KU Steam Power Plant Heat Recovery Component Energy Savings and Evaluation of Pumping System Power Consumption

By

Akeel Aigb Abdulla Al-Saedi

Submitted to the graduate degree program in Mechanical Engineering and the Graduate Faculty of the University of Kansas in partial fulfillment of the requirements for the degree of Master of Science

Dr. Ronald Dougherty _____

Thesis Advisor Chairman

Dr. Sara Wilson _____

Committee Member

Dr. Carl Luchies _____

Committee Member

Date Defended: December 19, 2016

The Thesis Committee for Akeel Aigb Abdulla Al-Saedi
certifies that this is the approved version of the following thesis:

KU Steam Power Plant Heat Recovery Component Energy Savings and Evaluation of Pumping System Power Consumption

_____

Chairperson Dr. Ronald Dougherty

Date Approved:

Abstract

Heat recovery is an essential process in any steam power plant because large amounts of energy are lost during the process of generating steam, whether with vented steam or drained hot water. So heat exchangers are used, to reclaim that energy before being wasted. According to the US Department of Energy, around 6,945 MMBtu/year could be saved by using a heat exchanger to reclaim vented steam energy under certain operation conditions [1]. Two heat exchangers are used in the KU steam power plant. One is as vent condenser to recover energy from steam and non-condensable gases that have to be vented from the deaerator to the atmosphere; and the other is to recover energy from blowdown water that has to be drained continuously from the boiler. Both the vented steam and the drained blowdown water have temperatures of 220-240 °F.

In this work, the recovered energy by both heat exchangers is analyzed and evaluated for the year 2016. The energy savings is computed based on the data gathered from January to August. For the rest of the year, energy savings is evaluated by using the relationship between the generated steam and the energy savings for the first eight months. The annual energy savings by the vent condenser in 2016 was $4.05\ x\ 10^9\ Btu$; while $8.92\ x\ 10^8\ Btu$ was saved by using the basement heat exchanger from January to September of 2016. Based on these, it was determined that about 5,291,500 ft^3 of natural gas was saved in the KU steam power plant in 2016 due to using both of the heat exchangers. This amount of fuel savings translated to $ 13,230 for the power plant.

Additional instrumentation has been installed at the vent condenser in order to assure that all needed data is gathered accurately. Internal temperature sensors (RTD type) were installed around the vent condenser to measure the fluid temperatures inside the pipes, instead of the surface sensors. A flow meter was installed in the condensed steam line exiting the vent condenser in order to determine the energy in that pipe line. In 2016, $3.3\text{x}10^8\ Btu$ was saved and added to the condensate water in the storage tanks by the condensed steam line; which means 352,000 ft^3 of natural gas was saved by the power plant. This fuel savings translated to about $ 880 for the power plant.

Flow rate calibration curves were produced using a calibration setup that was modified from a previous study [2] to calibrate the condensate water and condensed steam flow meters. The calibrated flow rates were about 6-7 gpm higher than the values recorded by those flow meters.

A thermal investigation has been conducted on the heat recovery components in the KU steam power plant. The average heat transfer rate from the steam to the boiler feed water during the deaeration process in the deaerator was evaluated. Investigation was performed to evaluate the flow type, efficiency, and the heat transfer rate in terms of the overall heat transfer coefficients for both of the heat exchangers.

Power consumption by the Worthington-D824 constant speed pump and the Grundfos CRE15-3 variable speed pump has been evaluated, based on new operating conditions in 2016. The flow rates of these pumps were adjusted using the flow meters' calibration curves that came from the calibration setup. Moreover, the discharge pressures of these pumps have been verified after applying comparative analyses by testing different pressure transducers with the pumping systems. Three approaches were used to evaluate the power consumption in order to verify the accuracy of the determined power. These approaches were: directly recorded power; pump curve power; and calculated power. In general, the power consumed by the Worthington pump was about 4% higher than that of the Grundfos pump.

The natural convection heat transfer coefficient around the vent condenser was calculated in order to determine the heat loss to the surroundings. The heat loss around the vent condenser was employed to determine the mass flow rates of the steam that enters the vent condenser and the non-condensable gases that are vented to the atmosphere. These mass flow rates were computed by applying mass and energy balances around the vent condenser. For instance, on 10/11/2016 at 12:12 PM, it was found that the flow rates of the DA's vented steam, condensed steam, and steam and non-condensable gases were 8.55 $\frac{lb_m}{min}$, 8.1 $\frac{lb_m}{min}$, and 0.46 $\frac{lb_m}{min}$, respectively.

A T-S diagram was developed, based on the new-found conditions and changes in the KU steam power plant, in order to visualize heat transfer and changes in temperature for the power plant's thermodynamic cycle. In this study, the T-S diagram's parameters were measured and recorded using thermocouples and data loggers that can measure temperatures of the steam around the power plant. Using this instrumentation helped to produce a more accurate T-S diagram.

With the basement deaerator, the vent condenser was isolated (by closing the steam line that comes from the DA) whenever the level control mode of the Grundfos pump was used because the pump pressure head was not sufficient to reach the vent condenser. The reason of isolating the vent condenser in this mode was to protect the vent condenser from overheating by the steam, since no cold fluid (condensate water) was flowing. As a result, less power was consumed by the VSP in this mode, but much more energy was wasted by not using the vent condenser. However, a new deaerator was installed in September of 2016 and located upstairs close to the vent condenser. So, in this case, new data needs to be gathered in order to calculate the energy savings when the vent condenser and the VSP's level control mode are used at the same time.

Also, it is recommended that the power plant staff install a control system that can control the make-up water flow rate to the storage tanks, instead of the manual valve that is used now. This system would have two advantages: control the make-up water flow automatically based on the water level inside the storage tanks; and protect the basement heat exchanger from thermal shock that happens due to sudden changes of the temperature caused by the immediate switching of the make-up line solenoid valve to fully open or fully closed.

To My Guardian Angels,

My Parents

Acknowledgements

I would like to thank Dr. Dougherty, my advisor, for his supervision, patience and encouragement throughout my work. His guidance, advice and support have been invaluable along this study. It has been a tremendous learning experience and I deeply grateful for it.

I would like to thank Dr. Sara Wilson and Dr. Carl Luchies for their time and contribution by being part of my committee. Also, I would like to thank Dr. Ku for his help during my lab work.

I would also like to express gratitude to The Higher Committee for Education Development in Iraq, HCED, for funding my study and the great opportunity for allowing me to pursue my ambition of getting my Masters of Science degree, as well as live this wonderful experience in the United States.

Also, I really appreciate all the time and effort of Robert Mills, Steve Bonebrake, Rick Ullery, and all of the staff of The University of Kansas steam power plant who worked with me regarding my project. They have been very helpful, and supportive.

I would also like to express my thanks to all of my friends, especially Anurag Nanda for all of the support and discussions that helped to improve this work.

Finally, I would like to thank my parents and all of my wonderful family from the depths of my heart for their support, patience, and continuous prayers.

Table of Contents

List of Appendices

List of Figures

List of Appendices Figures

List of Tables

List of Appendices Tables

Nomenclature

A_i Inner surface area for the heat exchanger tubes (in^2)

A_o Outer surface area for the heat exchanger tubes (in^2)

C_1 Flow rate conversion factor ($0.13368 \frac{ft^3/min}{gpm}$)

C_2 Power scale factor ($1714 \frac{lb_f\, gpm}{in^2\, hp}$)

C_3 Power conversion factor ($0.746 \frac{kW}{hp}$)

C_4 Pressure-to-head conversion factor ($2.31 \frac{ft-head}{lb_f/in^2}$)

C Natural gas price ($\$/ft^3$)

C_p Specific heat capacity ($\frac{Btu}{lb_m\ °F}$)

D Diameter of heat exchanger tubes or pipe lines (ft)

dT Temperature difference along the heat exchanger in parallel- and counter-flow cases (°F)

e_1 Percent difference between recorded and pump curve power values (%)

e_2 Percent difference between recorded and Eq. (4.27) or (4.33) power values (%)

e_3 Percent difference between pump curve and Eq. (4.27) or(4.33) power values (%)

e_{avg} Average error (%)

e_{RMS} Root mean square standard error (%)

g Acceleration of gravity ($32.2 \frac{ft}{sec^2}$)

Gr Grashoff number (-)

H Pump head (ft)

H_n Natural convective heat transfer coefficient ($\frac{Btu}{(ft^2)\ hr\ (°F)}$)

$\mathrm{H_{net}}$ Net head of a pump (ft)

$\mathrm{H_P}$ Discharge pressure head of a pump (ft)

$\mathrm{H_{static}}$ Static pressure head of a pump (ft)

h Specific enthalpy of fluid ($\frac{\mathrm{Btu}}{\mathrm{lb_m}}$)

h_{fi} Inner surface fouling heat transfer convection coefficient ($\frac{\mathrm{Btu}}{(\mathrm{ft^2})\ \mathrm{hr}\ (^\circ\mathrm{F})}$)

h_{fo} Outer surface fouling heat transfer convection coefficient ($\frac{\mathrm{Btu}}{(\mathrm{ft^2})\ \mathrm{hr}\ (^\circ\mathrm{F})}$)

hi Enthalpy for fluid at the inlet of heat exchanger ($\frac{\mathrm{Btu}}{\mathrm{lb_m}}$)

h_i Inner surface heat transfer convection coefficient ($\frac{\mathrm{Btu}}{(\mathrm{ft^2})\ \mathrm{hr}\ (^\circ\mathrm{F})}$)

h_o Outer surface heat transfer convection coefficient ($\frac{\mathrm{Btu}}{(\mathrm{ft^2})\ \mathrm{hr}\ (^\circ\mathrm{F})}$)

ho Enthalpy for fluid at the outlet of heat exchanger ($\frac{\mathrm{Btu}}{\mathrm{lb_m}}$)

K Thermal conductivity ($\frac{Btu}{(hr)\ ft\ (^\circ R)}$)

K_w Thermal conductivity of heat exchanger tube walls ($\frac{Btu}{(hr)\ ft\ (^\circ R)}$)

L Length of heat exchanger tubes or pipe lines (ft)

l_{cr} Characteristic length (ft)

LHV Lower heating value of natural gas ($\frac{\mathrm{Btu}}{\mathrm{ft^3}}$) for 7 inch water gauge pressure and a temperature of 60 °F

LMTD Logarithmic mean temperature difference (°F)

m Water/steam volumetric flow rate (gpm)

$\dot{m}$ Water/steam mass flow rate ($\frac{\mathrm{lb_m}}{\mathrm{min}}$)

Nu Nusselt number (-)

n Refers to number of error values (-)

n_1 Number of heat exchanger tubes (-)

n_2 Number of heat exchanger passes (-)

Pr Prandtl number (-)

Q Heat transfer rate ($\frac{\mathrm{Btu}}{\mathrm{hr}}$)

Q_{out} Heat loss due to natural convection ($\frac{\text{Btu}}{\text{hr}}$)

R_i Inner radius of heat exchanger tube wall (in)

R_o Outer radius of heat exchanger tube wall (in)

R_w Thermal resistance of heat exchanger tube wall ($\frac{\text{hr (°F)}}{Btu}$)

R^2 Correlation factor for fit of equation to data (-)

S_G Steam generated by boilers in the KU SPP ($\frac{\text{lb}_\text{m}}{\text{month}}$)

T Temperature (°F)

TDS Concentration of total dissolved salt solids of in water (ppm)

T_f Air film temperature around the vent condenser or steam pipe line ($°R$)

T_s Surface temperature of the vent condenser or steam pipe line ($°R$)

T_∞ Air temperature around vent condenser or steam pipe line ($°R$)

T_{1i} Inlet temperature of the hot fluid for heat exchanger (°F)

T_{1o} Outlet temperature of the hot fluid for heat exchanger (°F)

T_{2i} Inlet temperature of the cold fluid for heat exchanger (°F)

T_{2o} Outlet temperature of the cold fluid for heat exchanger (°F)

U Overall heat transfer coefficient ($\frac{\text{Btu}}{\text{(hr)°F (ft}^2\text{)}}$)

U_{eqv} Equivalent overall heat transfer coefficient of heat exchanger ($\frac{\text{Btu}}{\text{(hr)°F (ft}^2\text{)}}$)

U_{orig} Original overall heat transfer coefficient of heat exchanger ($\frac{\text{Btu}}{\text{(hr)°F (ft}^2\text{)}}$)

V Volume rate of consumed or saved fuel (ft^3/day) or (ft^3/min) or (ft^3/month)

W Work rate ($\frac{\text{Btu}}{\text{hr}}$)

$\dot{W}$ Power consumption (kW)

$\dot{W}_1$ Recorded power consumption (kW)

$\dot{W}_2$ Pump curve power consumption (kW)

$\dot{W}_3$ Power consumption from Eq. (4.27) or (4.33) (kW)

Greek

β Air thermal expansion coefficient ($\frac{1}{^\circ R}$)

γ Specific gravity of water (-)

ΔP Pressure increase developed across a pump (psig)

Δt Time interval (min or sec)

ΔT Temperature difference (°F)

ΔT_1 Temperature difference between two fluids at the inlet of heat exchanger (°F)

ΔT_2 Temperature difference between two fluids at the outlet of heat exchanger (°F)

η Efficiency (-)

η_{added} Added efficiency by heat exchangers (-)

η_{Boiler} Boiler thermal efficiency (-)

η_m Motor efficiency (-)

$\eta_{Overall}$ SPP's overall efficiency (-)

η_P Pump efficiency (-)

η_{VFD} Variable frequency drive efficiency of the Grundfos pump (-)

μ Air dynamic viscosity ($\frac{lb_m}{ft\ (\sec)}$)

ρ Density ($\frac{\mathrm{lb_m}}{\mathrm{ft^3}}$)

σ_e Standard deviation of errors (%)

Subscripts

1, 2	Different types of fluids in heat exchanger
a	Air
add	Energy added
after DA	Boiler feed water temperature before deaerator
before DA	Boiler feed water temperature before deaerator
BFW	Boiler feed Water
Boiler	Boilers in the KU SPP
c	Cold fluid in heat exchanger
c_st	Condensed steam from the vent condenser
cons. fuel	Consumed natural gas by boiler in the KU SPP
counter	Counter-flow type heat exchanger
cmp	Campus
CSP	Worthington D824 constant speed pump
DA	Deaerator in KU steam power plant
DA_st	Deaerator's vented steam and non-condensable gases
fuel	Natural gas fuel
G	Steam and non-condensable gases
H	DA's horizontal vented steam pipe line
h	Hot fluid
hex	Basement heat exchanger
i	Months (January-December) of energy calculations
in	Inlet temperature or flow rate
j	Refers to error between the Omega and Siemens flow meters
m_up	Make-up water
Omega	Omega FMG3002-PP magnetic flow meter
out	Outlet temperature or flow rate
P	Pumps in KU steam power plant
parallel	Parallel-flow type heat exchanger
rise	Temperature or pressure rise
sat	Saturated
sat1	Saturated steam at the outlet of the DA
sat2	Saturated steam at the inlet of the vent condenser
st	Steam generated in the KU steam power plant
str	Straight tubes of the heat exchanger
saved fuel	Total fuel saved by basement heat exchanger/vent condenser
saved fuel/hex	Fuel saved by using basement heat exchanger in the KU SPP
saved fuel/V.C.	Fuel saved by using vent condenser in the KU SPP
Smns1	Siemens flow meter in the condensed steam line of vent condenser
Smns2	Siemens flow meter in the constant speed pump discharge line
Smns3	Siemens flow meter in the variable speed pump discharge line
tank	Condensate water storage tank in KU steam power plant
tot	Total

U	U-tubes of heat exchanger
V	DA's vertical vented steam pipe line
V. C.	Vent condenser
VSP	Grundfos CRE15-3 variable speed pump
water	Condensate water in the KU steam power plant
w_i	Vent condenser inlet condensate water
w_o	Vent condenser outlet condensate water

Abbreviations

Aug.	August
BFW	Boiler feed water
bhp	Brake horsepower of pump
CSP	Constant speed pump (Worthington D-824)
DA	Deaerator in KU steam power plant
Dec.	December
G	Steam and non-condensable gases
GCS	Grundfos control system
hhp	Hydraulic horsepower of pump
Jan.	January
ppb	Parts per billion
ppm	Parts per million
RTD	Resistance temperature detector
Sept.	September
SPP	Steam power plant
VSP	Variable speed pump (Grundfos CRE15-3)

Chapter One: Overview and Details of Energy Recovery Components in the KU Steam Power Plant

This work was conducted on the main equipment in the KU steam power plant (SPP) that is related to energy savings and consumption. Savings are in the form of recovered energy, either from wasted steam or hot water in the heat exchangers that are used in the basement and on the first floor. Another energy savings investigation was conducted for the condensate water pumps (Worthington constant speed D-824 and Grundfos variable speed CRE 15-3) to calculate and analyze the power consumption of these pumps in different operation modes, and determine which pump type can reduce power demands. This information could be used in the life cycle cost analysis (LCCA) of Ref. 2 in order to determine the life cycle implications of this study's findings.

First of all, it is necessary to describe briefly the main equipment and parts of the KU SPP with its related water and steam lines, so that it will be easy to understand calculation of the energy that would be saved in these pieces of equipment. Figure 1 is a general schematic of the KU SPP components with which this project is connected.

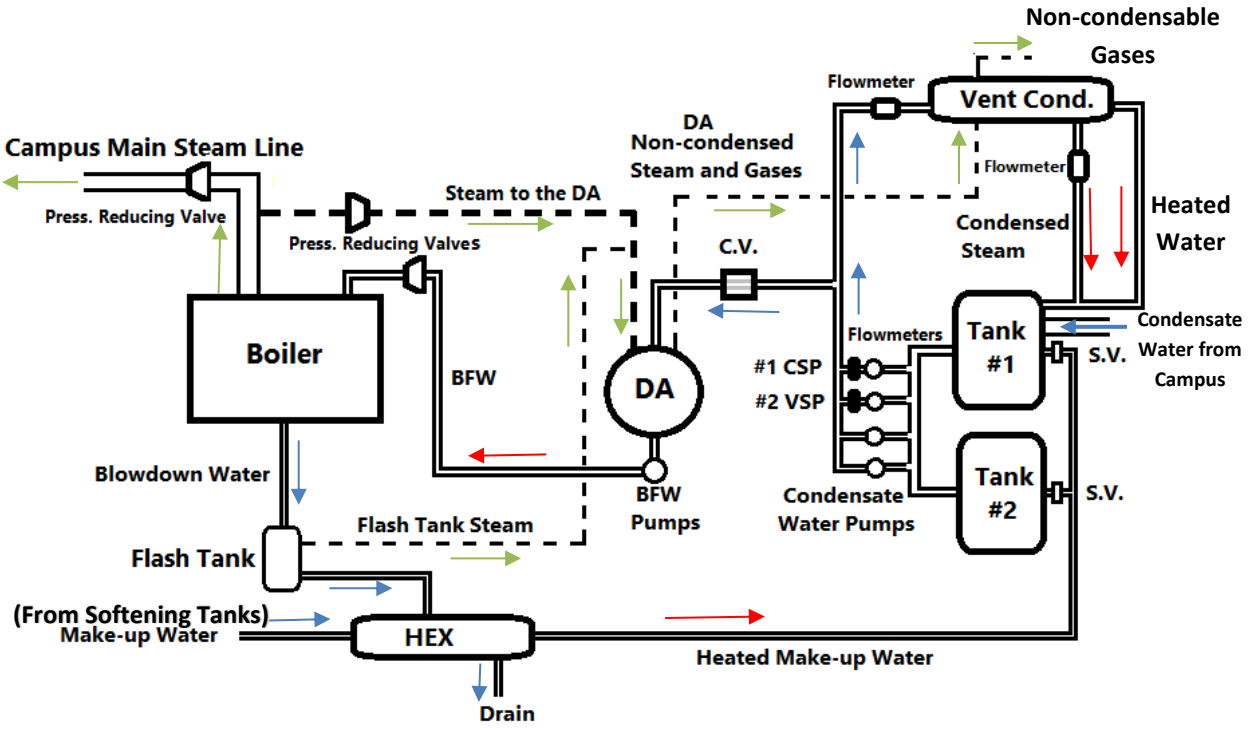

Fig. 1. Schematic of the KU SPP shows the main equipment and pathways for water and steam lines. Solid lines with blue arrows represent relatively cold water pipe lines; solid lines with red arrows represent relatively hot water pipe lines; and dotted lines with green arrows represent the steam pipe lines.

From Fig. 1, it can be seen that the KU SPP has no turbines because KU found that the cost of producing power by using turbines is more expensive than buying it from commercial suppliers. So the power plant is used just to produce steam for the campus. The power plant has condensate water storage tanks (labelled Tank #1 and Tank #2 in Fig. 1). These tanks store the condensate water that returns from the campus as well as receiving the make-up water from the city and the condensed steam from the vent condenser. Then that water is pumped from these tanks by using one of four pumps. Three of them are constant speed pumps, while the fourth is variable speed.

This study and the previous studies [2, 3, 4] investigate and compare the power consumption for the Worthington D-824 constant speed pump (labelled #1 CSP in Fig. 1) to that of the pair of Grundfos CRE 15-3 variable speed pumps (labelled #2 VSP in Fig. 1), which were installed in the KU SPP by Schmidt [4]. Each one of these pumps has a flow meter in its discharge line (Siemens flow meter, model Mag 5100 W DN 100) which was employed in this and the previous studies to make power calculations. These pumps push the water at a pressure of 40-50 psig to the deaerator (labelled DA in Fig. 1), but that pressure is reduced before entering the DA to 5-10 psig by a control valve (labelled C.V. in Fig. 1).

The DA's main function is preheating and reducing the oxygen and other gases' concentrations in the boiler feed water (explained in detail in Section 1.1). The excess steam and other gases from the DA line are directed to the vent condenser (labelled Vent Cond. in Fig. 1) on the first floor. The vent condenser is used to recover energy from the steam and gases that are vented from the DA by preheating the excess condensate water. Booster and feed water pumps (labelled BFW Pumps in Fig. 1) push the preheated water at a pressure of about 350 psig from the DA to the boilers; but that pressure is reduced to 175 psig by a pressure reducing valve before entering the boilers.

There are four boilers in the KU SPP. They generate steam at about 175 psig and 377 °F. After exiting the boilers, the steam is branched to two pipe lines. The main branch is for campus use which is reduced to a pressure of about 90 psig and a temperature of about 330 °F. The other branch's steam line is reduced to a pressure of about 5-10 psig and about 240 °F to feed the DA as a super-heated steam (shown in Fig. 1 as dashed lines). Due to the high TDS (Total Dissolved Solids) levels in the boiler feed water (about 3000-4000 ppm), water is bled continuously (termed "blowdown") from the boiler to dispose the sludge and mud that accumulates in the boiler header line. This blowdown water is directed to the flash tank, as shown in Fig. 1, having a pressure of 5-10 psig and a temperature of about 230 °F. Part of the blowdown water is flashed to steam in the flash tank due to the fact that the blowdown water pressure is greatly reduced which causes the water to flash to steam. Then that steam is vented to the DA to mix with the steam that comes from the boiler for the deaeration process. The remaining water in the flash tank is directed to the heat exchanger in the basement (labelled HEX in Fig. 1).

The basement heat exchanger has two essential purposes: to reclaim the energy from the hot blowdown water by exchanging its energy with the colder make-up water, and to cool that unneeded blowdown water to a temperature of about 140 °F for environmental purposes before draining to the sewer system. The heated make-up water that goes to the storage tanks is controlled by solenoid valves (labelled S.V. in Fig. 1) which provide access to the storage tanks as needed. More details and pictures regarding the equipment in Fig. 1 are shown in Chapter 1 of Nanda's thesis [3].

This chapter reviews and describes the energy recovery components that are used in power plants in general, and specifically the KU SPP. These components are the deaerator (DA) that is used to remove oxygen as well as other dissolve gases and preheat the boiler feed water, and the heat exchangers that are used in two different locations and deal with different fluids to recover energy from these fluids before they leave the SPP.

DA and heat exchanger fundamentals are explained and analyzed in general to understand their basic principles. New instruments, such as internal temperature sensors (RTDs) and a flow meter, have been installed around the vent condenser in order to measure the temperatures inside the pipe lines [instead of using external surfaces measurement], and in order to measure the flow rate in the condensed steam line in order to more accurately calculate the total reclaimed energy by the vent condenser.

A calibration system was rebuilt and modified from a previous study [2] in order to test and calibrate the condensate water flow meters. Flow rate calibration curves were produced for flow meters downstream of the Worthington and Grundfos pumps by employing the calibration results. These curves are used to determine and correct the error values that are associated with the flow meter readings. These curves were used to correct the recorded flow rates that are used in the energy and power consumption calculations in Chapters Three and Four.

1.1 The Deaerator

The DA is a device that is widely used to remove dissolved O_2 and CO_2 from the BFW [5]. The DA has multiple functions: stores water; provides positive section head to the BFW pumps; and pre-heats the BFW to a minimum temperature of 100 °C or 212 °F, which is the minimum saturation temperature that is required to remove dissolved gases from the feed water [5]. Moreover, heating the feed water to 100 °C helps to reduce thermal shock in downstream preheating equipment such as the economizer [6].

In particular, dissolved O_2 in the BFW causes serious damage in steam systems by attaching to the inner walls of the metal tubes, and any other metallic equipment, then forming oxides or rust.

Dissolved CO_2 combines with water to form carbonic acid that causes rapid corrosion of the tubes. The deaerator is designed to reduce O_2 to levels of about 7 ppb (or 0.005 cm³/liter) as well as eliminating CO_2 [5].

The design of the DA depends on the final desired O_2 concentration, which is in turn dependent on boiler operation conditions. If the O_2 concentration in the BFW is higher than 7 ppb and the boiler operates at high pressure values (greater than 200 psig), corrosion will build up in the tubes [6].

1.1.1 Deaerator Types in the KU SPP

There are two types of DAs: tray type and spray type. The tray DA has a domed section which is mounted above the main storage section and contains perforated trays (see Fig. 2). The feed water passes as droplets downward through the tray perforations to the main storage vessel. Meanwhile, steam enters at two locations, as shown in Fig. 2. The first steam branch enters directly below the trays to pass upward through the perforations and contacts the entering water which flows in the opposite direction. The second steam branch enters through nozzles in the bottom of the main vessel to mix with liquid water.

During this process, steam is cooled by direct contact with the incoming water. Most of that steam is condensed to water inside the DA, while a small fraction of the steam (about 5% to 14%) is vented with other gases (e.g., O_2 and CO_2) to the vent condenser [6]. More information on this venting process is provided in Section 1.4.

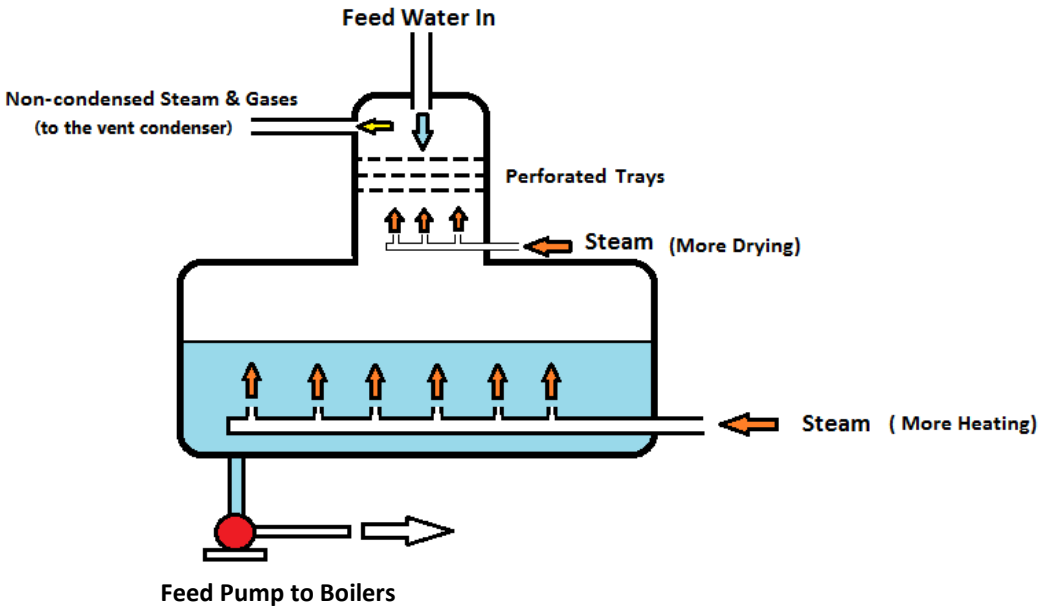

Fig. 2. Schematic diagram of a typical tray-type DA that is used in the basement of the KU SPP [based on Ref. 7]

The tray DA in the basement of the KU SPP works at a pressure of 5-10 psig and a temperature of about 225 °F. The condensate water that comes from the condensate storage tanks through the condensate water pumps has a pressure of approximately 5-10 psig after the DA control valve reduces it from a pressure of approximately 35-40 psig. The temperature of condensate water before the DA is on average about 160 °F; and the steam from the boilers enters the DA with the same pressure (i.e., 5-10 psig) but with a temperature of approximately 240 °F. So the water gains thermal energy by contacting and mixing with the steam to increase its temperature by about 75 °F.

The spray DA does not have a domed section, as shown in Fig. 3. The water is sprayed from the top of the tank while the steam enters through nozzles at the bottom of the tank. The steam mixes with the water and cools while condensing to liquid, and the non-condensed steam with the other gases is vented to the vent condenser (some energy recovery) or to the atmosphere (no energy recovery).

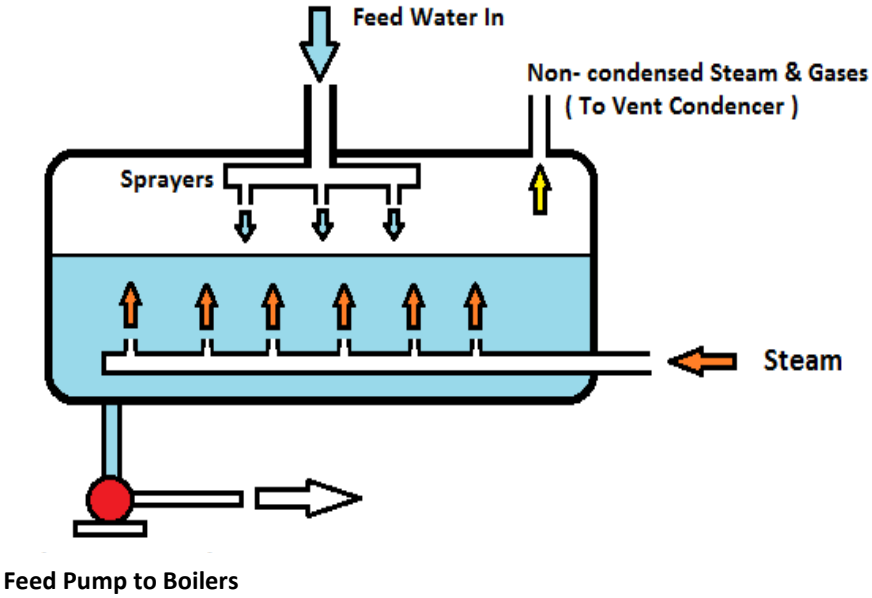

Fig. 3. Schematic diagram of a typical spray-type DA that is used on the first floor at the KU SPP [based on Ref. 8]

A tray DA is used in the KU SPP on the first floor as a standby for the main DA in the basement. This type of DA does not have trays, so it depends totally on the steam nozzles to deaerate the condensate water inside the tank. However, the deaeration process is enhanced by using chemicals (Sodium Sulphide) as O_2 scavengers. The pressure and the water level inside the DA are managed by a control valve to keep the operation pressure positive (5-10 psig) so as to prevent air from leaking into the DA, and to maintain the water level at about 52% (more details and pictures of the DA are in Chapter 1 of Nanda's thesis [3]).

Since high temperature steam is used in the deaeration process, the boiler feed water gains energy before it goes to the boilers. The greater the heat gained by BFW in the DA, the smaller the amount of fuel needed to form the steam inside the boilers; and that will save energy and enhance the boiler's efficiency. The average heat transfer rate between the steam and the condensate water during the deaeration process is evaluated in Chapter Two. This energy that is added to the condensate water in the DA translates into the natural gas [or liquid fuel] that is saved by using the DA, and, as a result, increases the power plant efficiency.

1.2 Heat Exchanger Basic Principles

A heat exchanger is a device that transfers heat between two fluids (e.g., liquid, steam, or gas). One fluid is relatively hot, while the other is relatively cold. The heat exchangers in the power plant are classified according to the liquid flow directions. When the two fluids flow in the same direction, the heat exchanger is termed parallel-flow; and when the fluids flow in opposite directions, this is a counter-flow heat exchanger. When the fluids flow perpendicular to each other, this is termed a cross-flow heat exchanger. The parallel-flow type, like the double-tube heat exchanger, is shown in Fig. 4a. The counter-flow type, like the shell-and-tube and the plate heat exchangers, are shown in Fig. 4b and Fig. 4c, respectively. The cross-flow type, like the finned-tube and the plate-fin heat exchangers, are shown in Figs. 4d and 4e, respectively.

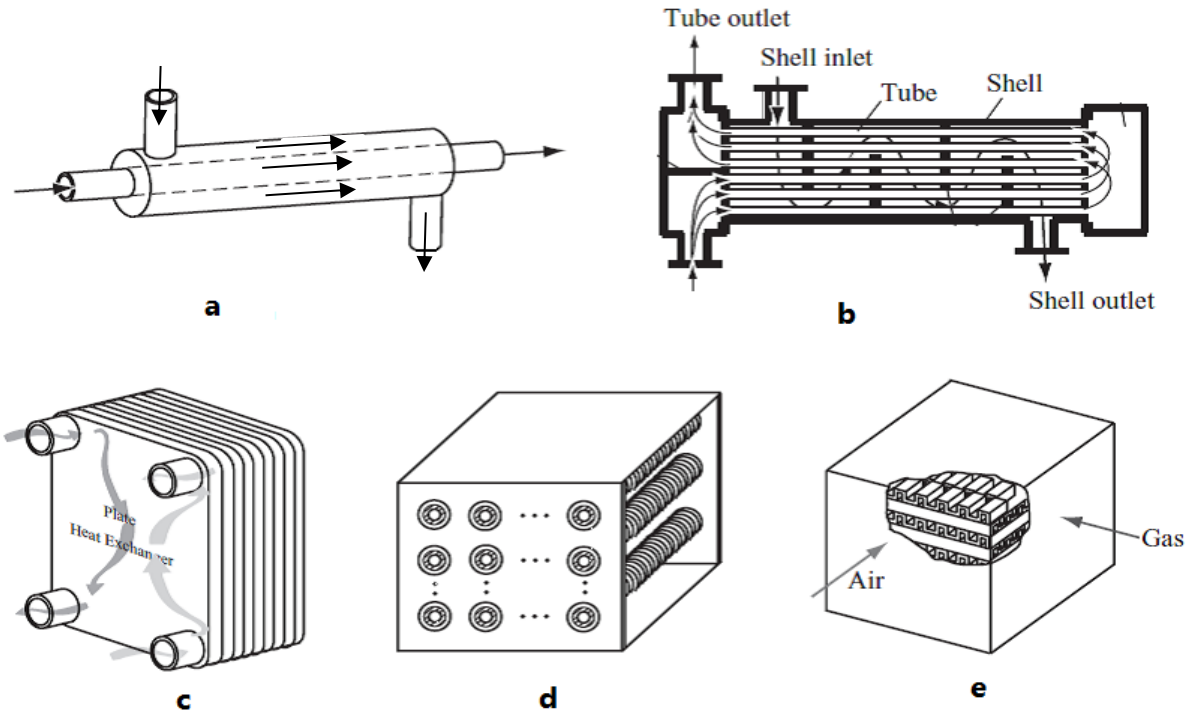

Fig. 4. Types of heat exchangers, according to the flow direction [reproduced from Ref. 9]

The KU SPP uses two shell-and-tube Bell & Gossett [10] heat exchangers in different locations for different purposes. One is used in the basement to heat make-up water and to cool the blowdown water at the same time, while the other heats the condensate water with the DA vented steam.

The heat exchange process depends basically on conduction and convection to heat a lower temperature fluid with a higher temperature fluid, such as hot liquid, steam, or gas. The KU SPP uses model SU-85-2 shell-and-tube heat exchangers, which are designed to handle steam in the shell and liquid water in the tubes [11].

Investigations have been conducted for this work by using basic heat transfer principles to evaluate the rate of heat transfer for the two types of heat exchangers in the KU SPP. Moreover, calculations are performed in Sections 2.3.1 to 2.3.2 in order to determine theoretically the type, as well as the efficiency, of the heat exchangers.

1.2.1 Heat Transfer Fundamentals

This section discusses, in general, the principles of heat exchangers. The common heat exchanger types that are used in most power plants are parallel-flow and counter-flow. These types are used specifically because of the flow capacity that they have and the type of the fluids that they can deal with in power plants. So, detailed heat transfer analysis is conducted for these two types in the KU SPP.

According to Bell and Gossett representatives [11], it is difficult to classify a steam-to-liquid heat exchanger as counter-flow or parallel-flow because these classifications are typically used when the process media in the heat exchanger are liquid-to-liquid. In the liquid-to-liquid case, one fluid exchanges its energy with another by means of sensible heat, while in the steam-to-liquid case, energy is transferred by the latent heat of the steam as its phase changes from steam to liquid.

The flow arrangement (shown in Figs. 5a and 5b) for both heat exchanger types shows that the hot fluid in the shell has an inlet temperature T_{1i} and reduced outlet temperature T_{1o} with a mass flow rate of $\dot{m}_1$, while the cooler fluid in the tubes has an inlet temperature T_{2i} and an increased outlet temperature T_{2o} with a mass flow rate of $\dot{m}_2$.

Figures 5a and 5b show the distribution, as well as the flow directions, of the fluids inside the heat exchangers in both types. From the law of the energy conservation, the heat transfer from the hot fluid (Q_h) is the same as the heat transfer to the cold fluid (Q_c), when the heat exchanger has no losses and the efficiency is 100%. Hence;

$$Q_h = Q_c \tag{1.1}$$

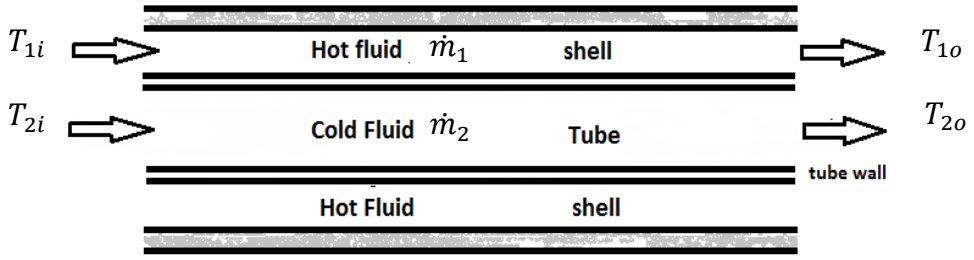

a. Parallel-flow heat exchanger

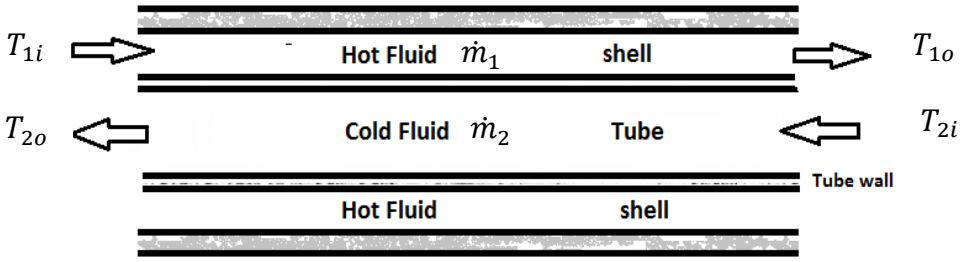

b. Counter-flow heat exchanger

Fig. 5. Shell-and-tube heat exchanger types [based on Ref. 13]

The heat transfer rate for the hot fluid is determined by the enthalpy change when the fluid's phase changes, for example from steam to liquid. The heat transfer rate is the product of the mass flow rate, the specific heat, and the temperature difference from the inlet to the outlet for a fluid when specific heat (C_p) is constant and there is no change of phase. For the hot fluid, where the inlet temperature is higher than the outlet temperature, this is expressed as

$$Q_h = \dot{m}_1(hi - ho)_1 = \dot{m}_1\, C_{p1}\, (T_{1i} - T_{1o}) \tag{1.2a}$$

For a cold fluid, where the outlet temperature is higher than the inlet temperature, the heat transfer is:

$$Q_c = \dot{m}_2(ho - hi)_2 = \dot{m}_2\, C_{p2}\, (T_{2o} - T_{2i}) \tag{1.2b}$$

Alternatively, heat transfer for a heat exchanger can be expressed in terms of an overall heat transfer coefficient (U) as

$$Q = U\, A_o\, LMTD \tag{1.3}$$

The term ($U\, A_o$) in Eq. (1.3) can be found in terms of the thermal resistances of the system, which depend on convection coefficients, fouling factors due to the corrosion and clinkers on the tube walls, and wall conduction thermal resistance.

All of the terms for the thermal resistance between the two fluids in the heat transfer process are shown as components of a resistance circuit in Fig. 6. The overall thermal resistance includes the inner and outer convection coefficients, the inner and the outer tube fouling coefficients, and the tube wall thermal conductivity.

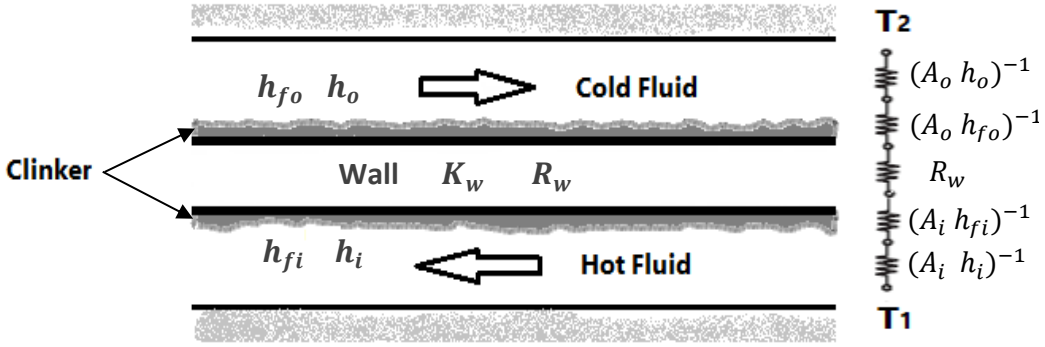

Fig. 6. Heat transfer thermal resistance circuit between the fluids in a heat exchanger [based on Ref. 9]

These resistance terms are represented as [9]

$$(UA_o)^{-1} = \frac{1}{A_i h_i} + \frac{1}{A_i h_{fi}} + R_w + \frac{1}{A_o h_o} + \frac{1}{A_o h_{fo}} \tag{1.4}$$

$A_i, h_i,$ and h_{fi} are the inner surface area, the inner surface convection coefficient, and the inner surface fouling coefficient, respectively. $A_o, h_o,$ and h_{fo} are the outer surface area, the outer surface convection coefficient, and the outer surface fouling coefficient, respectively. The thermal resistance (R_w) for the tube wall depends on the thermal conductivity (K_w) of the tube material, as well as the dimensions of the tube wall. So, for a tube:

$$R_w = \frac{ln(\frac{R_o}{R_i})}{2\pi K_w L} \tag{1.5}$$

All terms are defined in the Nomenclature.

Log mean temperature difference ($LMTD$) is the driving potential for heat transfer in Eq. (1.3), and it depends on the temperature differences throughout the heat exchanger for the hot and the cold fluids between the inlet and the outlet [9].

$$LMTD = \frac{\Delta T_1 - \Delta T_2}{ln(\frac{\Delta T_1}{\Delta T_2})} \tag{1.6}$$

The temperature differences in Eq. (1.6) can be seen in Figs. 7 and 8 for the flow direction types:
$\Delta T_1 = T_{1i} - T_{2i}$; $\Delta T_2 = T_{1o} - T_{2o}$ (parallel-flow)

$\Delta T_1 = T_{1i} - T_{2o}$; $\Delta T_2 = T_{1o} - T_{2i}$ (counter-flow)

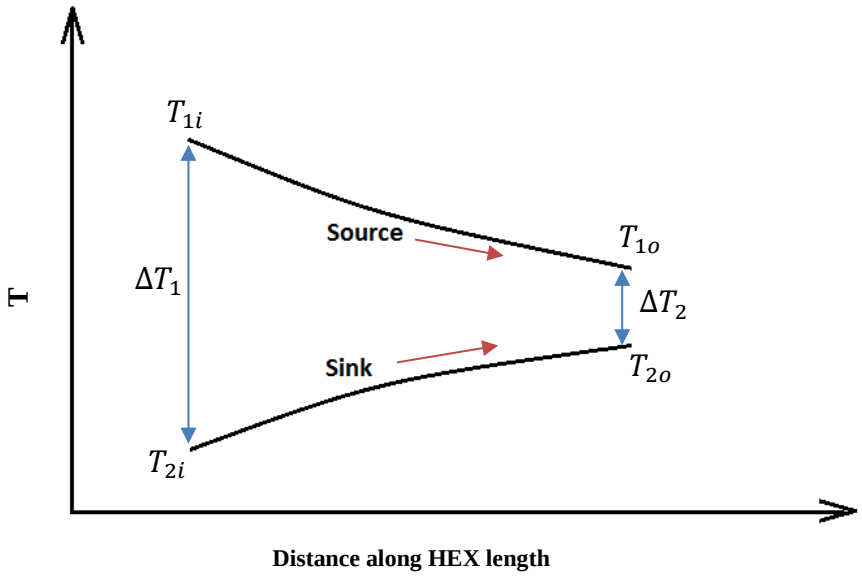

Fig. 7. Typical temperature profile for parallel-flow heat exchanger

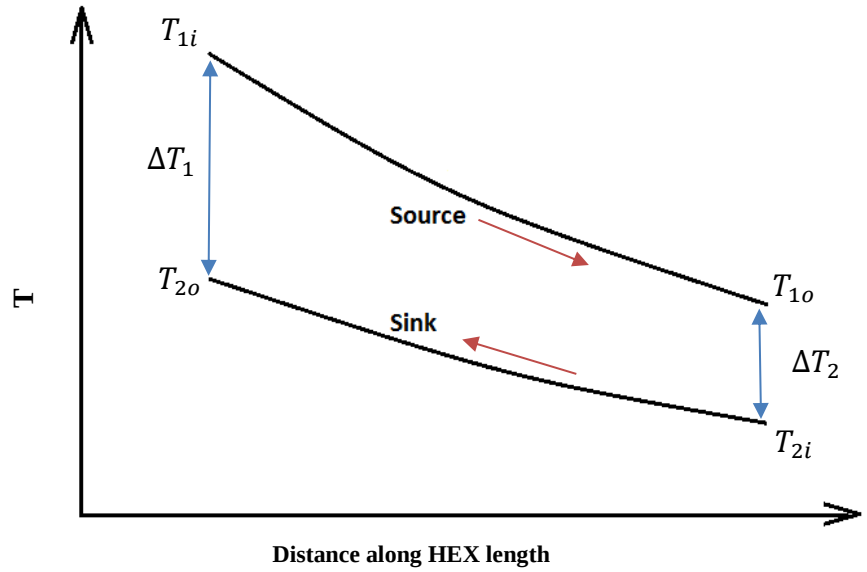

Fig. 8. Typical temperature profile for counter-flow heat exchanger

1.3 Basement Heat Exchanger

This heat exchanger is used in the basement of the KU SPP to heat the make-up water before it goes to the condensate storage tanks. That water enters the SPP at about 65 psig from the city supply system through water softening tanks in the basement of the SPP. The water softening tanks remove dissolved calcium and magnesium before the water passes through the heat exchanger. The city water flows through the heat exchanger's tubes at about 50-85 °F, while the boiler blowdown water flows through the shell at about 230 °F.

According to the manufacturer's specifications [10], this type of heat exchanger should deal with steam-to-water; but in the basement heat exchanger of the KU SPP, both fluids are liquid water. The cold city water enters the heat exchanger tubes between 50 °F and 85 °F, depending upon the season; and the boiler blowdown water enters the heat exchanger shell between 215 °F and 230 °F (see Fig. 9). After the water temperature is increased, it then goes into the storage tanks. The blowdown water temperature is reduced to approximately of 140 °F or below for environmental purposes, and is then dumped through a drain line to the sewer system.

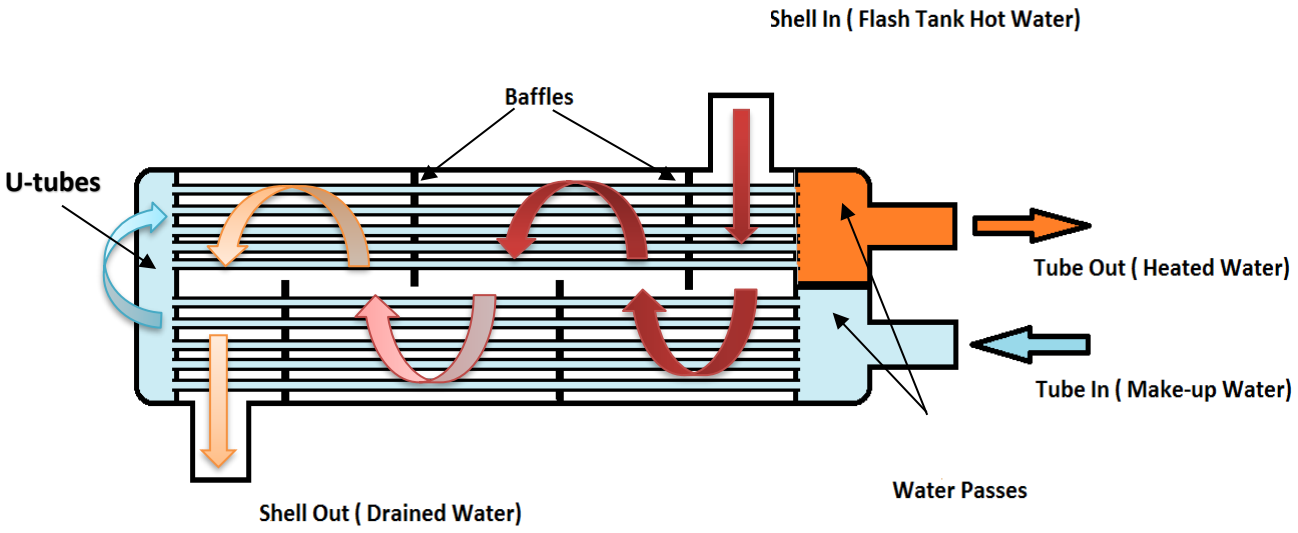

Fig. 9. Schematic of the basement heat exchanger for the flow arrangement of the KU SPP [based on Ref. 11]

From Fig. 9, it can be inferred that the heat exchanger is a shell-and-tube type with two passes, where the inlet hot water flows through the shell; and the baffles direct the hot water perpendicular to the flow of cold water in the tubes. These baffles make the hot fluid path longer in the shell in order to increase the heat transfer rate as well as the heat exchanger efficiency.

For the previous studies [2, 3], the heat exchanger specifications were not known. However, after determining the model number of these heat exchangers (Fig. 10, SU-85-2, Bell and Gossett [10, 14]), it was possible to obtain the needed information about these units from the manufacturer. This information helped to improve the thermal calculations of previous investigations [3] (i.e., verifying heating area, heat transfer rate, equivalent heat transfer coefficient "U_{eqv}", and estimating the heat exchanger efficiency). More details on the heat exchanger efficiency are given in Chapter Two.

Figure 10 shows the model number of the heat exchanger (see labelled area). The tag was found after removing the layer of glass wool insulation, which covers all of the heat exchanger in order to reduce heat loss to the surroundings. The information on the tag made it easy to obtain all other details from the manufacturer's website.

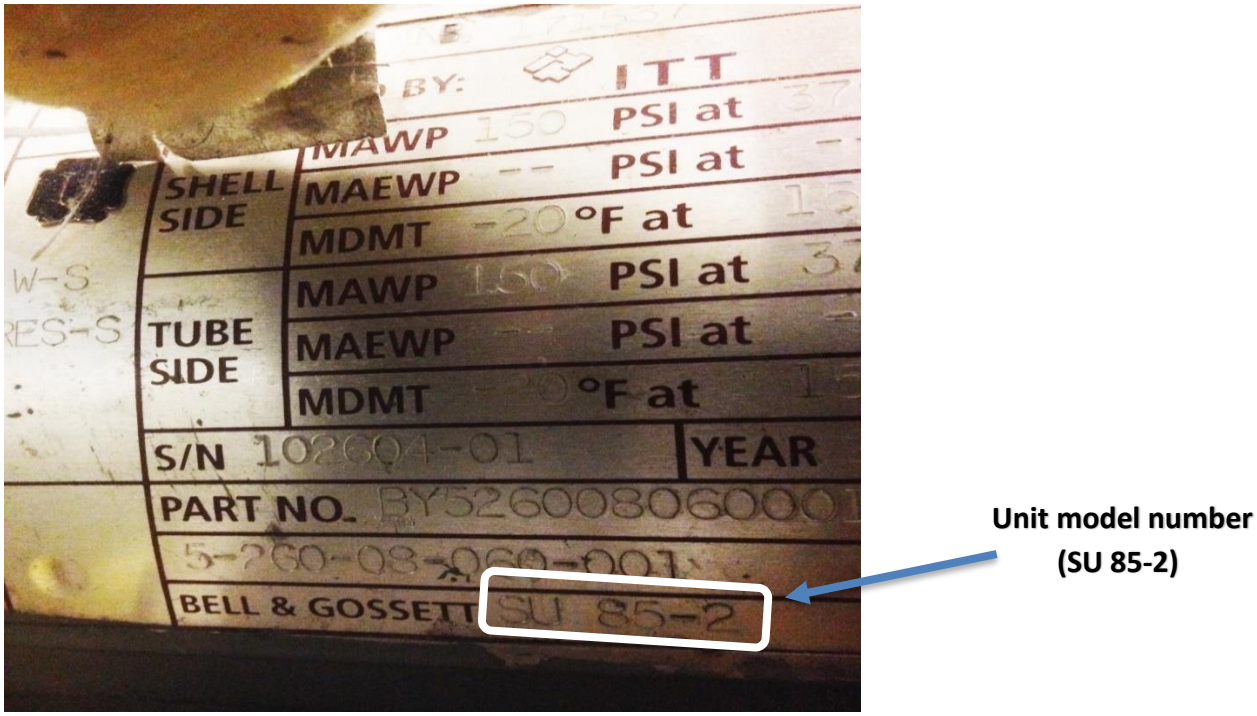

Fig. 10. Picture of a tag showing the model number of the KU SPP's basement heat exchanger

1.3.1 Data Acquisition System

As mentioned in Section 1.3, the basement heat exchanger handles liquid-to-liquid heat transfer. The liquids are the boiler blowdown water that flows through the shell, and the make-up water from the city which flows through the tubes. Surface contact probe temperature sensors (TMC6-HE**)** and a Hobo data logger (UX120-006M) were employed to measure and digitally record the temperatures for the inlet and outlet (see Apps. A1 and A2 for specifications of the Hobo logger and the sensors).

These surface sensors can measure within the temperature range of -40 °F to 212 °F with an accuracy ± 0.27 °F. The accuracy plot for temperatures out of this range is given in App. A2). For the previous study [3], the sensors were calibrated before they were installed; and they were in use for this study as investigation continued for the different seasons of 2016. Using the TMC6-HE sensors, it was possible to record the temperatures of the make-up water from the city, the heated make-up water, the boiler's blowdown water, and the water drained from the heat exchanger. These temperatures were helpful in calculating the energy savings from using the boiler's blowdown water before it was drained to the sewer system. They were also employed in the thermal calculations and investigation that are described in the Sections 2.2 and 2.3.

To calculate the energy saved by the heat exchanger, the make-up water flow rate was essential; but there was no flow meter in that pipe line to digitally record the water flow rate. However, there was a cumulative flow meter (Recordall Transmitter, Turbo 450 type, see App. A3) that the power plant staff used to manually record how many gallons of water were added to the storage tanks during each hour.

Downstream of the heat exchanger, solenoid valves in the make-up water pipe line were used to control the water flow to the condensate water storage tanks. These valves were opened or closed as needed, depending upon the water level inside the tanks, which prevented the tanks from overflowing. More details on the condensate water storage tanks, the solenoid valves, and the make-up flow meter are given in Nanda's thesis [3].

The data was recorded hourly on the SPP data sheet. During each hour, the solenoid valve might be opened or closed, so that meant the hourly recorded volume of water passed through the heat exchanger for only a few minutes when the valve was open during that hour. Simple calculations that depend on the temperature behavior of the water exiting the heat exchanger were used to determine the flow rate of the make-up water when the solenoid valve was in the open position (details of this process and the flow rate calculations are given in Section 3.2).

The solenoid's periodic opening/closing in the KU SPP has a damaging effect on the heat exchanger. This is due to the fluctuating thermal stresses in the tubes when the solenoid valve suddenly fully opens and fully closes, which causes sudden changes in the tubing temperatures. This is shown in detail in Section 3.2 with a graphical illustration of the temperature changes.

After studying the problem, an idea was suggested and discussed with the SPP staff as a substitute for using the solenoids valves. The idea was based on installing an electrically actuated valve in the make-up water pipe line before the solenoid valves, which could eliminate or reduce the thermal stresses on the heat exchanger by keeping the flow continuous at all time. The idea behind using the electric valve was to override the solenoid's sudden actions by keeping the electric valve partially open, yielding continuous water flow at all times.

The electric valve would be controlled by an analog signal (4-20 mA) from an ultrasonic level sensor installed on the storage tank. More details on the electric valve installation and its operation are discussed App. A4.

1.4 Vent Condenser

The vent condenser condenses the DA's vented steam; which then becomes a second make-up water source. In addition, some of the vented steam's thermal energy is transferred to the boiler feed water before it is released to the atmosphere with other non-condensable gases. Generally, the energy in the vent condenser is recovered in two forms: higher energy condensate water returns to the storage tanks; and the condensed DA's vented steam is another make-up source for the boiler feed water (quantity and other specifications of the condensed steam are given in Section 2.1.2).

The main purpose of the vent condenser is to reclaim as much as possible thermal energy from that steam and gases before they are released to the atmosphere. Meanwhile, all of the condensed steam is returned to the storage tanks, while the non-condensed steam and other gases (O_2, N_2, CO_2) are released. This reclamation adds more energy to the boiler feed water, and as a result, reduces the energy needed from consuming fuel in the burner and thus increases the boiler's overall efficiency.

The vent condenser is identical to the heat exchanger in the basement. They are both Bell & Gossett, shell-and-tube type, model SU-85-2; but the process fluids' phases are different than these of the basement heat exchanger. The vent condenser heats water with steam (as it should, according to the manufacturer's specifications [11]), while the basement heat exchanger deals with water-to-water, as explained in Section 1.3.

The condensate's temperature rises about 10-14 °F in the heat exchanger's tubes, while the steam enters the shell at a temperature of 220-230 °F and leaves the heat exchanger as saturated liquid water at 185-200 °F.

Regarding the vent condenser, all previous studies [2, 3] calculated the reclaimed energy from the steam by calculating the energy gained by the condensate water flowing through the vent condenser. However, that was not all of the energy gained using the vent condenser because the condensed steam that is returned to the storage tanks still has high thermal energy. Before this work, there was no data acquisition system in the condensed steam line to record the flow rate or the temperature. As a result, it was not possible to calculate the energy that was added to the storage tanks from the returned condensed steam.

After installing a flow meter in the condensed steam pipe line as well as installing internal temperature sensors (RTD) (details are given in Section 1.4.1), it is now possible to calculate the condensed steam's flow rate and thermal energy. In this case, the total saved energy is calculated

for the vent condenser, including the condensed steam's energy added to the condensate water in the storage tanks. That energy saves more fuel at the boilers. (The amount of fuel saved by the vent condenser is given in Section 3.4.)

1.4.1 Instrumentation and Data Acquisition System

In a previous study [2], the temperature readings in the inlet and outlet condensate water pipe lines were recorded manually from dial gauges in order to calculate the energy savings. A data logger and surface temperature sensors (i.e., HOBO UX120-006M and TMC6-HE; see Apps. A1 and A2) were used in the most recent study [3] for the condensate water pipe lines of the vent condenser in order to acquire and record the temperatures digitally.

The recorded temperatures from both previous studies [2, 3] for the vent condenser only recorded the inlet and outlet condensate water temperatures. The flow rate and the temperatures of the inlet and outlet steam were not recorded. So it was not possible to calculate the condensing steam's energy. On the other hand, the condensate water flow rate was recorded by a Cadillac SMAC Magnetic flow meter (see App. A5 for details). However, the surface temperature probes were not very trustworthy since the readings depended on conduction between the probe and the pipes' outer surfaces, which are affected by convection and radiation with the surroundings.

In addition, the accuracy of the measurement decreases as the temperature goes higher than about 70 ℃ (or 160 ℉), as shown in Fig. 11, where the error starts growing rapidly outside of the range of 0 ℃ to 70℃.

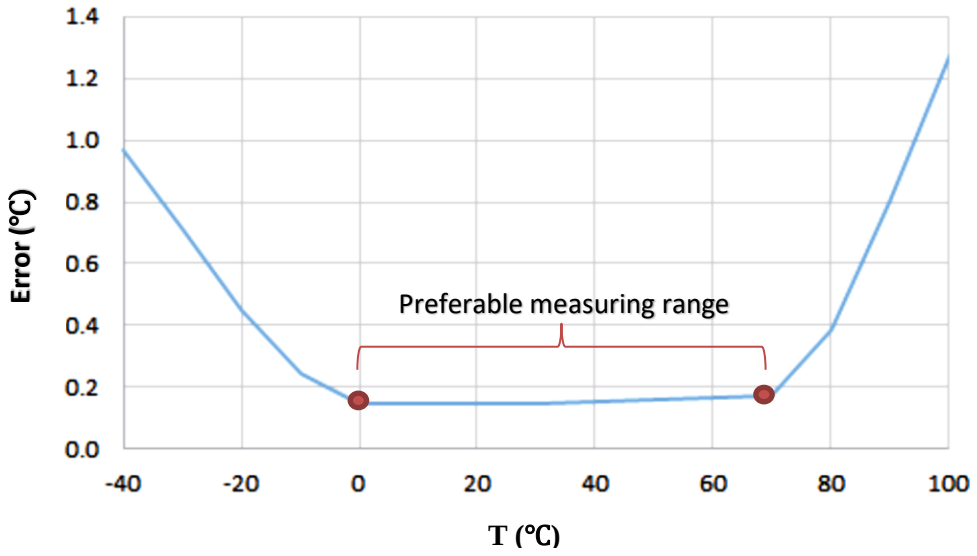

Fig. 11. The accuracy of the surface contact temperature probes (TMC6-HE) over the measurement range from −40 ℃ to 100 ℃ [reproduced from App. A2]

Since the temperatures in the vent condenser are sometimes higher than 160 °F, temperature sensors that have higher measuring ranges and can measure temperature inside the pipes were used, instead of surface contact sensors. Internal sensors ensure more accurate measurement regardless of the convection and radiation effects, as well as the ability to measure higher temperatures. Many options for internal sensors were considered, such as thermocouples and resistance temperature sensors. After weighing the benefits, resistance temperature detectors (RTD) were selected. This type of sensor employs a resistance that induces different voltage values as the temperature changes through the sensor.

These RTD sensors are the Omega PR-12-2-100 series (see App. A6) with analog signal transmitter type Omega TX92A-3 (see App. A6-1) to transform the RTD output voltage signal (0 -10 VDC) to an analog signal (4 to 20 mA); and this signal type was needed for the HOBO data recorders already in use.

The main reason for choosing RTDs is because the SPP staff are not able to make new holes in the water and steam pipe lines for installing new sensors. Such a process would require shutting down the power plant for one or two days, as well as having the possibility of leakage issues from the new fittings. So the SPP staff agreed to use the same thermowell holes that have been used for the dial gauge temperature probes, as shown in Fig. 12. This saved time and effort for the project and for the SPP staff.

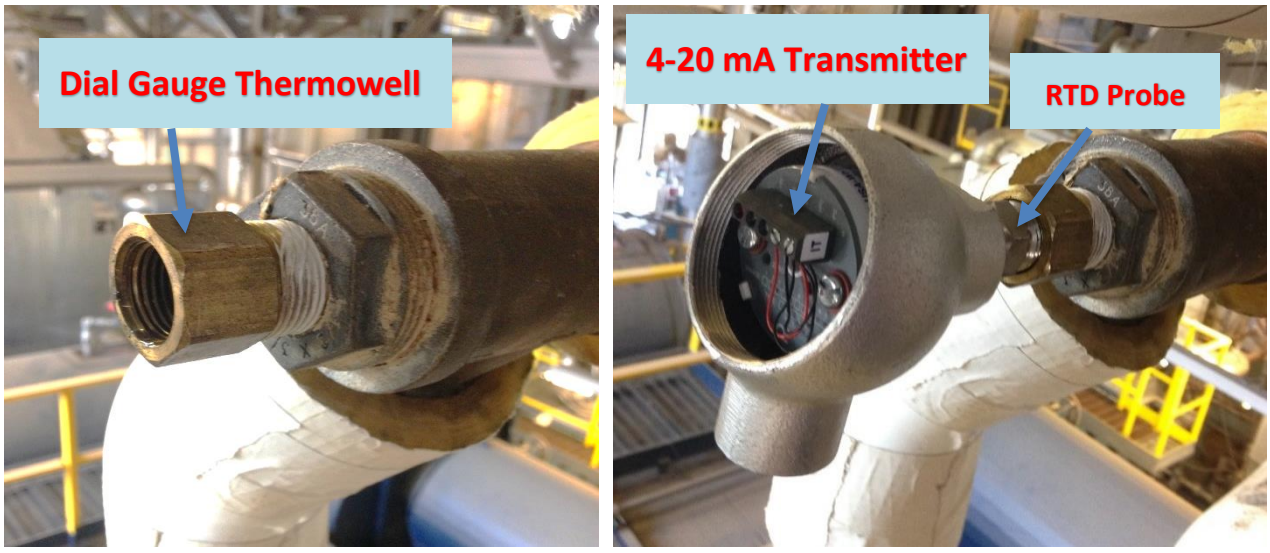

(a) (b)

Fig. 12. Thermowell in the inlet condensate water line that could be used with either dial gauge or RTD sensor. View (a) shows the dial gauge's thermowell; view (b) shows the RTD installed instead of the dial gauge.

The RTD sensor consists of two parts, as shown in Fig. 12b. The resistance probe (PR-12-2-100), that is 85 mm long and 6.3 mm in diameter, matching the thermowell hole's dimensions, goes inside the thermowell and produces the 0 to 10 VDC signal. The second part is the transmitter which transforms the signal of the resistance probe to the 4 to 20 mA data logger signal. The transmitter is powered with 8 to 50 VDC, which reflects a temperature range of 0 to 300 °F [15]. This range goes higher than the highest temperature in the vent condenser (see App. A6-1 for the internal sensor (RTD) specifications and measuring limits).

Three RTDs have been installed in the vent condenser. One each was installed in the inlet and outlet condensate water pipe lines, while the third was installed in the inlet steam pipe line that comes from the DA. A surface contact probe (TMC6-HE) was installed in the condensed steam line, because that pipe line does not have a thermowell in which the RTD can be installed, but only has a thermometer; and its fitting is not compatible with the RTD's probe.

Since this was the only pipe line in the vent condenser where the temperature is recorded by a surface contact probe, its reading was compared with other RTD readings in order to evaluate its estimated error.

It is essential to show the final wiring diagram (Fig. 13) because of the many issues that can arise with the wiring, especially with the output signals if the cables are not connected in the right way.

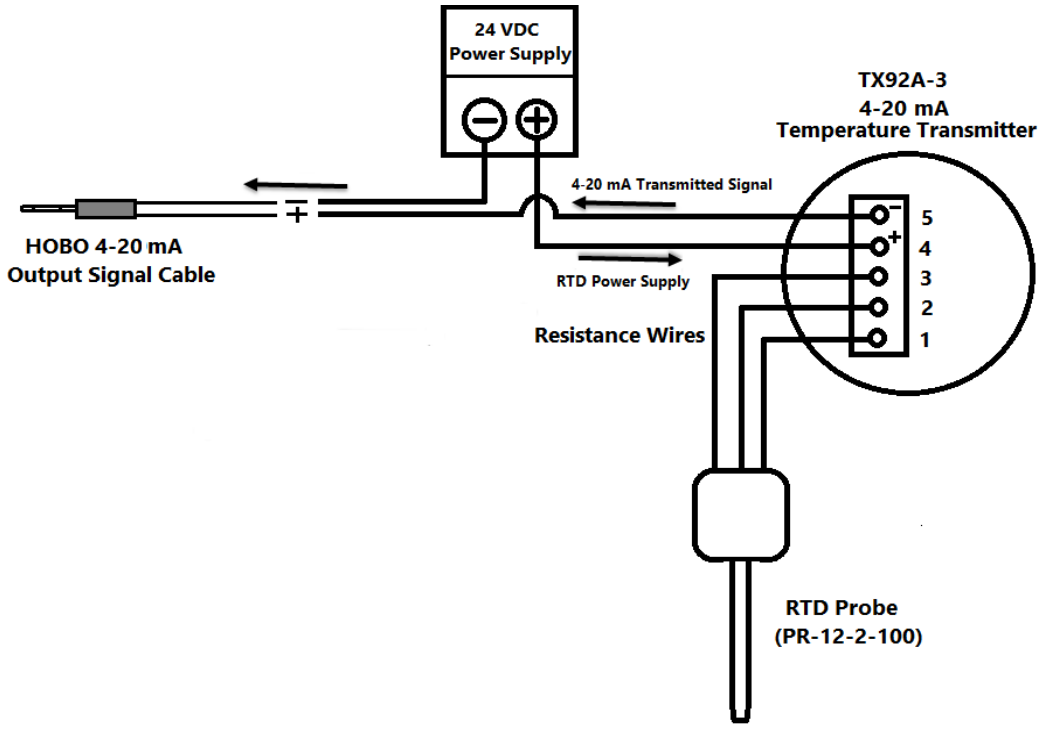

Fig. 13. Schematic wiring diagram for the RTDs installed around the vent condenser

Figure 13 shows the power and signal wires that run from the DC power supply to the RTD resistance probe. A 24 VDC power supply was used to power the TX92A-3 transmitter. In turn, the transmitter supplied voltage to the probe; and the probe sent back voltage but with different magnitudes due to the probe's resistance that changed with temperature. Eventually, the returned voltage was transformed by the transmitter to an analog signal (4-20 mA) so that it could be read and recorded by the HOBO data logger.

There were problems with the output signals of the RTDs during the initial tests. Unreasonable temperature values were recorded during these tests due to incorrect 4 to 20 mA signals. Section 2.1.1.a describes in detail the issues that were faced.

1.5 Flow Meter Calibration

The flow meters in the KU SPP were calibrated in a previous study [2] by building a flow meter calibration setup (see App. A7-1 for details about re-building the setup). The calibration system was built and used first to test and calibrate the condensate water flow meters that are used in the pipe line downstream of the condensate water pumps in the basement.

Also, it was used to calibrate a flow meter in the excess condensate water pipe line that goes to the vent condenser [2]. This calibration setup was rebuilt and modified for calibrating a different flow meter in this study. The following details the tests that were performed using this system.

1.5.1 Test and Calibration of Recirculation Line Flow Meter

As a part of the total reclaimed energy calculation for the vent condenser, there was a need to calculate the energy that is added to the condensate water in the storage tanks from the vent condenser's condensed steam line. To do so, a flow meter was installed in that pipe line to measure the flow rate of the condensed steam which allowed calculation of the total energy gained by the vent condenser.

Instead of purchasing a new flow meter, an old Siemens flow meter (Mag 5100 W DN 25; see App. A8), from the condensate water recirculation line, was selected, since that pipe line had not been used for the last few years by the SPP. The flow meter's last readings were in the negative flow rate range (-7 to -25 gpm). So, it was necessary to test and calibrate the flow meter before installing it in the vent condenser's condensed steam line.

The flow meter was re-calibrated using the calibration system after modifying the setup to fit the new flow meter. Most of the pipe lines and fittings in the setup were removed and replaced with different sizes in order to fit the Siemens flow meter (Mag 5100 W DN 25).

That calibration setup had been used in a previous study [2] to calibrate the Siemens flow meters (Mag 5100 W DN 100), located in the discharge line for the condensate water pumps, and also to calibrate the Cadillac flow meter in the condensate water pipe line before the vent condenser.

The pipe lines that were used before were 4 in and 2 in diameter, while a 1 in pipe line was needed for this process. After ordering all of the required materials, most of the pipe lines and fitting were dismantled from the calibration setup and new piping was installed. The modifications of the calibration setup with all of the needed materials are described in App. A7.

Figure 14 shows that the set up was composed of a water tank (100 gallon capacity), a Grundfos constant speed water pump (95 gpm, 330 psi, 15 HP, 3-Phase), an Omega FMG3002-PP magnetic flow meter measuring up to 180 gpm (see App. A9), a manual ball valve (2 in diameter) to manage the flow through the flow meters, and the Siemens flow meter (Mag 5100 W DN 25) capable of measuring up to 28 gpm (see App. A8).

The Grundfos pump moved the water from the tank to the Omega flow meter in the 1.5 in diameter pipe line. A clear pipe was installed upstream of the Grundfos pump in order to see if there were any bubbles flowing with the water because they can affect the flow meters' signals. Also, a 2 in diameter ball valve was installed directly before the pump in order to manage the water's flow manually as needed.

Then, the water flowed through the Siemens flow meter in the 1 in pipe line to the tank. Moreover, the electrical wiring for the Grundfos pump's control panel was changed to work with 460 VAC (it was wired in the previous study [2] to 230 VAC). The changes in the wiring were made according to the manufacturer's diagram in order to match the new power supply voltage (see App. A7-2 for the wiring graph).

Problems were encountered with rebuilding the calibration setup, such as a proper place to work on it and operate it due to the physical size, 3-phase power supply box and outlet, and water source. Previously, when the setup was built, the School of Engineering Machine Shop was used to build and operate the setup; but it was not possible to use that location because of additional restrictions that arose due to the new engineering building. As a result, the setup was re-engineered in order to fit in B171 LEA where it was re-built (see App. A7-1 for more details and schematics regarding these issues).

The Omega flow rate reading was considered to be the reference reading with which the faulty Siemens flow meter readings were compared. These data were recorded and saved using the HOBO data logger. Many tests were run and data was taken at different time intervals (1 second and 10 seconds); and the error values for the Siemens readings were calculated with respect to the reference readings from the Omega flow meter.

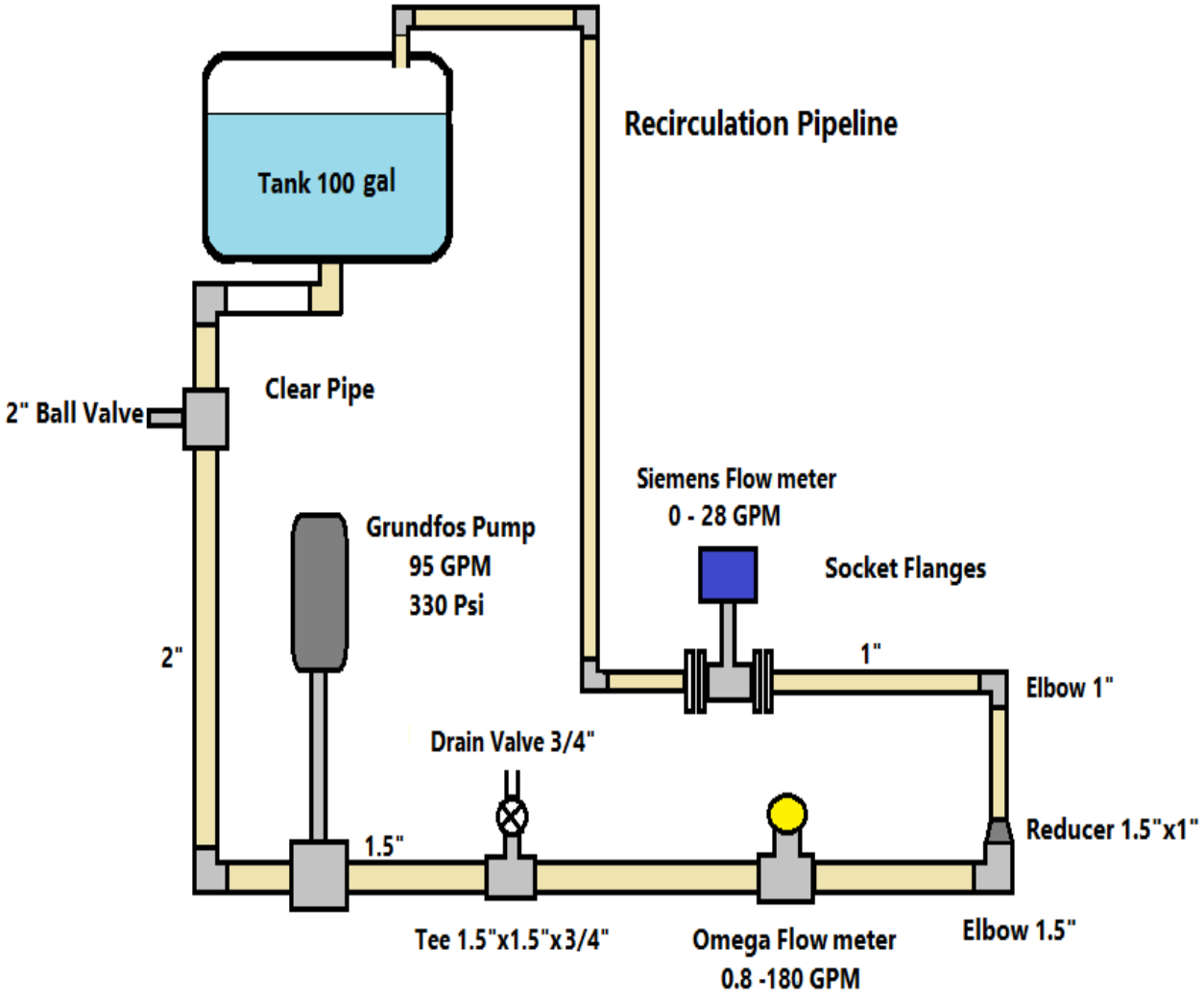

Fig. 14. Layout of the calibration setup's components

Data were taken for four main tests with flow rate varying from 5 to 28 gpm by opening/closing the 2 in ball valve. The reason for choosing this range of flow was because the Grundfos pump started making noise and vibrating below 5 gpm as a minimum value. Also, 28 gpm was chosen as the maximum value because this is the maximum of the Siemens flow meter (MAG 5100 W DN 25).

Test 1 was conducted using a 10 second time interval over a flow rate range from 10 gpm to about 47 gpm in order to check the accuracy of the maximum reading of the Siemens flow meter (see App. A7-3 for the flow rates of the four tests). It was noticed that, whenever the value 28.237 gpm was recorded, this meant that the pump's flow rate was higher than the Siemens flow meter's measuring limit, as shown in Fig. 15. The Omega flow meter continued to record higher flow rates for the times when the Siemens stopped measuring.

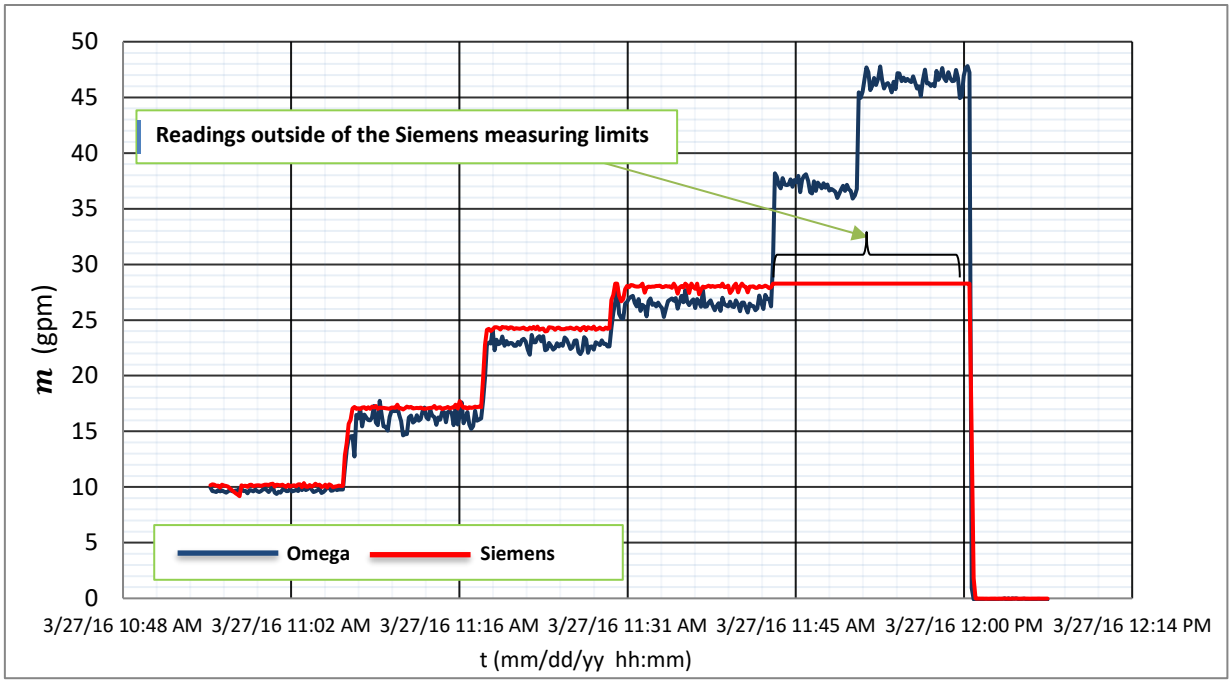

Fig. 15. Siemens and Omega flow rate readings for different flow ranges (Test 1)

All of the data in Tests 1 to 4 (App. A7-3) showed that the average Siemens flow meter readings were always higher than the Omega readings within an error of 5%. As shown in Fig. 15, data in Test 1 was taken over 10 second time intervals for ascending flow rate which was managed by the ball valve. Some tests were performed over 1 second time intervals for descending flow rate as shown in Test 4 of Fig. 16. The tests were performed in this way in order to check the Siemens meter's behavior under different operation conditions.

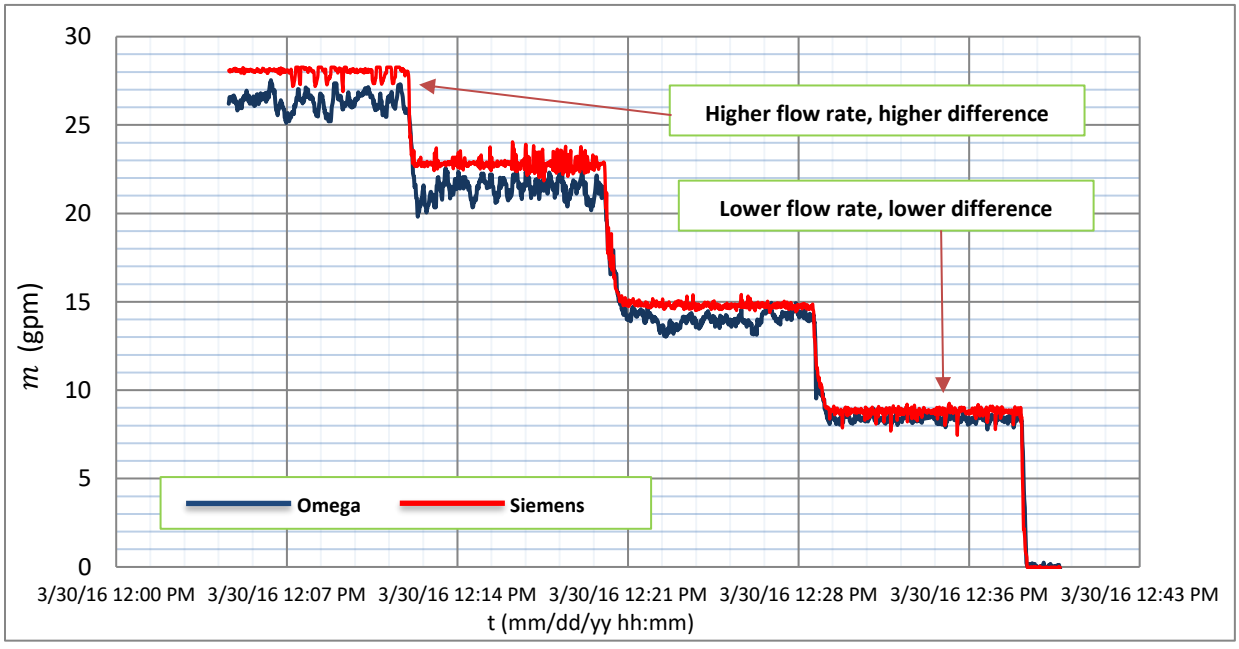

Fig. 16. Siemens and Omega flow rate readings for different flow ranges (Test 4)

The errors were calculated for each test. It was noticed that the error between the two flow meters' readings were almost zero at low flow rates (8 -10 gpm), but the error increased gradually as the flow increased (Figs. 15 and 16).

Table 1 shows the average error, the RMS error, and the standard deviations results for different flow rate ranges among the four tests. Table 1 shows that some of the lower flow rates (5-10 gpm) have higher error than others, which does not make sense if we compare these errors with the behavior shown by the graphs of Test 1 or 4.

In other words, the lower the flow rate, the lower the difference between the two flow meters' readings, and vice versa, according to the graphs of Test 1 and 4 (see marked flow rate values in Fig. 16). However, Table 1 does not show this to be true for all of the flow rate values. So for that reason, the RMS error was calculated since this method considers the absolute value of the difference between the two flow meters readings, which gives the actual difference or the error. (See Eqs. (A7-4a), (A7-4b), (A7-4c), and (A7-4d) in App. A7-3 for calculating the error, average error, RMS error, and standard deviation of the errors, respectively, for the 4 tests.) The standard deviation was determined for each flow rate range, which shows how far the Siemens readings deviated from the reference readings (i.e., the Omega flow meter).

Table 1. Errors and standard deviations of the Siemens flow meter in the recirculation pipe line for Tests 1-4

	$m\ (gpm)$	e_{avg} (%)	e_{RMS} (%)	σ_e (%)
Test 1	10	4.707	4.426	0.012
	17	6.357	6.548	0.022
	23	5.711	5.966	0.013
	27	5.108	5.561	0.015
Test 2	10	0.952	3.416	0.014
	17	8.738	3.503	0.041
	23	4.979	5.264	0.023
	28	1.184	3.428	0.019
Test 3	5	5.126	4.925	0.040
	10	4.722	4.834	0.017
	15	4.783	8.078	0.034
	20	5.936	6.785	0.024
	25	6.618	6.888	0.011
Test 4	27	7.027	6.231	0.071
	23	3.554	6.748	0.024
	15	2.607	5.799	0.031
	8	5.188	5.168	0.057

Figure 17 shows the overall results from the four calibrations tests as well as the determined correction equation for the Siemens flow meter. It shows the combined average data for all tests as a linear relationship with the correlation coefficient (R^2) that gives the deviation of the data from that linear relationship. The flow rate correlation equation that was derived from Fig. 17 was used to correct the Siemens MAG 5100 W DN 25 flow rate readings after installing it in the condensed steam pipe line of the vent condenser.

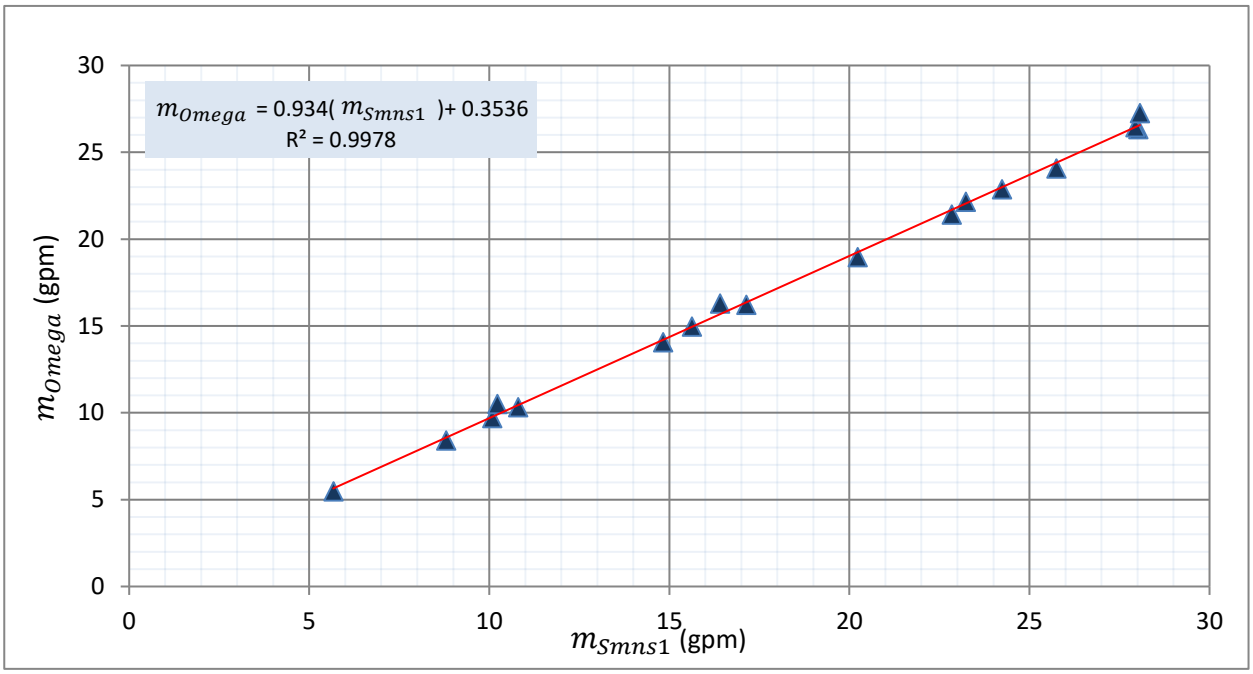

Fig. 17. Calibration curve for Siemens flow meter in the recirculation line, based on the data from Tests 1 to 4

Equation (1.7) was used to correct the Siemens flow meter readings, and the corrected values were employed in the energy savings calculations.

$$m_{c\_st} = 0.934(m_{Smns1}) + 0.3536 \quad (1.7)$$

The sensor part of the Siemens flow meter SITRANS F M MAG 5100 W has an overall error value of $\pm 0.2\ \%$ (see App. A8), while the Omega flow meter has an error value of $\pm 0.4\ \%$ from the manufacturer's specifications (see App. A9).

1.5.2 Analysis and Calibration of the CSP and VSP Flow Meters

In a previous study [2], calibration was performed for the Siemens flow meters (Mag 5100 W DN 100, see App. A8) downstream of the Worthington and Grundfos pumps. The results from those calibrations were employed in this analysis in order to determine the errors in these flow meters' readings.

The resulting error was used to correct the condensate water flow rate from the Worthington D-824 (CSP) and Grundfos CRE 15-3 (VSP). Those corrected flow rates can affect the power consumption calculations for these pumps (the power calculations are given in Chapter Four). In this project, row data was employed from a previous calibration [2] in order to determine the errors for the CSP and VSP flow meters.

Figure 18 shows the results for calibrating the flow meter downstream of Worthington D-824 CSP. The test results show that the Siemens flow meter readings were about 2.5% lower than those of the reference meter (i.e., Omega flow meter readings). Equation (1.8) was used to correct the current Siemens flow rate readings.

$$m_{CSP} = 1.0373(m_{Smns2}) - 0.9828 \quad (1.8)$$

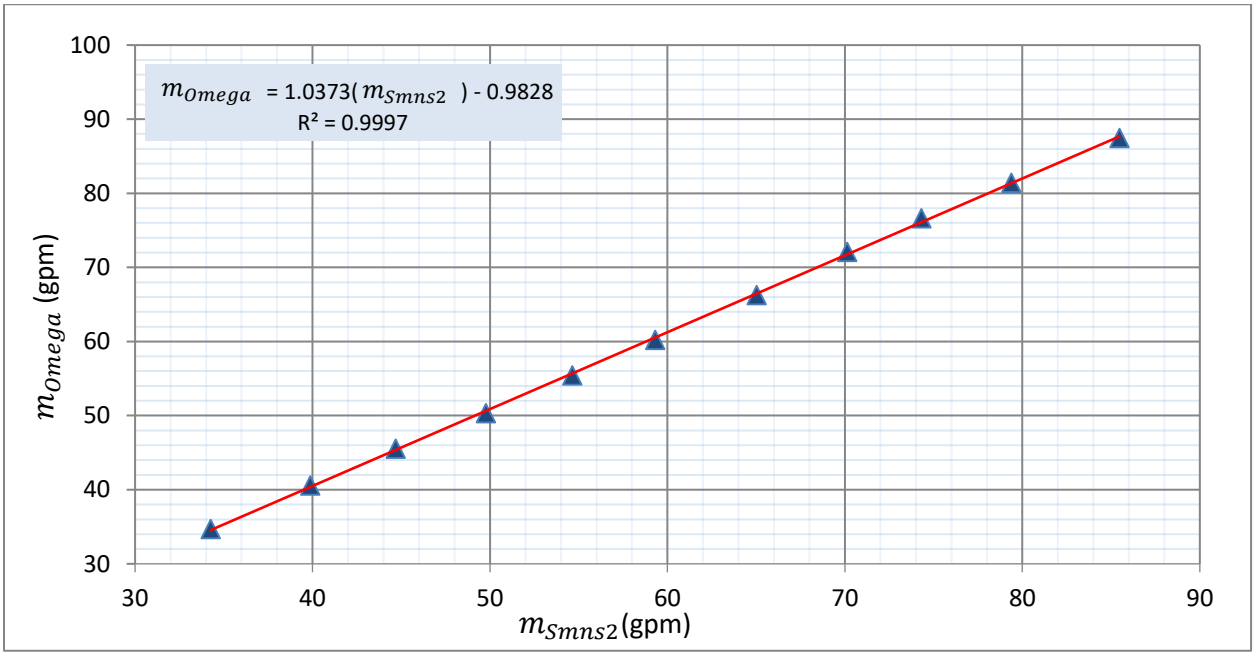

Fig. 18. Calibration curve of the Siemens flow meter in the Worthington CSP discharge line (based on Ref. 2 data)

The same work was done for the Grundfos CRE 15-3 VSP's flow meter. Figure 19 shows the calibration results for the Siemens flow meter downstream of the Grundfos VSP, which has almost the same average error as the CSP's flow meter (about 2.4%); and all of the readings were less than those of the reference meter (i.e., the Omega flow meter).

The VSP's flow rate was corrected by employing Eq. (1.9) which is the flow rate correlation equation between the two flow meters.

$$m_{VSP} = 1.0497(m_{\boldsymbol{Smns}3}) - 2.5575 \quad (1.9)$$

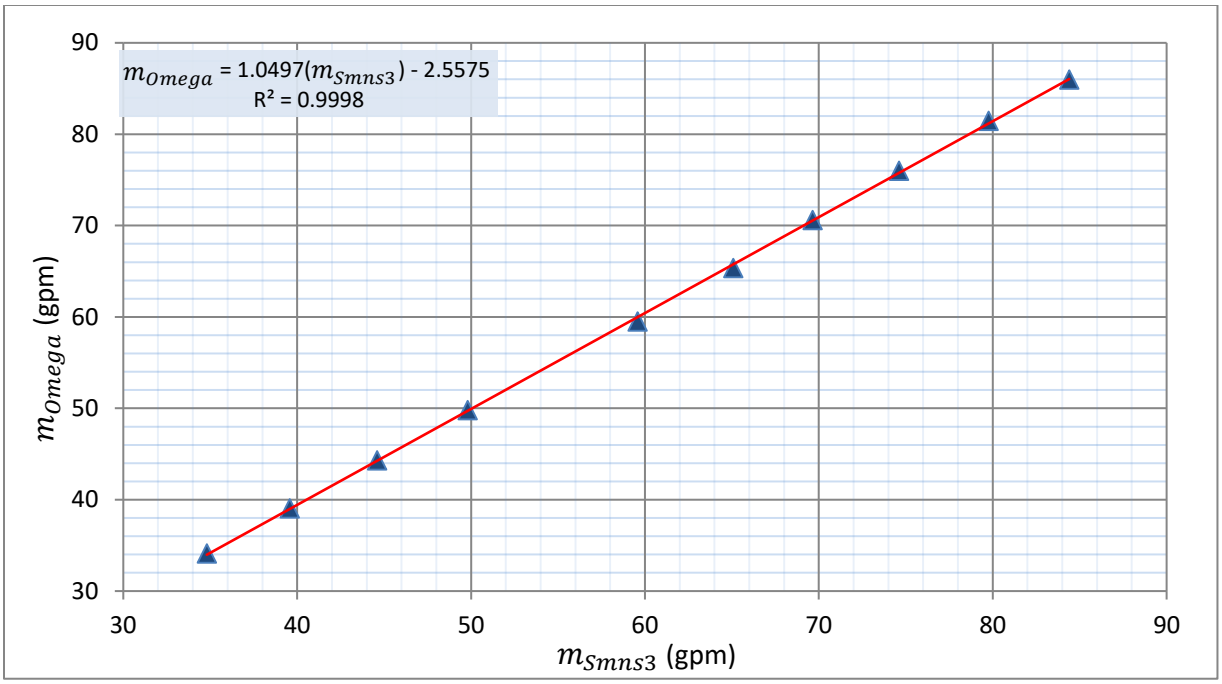

Fig. 19. Calibration curve of the Siemens flow meter in the Grundfos VSP discharge line (based on Ref. 2 data)

See App. A7-4 for graphs [Figs. (A7.f) and (A7.g)] of calibrating the Siemens flow meters downstream of the CSP and VSP. It has to be mentioned that the calibration curves in Figs. 18 and 19 were drawn in this study by using raw data that was recorded by Alabdullah during calibration tests that were conducted in a previous study [2].

In conclusion, this chapter describes the main components in the KU SPP, their design and function. The instrumentation and data acquisition systems around vent condenser and basement heat exchanger that were used in this study were explained. Flow calibration curves were produced based on the results of calibrating the Siemens flow meters downstream of the condensate water pumps and the vent condenser. The recorded flow rates of these flow meters were adjusted by the produced flow calibration curves.

Chapter Two: Investigation of the Energy Recovery Components and Evaluating the Measurement Instrumentation

This chapter presents evaluation data for the recently installed data acquisition instruments for the vent condenser. These instruments are internal temperature sensors (RTDs) and a Siemens flow meter. The RTDs were installed in the condensate water and the steam pipe lines. Moreover, a study was conducted on the Siemens flow meter that was installed in the condensed steam pipe line in order to evaluate the flow rate and the energy content in that pipe line. These instruments helped to more accurately calculate the total energy that was being saved by the vent condenser. This chapter also examines the DA in greater depth.

One of the DA's functions is to preheat the water entering the boiler, which helps to reduce the fuel consumption and increase SPP efficiency. So the heat transfer rate is computed for the DA and the boiler in order to estimate SPP efficiency. In a previous study [3], an investigation was conducted to determine the basement heat exchanger's type. So, a follow-on investigation is performed in this work to estimate types, efficiencies, and heat transfer rates of the heat exchangers that are used in the KU SPP, based on recently collected data.

2.1 Evaluation of the Newly Installed Instrumentation for the Vent Condenser

2.1.1 Internal Temperature Sensors (RTDs) in Condensate Water and Steam Lines

As stated in Section 1.4.1 and shown in Fig. 12, RTDs (PR-12-2-100-TX92A-3) have been installed in the inlet and outlet condensate water pipe lines of the vent condenser in place of the surface sensors (TMC6-HE) that were used previously [3]. Another RTD has been installed in the steam pipe line between the DA and the vent condenser.

A surface sensor has been installed in the condensed steam return pipe line. The RTDs record temperature directly inside the pipe lines, so these measurements are more accurate than surface sensor measurements which can be affected by the surrounding temperature through convection and the radiation.

Two types of savings calculations are shown in Chapter Three, comparing the old surface sensors (TMC6-HE)) with the new RTD sensors. It was necessary to evaluate the RTDs' performance by analyzing their readings with respect to the contact sensors as well as comparing with dial gauges that measure temperature at more than one point along the pipe lines. For example, there are two dial temperature gauges for the inlet condensate water at two different locations. One is in the storage tanks (see Fig. 1 for the KU SPP equipment and pipe line layout) and the other is directly before the vent condenser.

So these gauges were used to evaluate the internal sensors readings in order to determine whether their measurements were reasonable or not. The pipe line arrangement for the inlets and the outlets of the condensate water and steam for the vent condenser are shown, along with the temperature sensors, in Fig. 20.

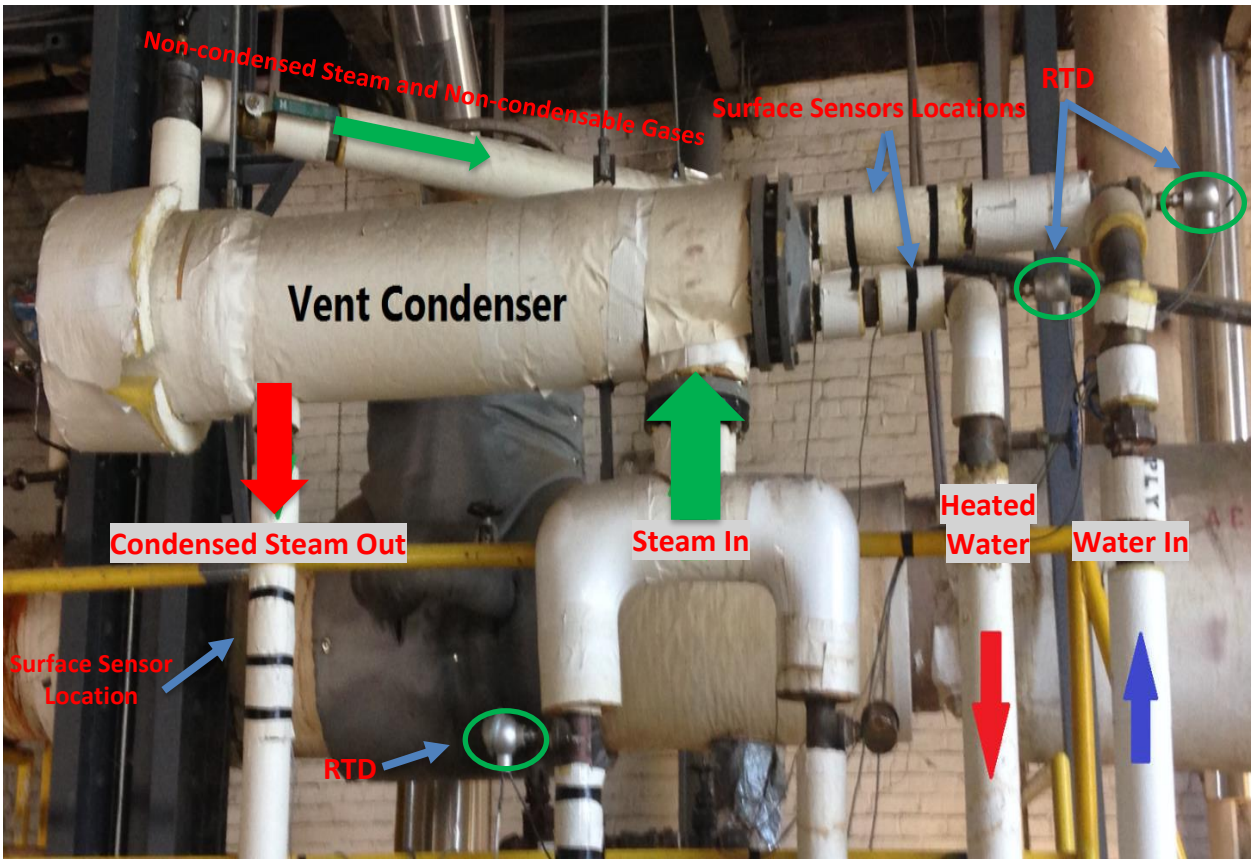

Fig. 20. Pipe lines with the temperature sensor types that are located around the vent condenser

According to surface sensor (TMC6-HE) readings, the inlet condensate water in the vent condenser has a temperature of about 155-180 °F, depending on the surroundings' temperature, while outlet condensate water is about 8-10 °F higher after recovering energy from the vented steam and gases. On average, the RTD temperature readings were higher than those of the surface sensors for both the inlet and the outlet condensate water (temperature rise and reading variations are given in Section 2.1.1.a)

2.1.1.a RTD Data Analysis

After installing internal sensors (RTD) at three positions inside pipe thermowells (i.e., inlet condensate water, outlet condensate water, and inlet steam) in the vent condenser, the Hobo data logger was used to record, at minute time intervals, the temperatures that were measured by the RTD sensors.

The temperature measurement range 0-300 °F of the RTD sensors (see App. A6) was set to the signal range 4-20 mA that is recorded by the Hobo data logger. The power supply cables and the signal cables were wired according to the manufacturer's wiring diagrams (see App. B1).

The first RTD test is shown in Fig. 21, where RTD1 represents the inlet condensate water temperature, RTD2 represents the outlet condensate water temperature, and RTD3 represents the inlet steam temperature which comes from the DA. Temperatures in Fig. 21 show that the values started negative and then stabilized at about 20 °F, which are incorrect values since all of the reading should be between 150 °F to 230 °F depending on sensor locations in the pipe lines.

Many tests were conducted in different ways; but for every trial, the values were negative and the readings behaved unreasonably. The wiring for the power supply and the output signal were changed and switched in different ways while attempting to solve the problem, but the output readings were the same. Initially, HOBO signal cables (type HOBO-Cable-4-20mA, see App. B1) were used to connect the RTD transmitters to the HOBO data logger (as shown in Fig. 22).

The errors were first thought to be caused by the cable, assuming it was not compatible with the RTD transmitter; but, after contacting the cable provider (Onset Computer Corporation), Onset confirm that these cables were proper for such signals (i.e., two wires with a 4-20 mA output signal).

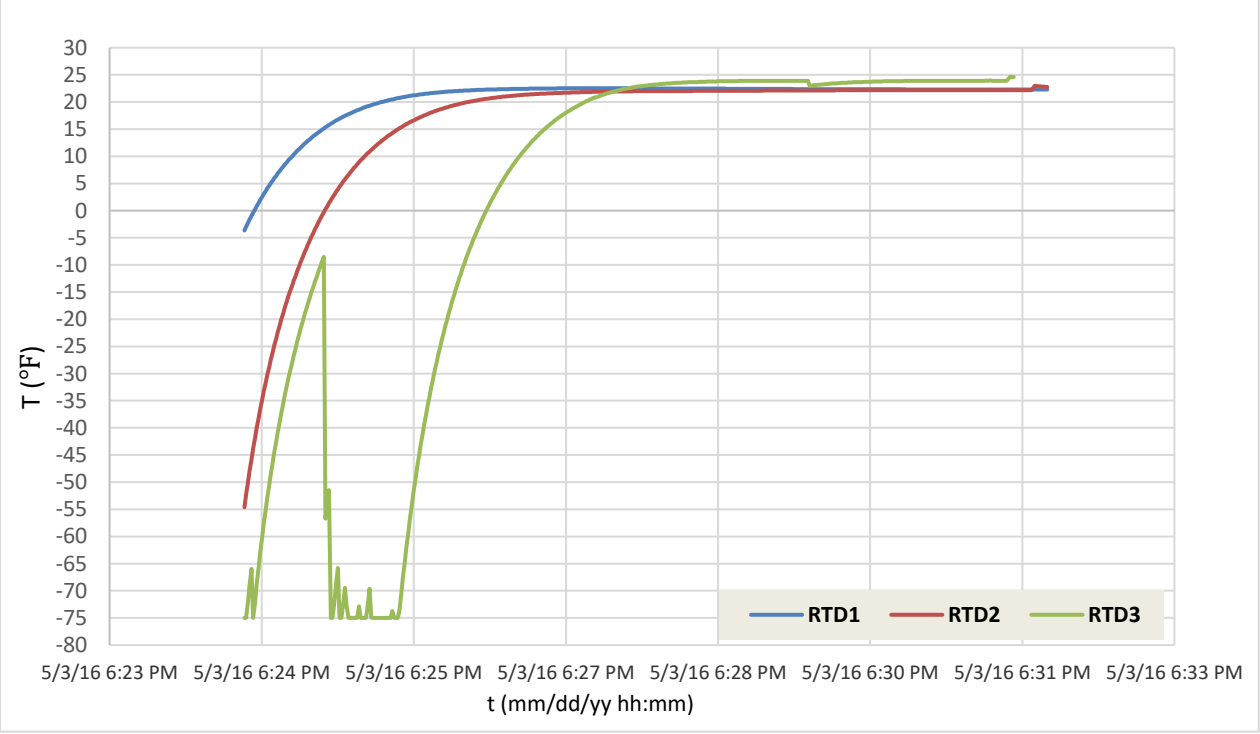

Fig. 21. False readings for the RTDs' first test in the vent condenser

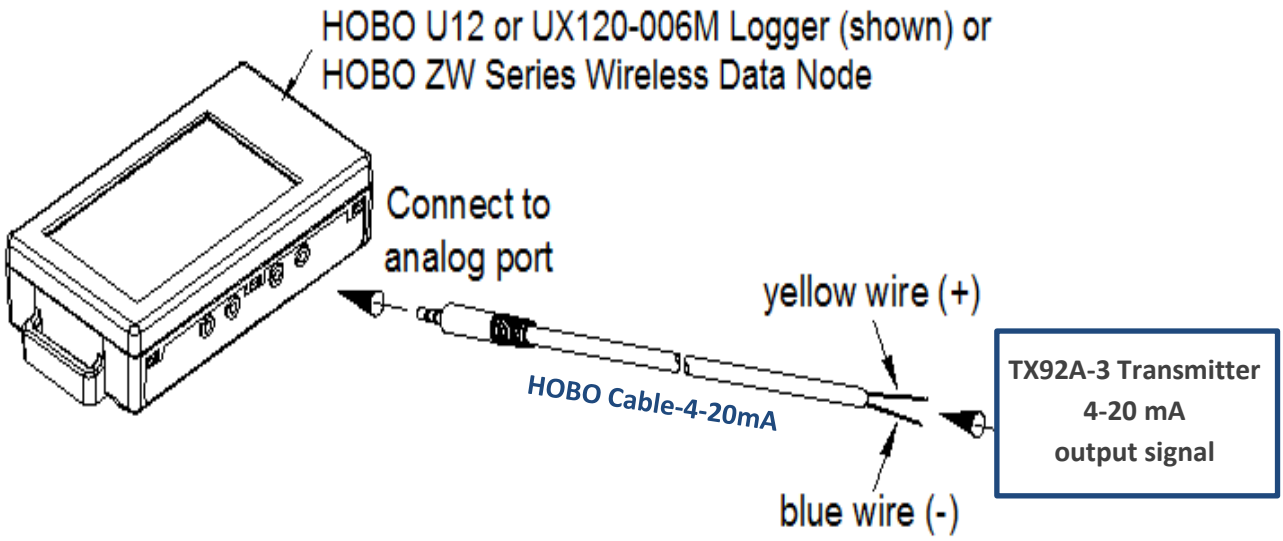

Fig. 22. Wiring diagram from the RTD's transmitter using HOBO cable
[reproduced from App. B1]

The Omega Company was contacted about the RTD calibration, and Omega confirmed that the RTDs were calibrated for the needed temperature range (i.e., 0-300 °F). Then new 4-20 mA signal cables were purchased and used instead of the old cables. Once the new cables were installed, all of the readings were correct.

Using the new cables (HOBO Cable-4-20 mA) and recording the vent condenser temperatures using the RTDs, new data was recorded and compared with that of the old temperature sensors (TMC6-HE surface sensors). The new recorded data showed readings with trends that were similar to those of the old surface sensors readings but with different magnitudes (see Fig. 23).

RTD readings were higher than the surface sensors by an average of about 4 °F for the outlet temperatures, and about 1-2 °F for the inlet temperatures. Figure 23 shows the inlet and the outlet condensate water temperatures for both types of sensors for the period of May 4 to May 6, 2016, which was the first test after fixing the cable problem. The readings for the first test showed that the RTD readings closely followed the surface sensors variation when the temperature increased or decreased dramatically.

According to the heat equation, the higher the ΔT, the greater the energy reclaimed by the vent condenser (see Eqs. (1.2a) and (1.2b) in Section 1.2). That means the reclaimed energy that was computed by using RTD sensor data was about 40% higher than that computed with the surface sensor data. There was about a 2 °F difference between the two sensor types in the inlet pipe line, while there was about a 5 °F difference between the two sensor types in the outlet pipe line.

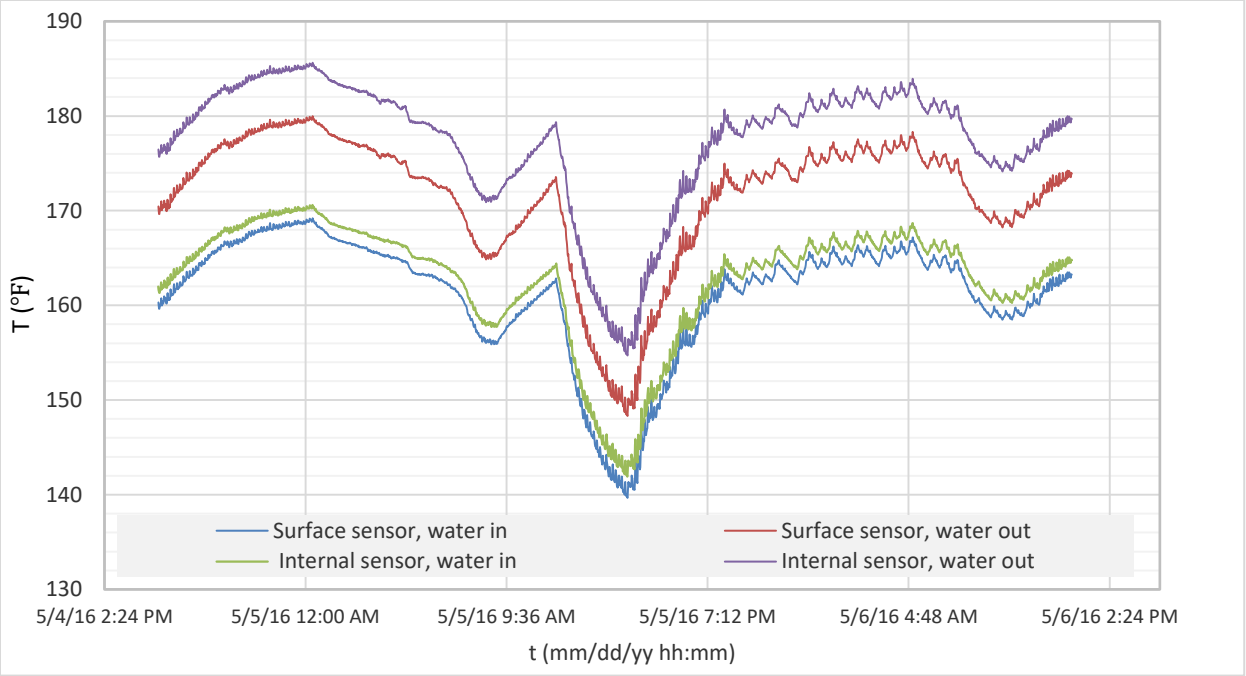

Fig. 23. Readings of the internal and surface sensors for the period May 4-6, 2016

Figure 24 shows that the temperature rise (ΔT) between the inlet and the outlet condensate water was about 10 °F for the surface sensor readings, while that rise was about 14 °F for the RTD readings.

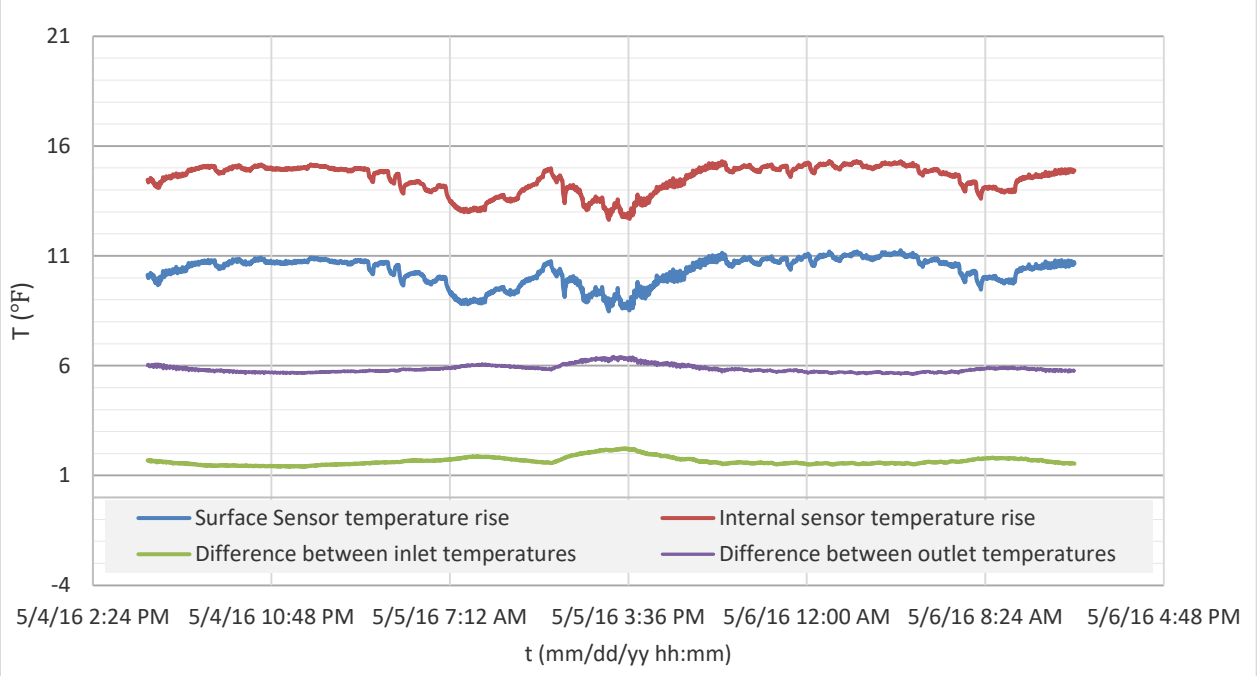

Fig. 24. Measured temperature rises and differences for condensate water pipe line of the vent condenser by internal and surface sensors for May 4-6, 2016

Figure 25 shows the temperature readings of the two types of sensors for 3 days, May 7-9; but the overall measured temperatures were higher than those in Fig. 23 due to a change in the outside temperature, which affected the condensate water temperature. Even though the measured temperatures were higher than those of the previous test, the temperature rises for both types of sensors were also about 2°F and 4 °F in the inlet and outlet pipelines, respectively, as shown in Fig. 26.

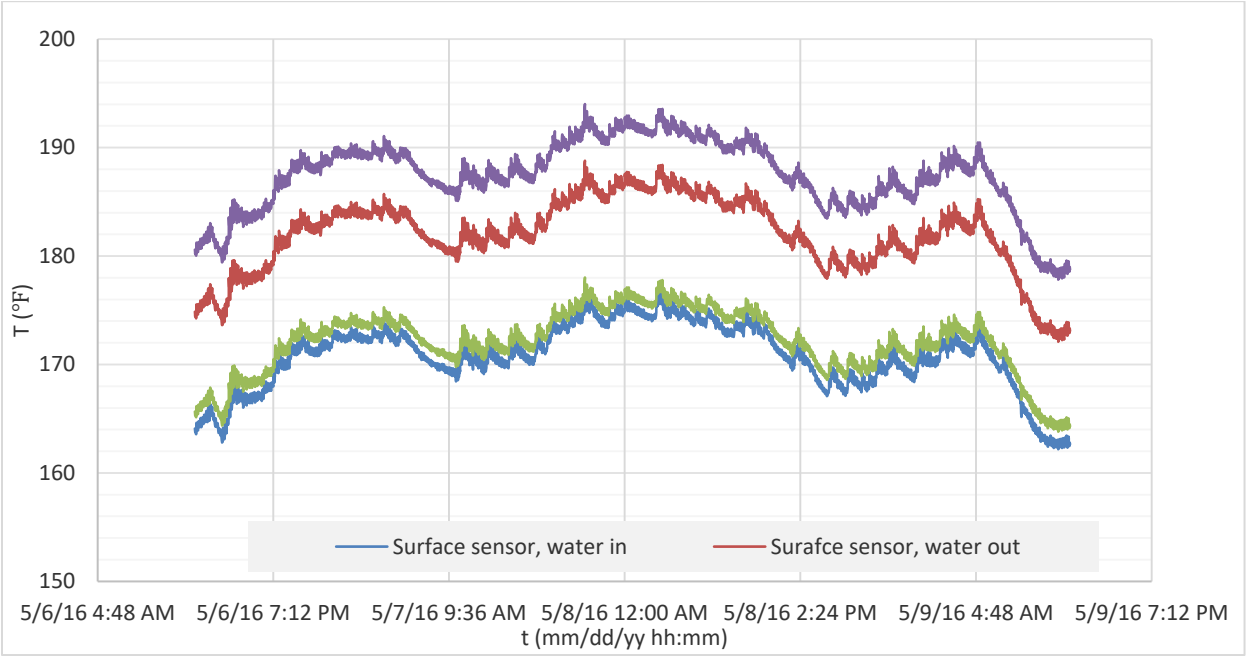

Fig. 25. Readings of the internal and surface sensors for the higher temperature ranges of the second test during the period May 7-9, 2016

In Fig. 26, The temperature rises that were measured by the internal and surface sensors were almost the same as shown in Fig. 24. There was about 11 °F when measured by the surface sensors and about 15.5 °F by the internal sensors. The difference between the two sensor readings in the same pipe line was about 1.5 °F for the inlet water pipe line, and about 5.5 °F for the outlet water pipe line.

Figure 27 shows readings for the inlet and the outlet temperatures of the internal and surface sensors for condensate water during the period May 9-15, 2016. The temperature rise of the condensate water from both types of sensors is given in Fig. 28, which was almost the same as the result of the other tests in Figs. 24 and 26. The differences between the two sensor types for the inlet was about 1 °F, and about 5 °F for the outlet. Figures 24, 26, and 28 show that the condensate water temperature rise measured by the internal sensors was higher by about 4 °F than that measured by the surface sensors, which means, as stated earlier, more energy savings were calculated when using the RTD readings.

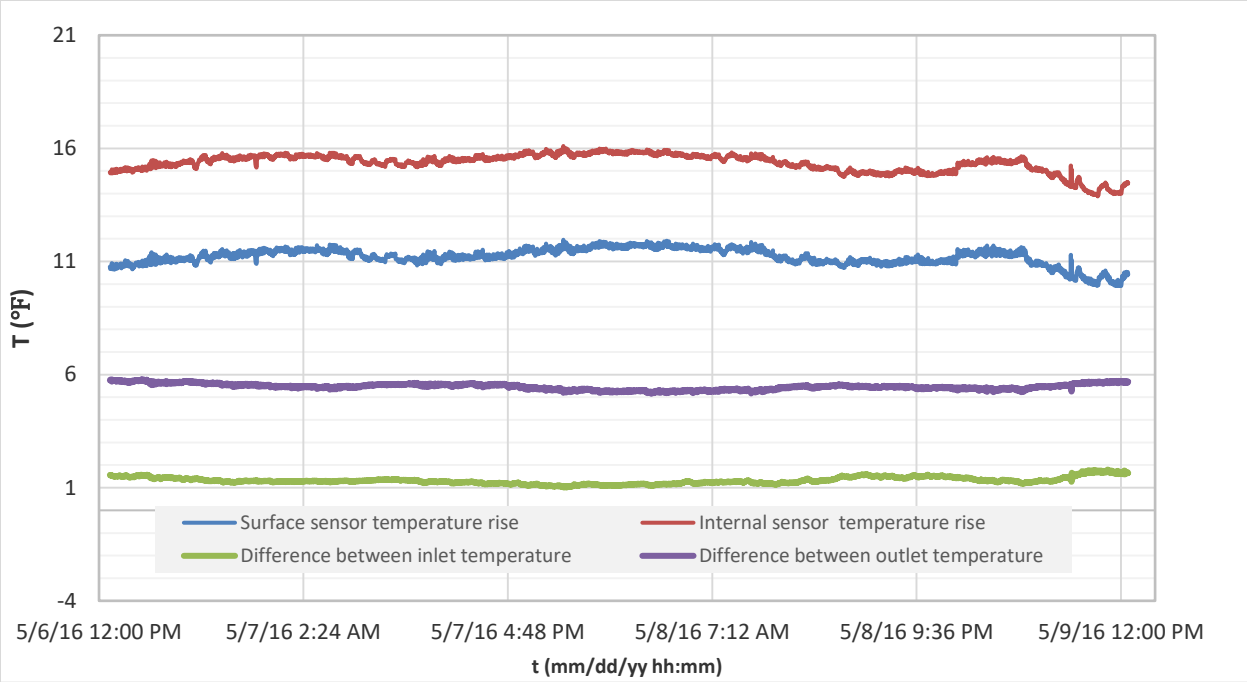

Fig. 26. Measured temperature rises and differences in the condensate water pipe line by internal and surface sensors during the period May 7-9, 2016

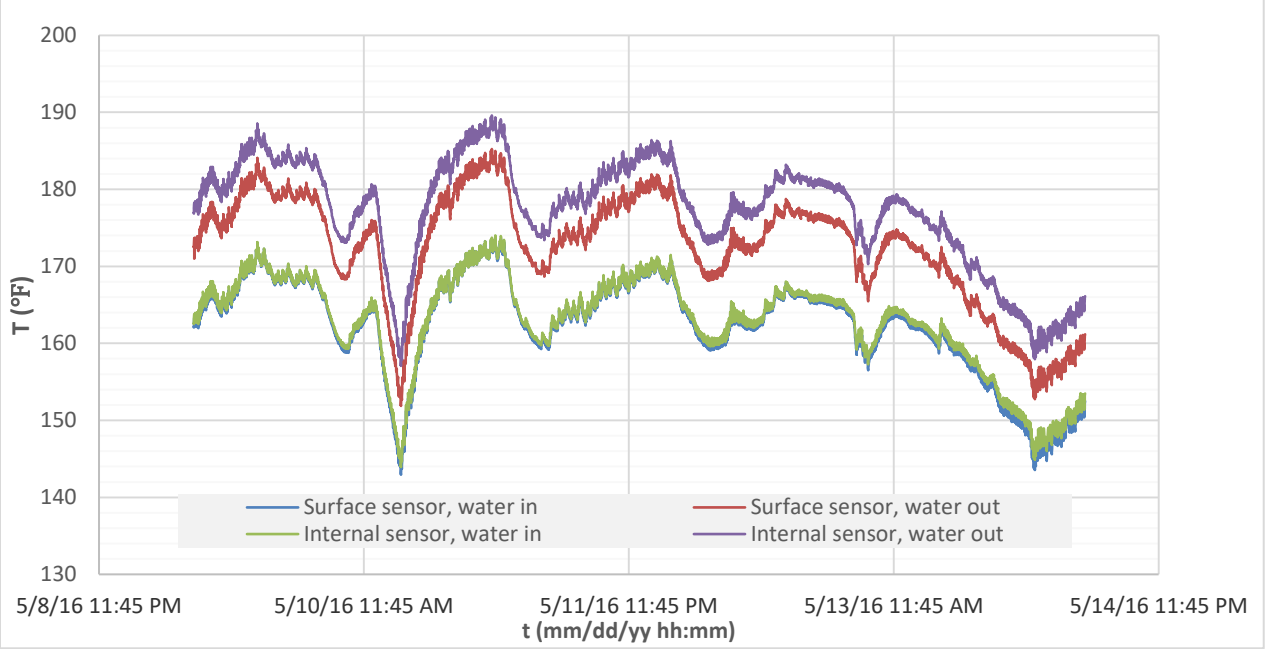

Fig. 27. Readings by internal and surface sensors of the inlet and the outlet condensate water in the third test during the period May 9-15, 2016

Figure 27 clearly shows how the temperatures changed sharply even within a short time period, such as within the same day on 5/10/2016; and that temperature fluctuation was due to the inlet condensate water temperature which was affected mainly by outside temperature.

The outside temperature affected how much of steam was needed in campus buildings, so the lower the outside temperature, the smaller the amount of steam needed, which meant less energy was removed from the steam. The internal and surface sensors followed each other stably during these fluctuations, which gives a clear sign of good measurement trends for both types of sensors.

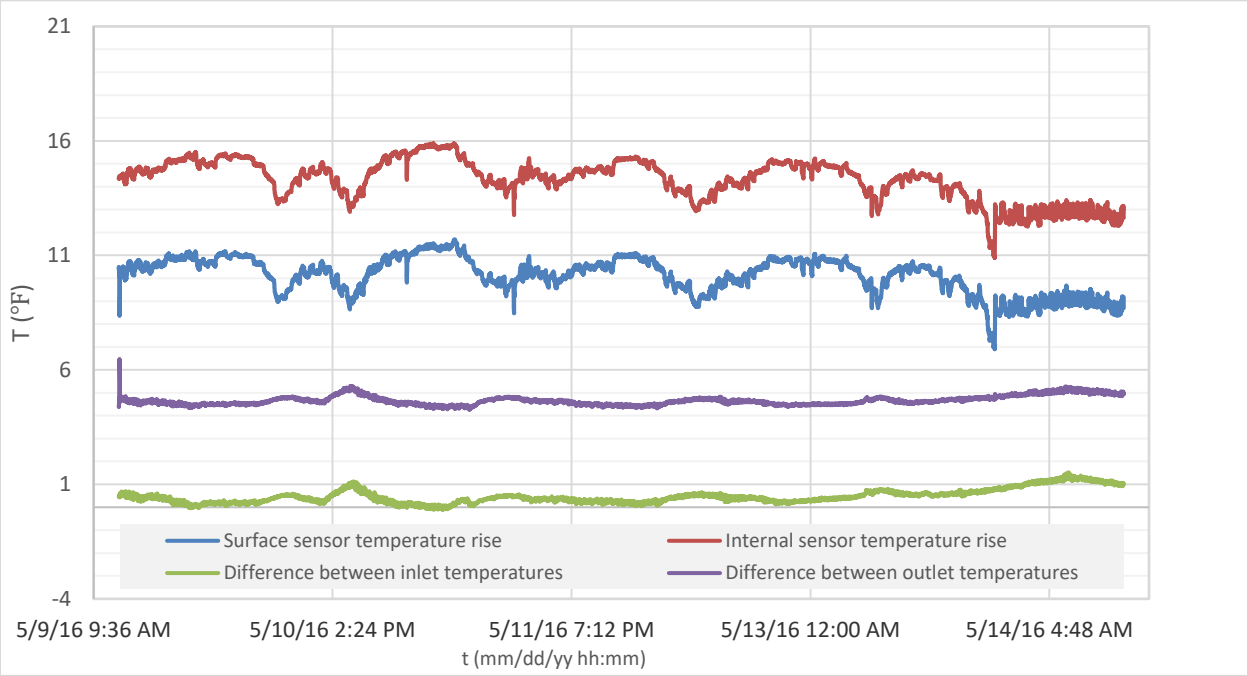

Fig. 28. Temperature rises and differences for the condensate water as measured by the internal and surface sensors during the period May 9-15, 2016

These data were taken for RTDs while the surface sensors were still located on the same pipe lines (until May 20). The reason for leaving the surface sensors after installing the RTDs was for comparative testing and evaluating the new sensor data as shown for the three test periods (i.e., Figs. 23, 25, and 27). The data from these tests were recorded every minute using the HOBO data logger for both the internal and surface temperature sensors. The internal sensors in the inlet and outlet condensate water lines of the vent condenser were tested continuously for about 10 days as shown in Figs. 23, 25, and 27 in order to record enough data for evaluating them over different temperature ranges and flow rates.

Then another RTD was installed in the inlet steam pipe line [that vented from the DA]. At that time, the surface sensors (TMC6-HE) were removed from the inlet and the outlet condensate water lines, and they were installed on the inlet and outlet steam pipe lines. That was because there were only two surface sensors available around the vent condenser, so they were removed from the condensate water lines and re-installed again on the steam lines in order to conduct new tests there.

As mentioned earlier, only the inlet steam pipe line had an internal sensor, while the outlet condensed steam pipe line had a surface sensor. This was because there is no thermowell in the condensed steam line to use for installing an internal sensor.

From the previous description, the internal sensors gave higher readings than the surface sensors for the inlet and the outlet pipe lines. However, even though both the internal and surface sensors were installed in the same pipe lines (i.e., inlet and outlet pipe lines), the differences between the two types readings in the inlet pipe line were not the same as in the outlet. For example, the difference between the internal and the surface sensors for the inlet line was about 1-2 °F, while the difference was about 5-6 °F in the outlet line. These differences are shown in Figs. 24, 26, and 28.

As a result, an evaluation, or test, was needed to figure out why the difference was higher between the two sensor types for the outlet than for the inlet. That evaluation began with double checking the RTDs' calibration in order to determine whether or not there was a problem with their measurement accuracy. So the RTDs were switched between the inlet and outlet pipe lines to see if the readings changed. The difference between sensor types was found to be the same (i.e., about 5 °F for the outlet and about 2 °F for the inlet).

The surface sensors were also checked the same way by switching the surface sensors between the inlet and the outlet pipe lines to compare the readings; but the values were almost the same. Then, after further considering the situation, the locations where the surface sensors contacted the outer surfaces of the pipe lines were changed as shown in Fig. 29 (the reason for this change is explained later in this section).

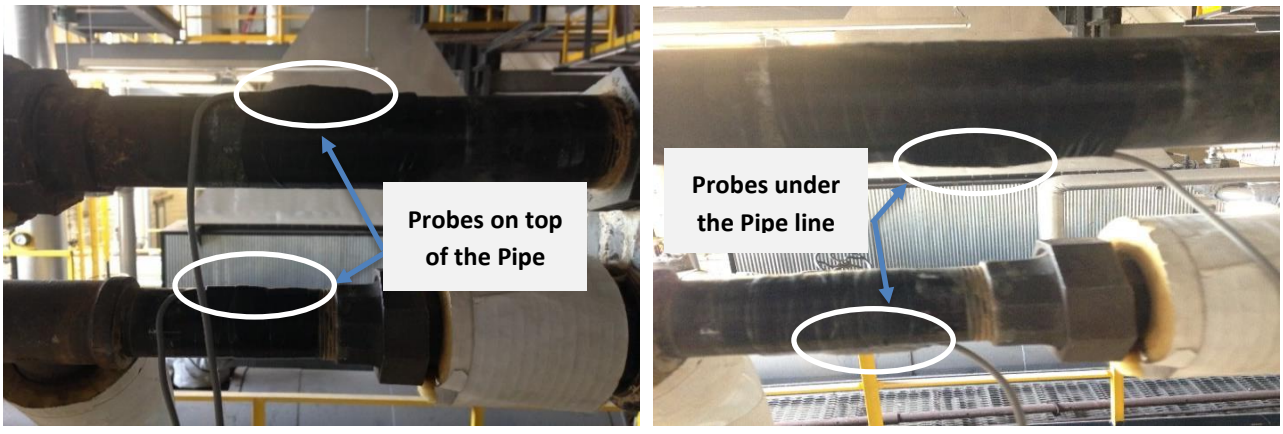

(a) (b)

Fig. 29. Pictures show the old and the new positions of the surface sensors for the condensate water inlet and the outlet pipe lines. In (a) the surface sensors are attached to the upper-most points of the pipe line; and in (b) the surface sensors are attached to the lowest points on the pipe lines.

After switching the surface sensors to the lowest points on the pipe lines, the differences between the internal and the surface sensors readings were almost the same for the inlet as for the outlet, as shown in Figs. 30 and 31.

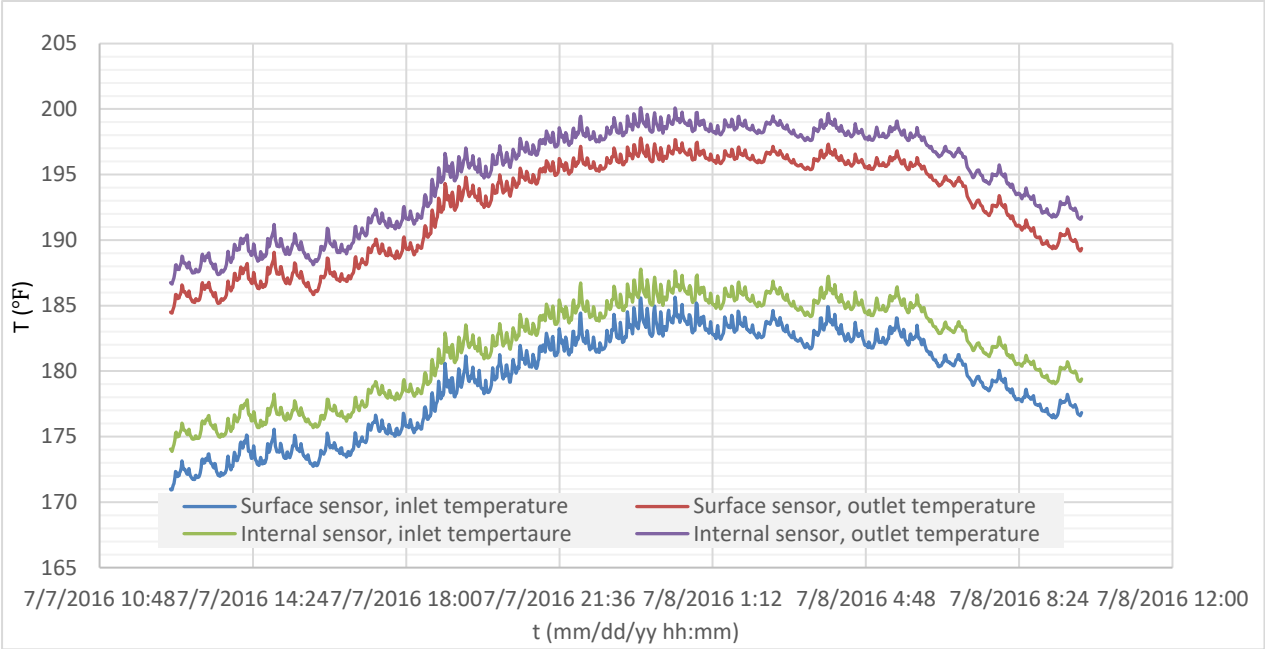

Fig. 30. Measured temperatures for the inlet and the outlet condensate water of the vent condenser after changing the surface sensors' locations on the pipe lines for the period July 7-8, 2016

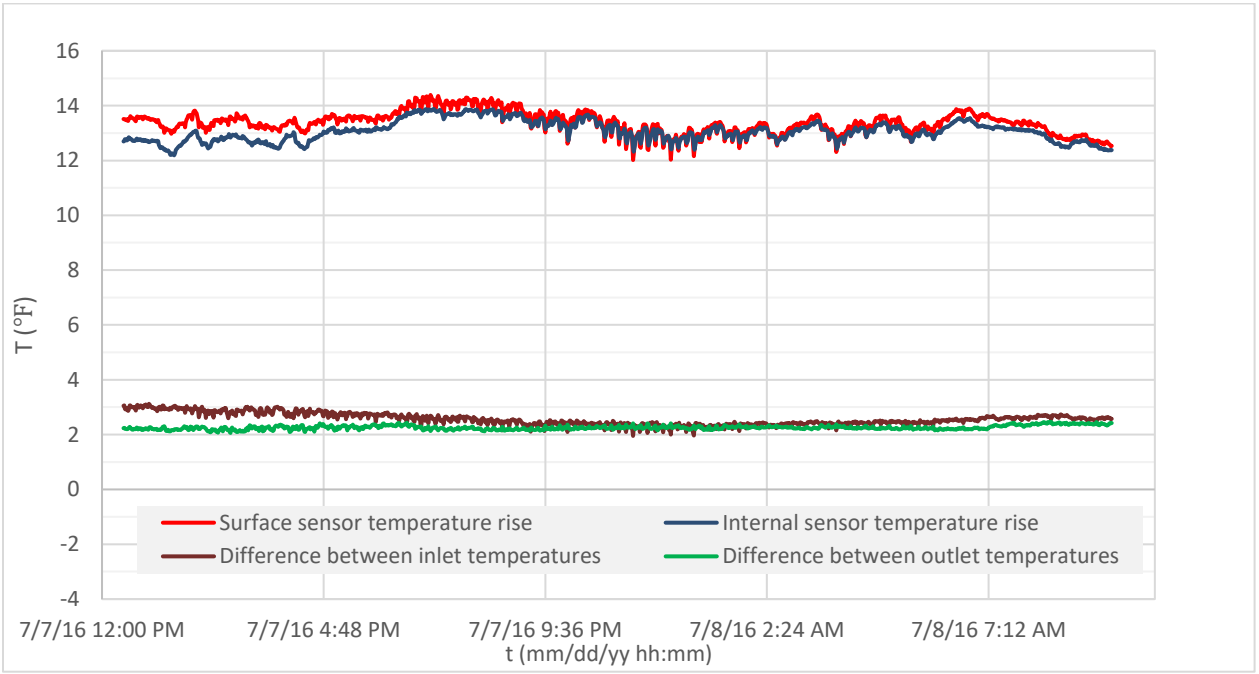

Fig. 31. Temperature rises and differences for the internal and surface sensors after re-locating the surface sensors to the undersides of the pipes during the period July 7-8, 2016

Even though Fig. 30 shows that the internal sensors (RTDs) readings were still higher than those of the surface sensors', Fig. 31 shows that the internal and the surface sensors have almost the same temperature rise (about 13 °F), and almost the same difference for the inlet and outlet pipe lines (about 2 °F).

A possible reason for location-dependent readings is that the pipe lines were not full of water, as expected, especially for the vertical outlet pipe line (see Fig. 20) due to gravity effects. So, if a pipe line was not full of water and the surface sensor was attached to the upper-most location on the pipe lines, this sensor would be measuring the temperature of the vapor inside the pipe, which is not exactly the water temperature (and vapor transfers heat poorly). When the sensors were re-located to the lowest side of the pipe, they were measuring the water temperature inside the pipe, even if it was not full of water.

See the schematic in Fig. 32 that illustrates the old and the new position of the surface sensor of the outlet condensate water pipe line. For the same pipe line, the measured temperatures in both positions were not the same due to different heat transfer coefficients of vapor and the liquid water.

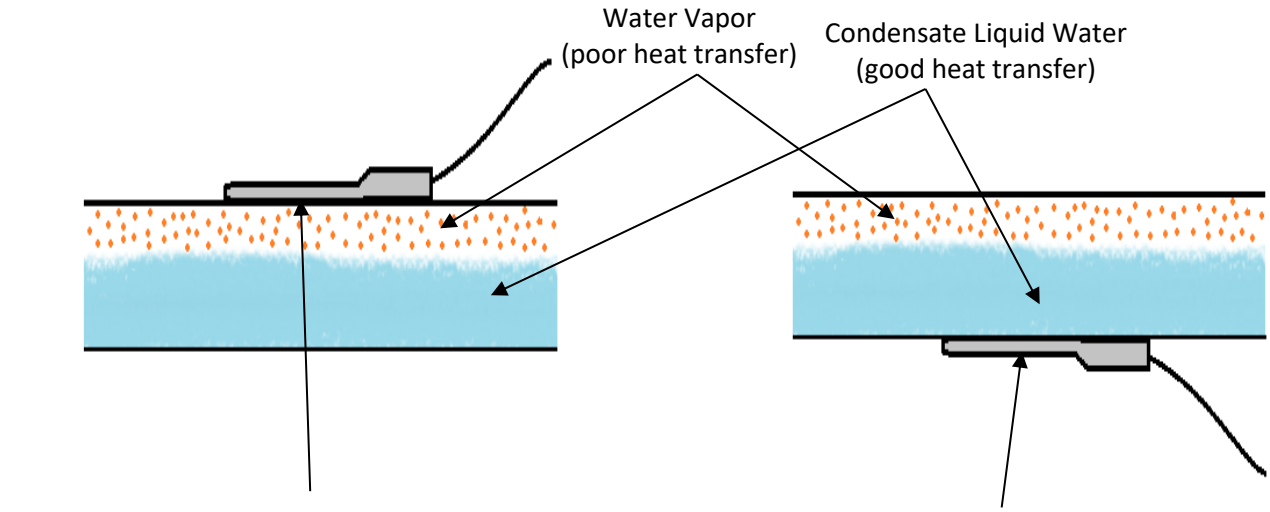

Fig. 32. Drawing for the outlet condensate water pipe line showing temperature measurement on upper vs. lower surfaces

By comparing Figs. 28 and 31, re-locating the surface sensors for the inlet condensate water line did not change the difference between the readings of the two types of sensors (i.e., internal and surface sensors), but the temperature difference for the outlet pipe line between the two types of sensors did change from about 4 °F [case (a) of Fig. 32] to about 2 °F [case (b) of Fig. 32].

That was because the inlet pipe line was assumed to be full of water since it is pumped by the condensate water pumps. So, it did not matter where the sensor was located around the pipe line. On the other hand, the outlet line was probably not full of water; so temperature measurement on the outside of the outlet pipe line was location-dependent. Figures 33 and 34 show temperature readings after changing the location of the surface sensors to the undersides the pipelines for the period July 8-10, 2016

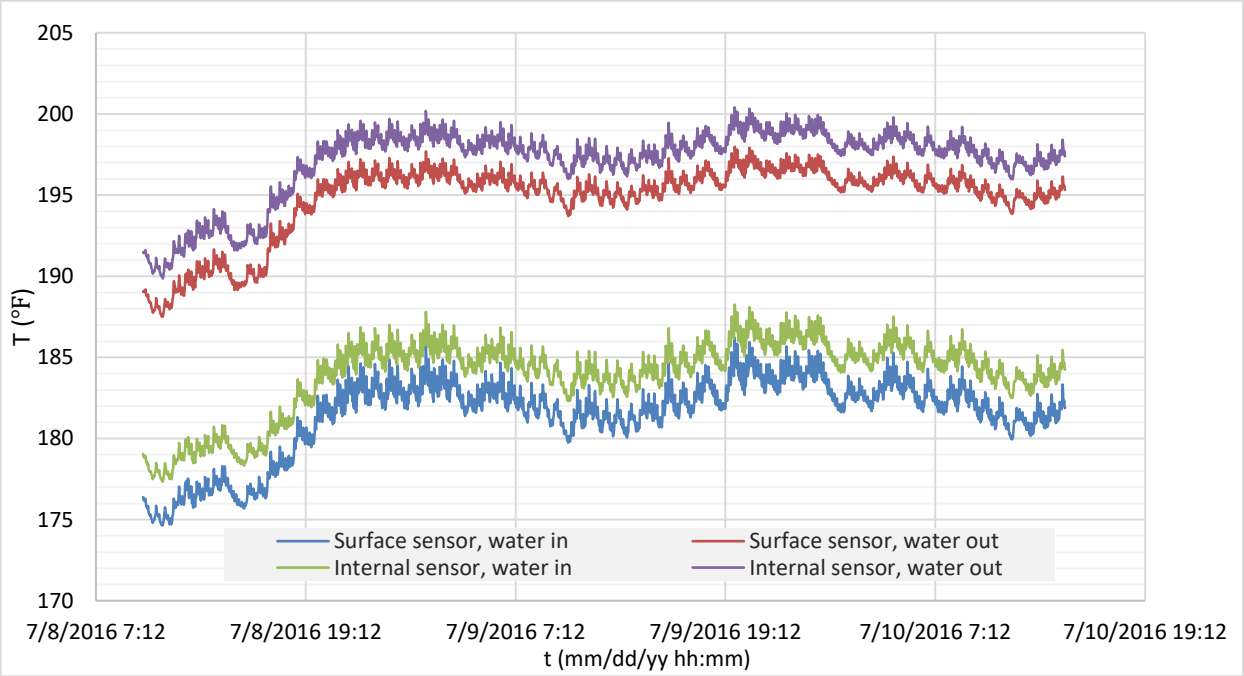

Fig. 33. Condensate water inlet and outlet temperatures measured by the internal and surface sensors after re-locating the surface sensors to the undersides of the pipe lines for the period July 8-10, 2016

Figure 33 shows also that the internal sensors read higher than the surface sensors for the inlet and the outlet pipe lines during the period July 8-10, 2016. Figure 34 shows that the temperature rise of the condensate water for both sensors types was almost the same (about 13 °F); and the differences between the two outlet temperatures and two inlet temperatures were about 2 °F because the internal sensors read higher than the surface sensors by about 2 °F. As stated earlier, the 2 °F difference between the two types of sensors is attributed to the temperature reduction when measuring external vs. internal values due to the effects of convection and radiation with the pipe lines' surroundings on the external sensors.

Three internal sensors (i.e., RTDs) were installed in the vent condenser pipe lines after testing and evaluating them: two in the inlet and outlet condensate water pipe lines, and the third was installed in the steam line that enters the vent condenser. A surface probe was installed on the condensed steam pipe line.

Thus there was a complete set of four temperature sensors around the vent condenser for its inlet and outlet lines. See Fig. 20 for the sensor positions around the vent condenser.

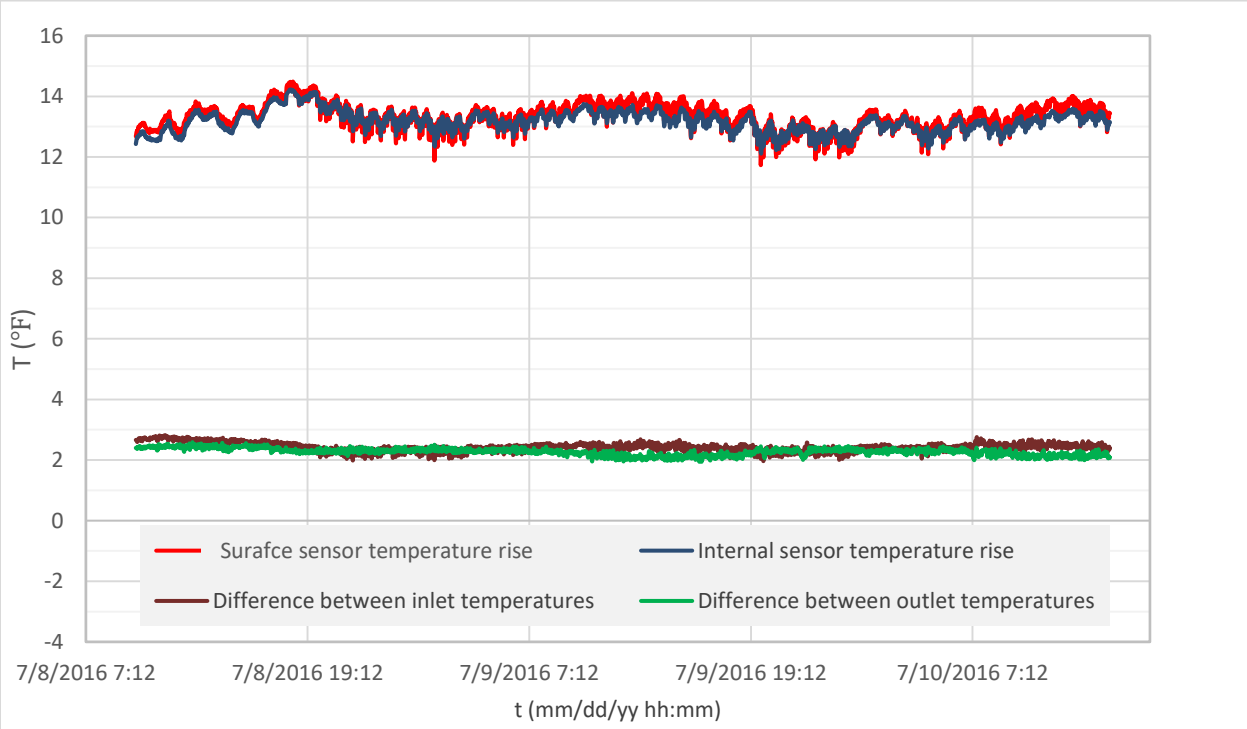

Fig. 34. Temperature rise in the condensate water pipe line, and the differences between the two sensor types after re-locating the surface sensors on the undersides of the pipe lines during the period July 8-10, 2016

Figure 35 shows readings for all temperature sensors of the vent condenser. Note that there are two types of readings for the inlet steam line: internal sensor and surface sensor. The reason for having two readings of the steam entering the vent condenser was to evaluate the internal sensor that was newly installed as compared to the surface sensor. The evaluation was conducted by comparing the two sensors' readings in order to check whether or not this pair for sensors had the same difference between their readings as the other sensor pairs in the inlet and outlet condensate water lines.

The internal sensor readings for the inlet steam pipe line were trusted more than those of the surface sensor. That was because it was found that the difference between the internal and surface sensors for that pipe line was the same as for the inlet and outlet for the condensate water pipe lines (i.e., 2 °F, see this difference in Fig. 35 for the inlet steam line). That means the internal sensor for the inlet steam line reads consistently with the others. So the internal sensor readings for the steam line were used in the energy savings calculations. Also, since the condensed steam pipe line temperature was measured by a surface sensor, 2 °F was added to the measured values in order to match this sensor to the RTD sensors in other pipe line.

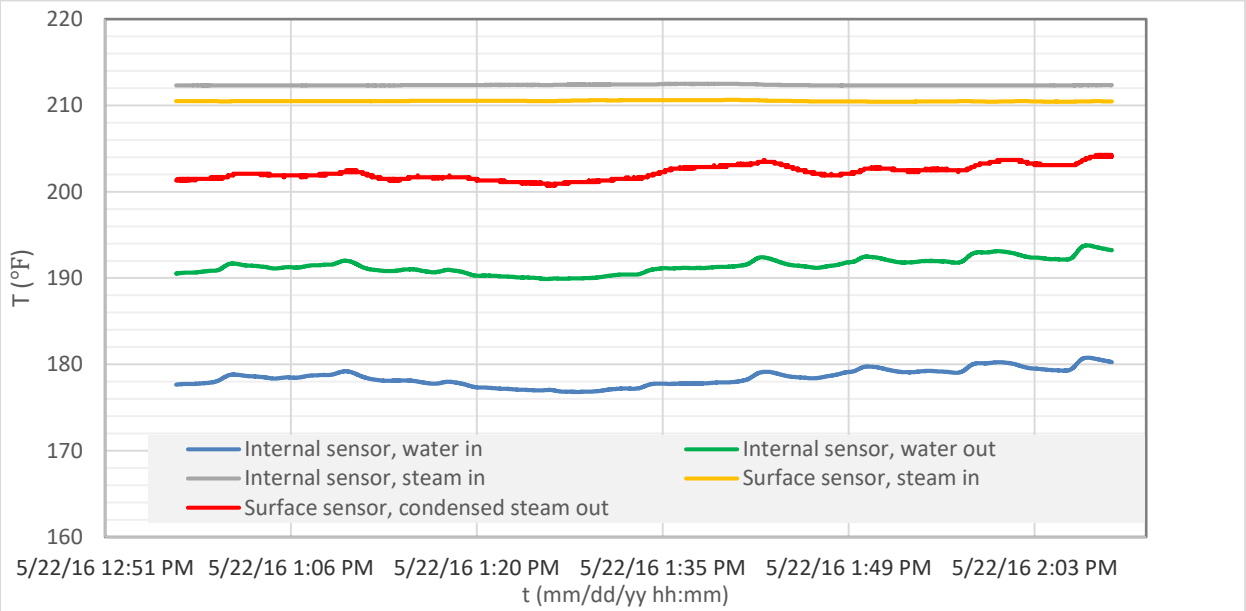

Fig. 35. Water and steam temperature readings for the inlets and outlets of the vent condenser on May 22, 2016

Readings in Fig. 35 were recorded for about one hour on May 22, 2016 in order to test all of the sensors after installing them around the vent condenser. This was done after removing the surface sensors from the inlet and the outlet condensate water pipe lines. The difference between the inlet and the outlet steam temperatures varied depending on the inlet condensate water temperature. That was because the inlet steam temperature was almost constant, while the condensed steam temperature clearly changed proportionally with condensate water temperature, as shown in Fig. 36.

The colder the condensate water entering the vent condenser, the greater the energy transferred from the steam to the condensate water during the condensation process. This is shown clearly in Fig. 36 where the temperature of the returned condensed steam decreased in proportion to the temperature of the condensate water.

States A and B are marked on Fig. 36 in order to show temperatures behavior around the vent condenser for the inlet and outlet steam lines. State B shows that the condensed steam temperature dropped when the inlet condensate water dropped. That was due to LMTD (Log Mean Temperature Difference) which is considered the driving force for exchanging energy between fluids in a heat exchanger. (LMTD's effect on heat exchange rate is described in Section 2.2.2.)

According to the heat transfer rate equation (see Eqs. (1.3) and (1.6)), LMTD increases whenever the temperature difference between the two fluids increases, which as a result increases the heat transfer rate from the steam to the condensate water.

Based on Fig. 36, the vent condenser's LMTD in Table 2 increased from 19.2 °F (state A) to 26.4 °F (state B) when the inlet condensate water temperature dropped about 11 °F between the two states. Even with this drop of the inlet condensate water temperature between the two states, the temperature rise was changed slightly (ΔT dropped about 1 °F, see in Table 2). Also, during these changes between states A and B, Fig. 36 shows that the condensate water flow rate was almost constant at about 88 gpm.

Table 2. LMTD increase for the vent condenser when the inlet condensate water temperature decreased

	State A	State B
T water in (°F)	183	172
T water out (°F)	196	184
T steam in (°F)	212	212
T condensed steam out (°F)	206	196
LMTD (°F)	**19.2**	**26.4**

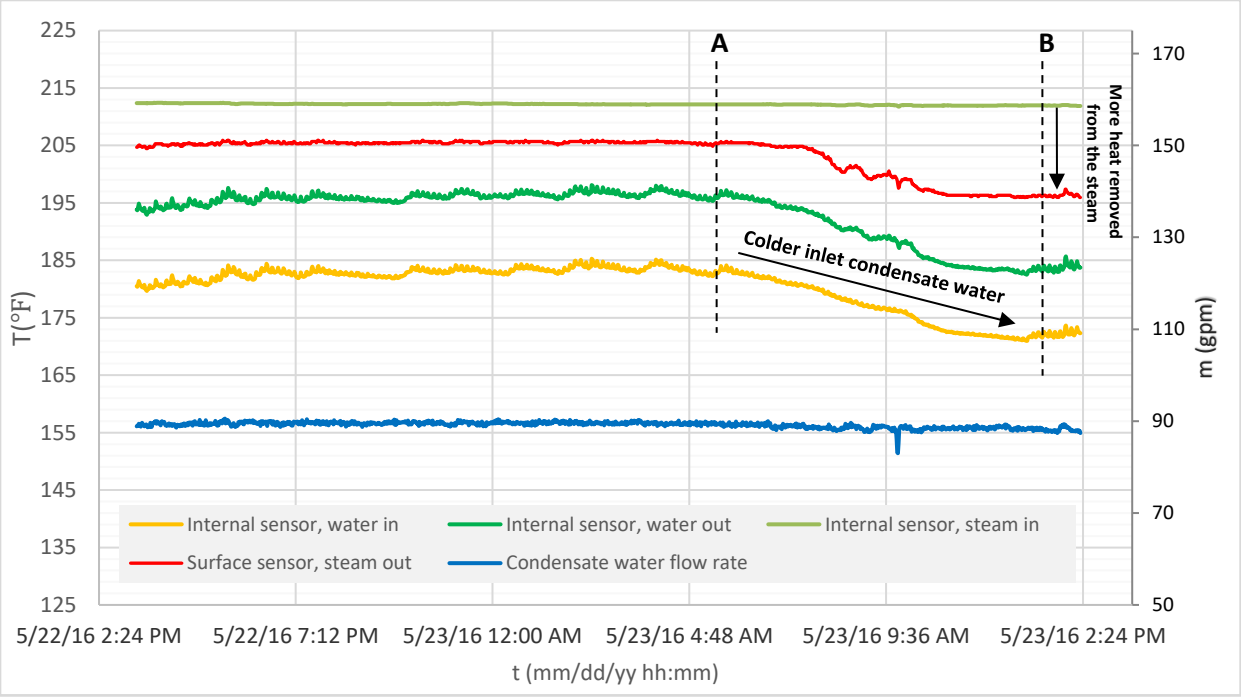

Fig. 36. Temperature changes around the vent condenser when inlet condensate water temperature dropped

Figure 37 shows that the drop in the steam's temperature changed dramatically from about 6 °F to about 16 °F, while the rise in the condensate water's temperature dropped slightly by about 1°F. It appears that the drop of condensed steam temperature at state B might attributed to an increase in the condensed steam flow rate. However, this flow rate was not measured since there was no flow meter installed in the pipe line; and that flow rate could not be calculated at that time.

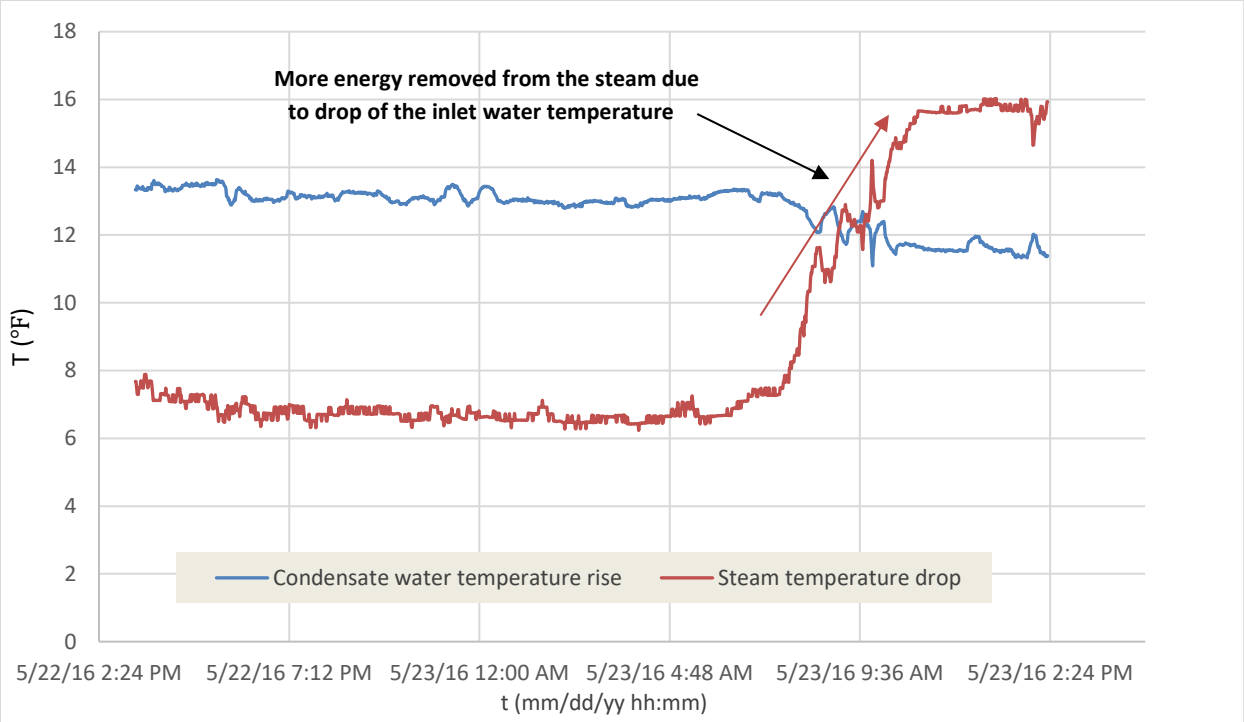

Fig. 37. Changes in the condensate water and steam pipe lines' temperatures due to a drop in the inlet condensate water temperature

2.1.2 Evaluating the Condensed Steam Flow Rate

The vented steam from the DA is re-directed to the vent condenser in order to recover some of the steam's thermal energy and add it to the condensate water. During the process of transferring this energy, the steam's latent energy is transferred to the lower temperature condensate water through the vent condenser's tubes inside the shell. The steam's energy drops in the shell, causing the steam to become liquid. That liquid water has high energy (180-200 °F), so it can be considered as another source of energy gained by using the vent condenser since that water is sent back to the storage tanks.

Previously, the flow rate of the condensed steam was not known because there was no flow meter in that pipe line. In this study, a Siemens flow meter (Mag 5100 W DN 25, SITRANS F M MAG 5100 W, see App. A8) was installed in the condensed steam pipe line (as shown in Fig. 38), after being tested and calibrated. A flow rate calibration curve was developed from the calibration tests in order to correct the flow meter readings (see Section 1.5.1).

The Siemens flow meter was installed in the pipe line's "wet leg" as shown in Fig. 38. The wet leg helps to assure that the flow meter is located where the pipe line is always full of liquid, in case the condensed steam flow is not enough to fill the line. The flow meter was for 1 in diameter pipes, so reducer and expansion joints were used before and after the flow meter in order to fit the 1.5 in diameter pipe.

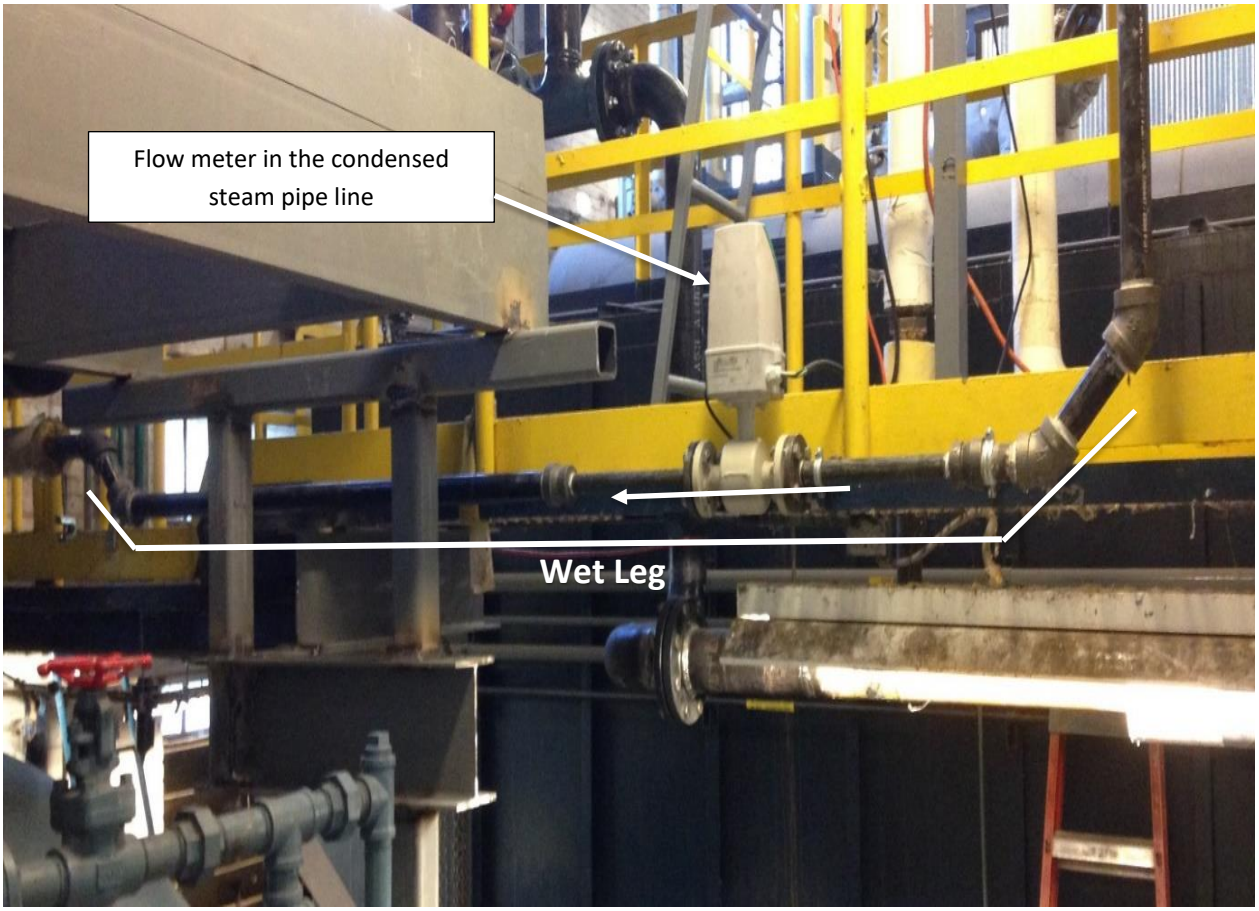

Fig. 38. Condensed steam pipe line out of the vent condenser with the newly installed Siemens flow meter in the wet leg

According to the manufacturer [16], the flow meter must be installed in a straight pipe line at least 10 in upstream of, and 5 in downstream of, the flow meter. In the 15 in of straight pipe line, no valves or any other flow restrictions are allowed because these could cause turbulence which affects the quality of the sensor signal. Thus, the flow meter was installed by the SPP staff with more than 1 ft upstream and 3 ft downstream, as shown in Fig. 38. That means the only issue was having 4 ft of full pipe flow.

2.1.2.a Acquired Flow Rate Data

The flow meter was installed and functional on September 10, 2016. So flow rate data for the condensed steam line was measured and recorded from that date forward. The condensed steam flow rate was found around 1-2.5 gpm. See Figs. 39 and 40 for the recorded flow rate on September 11-13, 2016. Since this flow meter was calibrated (see Section 1.5.1 for the calibration process) before being installed and there was an error associated with its readings, the recorded flow rate was calibrated by using the produced calibration curve.

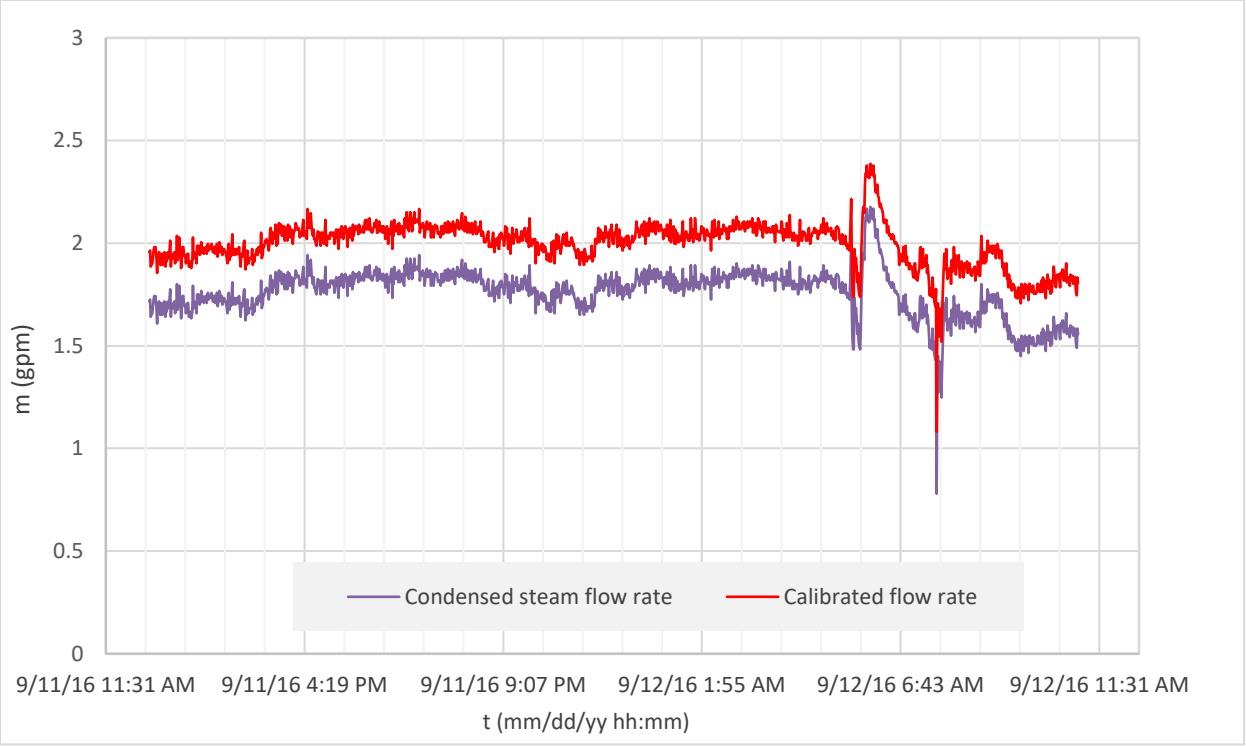

Fig. 39. Condensed steam flow rate compared to calibrated readings for the period September 11-12, 2016

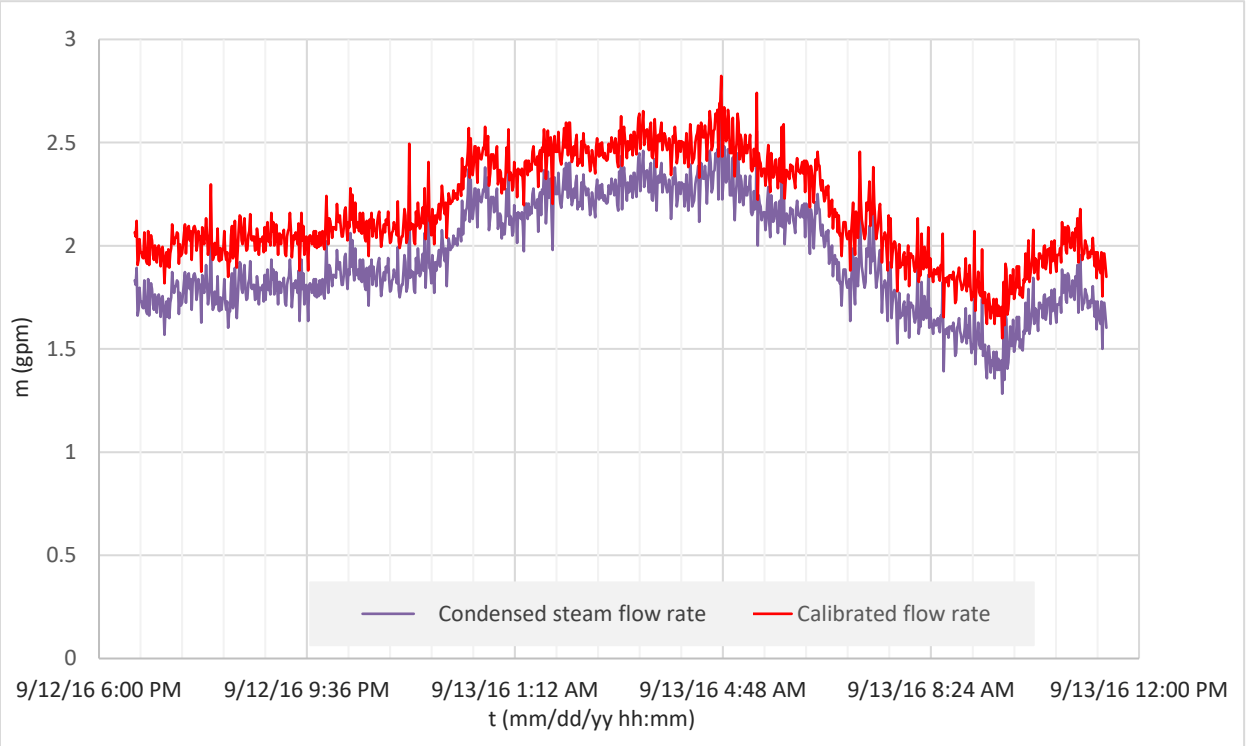

Fig. 40. Condensed steam flow rate compared to calibrated readings for the period September 12-13, 2016

From Figs. 39 and 40, it can be seen that the adjusted flow rate, which was based on the flow calibration curve (see Fig. 17 of Section 1.5.1), was about 0.25 gpm higher than the recorded value. The calibrated flow rate was employed in mass and energy balance investigation in Chapter Five.

It was important to understand why the flow rate of the condensed steam was fluctuating as shown in Figs. 39 and 40. So the condensed steam flow rate was compared with other parameters around the vent condenser in order to analyze the behavior of the condensed steam flow rate in conjunction with other data. Figures 41 and 42 give a better understanding of the relationship between the condensed steam flow rate and the temperature of the inlet steam, as well as the relationship with the flow rate of the inlet condensate water. For the period September 13-15, 2016, Fig. 41 shows that the flow rate of the condensed steam changed proportional to both of these parameters. The amount of condensed steam was affected by either the inlet steam temperature or the inlet condensate water flow rate, or both.

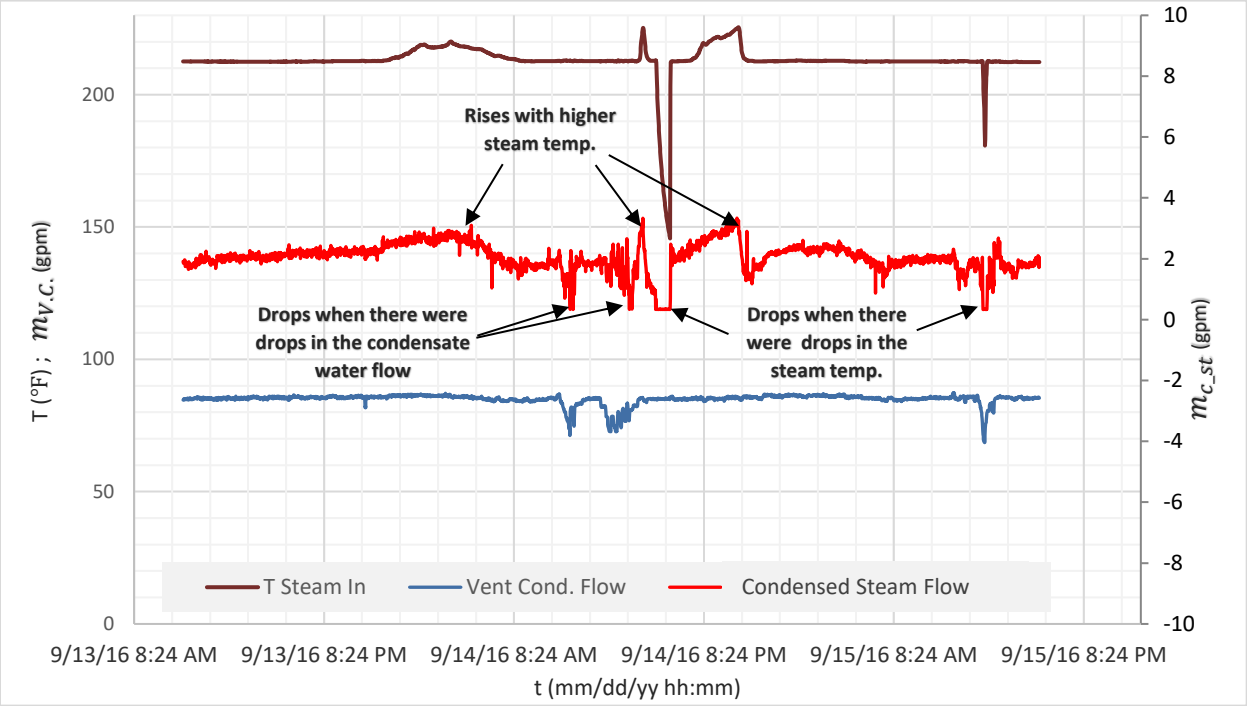

Fig. 41. Condensed steam flow rate varying with the steam temperature and inlet condensate water flow rate for the period September 13-15, 2016

Figure 41 shows that the main drops in the condensed steam flow rate happened at the same time when there were drops in the inlet condensate water flow rate and the steam temperature. Also, it can be seen that the rises in flow rate in Fig. 41 happened when there were higher steam temperatures.

When the steam temperature was lower, the temperature difference between the condensate water and the steam was lower; so less thermal energy was transferred to the condensate water, which meant less condensed steam generated. On the contrary, when the steam temperature increased, the temperature difference between the two fluids increased, so it appears that more steam was condensed to liquid water (refer to the flow rate of the condensed steam increasing/decreasing with the steam temperature in Fig. 41).

The flow rates of the condensate water and the condensed steam in the vent condenser were changing at the same time. Figure 41 shows, in some areas, that the condensate water and the condensed steam flow rates were decreasing at the same time. However, Fig. 42 shows that, at a fairly constant condensate water flow rate, the condensed steam flow rate increased at the same time that the inlet steam temperature increased. So, sometimes these parameters responded in the same "direction"; and at other times, they responded in opposite "directions".

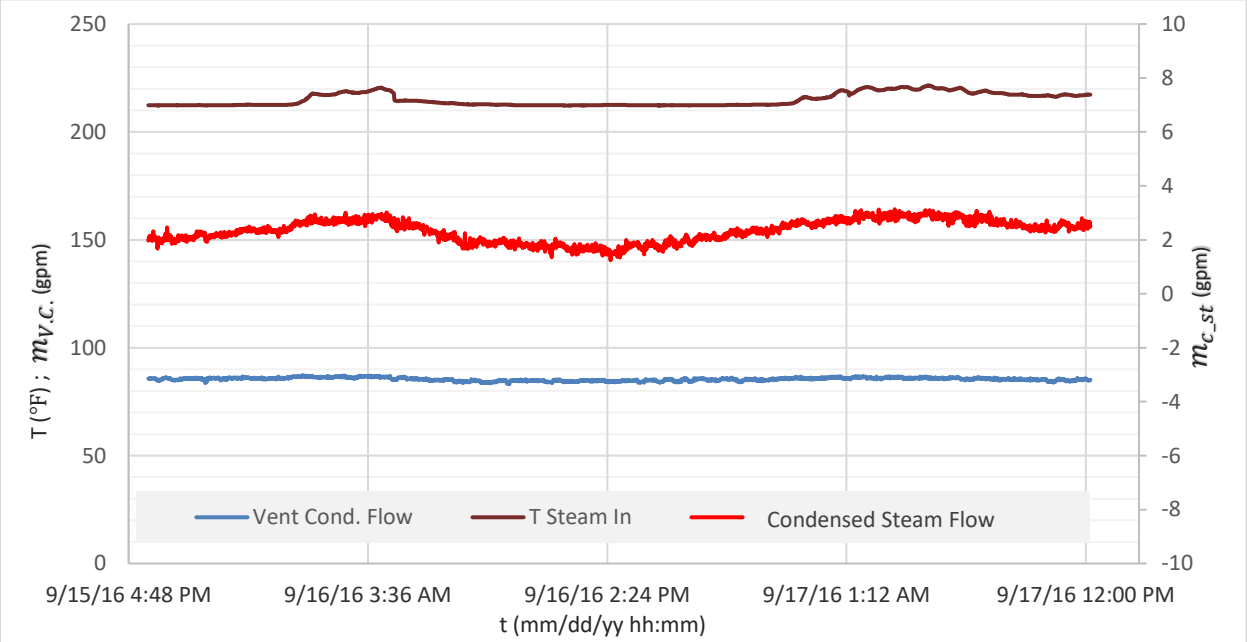

Fig. 42. Condensed steam flow rate varying with temperature of the steam for the period September 15-17, 2016

2.2 Heat Transfer Investigation of Energy Recovery Components

The average heat transfer rate was calculated for the KU SPP's heat recovery components. The heat transfer rate was calculated for the DA as a BFW preheater; and heat transfer was calculated using the overall heat transfer coefficients for the basement heat exchanger and the vent condenser when assuming parallel- and counter-flow.

Moreover, investigation was conducted to estimate the type, as well as the efficiency, of the heat exchanger that is used in the basement of KU SPP.

2.2.1 The Heat Transfer Rate in DA as Boiler's Preheater

The DA's operating principle is based on mixing hot fluid (steam from the boiler) with cold fluid (condensate water), and most of the steam is condensed to hot water. So, according to the conservation of energy, the DA increases the BFW energy by transferring energy from the steam to the condensate water. In addition, most of that steam is condensed to high temperature saturated water during the deaeration process, which also increases the BFW temperature, which enters the DA in the temperature range of 150-180 °F.

The temperature of the BFW downstream of the DA is increased to about 225 °F (on average). The energy gained helps to improve the boiler and the overall plant efficiencies because the BFW then needs less energy from burning the fuel to convert the water to steam.

It is useful to find the average heat transfer rates in the DA and the boiler during a specific time period, and estimate the DA-to-Boiler heat ratio. That ratio will show the energy added to the BFW in the DA, considering it to be a preheater to the boiler. According to the first law of the thermodynamics, heat transfer can be calculated for the BFW in the DA by knowing the water inlet and outlet temperatures, the water's specific heat capacity, and the water flow rate through the DA [17]:

$$Q_{DA} = \dot{m}_{DA}\, C_{P\,water}\, \Delta T_{rise} \tag{2.10}$$

$$\dot{m}_{DA} = \rho_{water}\, m_{DA}\, C_1 \tag{2.11}$$

The density and the specific heat capacity of the water in Eqs. (2.10) and (2.11) were found for the average between the inlet and outlet temperatures of the DA.

So, at 195 °F, $\rho_{water} = 60.3\ \frac{lb_m}{ft^3}$, $C_{p\,water} = 1.005\ \frac{Btu}{lb_m\,°F}$

while $C_1 = 0.13368\ \frac{\frac{ft^3}{min}}{gpm}$, which is the volumetric flow rate conversion factor [18].

$\dot{m}_{DA}$ in Eq. (2.11) was taken as the average flow rate of the DA feed water on March 7, 2016. Since there is no flow meter to measure the condensate water flow rate through the DA, that flow rate is computed as the main condensate water flow rate coming from the storage tanks minus the vent condenser flow rate.

$m_{DA} = m_{tot} - m_{V.C.} = 167\ gpm - 89\ gpm = 78\ gpm$

Then, from Eq. (2.11),

$$\dot{m}_{DA} = \left(60.3\ \frac{lb_m}{ft^3}\right)(78\ gpm)\left(0.13368\ \frac{\frac{ft^3}{min}}{gpm}\right) = 628.75\ \frac{lb_m}{min}$$

Here, the $\Delta T_{rise} = T_{after\ DA} - T_{before\ DA} =$ 55 °F. Then using Eq. (2.10) to calculate the energy gained by the condensate water,

$$Q_{DA} = (628.75\ \frac{lb_m}{min})(1.005\ \frac{Btu}{lb_m.°F})\ (55\ °F\ )(60\ \frac{min}{hr}) = 2.08\ x\ 10^6\ \frac{Btu}{hr}$$

This was the average energy gained by the BFW in the DA on March 7, 2016.

Next, the heat transfer rate in the boiler was calculated for the same time period. However, it is not possible to compute the boiler's heat transfer rate using Eq. (2.10) because it does not account for the phase change from liquid to steam. So, Eq. (2.12) was employed to calculate the heat transfer rate in the boiler.

$$Q_{Boiler} = \dot{m}\ (h_{st} - h_{BFW}) \tag{2.12}$$

The flow rate of the feed water and generated steam, as well as the enthalpies, are required to calculate the heat transfer rate. The steam flow rate is not the same as the BFW flow rate because of the continuous blowdown water being bled from the boiler (as explained in Chapter One), which makes the flow rate in and out of the boiler unequal. So Eq. (2.12) was modified to account for the actual fluid parameters in the boiler.

$$Q_{Boiler} = \dot{m}_{S_G}\ h_{S_G} - \dot{m}_{BFW}\ h_{BFW} \tag{2.13}$$

The blowdown water flow rate is not known since there is no flow meter in that pipe line. Blowdown was estimated in the previous study [3] to be 2% of the total BFW, so $\dot{m}_{S_G} \approx 0.98(\dot{m}_{BFW})$.

The enthalpies of the generated steam and the boiler feed water were found from the steam properties tables [16] as follows. The boiler feed water entered the boiler as a compressed liquid at an average temperature and pressure of 225 °F and 175 psig; so h_{BFW} was 193.67 $\frac{Btu}{lb_m}$. Steam is generated as saturated at a pressure of 175 psig and temperature of 377 °F (the pressure is constant along the boiler according to the T-S diagram, as shown in Section 5.4), so it was found that h_{st} was 1197.77 $\frac{Btu}{lb_m}$.

From the power plant daily log sheet on March 7, 2016 (see App. B2), the generated steam was (583600 $\frac{lb_m}{day}$). Substituting all information into Eq. (2.13) gives

$$Q_{Boiler} = (583600\ \frac{lb_m}{day})(1197.77\ \frac{Btu}{lb_m})(\frac{day}{24\ hr}) - (\frac{583600}{0.98}\ \frac{lb_m}{day})(193.67\ \frac{Btu}{lb_m})\left(\frac{day}{24\ hr}\right) = 24.32\ x10^6\ \frac{Btu}{hr}$$

This was the average heat transfer rate from the fuel (i.e., natural gas) to the BFW in the boiler on March 7, 2016. So, the heat ratio between the DA and the boiler

$$\text{Heat Ratio} = \frac{2.08\ x\ 10^6\left(\frac{Btu}{hr}\right)}{24.32\ x10^6\left(\frac{Btu}{hr}\right)}(100) = 8.5\%$$

This represents the percentage of energy saved in the boiler by using the DA as a preheater. Which increases the boiler efficiency since less fuel will be burned to convert the BFW to steam.

2.2.2 Heat Transfer Rate for Basement Heat Exchanger

Heat transfer rate was calculated for KU SPP's basement heat exchanger in terms of the overall heat transfer coefficient (U) of Eqs. (1.3) and (1.4) in Section 1.2.1. Most of the terms in Eq. (1.4) were not known. However, the value for the overall heat transfer coefficient (U) was found after knowing the model number of the heat exchanger and contacting the manufacturer [10]. By calculating the terms, A_o and $LMTD$, it was possible to determine the heat transfer rate using Eq. (1.3) without employing Eq. (1.4). The term A_o is the heating area, where heat transfer applies between the fluids in the heat exchanger. This is the total outside surface area of tubes inside the heat exchanger.

$$A_o = \pi D L_{tot} \tag{2.14}$$

Knowing the heat exchanger model number (SU-85-2), it was possible to determine some of the heat exchanger's specification. The first number (8) refers to the shell outer diameter of the heat exchanger in inches, which means it is 8 in. The second number (5) refers to the length of the tubes in feet, so it's 5 ft (or 60 in). The last number (2) refers to the number of tube passes.

There is no indication as to the number of tubes inside the heat exchanger from the model number; but after a specifications sheet was provided by the manufacturer (see App. B3), it was found that there were 22 tubes inside the shell for each pass; and the diameter of the tubes was 0.687 in [14]

Since the diameter of the heat exchanger shell is 8 in, it was estimated, reasonably, that the average length of the U-tubes that connect the heat exchanger's tubes between the two passes is 4 in (see Fig. 9 in Chapter One).

D= 0.6874 in (the outside diameter of the tubes). The total length of the tubes is the sum of the length of the straight tubes and U-tubes that connect the two passes.

$$L_{tot} = L_{str} + L_U$$

The straight tubes' total length is the number of tubes in each pass multiplied by the number of passes and the length of each tube. The U-tubes' total length is the length of the U-tubes multiplied by the number of them.

So, $L_{str} = (n_1)(n_2)(60\text{ in})$

$L_U = (n_1)(4\text{ in})$

where n_1 is 22, and n_2 is 2 [14]. (22 is the number of tubes in each pass; and 2 is the number of passes, see App. B3.)

Hence, $L_{tot} = 2728$ in. Using Eq. (2.14) gives $A_o = \pi D L_{tot} = 5891\text{ in}^2 = 40.9\text{ ft}^2$. This is the total heating surface area for the copper tubes inside the shell.

The result of this calculation was confirmed with the manufacturer by comparing this area with that in the specification document of the SU-85-2 unit. The manufacturer states that the heating surface area is 41 ft^2 $(or\ 5904\text{ in}^2)[10]$; and that is almost the same as the value computed from Eq. (2.14).

Even though the heating area was known from the manufacturer's document, it was computed just to verify the provided value. The difference between the calculated value and the manufacturer's value was felt to be related to the assumed length of the U-tubes, which means the length of the U-tubes could be a little longer than the assumed value of 4 in.

The overall heat transfer coefficient is used to calculate the heat transfer rate between the two fluids through the heat transmission surface. So it depends on the heat exchanger fluid's properties on both sides of the tube wall, as well as on the material of that wall (cast iron, copper, etc.). Since the heat exchangers in the KU SPP deal with water-to-water in the basement and steam-to-water on first floor, and the tubing was copper [10], the U values are those given in Table 3, according to Bell and Gossett's representatives.

Table 3. Heat exchanger U values for copper tubes with different process media [10, 18]

Process media in the heat exchanger		$U\ (\frac{Btu}{(hr)^\circ\text{F}(ft^2)})$
1	**Water-to-Water**	**60-80**
2	**Steam-to-Water**	**205**

In order to use Eq. (1.3) in Section 1.2.1, the logarithmic mean temperature difference ($LMTD$) is required. However, $LMTD$ was calculated for two cases: parallel-flow and counter-flow, because the type of the heat exchanger in the KU power plant was not known by the SPP staff.

From the temperature plots shown in Figs. 43 and 44 and the temperatures that are shown in Table 4, it was possible to calculate the basement heat exchanger's $LMTD$ for parallel- and counter-flow.

Table 4. Average values of the heat exchanger fluids' temperatures on May 9, 2016 (8:00 AM to 9:00 AM)

Make-up Water (temperature in) T_{2in}	Heated Make-up Water (temperature out) T_{2out}	Flash Tank Water (temperature in) T_{1in}	Drained Water (temperature out) T_{1out}
68.2 °F	**94.7** °F	**229** °F	**98.5** °F

The temperature data in Table 4 was taken on May 9 from 8:00 AM to 9:00 AM. The reason for using data from that time period is because the solenoid valves downstream of the make-up water pipe line were fully open during that period (this matter is explained briefly in Section 1.3.1, and it is explained in detail with graphs for the flow rate calculation procedure in Section 3.2).

Taking the data for that hour helped to calculate the make-up water flow rate through the basement heat exchanger accurately for each minute after recording the flow meter reading during that hour. The flow rate of the make-up water on average during that hour was about 10 gpm.

Case 1: Calculating Q, assuming parallel-flow

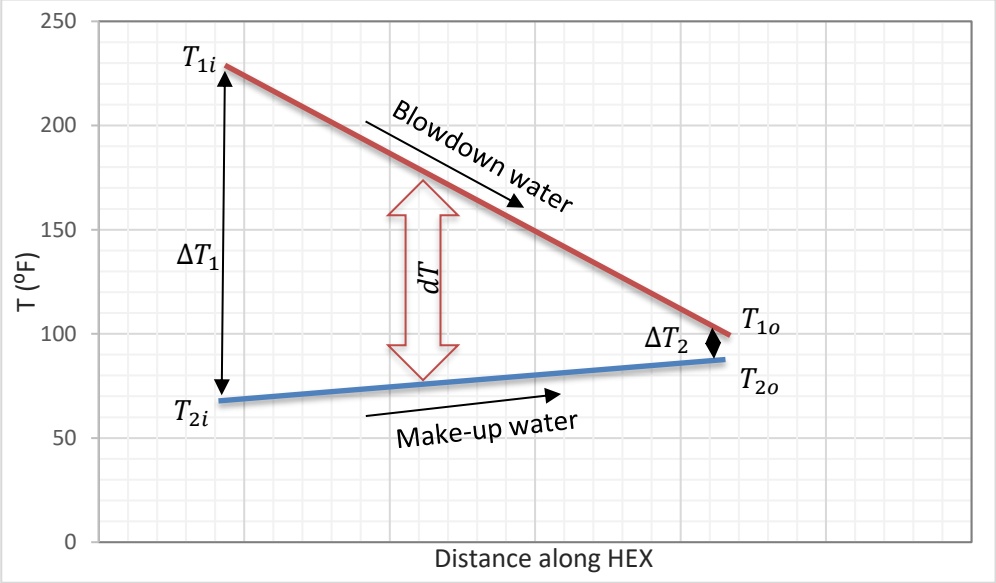

Fig. 43. Temperatures for the parallel-flow case for KU SPP's basement heat exchanger

For the parallel-flow case, the temperature differences in Fig. 43 are

$\Delta T_1 = T_{1i} - T_{2i} = 160.8$ °F and $\Delta T_2 = T_{1o} - T_{2o} = 3.8$ °F

so $LMTD = \frac{\Delta T_1 - \Delta T_2}{ln(\frac{\Delta T_1}{\Delta T_2})} = 41.9$ °F. The minimum water-to-water U value was selected from Table 3, assuming high fouling factors (h_f) for the inside and outside tubes walls, due to long time use. Hence, the May 9, 2016 heat transfer, assuming parallel-flow, was

$$Q_{parallel} = UA_o\ LMTD = \left(60\frac{Btu}{(hr)°\text{F}\ (ft^2)}\right)(41\ ft^2)(41.9°\text{F}) = \ 10.3\ x10^4\ \frac{Btu}{hr}$$

Case 2: Calculating Q, assuming counter-flow

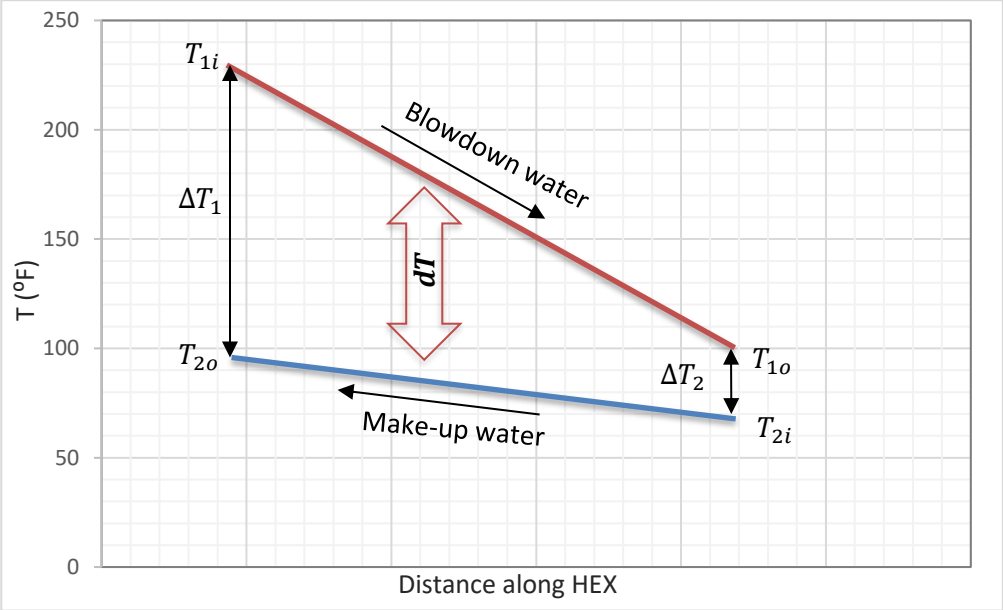

Fig. 44. Temperature for the counter-flow case of KU SPP's basement heat exchanger

For the counter-flow case, the temperature differences in Fig. 44 are

$\Delta T_1 = T_{1i} - T_{2o} = 134.3$ °F and $\Delta T_2 = T_{1o} - T_{2i} = 30.3$ °F

so $LMTD = \frac{\Delta T_1 - \Delta T_2}{ln(\frac{\Delta T_1}{\Delta T_2})} = 69.8$ °F

Now, the May 9, 2016 heat transfer rate for the counter-flow assumption was

$$Q_{counter} = UA_o\ LMTD = \ (60\frac{Btu}{(hr)\ °\text{F}\ (ft^2)})(41\ \ ft^2\ )\ (69.8\ °\text{F}) = \ 17.2\ x10^4\ \frac{Btu}{hr}$$

It can be seen that the counter-flow assumption gives a higher heat transfer rate (about 60% higher) than the parallel-flow assumption. That is because the driving force for the heat exchange, $LMTD$, is higher in the counter-flow case than in the parallel-flow case, which indicates that the counter-flow heat exchanger is more efficient to use for this application.

Moreover, it can be inferred from comparing Figs. 43 and 44 that the temperature difference (dT) between the fluids is more consistent along the counter-flow heat exchanger. So, as a result, this minimizes the thermal stresses in the heat exchanger. The temperature difference changes dramatically in the parallel-flow heat exchanger, which increases the effect of thermal stresses in the metal of the heat exchanger.

The lower and the upper tube passes for the inlet and the outlet make-up water are shown in Fig. 45a, while the number of the tubes in each pass is shown in Fig. 45b.

(a) (b)

Fig. 45. SU-85-2 heat exchanger cross-sections showing in view (a) the number of passes and in view (b) the number of tubes [reproduced from Ref. 14]

2.2.3 Heat Transfer Rate for Vent Condenser

The recovered energy from the steam by the vent condenser is equal to the additional thermal energy that would be needed in the boiler. So, ideally, if all of the steam's energy were recovered by the vent condenser, that energy equals the fuel energy that is needed to generate that amount of steam. At the KU SPP, the vent condenser reclaims energy from the DA's vented steam, as well as condenses most of that steam to liquid water that still has high thermal energy.

In this section, the vent condenser's heat transfer rate is calculated using the overall heat transfer coefficient "U" during a specific time period. This is an example of the energy that could be transferred between the steam and the condensate water. Energy recovery is calculated for two assumed flow cases (parallel- and counter-flow) and then compared with that calculated for the basement heat exchanger (in Section 2.3). This shows how heat transfer rate changes as a function of the types of process fluids and different temperature ranges.

The water temperature range in the vent condenser is different than that of the basement heat exchanger. For example, in May of 2016, the temperature change for the water-into and water-out-of the basement heat exchanger was about 60 °F to 100 °F, while the change was about 160 °F to 175 °F in the vent condenser.

The temperature plots in Fig. 46 shows the two cases combined on one graph. Parallel-flow is represented by the blue line; and counter-flow is the green line. Table 5 shows the average values of the inlet and outlet temperatures in the vent condenser on May 9, 2016.

Table 5. Average vent condenser fluid temperatures on May 9, 2016 (11:10 AM to 12:10 PM)

Condensate Water T_{2i}	Heated Condensate Water T_{2o}	DA Vented Steam T_{1i}	Condensed Steam T_{1o}
164.3°F	**178.4** °F	**219** °F (averaged from an analog gauge)	**180** °F (averaged from an analog gauge)

The temperatures in Table 5 were averaged over one hour on May 9, 2016. A data logger was used to record temperatures at one minute intervals for the inlet and the outlet temperatures of the condensate water (T_{2i} and T_{2o}). The inlet steam and the exiting condensed steam temperatures (T_{1i} and T_{1o}) were averaged while by observing analog gauges in the pipe lines during that hour because there were no instruments or temperature sensors in these lines to record the temperatures digitally.

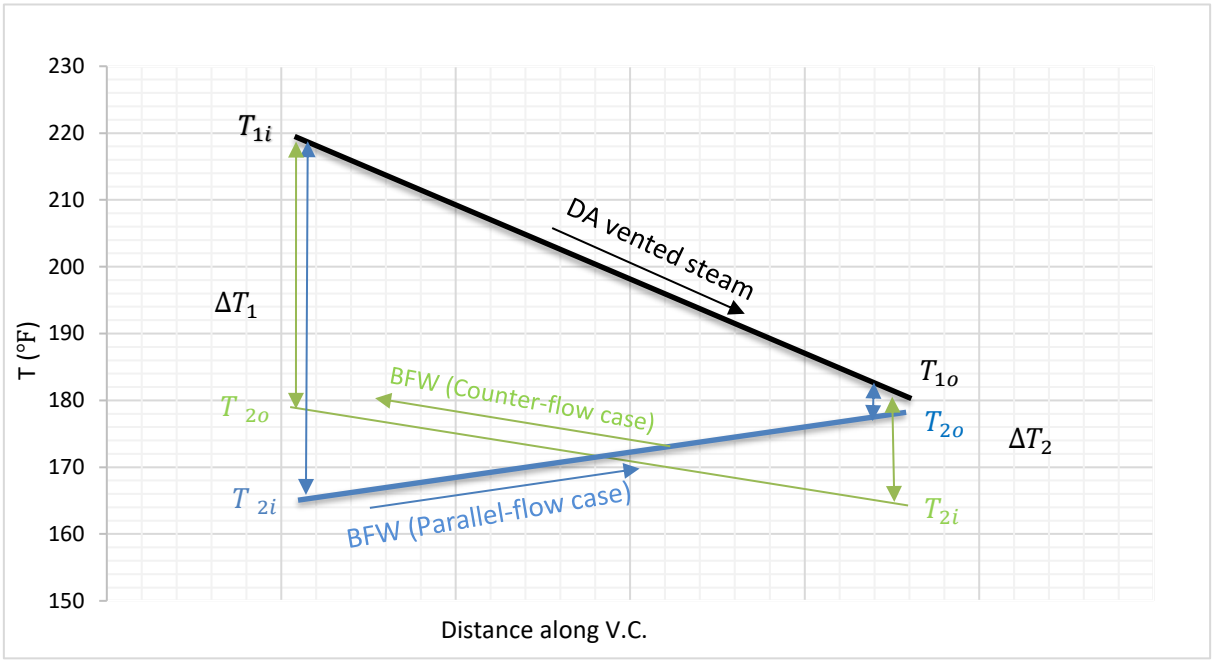

Fig. 46. Temperatures for two assumed flow directions for the vent condenser (parallel-flow in blue; counter-flow in green)

To calculate the heat transfer rate for the vent condenser for both cases, Eq. (1.3) was again used. Since the vent condenser is identical to the basement heat exchanger (SU-85-2), the heating surface area (A_o) is the same as that computed in Section 2.3 (41 ft^2).

The U value for the vent condenser is $205 \frac{Btu}{(hr)°\text{F}\ (ft^2)}$ since it handles steam-to-water (see Table 3 for the steam-to-water case). The main driving force of heat transfer between the fluids in the vent condenser is the logarithmic mean temperature difference ($LMTD$), and it was calculated as follows.

Case 1: Calculating Q assuming parallel-flow

Using the temperatures from Table 5 and the temperature profiles shown in Fig. 46,

$\Delta T_1 = T_{1i} - T_{2i} = 54.7\ °F$ and $\Delta T_2 = T_{1o} - T_{2o} = 1.6\ °F$. So, $LMTD = 15.03\ °F$

Using Eq. (1.3) and U=205 $\frac{Btu}{(hr)°F\,(ft^2)}$, gives $Q_{parallel} = 12.6\,x10^4\ \frac{Btu}{hr}$.

Case 2: Calculating Q assuming counter-flow

$\Delta T_1 = T_{1i} - T_{2o} = 40.6\ °F$ and $\Delta T_2 = T_{1o} - T_{2i} = 15.7\ °F$. So, $LMTD = 26.2\ °F$

Using Eq. (1.3) and U=205 $\frac{Btu}{(hr)°F\,(ft^2)}$ gives $Q_{counter} = 21.9\,x10^4\ \frac{Btu}{hr}$.

From the previous analysis, the heat transfer rate between the fluids was about 40% higher for the counter-flow assumption than for the parallel-flow assumption. This percentage difference was about 60% for the basement heat exchanger (in Section 2.3).

This percentage was higher for the basement heat exchanger because the temperature difference (ΔT) between the cold and the hot fluids was higher for the basement heat exchanger than for the vent condenser, as shown in Tables 4 and 5. Also, the LMTDs for both flow assumptions for the vent condenser were about 35% less than those of the basement heat exchanger.

2.3 Type and Efficiency of the Heat Exchangers in the KU SPP

The heat exchangers in the KU SPP have been studied to estimate the recovered energy that was added to the condensate water. However, there is not enough information about the heat exchangers' thermal specifications, such as the efficiency, and whether they are parallel-, counter-, or cross-flow heat exchangers. So, these specifications were evaluated by employing data that was recorded during the heat exchangers' operation.

2.3.1 Heat Exchanger Type

The classifications of the heat exchangers that are used in the KU SPP are not known, even after contacting the manufacturer regarding the model number (SU-85-2). According to the manufacturer [11], it is difficult to determine if heat exchangers are parallel- or counter-flow when they handle vapor and liquid.

According to the company's technical support [11], this is because the steam's energy is latent and not sensible; so the flow direction of the steam does not matter in that case.

In Sections 2.2.2 and 2.2.3, calculations were made of the heat transfer rates of the heat exchangers that are used in the KU SPP, as well as calculating the heat transfer areas. So, this section's analysis is used to determine the types of the heat exchangers in the KU SPP, based on the relationship [17]:

$Q_{water} = Q_{hex/V.C.}$; or

$$\dot{m}\ C_p\ \Delta T_{rise} = U\ A_o\ LMTD \qquad (2.15)$$

Using the terms $\dot{m}$, C_p, ΔT, U, and $LMTD$ for both flow cases from Sections 2.2.2 to 2.2.3, it is possible to calculate the apparent A_o from Eq. (2.15) in order to help in determining the heat exchanger type. The two flow cases' heat transfer areas can be calculated from Eq. (2.15) and compared to the actual area of 41 ft^2 that was calculated using Eq. (2.14) (or from the manufacturer's specifications [10]). Those heat transfer areas are given in Table 6.

Table 6. Calculated heat transfer area (A_o) for parallel- and counter-flow for the basement heat exchanger and the vent condenser

Flow Type	Basement Heat Exchanger $A_o\ (ft^2)$	Vent Condenser $A_o\ (ft^2)$
Parallel-Flow	91.5	199.1
Counter-Flow	**36.9**	114.2

From Table 6, it can be seen that both calculated areas for the vent condenser are higher than the actual area ($41\ ft^2$). So it is not possible to deduce whether the vent condenser is parallel-or counter-flow type; and that confirms the manufacturer's statement (Bell and Gossett) that it is difficult to classify the type of a shell-and-tube heat exchanger when it handles steam-to-water [12].

In the parallel-flow case, the basement heat exchanger's area was much higher than the actual area (about 55% higher); but for the counter-flow case, it was reasonably close to the actual area (10% lower). These results show that the vent condenser's type cannot be determined using the current information.

As a result, the vent condenser should also be checked to see if it is cross-flow. However, according to the manufacturer, U-tube heat exchangers cannot be classified as a single flow type because the two fluids flow parallel for one pass, while they flow counter for the other pass (see the directions of fluid flow in Fig. 9).

2.3.2 Heat Exchanger Efficiency

Since the heat exchanger is not a device with moving parts like a motor or a pump, it is not possible to calculate an efficiency in the typical sense of ideal vs. actual work. The efficiency can be calculated as "the ratio of the actual heat transfer to the heat transfer by the ideal heat exchanger. The ideal heat exchanger transfers the maximum amount of heat equal to the product of *UA* and the arithmetic mean temperature difference, and generates the minimum amount of entropy, making it the most efficient and least irreversible heat exchanger" according to Fakheri [20].

For insulated shell-and-tube heat exchangers, such as the units of the KU SPP (SU-85-2), if the energy removed from the hot fluid is equal to the energy added to cold fluid, the efficiency is equal to 1.

Instead of efficiency, the term "effectiveness" could be used when talking about heat exchangers. Effectiveness is a function of some of the heat exchanger specifications such as tube material, flow velocity, film coefficients, and the log mean temperature difference, which contribute to the overall heat transfer coefficient "U" of a particular heat exchanger [12].

The heat exchangers' age or time in service affects the effectiveness because the overall "U" value is changed by fouling coefficients due to chemical attack or deposits on the tube surfaces. The effectiveness of a heat exchanger is reduced by time. In other words, after using a heat exchanger for long time, the heat transfer rate between the two fluids will become lower than that of the new heat exchanger [11].

It may be difficult to estimate how much the effectiveness of a heat exchanger has changed with time. However, current effectiveness can be determined accurately by comparing the present values of the flow rates and temperatures with the original values. For example, if the flow rates remain the same, but the temperature differentials are reduced by 10%, this means that the effectiveness has dropped by 10% [11].

It is possible to use Eq. (2.15) to estimate the effectiveness if all of the operating conditions are known. The left hand side of this equation represents the actual heat transfer between the fluids, while the right hand side represents the ideal heat transfer that would be transferred between the fluids. So, effectiveness, is the ratio of the left side to the right side of Eq. (2.15).

Indeed, the U value on the right side changes with time due to many factors, such as fouling coefficients on both sides of the tube walls (see Eq. (1.6)). So Eq. (2.15) can be re-written in terms of the current equivalent U (U_{eqv}) to represent the actual heat transfer rate

$$\dot{m}\ C_p\ \Delta T_{rise} = U_{eqv}\ A_o\ LMTD \tag{2.16}$$

$$U_{eqv} = \eta\ U_{orig} \tag{2.17}$$

U_{eqv} is the current overall heat transfer coefficient, and U_{orig} is the original overall heat transfer coefficient. By knowing all of the terms in Eq. (2.16) which were used in Section 2.2.2 for the basement heat exchanger, it is possible to calculate U_{eqv} for the current operating conditions of the unit SU-85-2. From Eq. (2.16), it was found that U_{eqv}= 52.74 $\frac{Btu}{(hr)°\mathrm{F}\ (ft^2)}$.

Hence, we can estimate the current effectiveness of the heat exchanger from Eq. (2.17), assuming that the original U value was 60 $\frac{Btu}{(hr)°\mathrm{F}\ (ft^2)}$. This U value was chosen based on the minimum water-to-water value in Table 3 because of the high TDS in the make-up water (3000-4000 ppm, according to the SPP staff [38]), which means high deposits inside the heat exchanger tubes.

Thus, $\eta = \frac{U_{eqv}}{U_{orig}}$ (100%) = 88%.

This efficiency was determined based on the basement heat exchanger operating condition on May 9, 2016.

In conclusion, new temperature sensors were installed around the vent condenser in order to measure the fluids' temperatures more accurately. The new sensors can measure the temperature inside the pipe lines, instead of using surface sensors that measure the outer pipe surface temperatures which could be affected by the surroundings. It was found that the surface sensors measured about 2 °F less than the internal sensors on the inlet and outlet condensate water pipe lines due to heat loss. However, since this 2 °F temperature difference was the same in the inlet and outlet pipe lines, it did not affect the ΔT_{rise} in the heat transfer equation, and as a result, it did not affect the energy savings calculations.

Also, the condensed steam flow rate that exited from the vent condenser was determined after installing a flow meter in that pipe line. Knowing the flow rate of this line was helpful in computing the energy that was added to the storage tanks by the condensed steam. Heat transfer investigation for the heat exchangers in the KU SPP was conducted in order to estimate the efficiency as well as heat exchanger type. It was found that the efficiency was 88%, while the results in Section 2.3.1 showed that the heat exchanger type was neither parallel- nor counter-flow, so it is recommended to check if it is cross-flow or combination of the two types (i.e., parallel- and counter-flow).

Chapter Three: Annual Energy/Fuel Savings by the Vent Condenser and the Basement Heat Exchanger

As explained in Chapter Two, the KU SPP has two heat exchangers. They are used at different locations in order to recover waste energy. The first floor heat exchanger is used as a condenser for the DA's vented steam in order to recover and add that steam's thermal energy to the BFW before venting the remaining steam and non-condensable gases to the atmosphere. The basement heat exchanger handles the boiler blowdown hot water and transfers its energy to the make-up water before sending the blowdown water to the sewer system. The reclaimed energy from both heat exchangers is added to the condensate water in the storage tanks, which increases the BFW energy so that it will need, eventually, less energy to form steam in the boiler.

3.1 Vent Condenser Energy Savings

In this work, as a continuation of previous studies [2, 3], the annual energy savings, as well as fuel savings, from using the vent condenser is determined. The reclaimed energy is calculated for different periods throughout the year 2016 (January to August), and the monthly natural gas saved is computed based on the reclaimed energy and the SPP efficiency in order to estimate the impact on the SPP's yearly budget. Moreover, this investigation uses data from new temperature sensors installed around the vent condenser after May, 2016.

For this study, improved energy calculations for the condensed steam line are made, so that the total reclaimed energy by the vent condenser can be determined. It was possible to calculate the energy in the condensed steam line after a flow meter and temperature sensor have been installed in that pipe line. So the energy savings by the vent condenser is computed for three cases during the year 2016. The first case was from January to May using surface temperature sensors (contact probe type). The second case was from June to August using internal temperature sensors (RTD type). The third case was the determined energy in the condensed steam line (the energy in this case is computed in Section 5.1).

3.1.1 January to May Energy Savings

The temperatures and flow rates for the condensate water were recorded at minute intervals around the vent condenser throughout February, so reclaimed energy was calculated for each minute by employing Eqs. (2.10) and (2.11) from Section 2.2.1. Table 7 shows example results of these calculations for different days in February, 2016 in order to help explain the process of computing the energy savings based on the data gathered minute-by-minute.

Considering 2/01/16 12:00 AM as an example, the volumetric flow rate of the condensate water was computed using Eq. (2.11):

$$\dot{m}_{V.C.} = \rho_{water}\, m_{V.C.}\, C_1 = \left(60.8\ \frac{lb_m}{ft^3}\right)(77.9\ gpm)(0.13368\ \frac{\frac{ft^3}{min}}{gpm}) = 633.2\ \frac{lb_m}{min}$$

and the saved energy was computed using Eq. (2.10):

$$Q_{V.C.} = \dot{m}_{V.C.}\, C_{P\,water}\, \Delta T_{rise} = (633.2\,\frac{lb_m}{min})(\,1.005\,\frac{Btu}{lb_m\ ^\circ\mathrm{F}})(10.4\ ^\circ\mathrm{F}) = 6650.9\,\frac{Btu}{min}$$

where 170 °F was used as the average temperature between the inlet and the outlet. Water properties were [18]

$$\rho_{water} = \ 60.8\,\frac{lb_m}{ft^3}\text{, and }\ C_{p\,water} = 1.005\,\frac{Btu}{lb_m\ ^\circ\mathrm{F}}$$

Table 7. Vent condenser savings calculations based on example data taken on different days in February

Date/Time	m (gpm)	$\dot{m}$ (lb_m/min)	T_{in} (°F)	T_{out} (°F)	ΔT_{rise} (°F)	Q (Btu/min)
2/01/16 12:00 AM	77.9	633.2	157.0	167.4	10.4	6650.9
2/04/16 02:21 AM	77.8	633.1	157.5	167.0	9.5	6044.5
2/08/16 04:48 PM	81.9	665.9	152.1	160.5	8.4	5640.2
2/13/16 01:46 PM	89.6	728.9	159.6	166.9	7.3	5340.3
2/17/16 01:00 AM	88.4	718.4	161.6	171.7	10.1	7292.2
2/20/16 04:47 AM	88.5	719.3	150.1	160.0	9.9	7156.7
2/24/16 11:55 PM	84.1	683.8	157.3	167.9	10.6	7284.5
2/29/16 11:52 PM	82.5	671.2	160.5	170.8	10.3	6947.9

Data in Table 7 was chosen randomly from February's recorded readings in order to analyze the main factors that affect reclaimed energy by the vent condenser. From Table 7 and Fig. 47, it can be seen that temperature rise for the condensate water was dependent upon two factors: the flow rate and the inlet temperature. The higher the condensate water flow rate, the lower the temperature rise (for example, refer to section A of Fig. 47). This is because fluid velocity increases proportionally with flow rate (assuming no change in pipe diameter), which means less time to gain heat from the steam.

Moreover, the higher the inlet condensate water temperature, the lower the temperature rise. For example, at 01:46 PM on 2/13/16, from Table 7, ΔT_{rise} is the lowest among other values (7.3 °F) because T_{in} was relatively high as compare to other temperatures. As a result, after calculating the full month's energy savings using minute-by-minute data, as show in Table 7, the total energy savings in February was $282{,}370{,}000\ Btu$ when the total steam generated from the boilers was $31{,}546{,}300\ lb_m$.

The energy savings for March was calculated in the same way as for February. The flow rate and temperature were digitally recorded every minute during the month.

The total reclaimed energy in March by the vent condenser was $315{,}420{,}000$ Btu, and the total steam generated by the boilers was $24{,}297{,}800\ lb_m$.

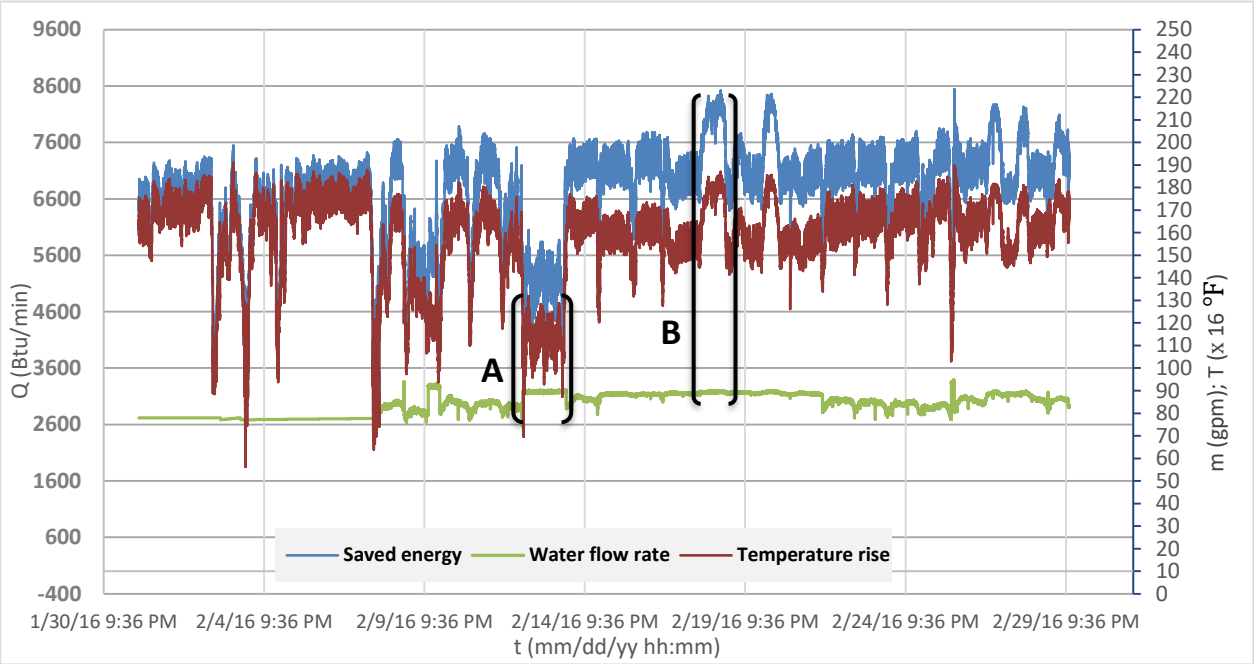

Fig. 47. Energy savings by the vent condenser in February, 2016 (actual temperature is multiplied by 16)

It can be seen from Fig. 47 that temperature rise was inversely related to flow rate. The reclaimed energy in Fig. 47 was produced, according to the heat transfer equation (Eq. (2.10)), from the mass flow rate of the condensate water and the temperature rise. In order to show the how the energy savings was affected by the flow rate and temperature rise of the condensate water, section A and B were taken as examples. In section A, the average mass flow rate was 725 $\frac{lb_m}{min}$, and the temperature rise was 8 °F; so that gave 5800 $\frac{Btu}{min}$ as the energy savings. In section B, it can be seen that the reclaimed energy was affected mainly by the temperature rise, while the flow rate of condensate water was fairly constant. Section B had an average flow rate of 720 $\frac{lb_m}{min}$, and the temperature rise was 11.3 °F; so that gave 8000 $\frac{Btu}{min}$ as the energy savings.

In the same way as shown in Table 7 for calculating February savings, in April, the total energy savings was $325{,}100{,}000\ Btu$, and the total steam generated by the boilers was $19{,}774{,}300\ lb_m$. For May, saved energy in the vent condenser was $343{,}030{,}000\ Btu$, and the total steam generated was $16{,}635{,}600\ lb_m$. In May, the energy savings and the steam generated were scaled to 30 days, instead of the 27 days during which data was actually taken. Data was not available for the end of May, because the power plant was shut down for the last 4 days for annual maintenance.

It can be seen that, as the generated steam reduced, the vent condenser's energy savings increased. Figure 48 shows the trend of the March energy savings, as well as the trends for flow rate and temperature rise.

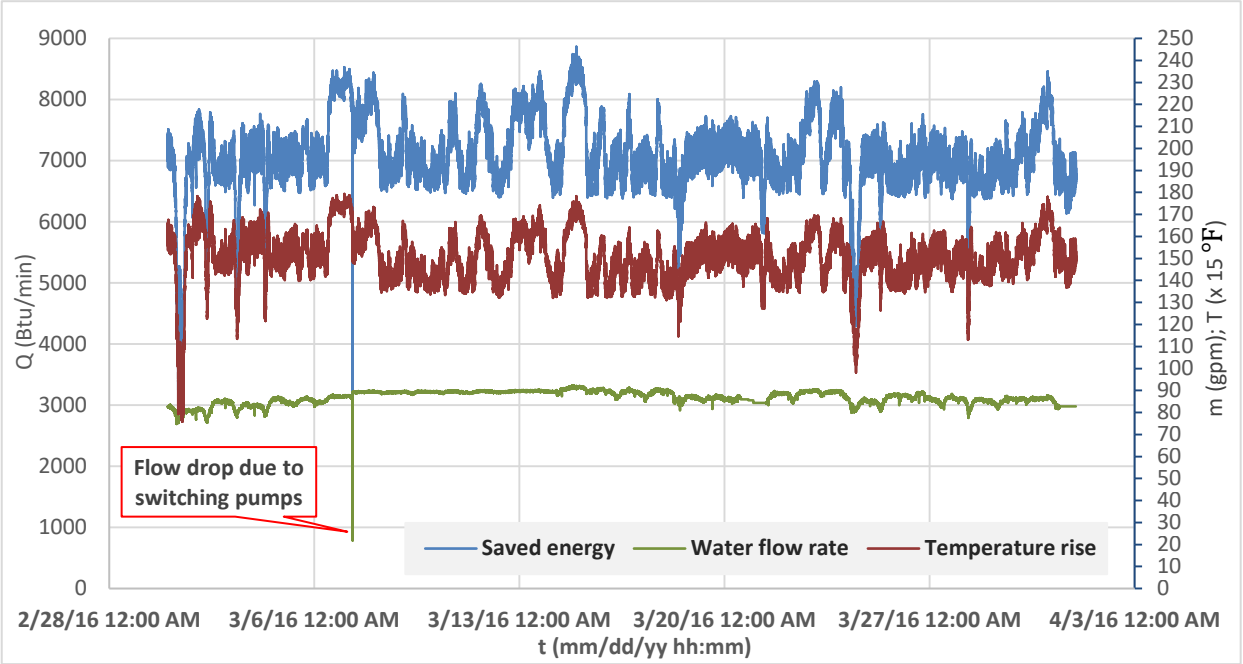

Fig. 48. Energy savings by the vent condenser in March, 2016 (actual temperature is multiplied by 15)

The calculated energy in the vent condenser from February to March was computed based on surface temperature sensors (TMC6-HE), while the calculated energy after May was based on internal temperature sensors (RTDs).

3.1.2 June to August Energy Savings

The energy savings from June to August was on average higher than that of previous months, even if the flow rate was assumed to be the same, because these calculations were based on internal sensor (RTDs) readings instead of surface sensor readings. According to data analysis in Section 2.1.1.a, the recorded temperature rise of the condensate water was higher when using internal sensors (RTDs), which translated to higher energy savings in comparison to savings calculated using surface sensor data.

The energy savings in June was $396{,}280{,}000\ Btu$. Data in Table 8 was chosen for a few example days in June, in order to compare the results with these from months when the surface sensors were used. Table 8 shows that the vent condenser's condensate water flow rate in June was on average higher than in other months due to lower steam demand, which translates to more excess condensate water being sent to the vent condenser.

As explained for Table 7, the energy savings is dependent upon the temperature rise and the mass flow rate of the condensate water, according to Eq. (2.10). Table 8 shows the calculated energy savings by the vent condenser by using data gathered at different times in June as examples.

Table 8. Vent condenser savings calculations based on example data taken on different days in June

Date/Time	m (gpm)	$\dot{m}$ (lb_m/min)	T_{in} (°F)	T_{out} (°F)	ΔT_{rise} (°F)	Q (Btu/min)
6/01/16 12:00 AM	93.6	761.4	180.6	192.8	12.1	9284.7
6/04/16 1:49 AM	94.3	767.0	179.9	192.1	12.2	9419.3
6/08/16 7:12 PM	90.3	734.1	178.0	190.8	12.7	9369.6
6/13/16 1:37 PM	90.2	733.2	178.8	191.1	12.2	9005.6
6/17/16 1:28 AM	91.0	739.8	186.3	198.7	12.3	9137.6
6/20/16 7:35 PM	86.8	705.7	183.0	196.5	13.4	9524.9
6/24/16 10:39 PM	87.3	710.1	184.2	197.2	13.0	9237.9
6/29/16 10:18 PM	92.6	753.0	183.3	195.7	12.4	9359.0

Figure 49 shows the energy that was reclaimed from the DA's vented steam in June after installing internal sensors (RTDs) in the inlet and outlet condensate water pipe lines.

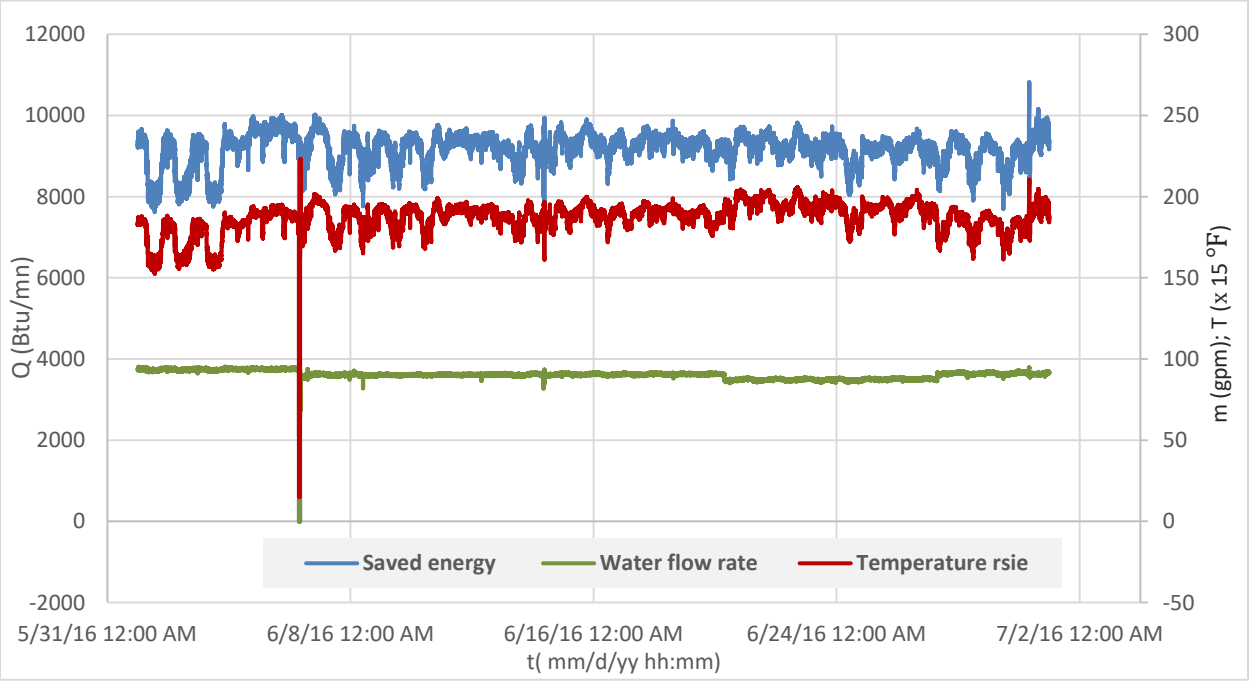

Fig. 49. Energy savings by the vent condenser in June, 2016 based on internal sensor (RTDs) readings (actual temperature is multiplied by 15)

Table 9 shows the monthly energy savings for February through August, with the difference between each two consecutive months computed in order to evaluate how the energy savings changed after using the internal temperature sensors in June.

Table 9. Differences in the reclaimed energy from February to August, 2016

Month	$\boldsymbol{Q_i}$ (*Btu*/30 days)	$\Delta\boldsymbol{Q}=\boldsymbol{Q_{i+1}}-\boldsymbol{Q_i}$ (*Btu*)
February	292,100,000	13,150,000
March	305,250,000	19,850,000
April	325,100,000	18,000,000
May	343,100,000	**53,180,000**
June	396,280,000	4,610,000
July	400,890,000	-23,010,000
August	377,880,000	N/A

It can be seen that the difference in the reclaimed energy from June to May (53,243,820 *Btu*) is much more than between any other two months (the next biggest difference was 23,010,000 *Btu*). The reason of this high difference value between May and June was attributed to the effect of using internal temperature sensors (RTDs) in June, because this type of sensor recorded higher temperature rises than those of the surface sensors which translated to higher energy savings.

The difference between July and August energy savings was negative. That was because the monthly flow rate for the two months was almost the same, but the outside temperature dropped in August which reduced the temperature rise through the vent condenser, and resulted in lower energy savings.

The calculated energy savings for the months of February to August have been analyzed with respect to the steam generated by the boilers. For more steam generated, less condensate water flows through the vent condenser, which means lower energy reclamation.

The outside temperature directly affects the temperature of the returned condensate water from the campus to the storage tanks of the KU SPP. During the hotter months of the year (i.e., April to August), the use of the steam is reduced, so the returned condensate water has a higher temperature. Table 10 shows the monthly generated steam which was provided by the SPP's data sheets in column A (see App. B2) as well as the computed energy savings for the vent condenser for each month in column B.

Table 10. Monthly generated steam and the vent condenser energy savings

Month	A	B	C	D
	S_G ($\frac{\text{lb}_\text{m}}{\text{month}}$)	Q ($\frac{\text{Btu}}{\text{month}}$)	S_G ($\frac{\text{lb}_\text{m}}{\text{30 days}}$)	Q ($\frac{\text{Btu}}{\text{30 days}}$)
January (31 days)	41,573,600	265,430,000	40,232,516	256,870,000
February (29 days)	31,546,300	282,370,000	32,634,103	292,110,000
March (31 days)	24,297,800	315,420,000	23,514,000	305,250,000
April (30 days)	19,774,300	325,100,000	19,774,300	325,100,000
May (27 days)	14,972,100	308,730,000	16,635,667	343,100,000
June (30 days)	13,154,700	396,280,000	13,154,700	396,280,000
July (31 days)	13,540,900	414,250,000	13,104,097	400,890,000
August (31 days)	13,522,100	390,480,000	13,085,903	377,880,000

In order to have the same basis for evaluation, the generated steam and the saved energy in columns A and B were scaled to 30 days in columns C and D, instead of per calendar months. The calculations for January's saved energy were based on just a few days during the month because of the lack of recorded data. Data gathered in Table 10 shows that the relationship between the steam generated and reclaimed energy is inversely related. When the steam generated was reduced from January to August due to less demand, more energy was reclaimed.

An energy curve was plotted based on the computed monthly energy savings in order to determine the relationship between the energy savings by the vent condenser and the generated steam, as shown in Fig. 50. The curve was helpful to estimate other month's energy savings when data was not available. Figure 50 shows that the higher the generated steam, the lower the energy saved by the event condenser. This is because, when the boilers generated more steam, more water went to the DA, which means less excess condensate water going to the vent condenser.

For example, January was the coldest month, among others in the plot; and the steam generated was the least, but the reclaimed energy was the lowest. On the other hand, July, as a hot month, had the highest reclaimed energy by the vent condenser with a low generated steam. Because of the outside temperature changing (to relatively cooler weather) from July to August, in addition to the effect of newly installed instruments (i.e., the internal temperature sensors around the vent condenser), August had a drop in the computed energy savings.

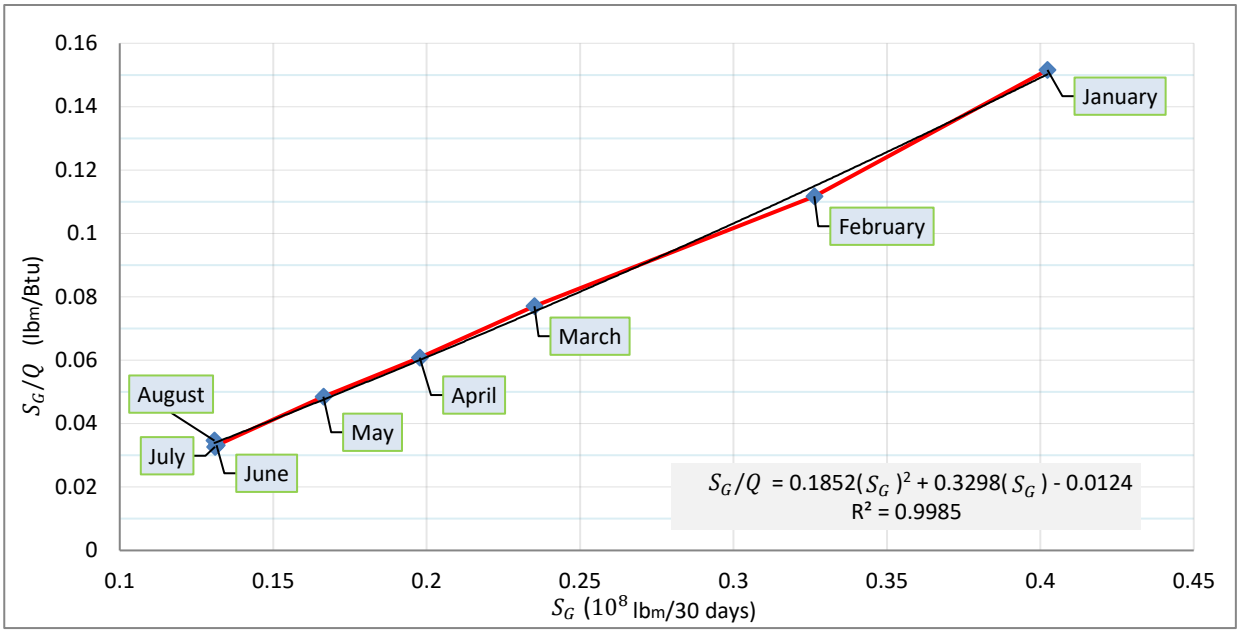

Fig. 50. Energy savings curve fit for the vent condenser from January to August

A polynomial relationship resulted from Fig. 50. The relationship is:

$$Q_i\left(\frac{Btu}{30\ days}\right) = \frac{\left(S_G\left(\frac{lb_m}{30\ days}\right)\right)_i}{0.1852\left(\left(S_G\left(\frac{lb_m}{30\ days}\right)\right)_i x10^{-8}\right)^2 + 0.3298\left(\left(S_G\left(\frac{lb_m}{30\ days}\right)\right)_i x10^{-8}\right) - 0.0124} \quad (3.18)$$

Before calculating August's energy savings from data, Eq. (3.18) was used to estimate August's energy savings (see Table C1.2 in App. C1 for January-July's calibration equation and accuracy). August's estimated energy value was 103% of the actual computed value. Then, Eq. (3.18) was used to predict energy savings for September to December. So, Eq. (3.18) was used to compute the estimated energy values for September to December of 366,027,423 Btu, 352,555,871 Btu, 313,997,761 Btu, and 293,334,988 Btu, respectively.

Equation (3.18) was also used to estimate energy savings for the months that were used to develop the equation (i.e., January to August). It was found that the estimated values' accuracy was 96%-103% (see Table C1.1 in App. C1). As a result, Eq. (3.18) can be employed to predict and estimate the energy that would be saved for any desired month during the year 2016.

In order to evaluate the annual energy savings in 2016, the equation:

$$Q_{2016} = \sum_{i=Jan.}^{i=Aug.} Q_i + \sum_{i=Sept.}^{i=Dec.} Q_i \quad (3.19)$$

was based on collected data from January to August, and on the estimated energy from September to December, 2016 (from Eq. (3.18)). In this study, the steam generated in December was estimated, based on the amounts from the last two years (see App. C1, Table C1.4). This is because December's steam generated was not available at the time this thesis was written.

The computed energy savings in the first summation of Eq. (3.19) is $2.7\ x\ 10^9\ Btu$, while the estimated energy savings in the second summation is $1.35\ x\ 10^9\ Btu$. So, the annual energy savings by using the vent condenser in 2016 was $4.05\ x\ 10^9\ Btu$. This energy is translated to saved fuel in Section 3.4 after calculating the SPP's efficiency.

3.2 Basement Heat Exchanger Energy Savings

The reclaimed energy from the basement heat exchanger comes from boiler blowdown water that has a temperature of 220-230 °F, transferring energy to the city make-up water that goes to the storage tanks. Even though the basement heat exchanger and the vent condenser are identical, the process of calculating reclaimed energy for the basement heat exchanger is different. That is because there is no flow meter in the make-up water pipe line to digitally record the flow.

As explained in Section 1.3.1, make-up water comes from the city after being softened by the softener tanks. Then it passes through a flow meter (Recordall Transmitter, Turbo 450 type, see App. A3) to cumulatively sum the gallons of water added to the storage tanks.

The flow of water into the tanks is controlled by electrical solenoid valves downstream of the heat exchanger in order to keep the water level inside the tanks at the desired set point. These valves open whenever the water level is less than about 55% of the tanks' total height, and they close when the level is higher than about 65%. (The levels where the solenoid valves open/close were visually estimated by observing the tanks' sight glass with the valves opening/closing.)

The Turbo 450 flow meter measures the amount of water cumulatively, and the SPP staff record its reading hourly to document how many gallons of water have been used. For savings calculations, the difference between hourly readings is divided by 60 minutes in order to estimate the average flow rate through the heat exchanger. However, a problem with the energy calculations for the basement heat exchanger resulted because the flow rate through the heat exchanger is discontinuous due to the solenoid valves opening/closing.

That means dividing the difference between hourly readings by 60 minutes was not correct, because, during that hour the solenoid valves could be closed for an unknown time. So, a mathematical analysis was employed in the previous study [3] in order to estimate the actual minute-by-minute flow rate when the valves were open, based on the temperature rise behavior of the make-up water line.

The temperature rise for the make-up water line can indicate when the solenoid valves are closed or open, as shown in Fig. 51; and this helped to know approximately how many minutes during an hour make-up water flowed through the basement heat exchanger.

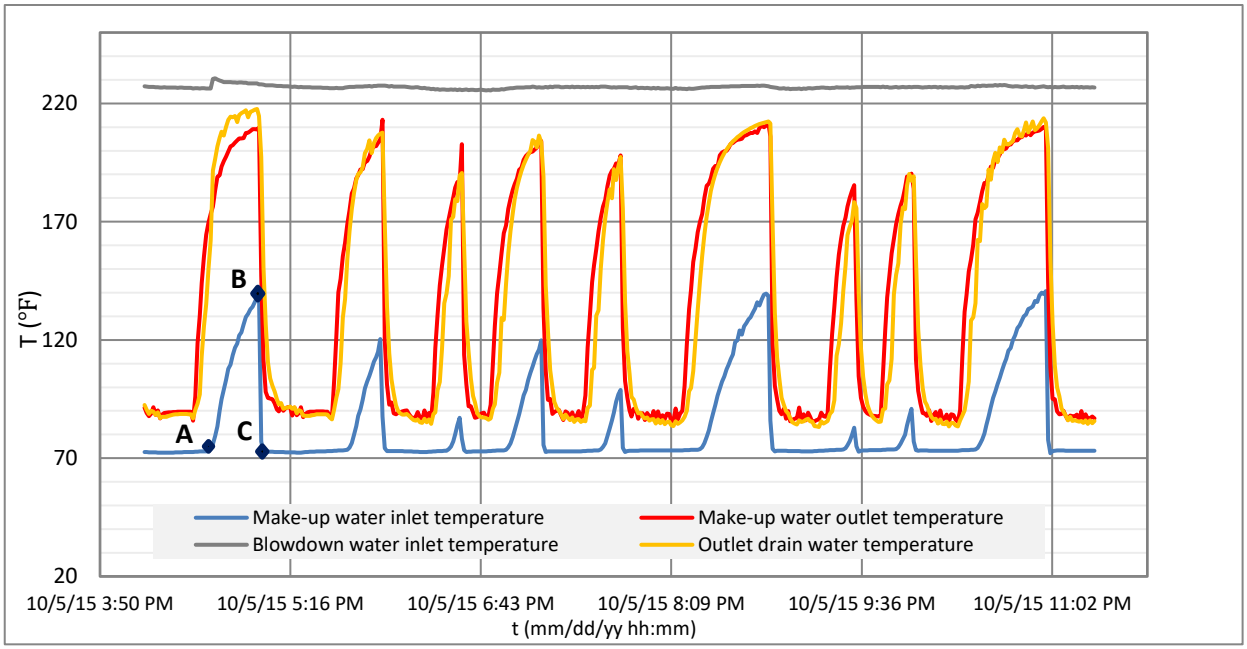

Fig. 51. The effect of opening/closing the solenoid valves on the inlet and outlet temperatures of the basement heat exchanger

When the solenoid valves close, no make-up water flows through the heat exchanger tubes, while the hot blowdown water keeps flowing through the shell. As a result, the heat exchanger metal overheats because there is no cold water flowing to absorb the blowdown water's energy. Figure 51 shows the sudden rises and drops in the temperatures of the basement heat exchanger's fluids due to the solenoid valves opening/closing. These sudden changes in temperature could cause thermal stresses in the heat exchanger's metal components, which could lead to failure of the inner tubes. According to power plant employees, in the past, this type of failure caused damage to two heat exchangers in the basement of the KU SPP [22].

In Fig. 51, Point A was when the solenoid valves started closing, and caused a dramatic rise of the temperatures for the inlet and outlet make-up water. The temperature rise continued from Point A for about 20-25 minutes until the valves started opening again at point B. Then a drop in the temperature continued for about 4-5 minutes to point C, returning to the normal temperature of the inlet make-up water. All other temperature pulses in Fig. 51 were due to the opening/closing of the solenoid valves as explained for points A-B-C. For the energy savings calculations, the readings when the solenoid valves were closed should be ignored in order to determine the real temperature readings when there was water flow.

In a previous study [3], to determine the time periods when the valves were closed, the temperature rise was employed as shown in Fig. 52. The temperature rise pulses were employed to figure out when the solenoid valves were closed (shown between points A and C in Fig. 51). However, the temperature rise readings were not stable and neither was the flow (see the

temperature rise fluctuation in the green circle of Fig. 52); so temperature and flow rate ratios were employed as factors to help estimate the flow rate variation due to the temperature variation (the ratio method of calculation was used and shown in Nanda's thesis [3]).

During this study, an easier method was used to determine the actual flow rate when the valves were closed by employing the inlet temperature of the make-up water, instead of the temperature rise. This method was used because the action of the solenoid valves had a clear effect on the make-up water's inlet temperature; and it can be seen from Fig. 52 that it is much easier to figure out where the temperature pulses started and ended. That is because the inlet temperature was more stable than the temperature rise between the pulses (compare reading behaviors in the black and green circles of Fig. 52). Moreover, as long as the inlet temperature readings were stable, there was no need to use the factors that were used in the previous study [3] to correct the flow rate when the temperature varied.

Since the ratio method of Ref. 3 was not used to estimate the flow rate variation as the temperature changed, the flow rate in this study, during any hour, was divided equally among the minutes during that hour when the valves were open. That is because the solenoid valves, in fact, were either fully opened or fully closed, so the make-up water either flowed or not, which means the flow rate would have been relatively constant when the valves were open. So, the variation in the temperature rise (when the valves were open) was attributed to the blowdown water flow rate varying and not due to variation in the make-up water flow rate. The blowdown water flow rate is unequally bled from the boiler, which affects the temperature rise by the amount of the hot blowdown water flowing through the heat exchanger.

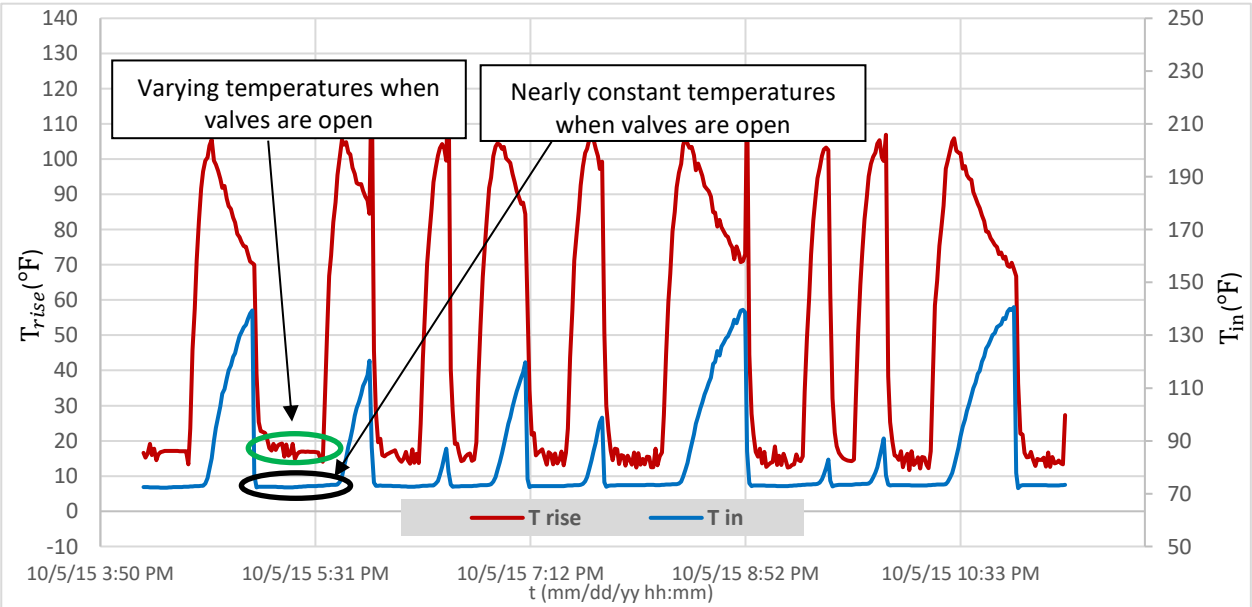

Fig. 52. Comparison of the effect of opening/closing the solenoid valves on the inlet temperature and the temperature rise of the make-up water

As an example of the February energy savings calculations, Fig. 53 shows the inlet, outlet, and rise of the make-up water temperature on February 28, 2016. The low temperature readings between the pulses are when the solenoid valves were open, while the pulses represent the temperature readings when the valves were closed.

It can be seen that the most stable temperature readings between the pulses were for the inlet temperature; and it was easiest to recognize when the temperature pulses started and ended. When the valves closed, the inlet make-up water temperature increase took about 20 minutes, while it dropped to the normal temperature about 5 minutes after the valves opened. For example, in looking at data shown in Fig. 53, inlet temperature pulses indicated the valves were closed for about 20 minutes for most of these pulses. For the data excluding the pulses, inlet temperature ranged approximately between 51 and 53 °F, and those time periods were when the values were open. So energy calculations were made for these time periods, excluding the pulses areas since no make-up water was flowing through the basement heat exchanger during the temperature pulses.

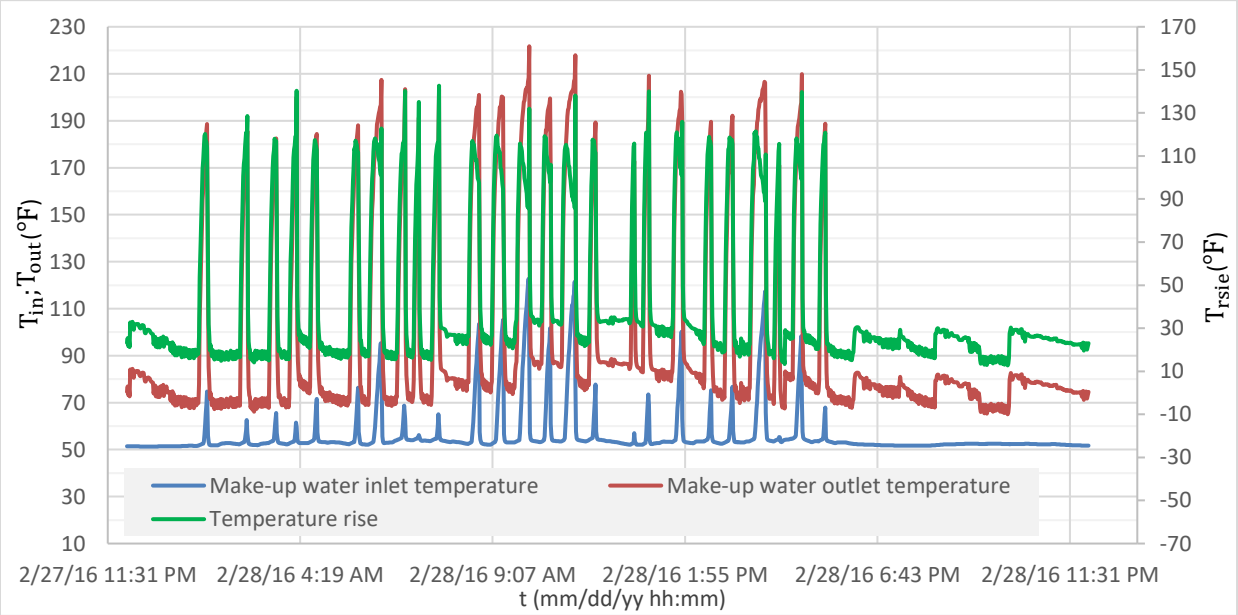

Fig. 53. Basement heat exchanger's inlet, outlet, and change in make-up water temperature on February 28, 2016

The same energy savings calculation process was used for all other months. On March 2, 2016 (Fig. 54), the same process was employed to determine when the valves were closed. The temperatures between the pulses were about 52 °F to 55 °F (these temperature ranges are different for different test dates depending on the inlet temperature of the make-up water), so any value above 55 °F was not considered because the valves were closed. Similar to the vent condenser, Eq. (2.10) was used to calculate the energy saved during each minute of each month. However, for the basement heat exchanger, the monthly energy saved was evaluated from using

a few days of data, instead of that for the whole month, because it would be extremely time consuming to perform the minute-by-minute assessment for the whole month, as is obvious from looking at Figs. 53 and 54.

The make-up water flow rate was taken from the SPP's data sheet (see App. B2). The flow rate for any chosen hour was divided among the minutes between the pulses during that hour in order to determine the actual flow rate through the heat exchanger when the valves were open. The analysis, as explained for Figs. 53 and 54, was conducted for each hour when calculating the reclaimed energy. See App. C2 for plots of the temperatures resulting from this process.

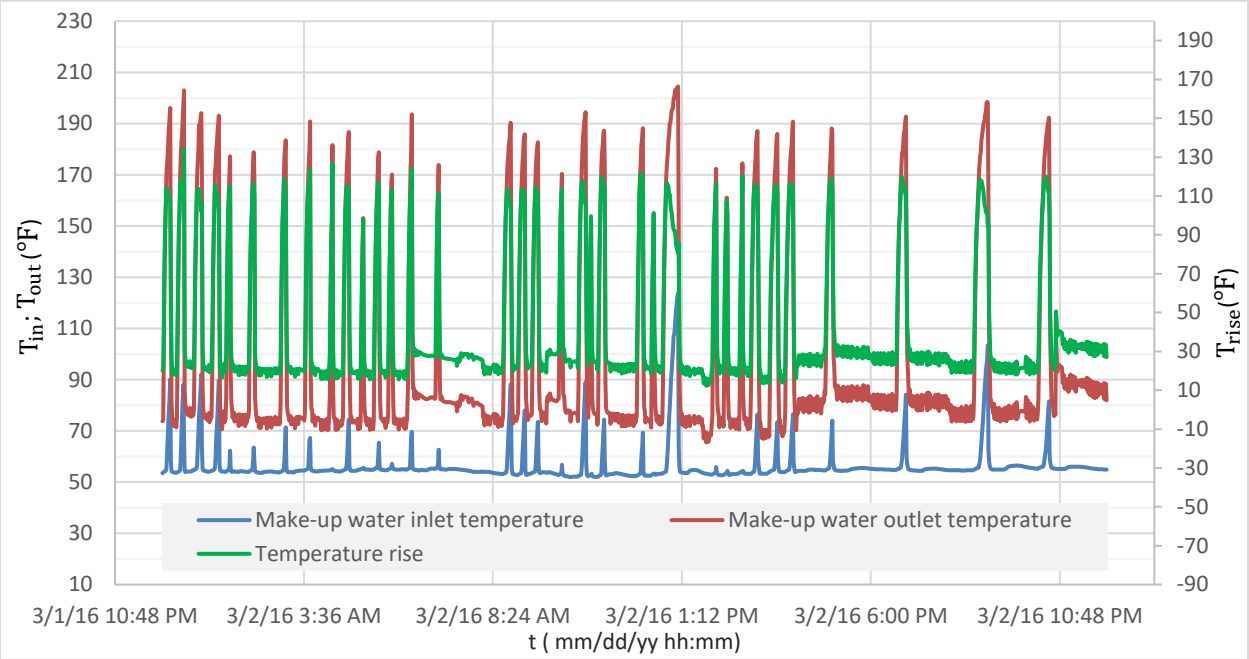

Fig. 54. Basement heat exchanger's inlet, outlet, and change in make-up water temperature on March 2, 2016

The computed energy savings in February was 134,320,000 *Btu* (Table 11). This energy represents the reclaimed energy from the boiler blowdown water before disposing of it in the sewer system. That energy was transferred to 610,090 lb_m of make-up water that was added to the storage tanks. In March, 139,2000,000 *Btu* was reclaimed and transferred to 612,300 lb_m of make-up water.

Table 11 shows the reclaimed energy by the basement heat exchanger for the months of January to September, along with the amounts of make-up water. The relationship between the basement heat exchanger's make-up water flow rate and the energy savings were proportional, unlike the inverse relationship between the generated steam and the energy savings of the vent condenser. Table 11's columns A and B are the monthly make-up water that was added to the storage tanks, and the energy that was transferred to the make-up water, respectively.

The values in columns C and D are the monthly values from columns A and B, but scaled to 30 days, instead of the calendar months, in order to have same basis for evaluation.

Table 11 and Fig. 55 show that the larger the make-up water flow rate through the heat exchanger, the greater the energy reclaimed from the blowdown water.

Table 11. Monthly make-up water and reclaimed energy by the basement heat exchanger

Month	A	B	C	D
	$\dot{m}_{m-up}$ $(\frac{\text{lb}_\text{m}}{\text{month}})$	Q $(\frac{\text{Btu}}{\text{month}})$	$\dot{m}_{m-up}$ $(\frac{\text{lb}_\text{m}}{\text{30 days}})$	Q $(\frac{\text{Btu}}{\text{30 days}})$
January (31 days)	785,180	199,650,000	759,852	193,210,00
February (29 days)	610,090	134,320,000	631,128	138,960,000
March (31 days)	612,300	139,200,000	592,548	134,710,000
April (30 days)	464,410	83,560,000	464,410	83,560,000
May (27 days)	361,610	75,840,000	401,789	84,260,000
June (30 days)	314,747	62,680,000	314,747	62,680,000
July (31 days)	299,290	55,870,000	289,635	54,100,000
August (31 days)	470,600	64,460,000	455,419	62,380,000
September (30 days)	556,020	76,153,050	556,020	76,153,050

The power plant consumed more make-up water in January in order to meet the campus demand for steam because of the low outside temperature. As a result, using Eq. (2.10), January had the largest reclaimed energy. The outside temperature increased from January to July, so less steam was needed, which meant that less make-up water flowed through the heat exchanger (Fig. 55). The large increase in make-up water in August and September as shown in Table 11 was because the SPP staff started using a water purifier (RO unit).

The RO unit reduced the water's TDS from about 3000-4000 ppm to less than 100 ppm [38]. So, much water was wasted while testing the new unit in August and September, and that caused the jump in the make-up water after July as shown in Fig. 55.

Thus, August and September's reclaimed energy values were not considered in the curve fit because it would be not accurate to considered the wasted water in energy estimation. By using January to July's reclaimed energy, a more accurate relationship between the make-up water and reclaimed energy was produced.

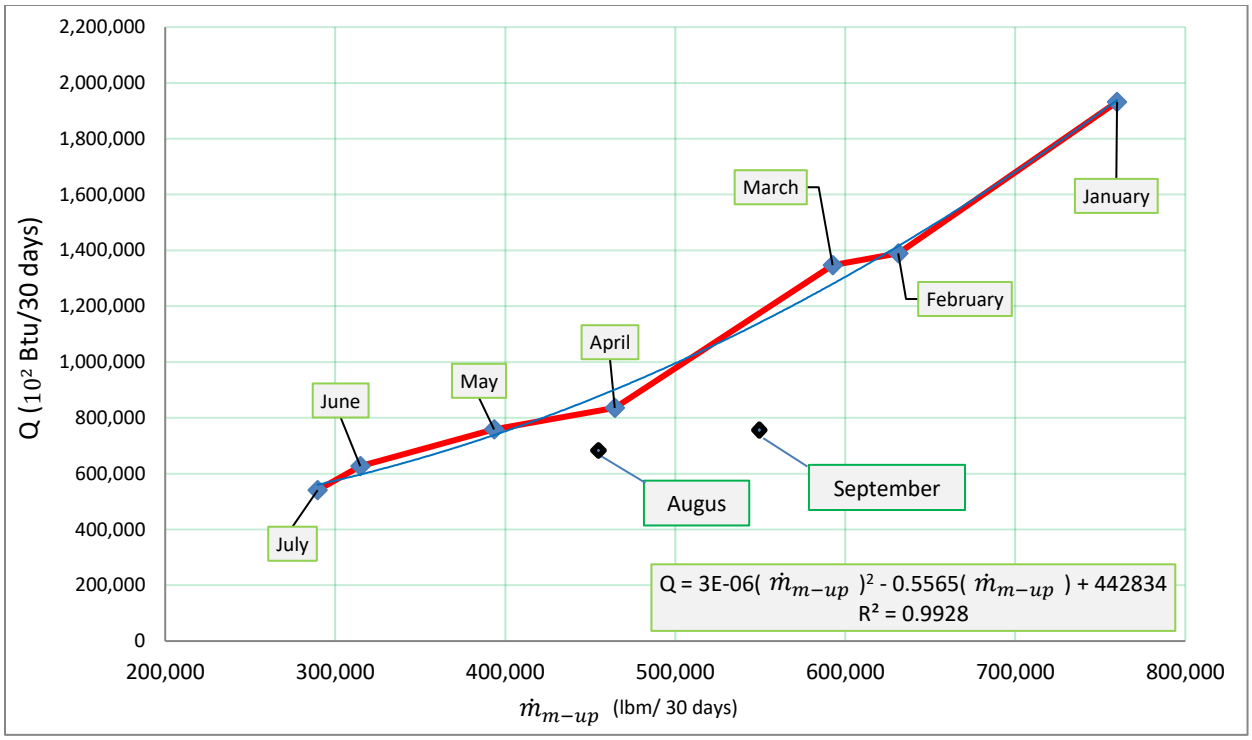

Fig. 55. Energy savings results from January to September for the basement heat exchanger

A polynomial relationship was determined from the curve in Fig. 55 in order to estimate the reclaimed energy by the basement heat exchanger for any month (Q_i) based on the make-up water in that month ($(\dot{m}_{m\_up})_i$).

$$Q_i = 10^2 \left[3x10^{-6}\left(\dot{m}_{m\_up}\right)_i^2 - 0.5565\left(\dot{m}_{m\_up}\right)_i + 442834\right] \quad (3.20)$$

As for the vent condenser energy curve of Eq. (3.18), the accuracy of this equation was evaluated by using the months of January-July to predict other month's reclaimed energy. The accuracy of this relationship was between 87-100%. This accuracy was founded by taking the ratio of the estimated values by Eq. (3.20) to the real values (see App. C1, Table C1.3, for the accuracy of the estimated energy values). This relationship has less accuracy than that of the vent condenser energy because the monthly energy calculation for the basement heat exchanger was based on only a few days (usually four days) to evaluate the whole month. So the evaluated energy value that was based on four days may be subject to error.

Similar to the calculations of the vent condenser's energy savings, the total energy reclaimed by the basement heat exchanger from January to September was about $8.92\ x\ 10^8\ Btu$. However, since the basement heat exchanger was disconnected in October, 2016, Eq. (3.20) is not applicable for months after September. Section 3.4 shows this energy translates into saved fuel for the KU SPP.

3.3 Boiler and Overall Plant Efficiency Calculations

The efficiency of a power plant is a major consideration, due to its impact on power consumption/production. The more efficient the steam generators are, the more fuel is saved in the process of forming steam. After calculating the monthly energy reclaimed by using the vent condenser and basement heat exchanger, the amount of fuel (i.e., natural gas in the KU SPP) that would be saved in the steam generator was calculated. The boiler efficiency and the overall plant efficiency were needed in order to determine the amount of saved fuel. The boiler efficiency is provided by the SPP daily log sheets, which is computed by the boiler's control system. However, the boiler efficiency was re-calculated for this study as

$$\eta_{Boiler} = \frac{Q_{out/Boiler}}{Q_{add/fuel}} = \frac{\dot{m}_{st}\ h_{st} - \dot{m}_{BFW}\ h_{BFW}}{LHV_{fuel}\ V_{cons.\ fuel}} \tag{3.21}$$

The data that was used in the efficiency calculations was also provided in the SPP's log sheets (see App. B2 for SPP's monthly log sheets). Here, the energy added by the boiler was represented by the steam energy that was gained from burning the fuel. The generated steam's mass flow rate and the volume of consumed fuel were provided by the SPP's monthly log sheets. The value of the natural gas LHV is 1018.6 $\frac{Btu}{ft^3}$ [21]. As mentioned in Section 2.2.1, the mass flow rate of the generated steam represents about 98% of the BFW because of the continuous dumped blowdown water that was estimated to be about 2% of the BFW. Assuming that the operating conditions of the boilers were constant, the enthalpy of the generated steam was founded to be 1197.7 $\frac{Btu}{lb_m}$ at 175 psig and 377 °F, while the enthalpy of the BFW was founded to be 193.67 $\frac{Btu}{lb_m}$ at 175 psig and 225 °F [17].

The only changing terms that drive boiler efficiency in Eq. (3.21) are the generated steam mass flow rate, the feed water mass flow rate, and the volume flow rate of the consumed fuel. For example, using the SPP log sheet data for March 7, 2016, the boiler efficiency given by Eq. (3.21) was

$$\eta_{Boiler} = \frac{\left(583600\ \frac{lb_m}{day}\right)\left(1197.7\ \frac{Btu}{lb_m}\right) - \left(\frac{583600}{0.98}\ \frac{lb_m}{day}\right)\left(193.67\ \frac{Btu}{lb_m}\right)}{\left(1018.6\ \frac{Btu}{ft^3}\right)\left(590600 \frac{ft^3}{day}\right)}(100) = 97\%$$

There are four boilers in the KU SPP. They are labeled on site as boilers 1, 2, 7, and 8; and the efficiency is different for each boiler.

Since the vent condenser and the basement heat exchanger recover energy and add it to the BFW, less fuel is needed to generate steam in the boiler, and that increases the boiler efficiency. The recovered energy from both heat exchangers has to be taken into account in the efficiency

calculation; so the boiler and the overall plant efficiencies were computed in order to find how much fuel could be saved. Equation (3.22) represents the overall efficiency, which includes the energy added by the vent condenser and the basement heat exchanger.

$$\eta_{Overall} = \eta_{Boiler} + \eta_{added} = \eta_{Boiler} + \frac{Q_{V.C.} + Q_{hex}}{LHV_{fuel}\ V_{cons.\ fuel}} \quad (3.22)$$

In January for instance, the energy savings by the vent condenser and the basement heat exchanger was 265,430,000 Btu, and 199,650,000 Btu, respectively. The consumed fuel was 44,377,800 ft^3; and the calculated boiler efficiency was 92%. So the added efficiency by both heat exchangers was:

$$\eta_{added} = \frac{\left(265{,}430{,}000\,\frac{Btu}{month}\right) + \left(199{,}650{,}000\,\frac{Btu}{month}\right)}{\left(1018.6\,\frac{Btu}{ft^3}\right)\left(44{,}377{,}800\,\frac{ft^3}{month}\right)}(100) \cong 1\%$$

This efficiency is added to the boiler efficiency in order to get the overall plant efficiency due to using both heat exchangers.

So, $\eta_{Overall} = \eta_{Boiler} + \eta_{added} = 93\%$.

The energy reclamation rates in the vent condenser and the basement heat exchanger were calculated on per a minute basis because all of the data is digitally recorded by minute. So the overall all plant efficiency was also computed by minute. However, the efficiency values for the boiler and the overall plant were averaged on a monthly basis from January to August and are shown in Table 12.

Table 12. Monthly boiler and overall plant computed efficiencies

Month	η_{Boiler}	η_{added} (due using both heat exchangers)	$\eta_{Overall}$
January	0.92	0.010	0.930
February	0.88	0.014	0.894
March	0.96	0.018	0.978
April	0.87	0.018	0.888
May	0.89	0.020	0.910
June	0.91	0.031	0.941
July	0.87	0.029	0.899
August	0.93	0.025	0.955

According to Eq. (3.22), the relationship between the consumed fuel in the boiler and the η_{added} is inversely proportional. So the added efficiency by the heat exchangers in Table 12 increased from January to June because the generated steam decreased during those months. (See the steam generated in Table 10.) In July and August, the steam generated started increasing again.

According to the efficiency calculations, the most efficient boilers are 7 and 8 because they were recently installed in the power plant. The efficiency calculations also showed that the higher efficiency values in Table 12 were associated with the months of January, March, June, and August, which was when boilers 7 and 8 were used (see App. B2 for which boilers were used within a given month).

3.4 Natural Gas Savings by Heat Exchangers in the KU SPP

The recovered energy from both heat exchangers in the SPP was employed to estimate the amount of natural gas that would be consumed in the boilers if no heat exchangers were used. The higher the recovered energy, the lower the amount of fuel consumed in transforming water to steam.

As explained previously, computing the saved fuel is affected by the boiler efficiency. The efficiency was calculated in the Section 3.3 for the boiler and the overall plant. However, a point-of-view might be discussed about which efficiency should be employed in the fuel savings calculations. Since the recovered energy by the heat exchangers was added to the BFW in the storage tanks, that means the BFW had higher energy than when no heat exchangers were used. So, it appears that the recovered energy by the heat exchangers was already taken into account in the boiler efficiency calculations, even if the η_{added} was not added to find $\eta_{Overall}$. However, for comparison purposes, calculation of the saved natural gas was made for two cases: using the boiler efficiency, and using the overall plant efficiency, in order to determine the size of the added efficiency and how it could impact the amount of saved fuel.

In Eq. (3.21), the efficiency equation was written in terms of the increased energy in the steam leaving the boiler divided by the energy released from the consumed fuel. It also can be written in terms of the energy and fuel saved by the vent condenser and basement heat exchanger as

$$\eta_{Boiler} = \frac{Q_{V.C./hex}}{LHV_{fuel}\ V_{saved\ fuel}} \tag{3.23}$$

So the saved fuel can be found by rearranging Eq. (3.23) as

$$V_{saved\ fuel} = \frac{Q_{V.C./hex}}{\eta_{Boiler}\ LHV_{fuel}} \tag{3.24}$$

Or, if we consider the overall plant efficiency, then the saved fuel is:

$$V_{saved\ fuel} = \frac{Q_{V.C./hex}}{\eta_{Overall}\ LHV_{fuel}} \tag{3.25}$$

For instance in February, 282,370,000 Btu was saved by the vent condenser, and 134,320,000 Btu was saved by the basement heat exchanger; and the efficiencies were 88% and 89.4% for the boiler and the overall plant, respectively. So the fuel saved by both heat exchangers was

$$V_{saved\ fuel/V.C.} = \frac{282{,}370{,}000\ \frac{Btu}{February}}{0.88(1018.6\frac{Btu}{ft^3})} = 315{,}010\ \frac{ft^3}{February}$$

$$= \frac{282{,}370{,}000\ \frac{Btu}{February}}{0.894(1018.6\frac{Btu}{ft^3})} = 310{,}080\ \frac{ft^3}{February}$$

$$V_{saved\ fuel/hex} = \frac{134{,}320{,},877\ \frac{Btu}{February}}{0.88(1018.6\frac{Btu}{ft^3})} = 149{,}850\ \frac{ft^3}{February}$$

$$= \frac{134{,}320{,}000\ \frac{Btu}{February}}{0.894(1018.6\frac{Btu}{ft^3})} = 147{,}510\ \frac{ft^3}{February}$$

The difference between the two amounts of saved fuel for the vent condenser (i.e., 4930 ft^3) and for the basement heat exchanger (2340 ft^3) was due to using the overall efficiency instead of the boiler efficiency.

The saved fuel values shown above for February were computed based on the monthly energy savings as examples; but the actual calculations were based on minute-by-minute data for both heat exchangers. Examples of minute interval fuel savings calculations are shown in Tables 13 and 14 during 30 minute periods for both heat exchangers in order to show the difference between the fuel savings for the two heat exchangers during the same time period. The fuel savings were summed minute-by-minute for the whole month to get the total monthly fuel saved in Table 15.

Table 13. Example calculation of the fuel saved by the vent condenser for 30 minutes on July 1, 2016

Date and Time	T_{rise} (°F)	$\dot{m}$ (lb_m/min)	Q (Btu/min)	η_{Boiler}	V (ft^3/min)	$\eta_{Overall}$	V (ft^3/min)
7/1/16 12:01 AM	12.68	744	9484	0.87	10.70	0.90	10.34
7/1/16 12:01 AM	12.62	745	9452	0.87	10.64	0.90	10.29
7/1/16 12:02 AM	12.58	747	9452	0.87	10.64	0.90	10.30
7/1/16 12:03 AM	12.55	747	9431	0.87	10.62	0.90	10.27
7/1/16 12:04 AM	12.62	744	9436	0.87	10.63	0.90	10.28
7/1/16 12:05 AM	12.68	750	9569	0.87	10.78	0.90	10.42
7/1/16 12:06 AM	12.72	746	9542	0.87	10.75	0.90	10.39
7/1/16 12:07 AM	12.73	750	9591	0.87	10.80	0.90	10.45
7/1/16 12:08 AM	12.76	744	9539	0.87	10.74	0.90	10.39
7/1/16 12:09 AM	12.62	740	9389	0.87	10.57	0.90	10.23
7/1/16 12:10 AM	12.50	749	9411	0.87	10.60	0.90	10.25
7/1/16 12:11 AM	12.53	746	9400	0.87	10.59	0.90	10.24
7/1/16 12:12 AM	12.61	746	9455	0.87	10.65	0.90	10.30
7/1/16 12:13 AM	12.65	746	9493	0.87	10.69	0.90	10.34
7/1/16 12:14 AM	12.67	748	9525	0.87	10.73	0.90	10.38
7/1/16 12:15 AM	12.66	746	9500	0.87	10.70	0.90	10.35
7/1/16 12:16 AM	12.67	745	9485	0.87	10.68	0.90	10.33
7/1/16 12:17 AM	12.59	749	9477	0.87	10.67	0.90	10.32
7/1/16 12:18 AM	12.52	745	9381	0.87	10.56	0.90	10.22
7/1/16 12:19 AM	12.49	746	9365	0.87	10.55	0.90	10.20
7/1/16 12:20 AM	12.51	749	9418	0.87	10.61	0.90	10.26
7/1/16 12:21 AM	12.50	743	9335	0.87	10.51	0.90	10.17
7/1/16 12:22 AM	12.47	746	9352	0.87	10.53	0.90	10.19
7/1/16 12:23 AM	12.40	748	9323	0.87	10.50	0.90	10.15
7/1/16 12:24 AM	12.35	746	9254	0.87	10.42	0.90	10.08
7/1/16 12:25 AM	12.25	748	9208	0.87	10.37	0.90	10.03
7/1/16 12:26 AM	12.18	750	9186	0.87	10.34	0.90	10.01
7/1/16 12:27 AM	12.11	744	9060	0.87	10.20	0.90	9.87
7/1/16 12:28 AM	12.05	743	9003	0.87	10.14	0.90	9.81
7/1/16 12:29 AM	11.90	745	8913	0.87	10.04	0.90	9.71
7/1/16 12:30 AM	12.03	747	9039	0.87	10.18	0.90	9.85
		Total:	299,900 $\frac{Btu}{30\ min}$		337.8 $\frac{ft^3}{30\ min}$		326.7 $\frac{ft^3}{30\ min}$

Table 14. Example calculation of the fuel saved by the basement heat exchanger during 30 minutes on

July 1, 2016

Date and Time	T_{rise} (°F)	$\dot{m}_{m-up}$ (lb_m/min)	Q (Btu/min)	η_{Boiler}	V (ft^3/min)	$\eta_{Overall}$	V (ft^3/min)
7/1/16 12:00 AM	18.73	77.80	1464	0.87	1.65	0.90	1.60
7/1/16 12:01 AM	18.14	77.80	1418	0.87	1.60	0.90	1.54
7/1/16 12:02 AM	17.81	77.80	1392	0.87	1.57	0.90	1.52
7/1/16 12:03 AM	17.65	77.80	1380	0.87	1.55	0.90	1.50
7/1/16 12:04 AM	17.50	77.80	1368	0.87	1.54	0.90	1.49
7/1/16 12:05 AM	17.49	77.80	1367	0.87	1.54	0.90	1.49
7/1/16 12:06 AM	22.68	77.80	1773	0.87	2.00	0.90	1.93
7/1/16 12:07 AM	17.89	77.80	1398	0.87	1.58	0.90	1.52
7/1/16 12:08 AM	29.27	77.80	2289	0.87	2.58	0.90	2.49
7/1/16 12:09 AM	26.81	77.80	2096	0.87	2.36	0.90	2.28
7/1/16 12:24 AM	24.02	77.80	1877	0.87	2.11	0.90	2.05
7/1/16 12:25 AM	19.38	77.80	1515	0.87	1.71	0.90	1.65
7/1/16 12:26 AM	16.64	77.80	1301	0.87	1.47	0.90	1.42
7/1/16 12:27 AM	15.06	77.80	1177	0.87	1.33	0.90	1.28
7/1/16 12:28 AM	14.74	77.80	1152	0.87	1.30	0.90	1.26
7/1/16 12:29 AM	25.67	77.80	2007	0.87	2.26	0.90	2.19
		Total:	24,900 $\frac{Btu}{30\ min}$		28.1 $\frac{ft^3}{30\ min}$		27.2 $\frac{ft^3}{30\ min}$

It can be seen from Table 14 that the energy and the fuel savings calculations for the basement heat exchanger were for just 16 minutes instead of 30 minutes because the solenoid valves were closed for 14 minutes during that period. So, during the 30 minute period, the calculations were actually just for 16 minutes.

Tables 13 and 14 show that the total vent condenser energy savings for 30 minutes was 299,900 *Btu* with an average of 9371 *Btu/min*; and the basement heat exchanger saved 24,900 *Btu* with an average of 1451 *Btu/min*. The vent condenser fuel savings for that period was around 330 ft^3, with an average of 10.3 ft^3/min, and the basement heat exchanger saved around 27.6 ft^3 with an average of 1.6 ft^3/min .

The difference between heat exchangers was attributed to the high water flow rate through the vent condenser in comparison to that of the basement heat exchanger, even though the temperature rise was higher for the basement heat exchanger.

Table 15. Monthly fuel savings by both heat exchangers based on boiler and overall

plant efficiencies

Month	Vent Condenser		Basement Heat Exchanger	
	V_{saved} based on η_{Boiler} (ft^3 /month)	V_{saved} based on $\eta_{Overall}$ (ft^3 /month)	V_{saved} based on η_{Boiler} (ft^3 /month)	V_{saved} based on $\eta_{Overall}$ (ft^3 /month)
January	283,300	280,170	213,090	210,730
February	315,380	310,490	149,410	146,740
March	324,020	317,740	144,280	141,880
April	366,300	358,580	94,050	92,170
May (27 days)	342,700	336,760	84,600	82,720
June	425,950	413,870	66,290	65,460
July	466,480	451,180	63,040	60,940
August	413,240	402,670	68,260	66,470
September	408,350	399,270	84,957	83,070
October	406,430	397,400	N/A	N/A
November	350,300	342,520	N/A	N/A
December	338,160	330,640	N/A	N/A
Total:	**4,440,610**	**4,341,290**	**967,980**	**950,180**

Table 15 shows that from January to July, the fuel saved by the vent condenser increased, while the fuel saved by the basement heat exchanger decreased. That was because the lower the steam generated by the boiler, the greater the condensate water flow was through the vent condenser, which means more energy was reclaimed. On the other hand, with lower generated steam, less make-up water was needed, so less energy was recovered from the boiler blowdown water. After July (August to December, 2016), the fuel saved by the vent condenser started decreasing again, while the fuel saved by basement heat exchanger started increasing. This change happened due the outside temperature that started decreasing again, which affected the amount of the steam generated.

To calculate how much fuel savings reduced the SPP budget, the cost of natural gas was needed. A standard price of \$0.0053/ft^3 was used in the previous studies [2, 3] according to the campus energy engineer [21]. However, because of the recent global oil crisis, this cost has reduced to about \$0.0025/ft^3 (last updated in May of 2016), according to the U.S. Energy Information Administration [23].

Figure 56 shows the natural gas prices for the last 15 years for different consumers. The price used in this study was the "Electric Power Price". So, according to this price (\$0.0025/ft^3), the annual savings from using the vent condenser in 2016 was about \$10,850, and from using the basement heat exchanger was about \$2,380 (by considering the fuel amounts that were calculated based on the plant efficiency).

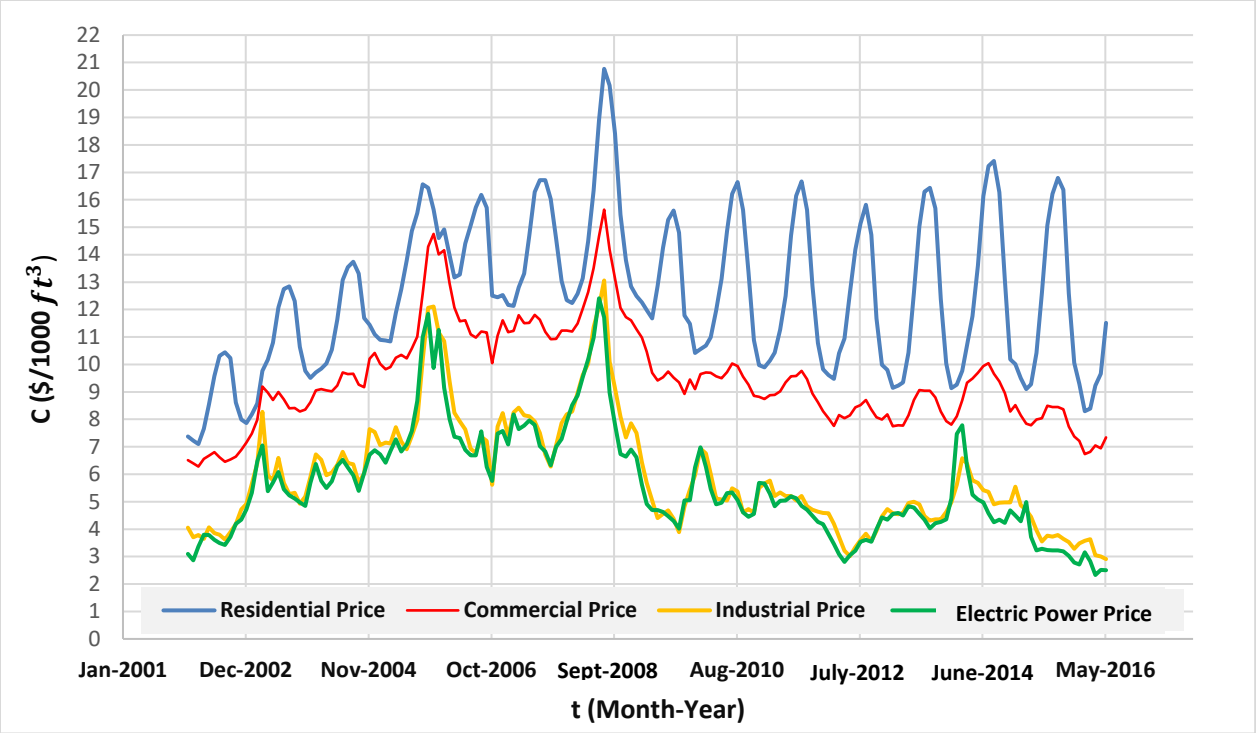

Fig. 56. Standard natural gas cost over the last 15 years for different types of consumers [reproduced from Ref. 23]

In conclusion, the total energy reclaimed from the DA's vented steam by the vent condenser in 2016 was about $4.38\ x\ 10^9\ Btu$ as heated condensate water and condensed steam. While $8.92\ x\ 10^8\ Btu$ as heated make-up water was reclaimed from the boilers' blowdown water by using the basement heat exchanger between January to September of 2016. The total natural gas savings by using both heat exchangers in the KU SPP was about $5.64\ x\ 10^6\ ft^3$, which represents about $ 14,110 for the power plant.

Chapter Four: Re-evaluation of CSP/VSP Power Consumption Based on Calibrated Flow Rates and New Operating Conditions

The pumping system in the KU SPP has four pumps to pump the condensate water at a pressure of 40-50 psig to the DA and the vent condenser (explained in Chapter One). In order to balance "wear" on the pumps, each one is run for one week during each month. Three of these pumps are constant speed pumps, while the fourth is a pair variable speed pumps, which were previously installed by Schmidt [4]. Two pumps are involved in the power evaluation: the constant speed pump (CSP) is a Worthington D-824 (see App. D1), and the variable speed pumps (VSP) are Grundfos CRE 15-3 (see App. D2). The pair of variable speed pump are connected to the same suction and discharge pipe lines, and they can work together or separately depending upon need. The control system of the VSP has two operation modes: pressure control mode which drives the pumps' speeds depending upon the desired discharge pressure, and level control mode which drives the pumps' speeds depending on the desired condensate water level inside the DA.

Power consumption and evaluation were conducted in the previous studies [2, 3, 4] based on the two types (CSP and VSP) of pumps, as well as the two operating modes for the Grundfos VSP. The power consumption for the pumping systems was based on calibrated flow rates using calibration curves (see Section 1.5.2) for the Siemens flow meter downstream the CSP and VSP. Data was recorded around the Worthington and Grundfos pumps by employing flow meters, pressure transducers and power transmitters (these instruments are given in detail in Sections 4.1 and 4.2). This data was recorded continuously as long as these pumps were running in order to compute the annually consumed power of the CSP and VSP.

4.1 Constant Speed Pumping System (CSP)

In previous studies [2, 3], three methods were used to determine the power of the CSP in the KU SPP. Those methods were: recording the consumed power using a power meter with a data logger; using the Worthington pump's performance curves (see the pump curve in App. D1), and computing the power based on the pump operating's characteristics. These three methods can be used to verify the pump's consumed power for different operating conditions. For comparison, the percentage error was computed among the three methods. In this study, the calculated power consumption is based on corrected flow meter readings by employing the calibration curve from Fig. 18.

Even though the Worthington pump has a constant rotational speed and impeller diameter, the output pressure varies between 40-50 psig, because it depends on the system operating point (where the pump curve and the system curve intersect).

The condensate water loses 7-10 psig between the pumps and the DA due to DA elevation change, frictional losses in the pipes, and elbow and valve losses in the pipe line. Then, pressure is reduced to 8-10 psig by the control valve in order to meet the DA's operating conditions. For any pumping system, the performance curve is essential for evaluating the required power and the efficiency at any operating point of the system.

For a known pump, the impeller diameter and motor speed are constant, so the pump curve is fixed. The operating point on the pump's curve is dependent upon the characteristics of the pumping system in which it is operating. The operating point of a pump is a relationship between pump flow rate and hydraulic losses in a system. So, this point changes as the system's properties change, such as frictional losses in the pipe line and valves opening/closing.

The operation point can be represented as parabolic shape, shown in Fig. 57, because the frictional losses vary with flow rate squared for the system curve. A pump curve is essentially experiential data on a pump's ability to produce a flow rate versus discharge head.

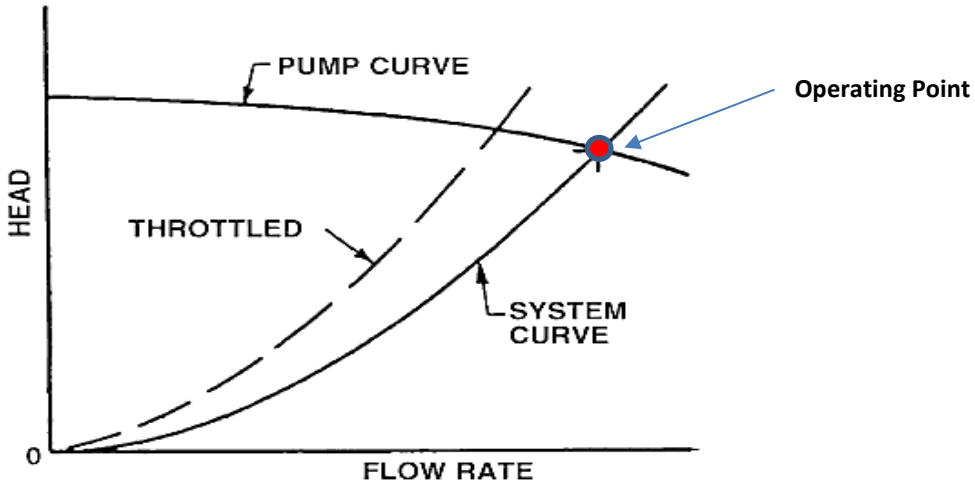

Fig. 57. Typical pump curve for a constant speed pumping system
[reproduced from Ref. 24]

By plotting the system curve and pump curve together, the following can be determined:

1. where the pump will operate on the curve.
2. changes that may occur in the pump's operating conditions, including the pump efficiency [24].

The performance curve in Fig. 57 is for a pumping system where the suction and the discharge levels are the same; so there is no static head in the system curve.

The system curve in this case starts at zero head and zero flow, so a parabolic shape results from the frictional losses along the pipe line. However, the shape of the curve can be changed when a throttling valve is used, such as the DA's control valve of the KU SPP.

The system curve can be started from a positive or negative head in addition to the frictional losses through the pumping system. A positive static head shifts the curve up for the pump at the zero flow rate (see Fig. 59).

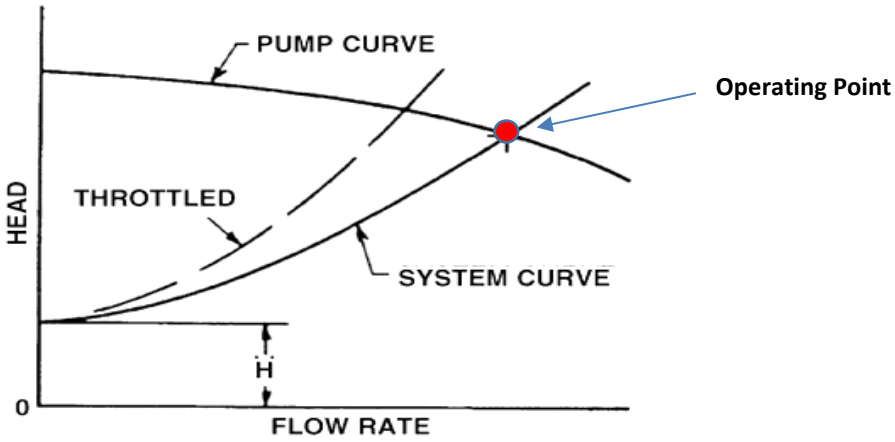

Fig. 58. Typical pump curve for a constant speed pumping system with a positive static head (H) [reproduced from Ref. 24]

For a specific system, same flow occurs due to gravity alone. That means the suction side head of the pump is above that of the discharge side, and such a system has pump curve with negative initial head (see Fig. 59).

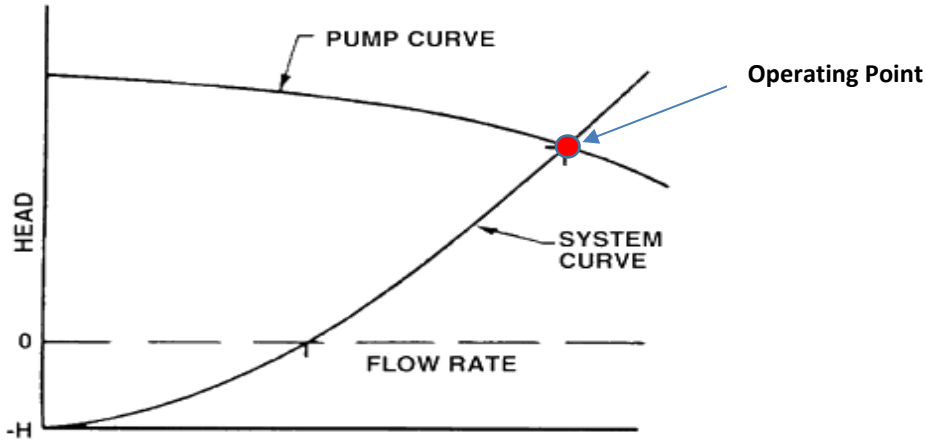

Fig. 59. Typical pump curve for a constant speed pumping system with a negative static head (-H) [reproduced from Ref. 24]

For the KU SPP condensate water pumping system, the Worthington pump curve is fixed, but the system curve is mainly affected by the throttle valve in the condensate water pipe line before the

DA. That valve has a major effect on the operating point of the system curve since it affects the pump flow rate and discharge pressure (or the positive static head). Figure 60 shows the performance curve for the Worthington D-824 (CSP). The pump's power and the efficiency can be found in Fig. 60 by knowing the flow rate (in gpm) or the pressure head (in ft).

The marked point (red triangle) on the pump curve in Fig. 60 represents the maximum operational limit of the Worthington pump that is used in the KU SPP. The operational limits for the Worthington pump in the KU SPP are 225 gpm and 105 ft for the pump discharge flow rate and pressure head, respectively.

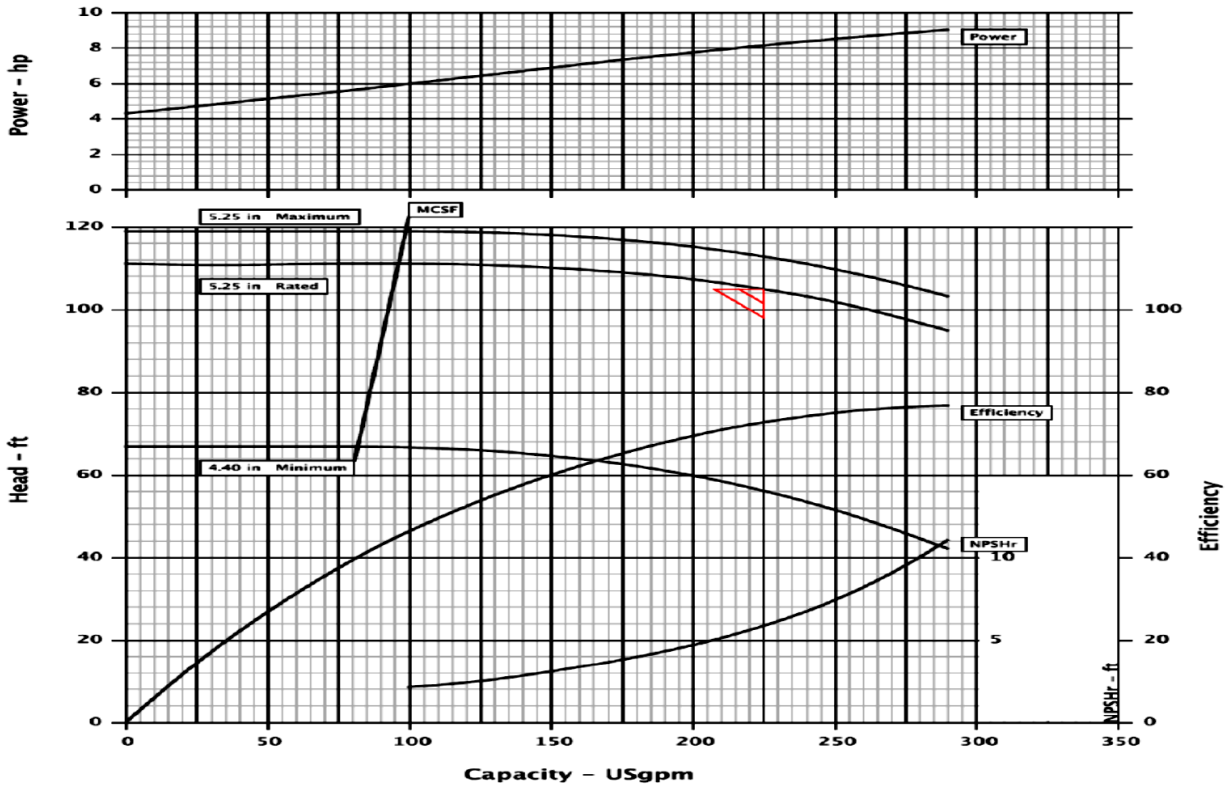

Fig. 60. Worthington D-824 performance curve [reproduced from App. D1]

By knowing the flow rate and discharge pressure of the pump, the hydraulic horsepower of the pump can be computed (see Eq. 4.27). Once the hydraulic horsepower is known, the brake horsepower can be determined as

$$\dot{W}\ (bhp) = \frac{\dot{W}\ (hhp)}{\eta_P} \tag{4.26}$$

based on the pump efficiency that can be found from the manufacturer's pump curve (Fig. 60). For power in kW, and given the overall efficiency of the pumping system (i.e., the pump and the motor efficiencies) the total brake power of the pumping system is [25]

$$\dot{W} = \frac{m\ \Delta P}{C_2\ \eta_P\ \eta_m}\ (C_3) \tag{4.27}$$

where $C_2 = 1714\ \frac{lb_f\ gpm}{in^2\ hp}, and\ C_3 = 0.746\ \frac{kW}{hp}$. All terms in Eqs. (4.26) and (4.27) are defined in the Nomenclature; and ΔP is the pressure rise from the suction to the discharge sides of the Worthington pump.

The efficiency that is found from the performance curve of the Worthington pump in Fig. 60 is the pump efficiency (η_P), while the motor efficiency (η_m) was 0.875, as shown on the manufacturer's specification tag (a picture of the motor tag is in App. D1-1).

4.1.1 Re-evaluation of the Power Consumption for the Worthington CSP Based on the Flow Rate Calibration Curve

Even though the Worthington pump in the KU SPP has a fixed rotational speed, the power is not constant because of the changing operating point on the pump curve. The operating point is dependent upon the pump flow rate and discharge pressure (including static head). The operating point for the Worthington pump varies with throttling by the DA's control valve in order to control how much condensate water is needed in the DA to meet the steam demand.

A Siemens flow meter (Siemens Mag 5100 W DN 100, see App. A8) and a pressure sensor (Omega pressure transducer PX43E0-200GI, see App. D3) are employed to measure the flow rate and the pump's discharge pressure at minute time intervals, and these data is recorded by the HOBO data logger. A power monitoring transducer (Veris Power Monitoring H8044-0100-2 current transducers, see App. D4) is employed to record the power consumption by the pump. All measuring sensors and instruments were installed by Schmidt in a previous study [4]. It was found later during this study that the Omega pressure sensor was reading about 2 psig higher than the actual value. So, this sensor was replaced with a Danfoss pressure sensor (MBS3000, see App. D6), and that pressure reading error was corrected in the power calculations that were based on the Omega sensor.

The power consumed by the Worthington pump was recorded at minute time intervals for a week every month from February until August. During February 8-15, 2016, the pump's average flow rate was 192.2 gpm, the average discharge pressure was 44.11 psig, and the average recorded power consumed was 5.45 kW. However, the recorded flow rate was corrected by using the correction equation (Eq. (1.8)) from the calibration curve in Fig. 18. So, the flow rate value that was considered in the power calculations was the calibrated value, which is 198.8 gpm, instead of 192.2 gpm.

The power was evaluated by another method using the pump curve in Fig. 60. The required power and the efficiency of the pump were read from the performance curve depending only on the calibrated flow rate. Therefore, the power consumption was found to be 5.8 kW during the period February 8-15, 2016.

The consumed power by the Worthington pump was also computed by employing Eq. (4.27) in order to verify the validity of the recorded power consumption by more than method. For instance, the consumed power during the same period in February, 2016 was calculated based on the average data gathered during that week as (which is based on the calibrated flow rate)

$$\dot{W} = \frac{(198.8\ gpm)\ (42.46\ psig)}{\left(1714\ \frac{lb_f\ gpm}{in^2\ hp}\right)(0.69\ x\ 0.875)}\left(0.746\ \frac{kW}{hp}\right) = 6.08\ kW$$

where ΔP is difference between the pump discharge pressure (44.11 psig) and the suction pressure (average 1.65 psig) on the inlet side of the Worthington pump. This was the average brake horsepower (in kW) for the Worthington pumping system. The pump efficiency was determined to be 69% from the pump performance curve by using the calibrated flow rate (198.8 gpm). The three power calculations show that the Eq. (4.27)'s power value was the highest among the three methods.

Figure 61 shows the recorded data for the CSP from February 8-15, 2016. The sudden effect of throttling can be recognized from the data plot of the flow rate and the discharge pressure. The areas in the red circles (as examples) show when the DA's control valve throttled the flow more. Also, it can be seen in Fig. 61 that the corrected flow rate was higher most of the time, approximately 6-7 gpm, than the recorded flow rate from the Siemens flow meter sensor; and that difference makes the calculated power higher when using Eq. (4.27).

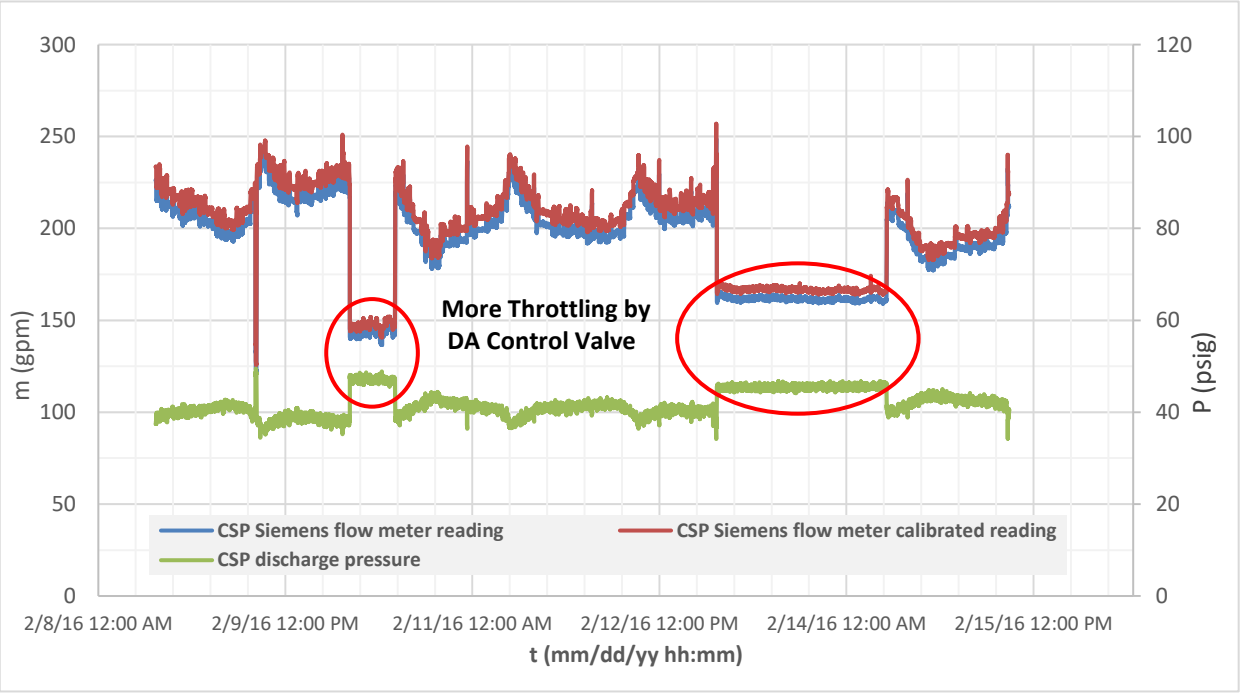

Fig. 61. Worthington CSP flow rate and pressure readings for February 8-15, 2016

Due to the high steam demand during March 14-20 (Fig. 62), more condensate water was needed by the DA, so the DA control valve opened for more condensate water to flow in; and, as a result, the pump's discharge pressure went down. The pump's characteristics in March were an average of 183 gpm, 44.2 psig, and 5.74 kW.

The pump curve shows that the average power was 5.67 kW based on the calibrated flow rate. Employing Eq. (4.27), the consumed power by the Worthington during that period was determined to be 4.47 kW using the calibrated flow rate.

Since the DA control valve was releasing more water to meet the steam demand during the period of March 14-20, 2016, the flow rate and the discharge pressure were inversely related as shown in Figs. 62 and 63. So, in Fig. 62, flow and pressure characteristics are analyzed on the first day (March 14 or Point A) and on the last day (March 20 or Point B) of that period in order to understand how the power and the efficiency respond to such a change in the operating conditions.

At Point A, when the flow was about 157 gpm, the recorded power was 5.4 kW, and the pumping system efficiency was 60%. At Point B, the power was 6.1 kW, and the efficiency was about 72% when the condensate water flow rate was about 220 gpm.

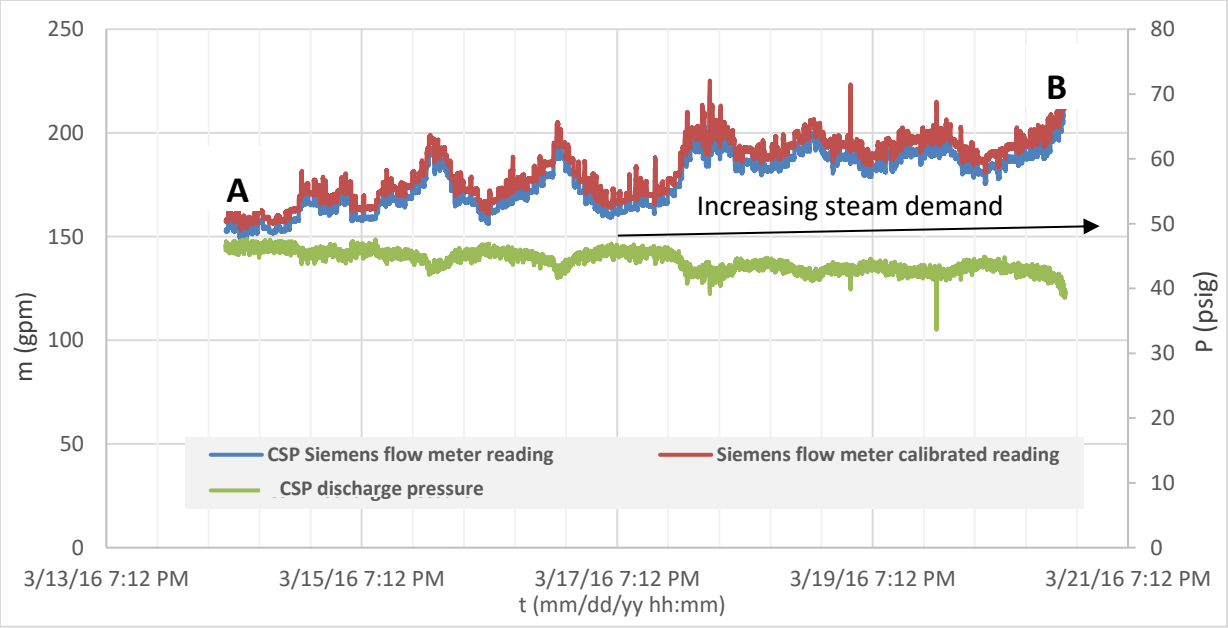

Fig. 62. Worthington CSP flow rate and pressure readings for March 14-20, 2016

The pump curve in Fig. 60 shows that, even though the Worthington pump consumed more power as the flow rate increased, the pump efficiency also increased. That can be explained because pump efficiency is proportional to the hydraulic horsepower of the pump, which is dependent mainly on the produced flow rate and pressure, according to Eq. (4.27).

Figure 63 shows the recorded flow rate and the discharge pressure of the pump for April 4 to 11, 2016. The average calibrated flow rate was about 150 gpm, and the discharge pressure was about 47 psig (see Tables 16 and 17 for power consumption during this period). The vent condenser pipe line was isolated between 4/6/16 8:49 AM and 4/8/16 9:09 AM due to urgent pipe line maintenance. As a result, the pressure in the pipe line before the vent condenser increased suddenly from about 42 psig to 51 psig because the condensate water was trapped in the vent condenser pipe line. This caused the flow rate to drop from about 175 gpm to 75 gpm during that period.

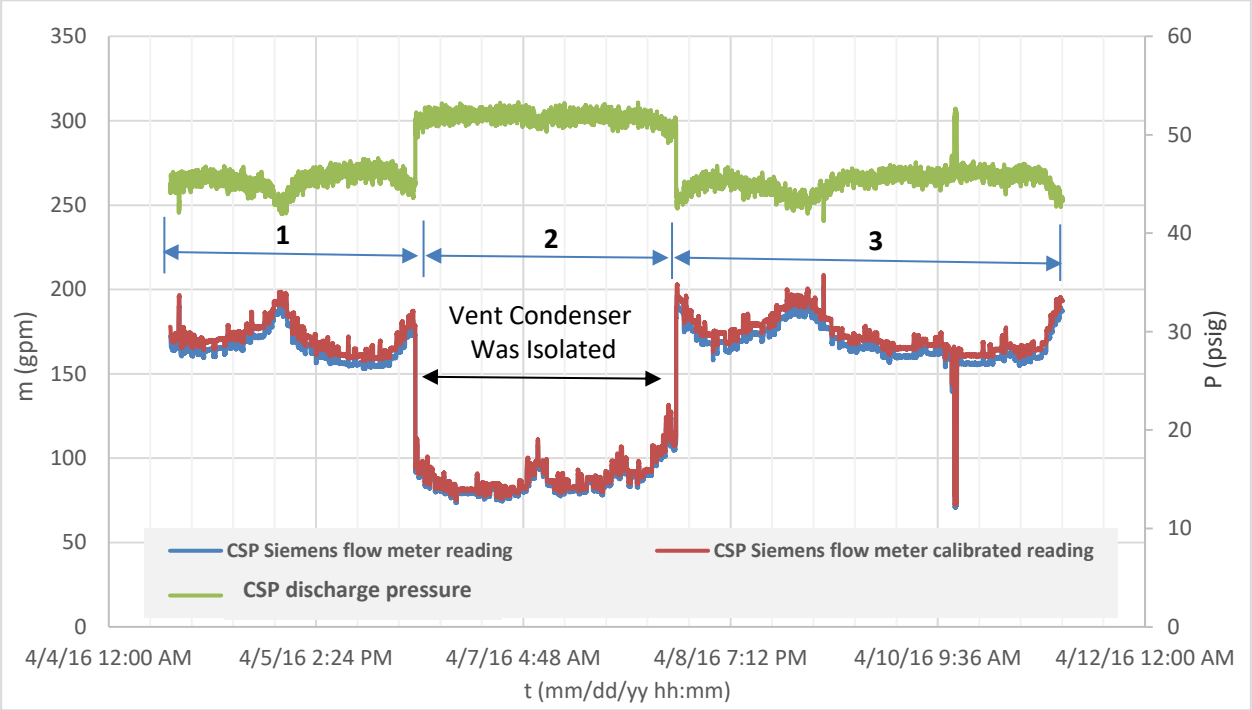

Fig. 63. Worthington CSP flow rate and pressure readings for April 4-11, 2016

All gathered data (i.e., power, flow rate, and pressure) around the pump was averaged for use in the power calculation, but it was not accurate to use the average values for some months when the data was varying in different operating ranges, such as in Figs. 61, 62, and 63. So, time-weighted readings were used for the periods when there were dramatic changes (see reading changes in Figs. 61, 62, and 63). For example, for April, the data was time-weighted based on three time periods (see Fig. 63).

Power evaluation based on the three approaches (i.e., recorded, pump curve value, and Eq. (4.27)) was performed for each period separately. Then, the three periods were time-weighted as shown in Table 16.

Table 16 shows the three periods in Fig. 63 with time-weighting for each period, where the total time for the three periods was 165.5 hours.

Table 16. Time-weighted power consumption calculation for April, 2016 data shown in Fig. 63

	Period 1 (171.5 gpm; 45 psig)	Period 2 (88.7 gpm; 51.8 psig)	Period 3 (173 gpm; 45.3 psig)
Power by Power Transducers $\dot{W}_1$ (kW)	5.60	4.47	5.60
Power by Pump Curve $\dot{W}_2$ (kW)	5.43	4.33	5.37
Power by Eq. (4.27) $\dot{W}_3$ (kW)	5.12	4.38	5.19
Period Time-weighted $(\frac{Period\ Length\ (hr)}{165.5\ (hr)})$	$\frac{45.4}{165.5}$	$\frac{48.1}{165.5}$	$\frac{72}{165.5}$
Total Time-weighted $\dot{W}_1$ (kW)	5.60 $(\frac{45.4}{165.5})$ + 4.47 $(\frac{48.1}{165.5})$ + 5.60 $(\frac{72}{165.5})$ = 5.27		
Total Time-weighted $\dot{W}_2$ (kW)	5.43 $(\frac{45.4}{165.5})$ + 4.33 $(\frac{48.1}{165.5})$ + 5.37 $(\frac{72}{165.5})$ = 5.09		
Total Time-weighted $\dot{W}_3$ (kW)	5.12 $(\frac{45.4}{165.5})$ + 4.38 $(\frac{48.1}{165.5})$ + 5.19 $(\frac{72}{165.5})$ = 4.94		

The time-weighting process was conducted for February, March, and April. It was not needed for other months (May, June, July, and August) because all readings during those months were consistently in the same ranges. So time-weighting would not change the final result (see App. D5 for plotted data for May, June, and July). Table 17 shows the average power consumption by the Worthington constant speed pump for the months of February to August for the three different approaches.

Table 17. Comparative evaluation of power consumption of the Worthington CSP as determined by three methods, from February to August, 2016

Month, days	Recorded Power by Data Logger $\dot{W}_1$ (kW)	Power Based on the Pump Performance Curve $\dot{W}_2$ (kW)	Power Computed by Eq. (4.27) $\dot{W}_3$ (kW)
February, 8-15	5.95	5.80	5.54
March, 14-20	5.74	5.50	5.59
April, 4-11	5.27	5.09	5.65
May, 3-9	5.48	5.15	5.68
June, 1-6	5.19	4.92	5.34
July, 2-9	5.52	5.37	5.54
August, 22-29	5.63	5.37	5.68

The percent differences among the three power results are shown in Table 18. Equation (4.28) was employed to determine the difference between recorded and the pump curve values. Equation (4.29) was employed to determine the difference between recorded and computed [from Eq. (4.27)] values. Equation (4.30) was employed to determine the difference between pump curve and computed (from Eq. (4.27)) values.

$$e_1\ (\%) = \frac{\dot{W}_1 - \dot{W}_2}{\dot{W}_1}\ (100) \tag{4.28}$$

$$e_2\ (\%) = \frac{\dot{W}_1 - \dot{W}_3}{\dot{W}_1}\ (100) \tag{4.29}$$

$$e_3\ (\%) = \frac{\dot{W}_2 - \dot{W}_3}{\dot{W}_2}\ (100) \tag{4.30}$$

The idea behind calculating the differences was to determine which two methods of calculating the power consumption agreed better, which indicated the more trustworthy approach (or approaches) to be considered in the Worthington power consumption evaluation.

Table 18. Percent differences among the three methods of calculating the power consumption of the Worthington pump

Month, days	e_1 (%)	e_2 (%)	e_3 (%)
February 8-15	2.52	6.84	4.43
March 14-20	4.18	2.64	-1.61
April 4-11	3.42	-7.13	-10.92
May 3-9	6.02	-3.65	-10.29
June 1-6	5.20	-2.84	-8.84
July 2-9	2.72	-0.41	-3.22
August 22-29	4.60	-0.89	-5.75

Table 18 shows that the most stable difference values were between the recorded power and the pump curve power (i.e., e_1), while e_2 and e_3 fluctuated between positive and negative values. It was concluded from Tables 17 and 18 that the most trustworthy power value was $\dot{W}_1$ for the following reasons. Table 18 shows that e_1 was more stable because of more consistent readings of $\dot{W}_1$ and $\dot{W}_2$. However, the power and the efficiency that were found from the pump curve may have been subject to about a 3-5% error because they were determined based on using the pump curve chart manually. That chart has some error in reading values, especially the power value because the chart can give the same power value for any flow rate value within about $\pm$ 5 gpm (see Fig. 60), which means inaccurate readings of $\dot{W}_2$.

Since $\dot{W}_3$ was dependent upon the data that were gathered by the flow and pressure instrumentation, that means the computed power was subject to many errors which were

associated with the employed instrumentation. Pump aging may have also reduced the pump efficiency over time which increased the consumed power. Thus, the computed power by Eq. (4.27) may have been higher than that shown in Table 17, which would increase the value of e_3.

In conclusion, the power value obtained by power monitoring transducers ($\dot{W}_1$) can be considered as the most trustworthy value in the Worthington power consumption calculations because this method depends on measuring the current flow through the pump power supply wiring with high accuracy ($\pm$1%) of the rated current reading [26].

4.2 Variable Speed Pumping System (VSP)

The Grundfos CRE15-3 pumping system (HYDRO MPC E 2CRE15-03 3X460V BASIS 60Hz, see App. D2) is a pair of pumps that work simultaneously in a controlled process depending on desired set point of pressure or level. These pumps are rotational speed controlled, and each pump is equipped with an integrated variable frequency drive motor (VFD). The system performance is adapted to the load or the demand through cutting in/out the pumps. The pumping system can provide a pressure of 232 psig and a flow rate of 244 gpm as a maximum operating limit [27]. This system can operate in two control modes: pressure and level.

4.2.1 Pressure Control Operation Mode

The pressure control operation mode depends on setting the desired discharge pressure of the pumps. For the Grundfos CRE15-3, the pressure mode target is set to 3 bar (43.5 psig). The GCS has a pressure sensor (Danfoss pressure transducer MBS 3000, see App. D6) to read the discharge pressure of the pumps and compare it with the set point. The VFD system runs one or both pumps, or operates them at different rotational speeds in order to maintain the pressure set point when the flow rate demand of the condensate water varies.

As an operational principle, this mode is similar to that of the Worthington CSP because the pumps' discharge pressure in this case still needs to be controlled at the DA in order to reduce the pressure to 8-10 psig. Even though the needed pressure in this mode is constant, the pumps' speed varies usually between 86%-99% of full speed, in order to meet the flow demand.

It is possible to run the pumps in the pressure control mode at low pressures (about 8-10 psig at the DA) to meet the DA required pressure. So there would be no need to use the control valve before the DA. The advantage of this mode is saving more energy by running the pumps at low pressure, as well as there would be no losses due to diverting the excess condensate water. However, there is a disadvantage in operating at low pressure because that pressure will not be high enough to force the condensate water reach the vent condenser; so no energy is recovered from the DA's vented steam.

4.2.2 Level Control Operation Mode

The level control mode depends on the desired set point of the condensate water level inside the DA. The VFD controls the pumps' speeds to increase and decrease the flow rate in order to keep the water level at 52% of the tank's total volume capacity. There is a magnetic level transducer, Gems-Suresite [28], that was installed by Schmidt [4] at the DA tank in order to sense the water level and send the signal to the GCS. The discharge pressure of this mode is lower than that of the pressure mode (about 10-25 psig), and the DA control valve is kept fully open. That is because there is no need to use the control valve to reduce the pressure as long as the target tank level is maintained by the pumping system.

So, with this pressure range (i.e., 10-25 psig), the provided pressure head is between 25-60 ft. which is, in some cases, not enough to reach the vent condenser on the first floor because the vent condenser is at an elevation of about 40 ft. above the pumps (which means at least 17 psig is needed, see Eq. (4.31)). Since 10-25 psig is not always enough to push the condensate water to the vent condenser, the vent condenser's steam pipe line is isolated by closing a manual valve, whenever this mode is used. The vent condenser is isolated whenever the level mode is used because, only the steam would flow through the vent condenser, while no condensate water would flow due to the low pressure head. This would increase the temperature of the vent condenser's metal to more than 200 $^{\circ}$F. So the steam line had to be closed in order to keep the vent condenser from overheating.

At high flow demand, both pumps run at full speed; and once the demand is met, the VFD starts reducing both pumps speed until they reach 70% of full speed. Then if the flow rate needs to reduce further, one of the pumps is shut down, while the other keeps running until it reaches 42% of full speed. This is the minimum performance point of the VSP pumping system. The minimum performance was set at 42% of full speed after many operational trials had been conducted in the previous studies [2, 4]. The minimum performance mode was set in order to keep condensate water flowing into the DA whenever the set point is met.

The minimum performance mode was also used to protect the piping and pumping systems from steam backflow from the DA to the pumps, by keeping the condensate water always flowing toward the DA. Once the pumps speeds went below 42%, the pressure in the condensate water pipe line was not enough to overcome the DA's steam pressure, which caused pressure hammering in the pipe lines, according to Alabdullah [2].

Whenever the condensate water level went below 52% of the DA's full level, the minimum performance mode was deactivated; and the running pump started speeding up until it reached 70% of full speed. Once this speed was reached, the other pump was automatically activated by the GCS in order to run simultaneously and maintain the desired set point.

4.2.3 Re-evaluation of the Power Consumption for the Grundfos CRE15-3 VSP Based on the Flow Rate Calibration Curve

The operating principle of the VSP is different than that the CSP because the operating point of the Worthington is dependent only upon changes in the system curve due to DA control valve action. The CSP pump curve is fixed since the impeller diameter and the pump rotational speed are constant. On the other hand, the operating point of the Grundfos pumps is dependent upon both pump curve and the system curve. The pump curve changes with the pump rotational speed. Figure 64 shows the Grundfos CRE15-3 pump curves at different speeds.

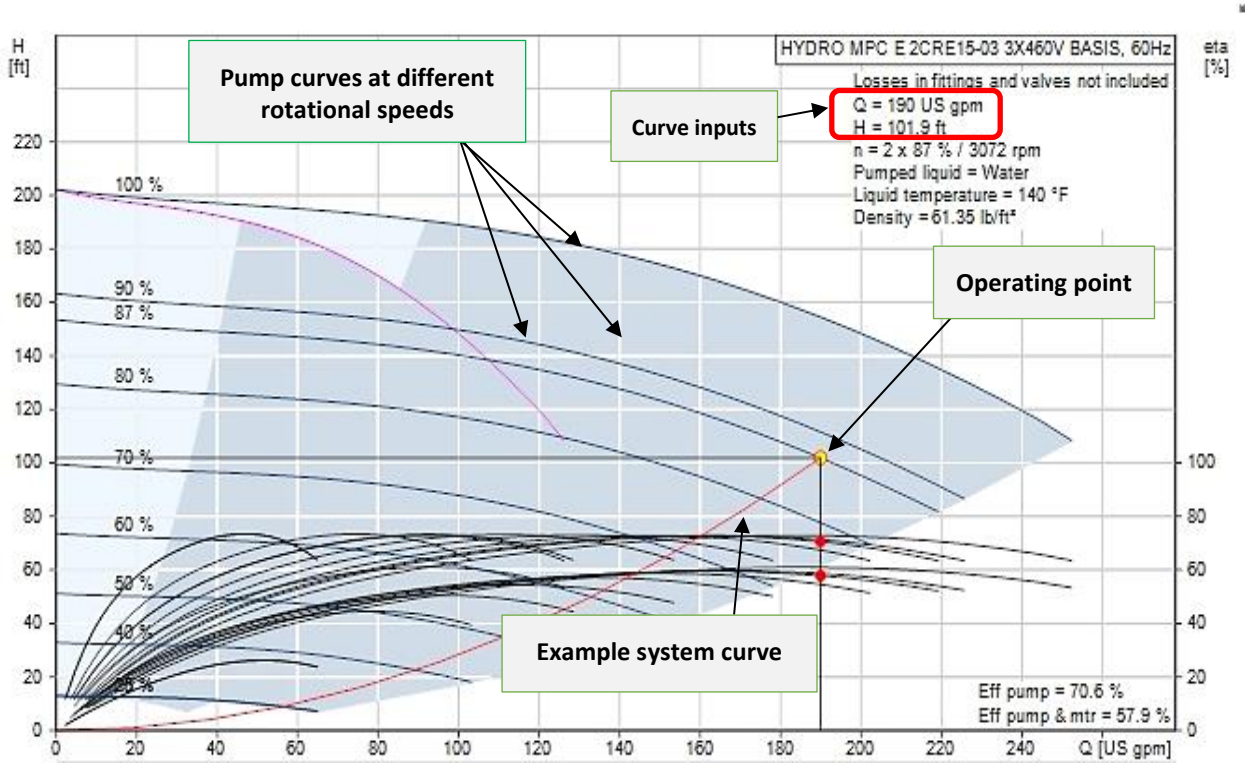

Fig. 64. Grundfos CRE15-3 variable speed pumping system curve [29]

Figure 64 shows a sample of the multiple pump curves for the Grundfos CRE15-3, unlike the constant speed pumping system that has just one curve. As an example, the operating point in Fig. 64 is defined at the pump speed (87 % line) with a flow rate 190 gpm. The pumps' power, the pump efficiency and the overall pumping system's efficiency are determined by using the flow rate and pressure head as the curves inputs. So, these inputs produce the operating point in the performance curve as shown in Fig. 64.

The system curve is dependent upon the flow rate and pressure head (in ft.) for a variable pumping system. However, since the pressure control mode maintains the pressure constant around the set point, which means the pump head is almost constant, the system curve is dependent upon the flow rate only.

The operating point at which the system curve and the pump curve intersect is defined by flow rate and pressure head. The system curve for the pressure control mode is the same as for the Worthington pump because the system is affected by DA control valve throttling.

For a pumping system, 1 psig is required to lift 62 °F water 2.31 ft. [30]. Thus, Grundfos CRE15-3 pressure head was found as [31]

$$H = \frac{C_4\,\Delta P}{\gamma} \tag{4.31}$$

where C_4 is $2.31\frac{ft-head}{\frac{lb_f}{in^2}}$, and specific gravity for the condensate water (γ) at about 160 °F is 0.975. See Fig. 65 for the specific gravity of water at different temperatures. ΔP in Eq. (4.31) was employed instead of the discharge pressure, so H was computed for the pump's real head by excluding the static head due to the pump's inlet pressure.

The net pump head was also computed by subtracting the static head due to the inlet pressure from the pump head due to the discharge pressure as

$$H_{net} = H_P - H_{static} \tag{4.32}$$

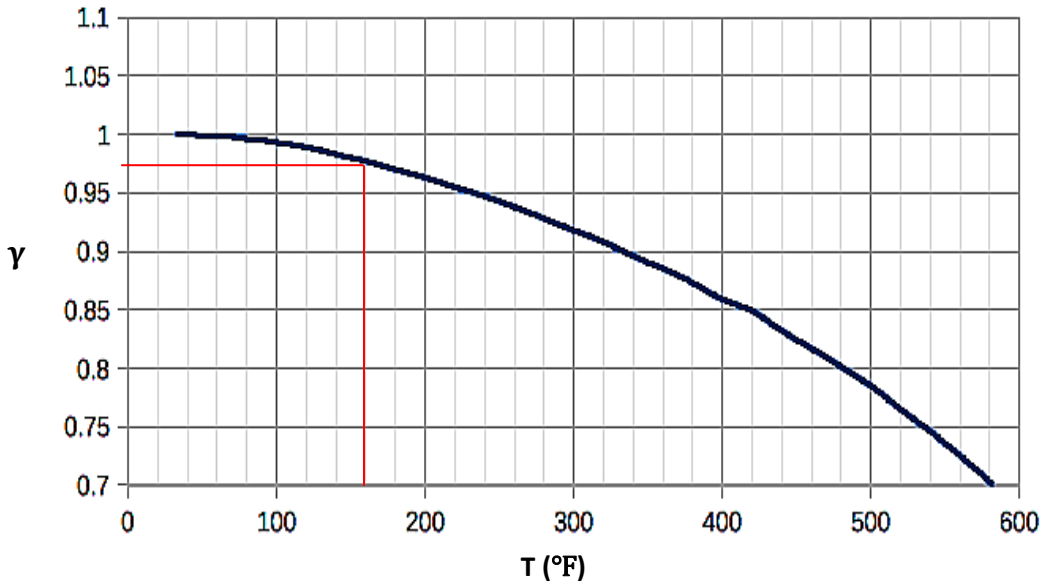

Fig. 65. Water specific gravity chart for 32-580 °F [reproduced from Ref. 32]

The GCS recorded the pumps' discharge pressure, rotational speeds, flow rate, and power consumption. Grundfos E-product PC Tools (see App. D2-1) was used in order to continuously monitor and record these data from the control system.

These parameters were recorded for irregular time intervals (Δt), because the GCS recorded data only when a change occurs in these parameters. However, the Siemens flow meter (Siemens Mag 5100 W DN 100, see App. A8), and the Danfoss pressure sensor (MBS 3000, see App. D6) measured the flow rate and the pump's suction pressure at minute intervals.

Equation (1.9) (see Section 1.5.2) from the flow rate calibration curve in Fig. 19 was employed to correct the Siemens flow meter readings. The average value of the calibrated flow rate was higher by about 5-8 gpm than the recorded flow rate. On the other hand, the flow rates that were recorded by the GCS were, on average, 20-45 gpm higher than the Siemens readings. So, after the Siemens flow rate readings were adjusted using the flow rate calibration curve, the difference from the GCS was reduced to about 13-38 gpm. So, this difference was still high even after using the flow calibration curves.

For the periods March 8-14 and April 13-15, 2016, Figs. 66 and 67 show the flow rate difference between the GCS and the Siemens flow meter readings. Both figures show that the discharge pressure was fairly constant, around 42.9 psig, because of the Grundfos pump pressure control mode. During March and April, the flow rate varied around 180 gpm as measured by the Siemens flow meter, but varied around 200 gpm as recorded by the GCS.

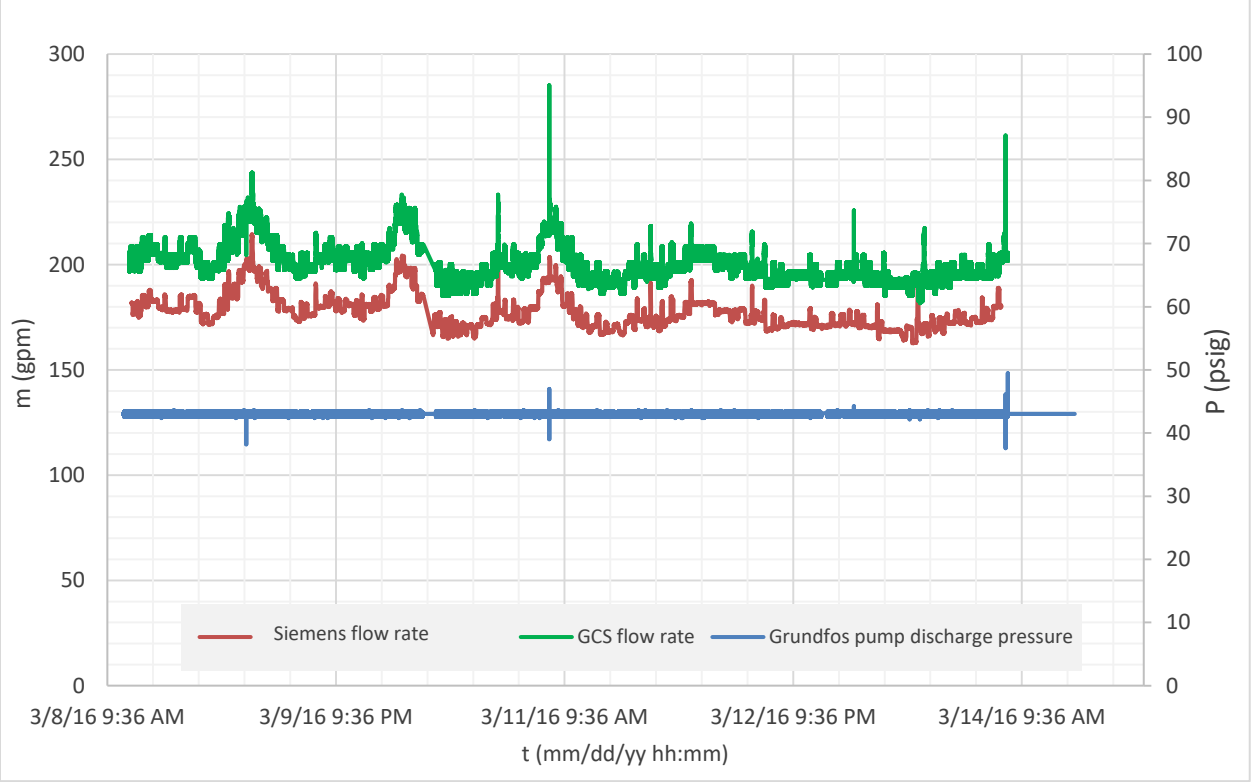

Fig. 66. The flow rate that was read by the GCS and the Siemens flow meter for March 8-14, 2016

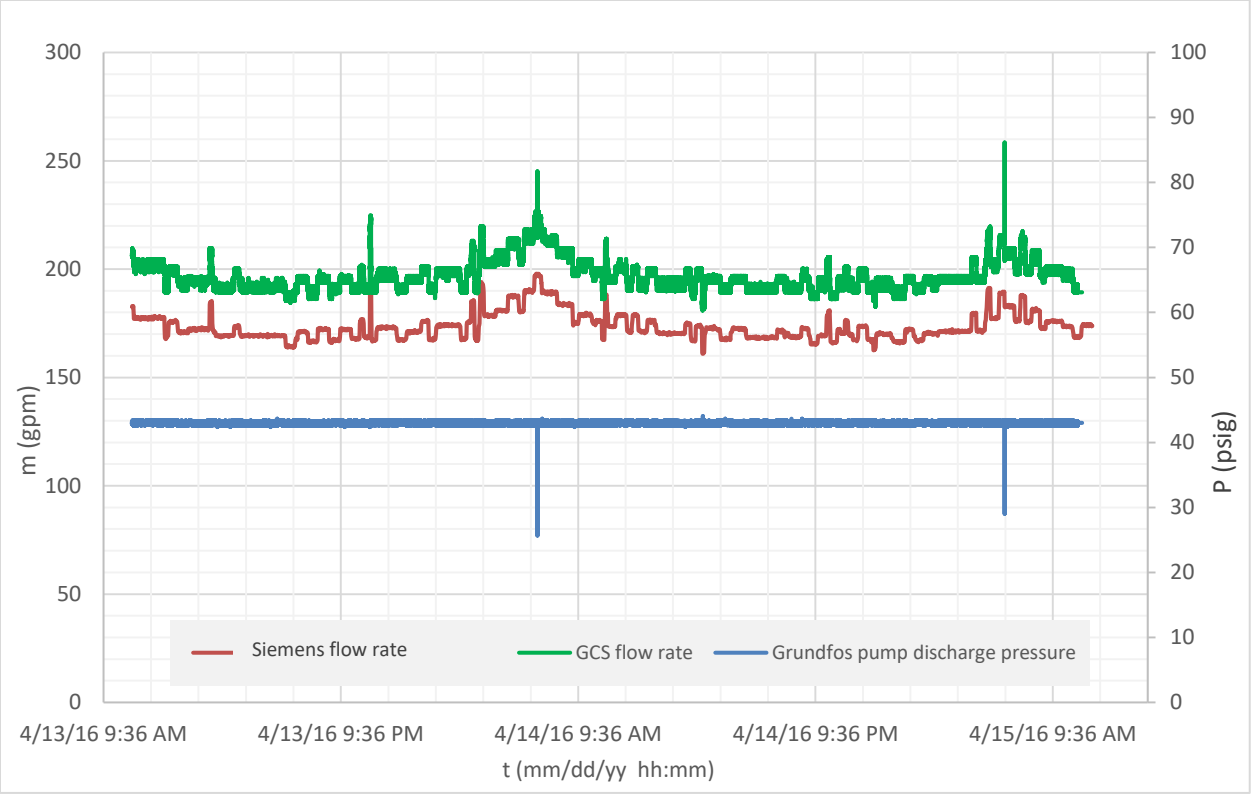

Fig. 67. The flow rate that was read by the GCS and the Siemens flow meter for April 13-15, 2016

The power consumption comparison was based on the power that was recorded by the GCS, taken from the pump curve and computed power using the gathered data (see Eq. (4.33)). Since the power obtained from the pump curve and Eq. (4.33) depended upon the flow rate, the power comparison was conducted twice: by using the GCS flow rate, and the Siemens flow rate. The corrected Siemens flow meter readings were considered to be trustworthy since the flow meter was calibrated (see Section 1.5.2).

Table 19 shows the average flow rates that were recorded by the GCS and the Siemens flow meter, as well as the pump speed and discharge pressure. In February, the pump's speed was higher than for other months because the of the high BFW demand. The higher the pump speed, the greater the flow rate provided at the same pressure. Also, it can be seen from Table 19 that, even though the pump's speed was changed by the GCS in order to maintain the required BFW, the discharge pressure was consistent at about 43 psig.

No data was recorded from the Siemens flow meter in June because the DC power supply and the Hobo data logger were moved during that period to conduct a temperature analysis and tests related to the vent condenser's new RTD sensors.

Table 19. Grundfos pump operation data from February to August according to the GCS and the Siemens flow meter

Month, days	Pumps Speed [percentage of full speed]	P (psig)	m (gpm) [from the GCS]	m (gpm) [calibrated Siemens flow rate]
February 15-22	94 %	42.99	228.5	189.9
March 7-14	88 %	42.98	200.6	177
April 11-18	88 %	42.98	195	175
May 9-14	88 %	42.98	202.5	175.5
June 11-15	86 %	42.92	185.3	No data recorded
July 4-11	85 %	42.92	181	161
August 1-8	88%	42.98	195	160.3

Since the pressure loss between the pumps and the DA is about 8 psig due to piping and the DA's elevation, and the required pressure in the DA is about 10 psig (as a maximum), the condensate water pressure in Table 19 could be set to about 18 psig, instead of about 43 psig. So, a lower power pump could be used to save power. In addition, there would be no need, in this case, to use the DA control valve to throttle the surplus pressure and flow. However, by setting the Grundfos pump discharge pressure to 18 psig (or using a low power pump to provide this pressure), the pressure head is not large enough for the condensate water to reach the vent condenser (at least 17 psig is needed to reach the vent condenser, according to its elevation); so no energy could be recovered from the vented steam.

However, it was found from a previous study [3] that the yearly savings by using the vent condenser was $20,498, while the yearly savings by using a low power pump (meaning that the vent condenser was not used) was $2,505 (see Table 11, Section 4.iii of Ref. 3). So, setting the pump to pressure of 20 psig or using low power pump would not be efficient with regard to possible savings.

Equation (4.27) can be written for the Grundfos CRE15-3 to compute the required pump power. Taking into account the motor, pump and VFD efficiencies, the Grundfos power calculation gives [25]

$$\dot{W} = \frac{m\ \Delta P}{C_2\ \eta_m\ \eta_P\ \eta_{VFD}}\ (C_3) \tag{4.33}$$

All terms are defined in the Nomenclature. The pump and motor efficiencies can be determined from the manufacturer's pump curve (see Figs. 68 and 69).

The VFD efficiency is not known or determined by the pump curve. After contacting the manufacturer, it was found that the VFD efficiency is included with the efficiency that is determined from the curve as an overall efficiency. Figure 68 shows the pump curve for the Grundfos pump during March 7-14, 2016 when using the average GCS flow rate (200 gpm) and the net pump head (98 ft). The net head means that the suction head (≈ 4 ft.) due to the suction pressure (1.7 psig) was subtracted from the pump head (102 ft). The flow rate and net pump head are used as the pump curve's inputs in order to specify the operating, or duty, point of the pump.

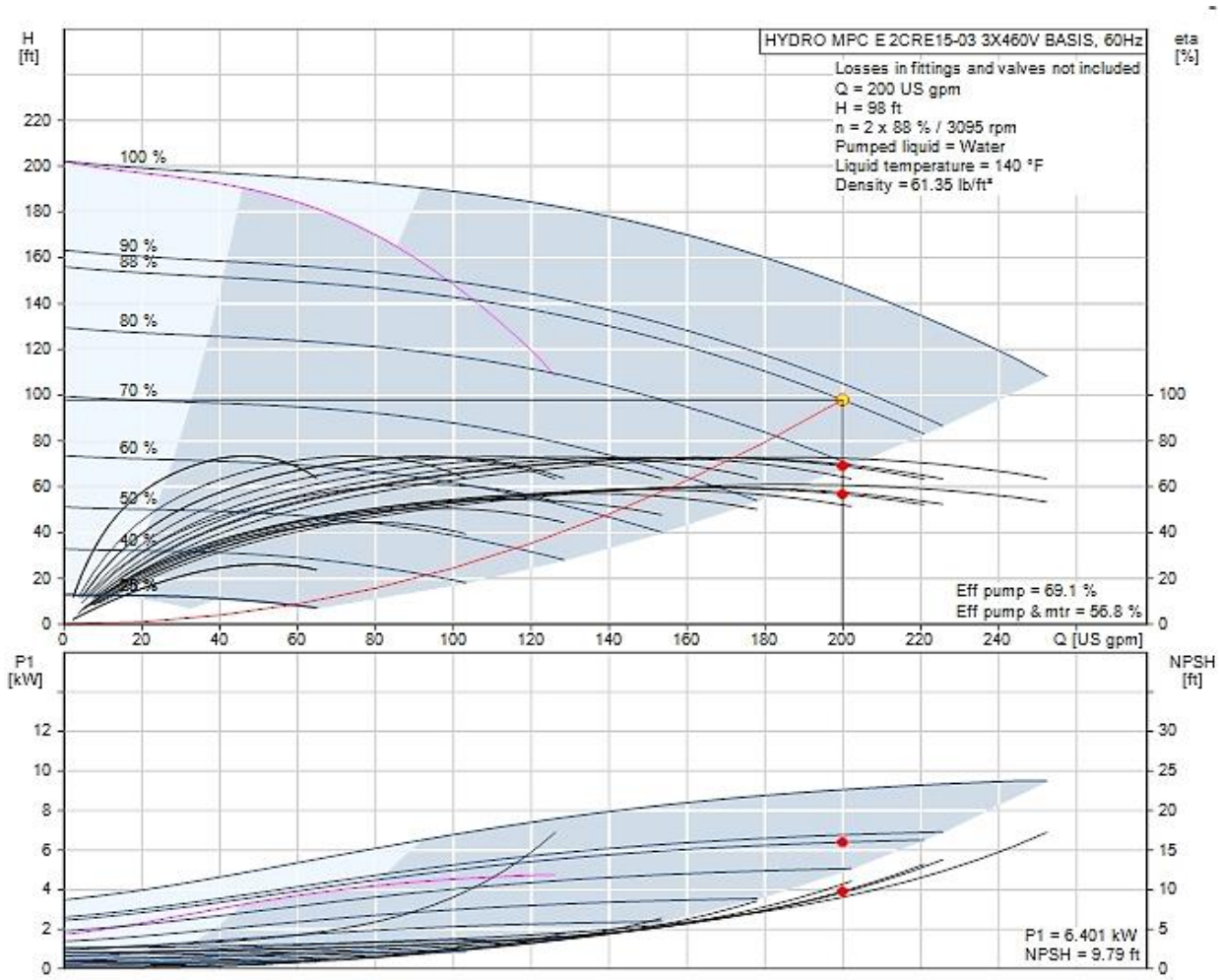

Fig. 68. Performance curve based on the GCS flow rate for March 7-14, 2016 [reproduced from Ref. 29]

It can be noted from Fig. 68 that the operating point of the pump is located at the 88% curve, which represents the pump's actual speed as a percentage of full speed (see Table 18 for the actual recorded percentage speeds). The consumed power that was determined by the pump curve in Fig. 68 was 6.4 kW, and the overall efficency (which included those of the pump, motor, and VFD) was 56.8 %.

Furthermore, the required power that was computed by Eq. (4.33) was 6.35 kW, while the the power that was recorded by the GCS was 6.4 kW. So, the power obtained from the recorded data was about 1.6% less than the recorded or the pump curve values.

Figure 69 shows the performance curve that was based on the average Siemens calibrated flow rate (177 gpm) instead of the GCS's flow rate, and the net pump head for determining the operating point. The consumed power from the pump curve in Fig. 69 was about 5.53 kW, and the overall efficiency was 58.2 %. The required power that was computed by Eq. (4.33) was 5.47 kW. See Table 19 for each month's power that was obtained by the three different approaches.

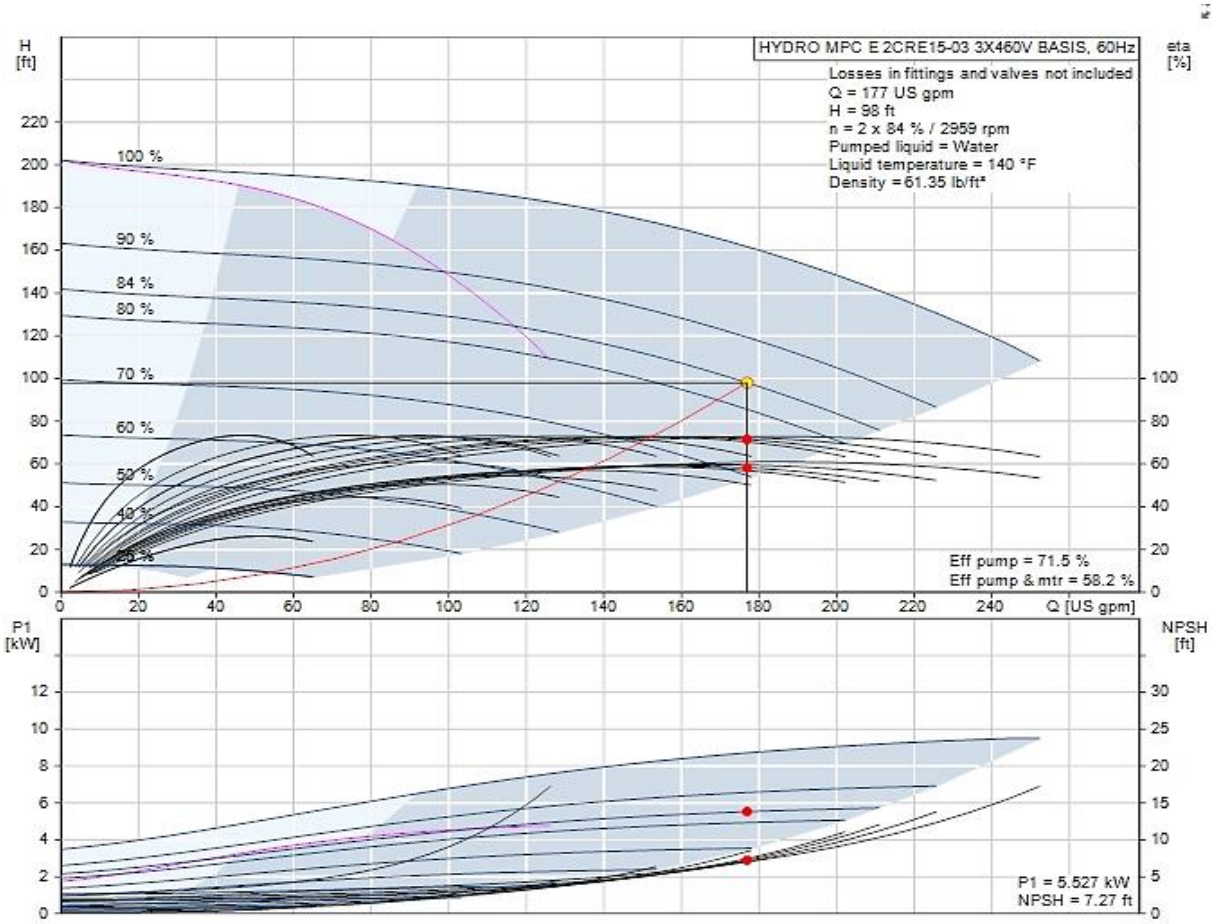

Fig. 69. Pump curve based on the Siemens meter's flow rate for March 7-14, 2016 [reproduced from Ref. 29]

So, the pump curve gave about 13% less than the GCS's recorded power; and the computed power was about 14.5% less than the GCS's recorded power. However, the Grundfos pump power calculation and evaluations were based on the Siemens calibrated flow rate instead of the GCS's flow rate. This is because the GCS flow value is not measured physically by a flow meter or any other measuring device, but is found using a theoretical relationship between the pump speed and head.

This was confirmed because, whenever the GCS's flow rate was applied to the pump curve, the operating point was located on a pump curve where the speed was the same as the actual recorded speed in March. See Table 19 and Fig. 69 for the actual recorded speed and estimated speed from the pump curve.

That information was interpreted as follows. The GCS employs the pump speed and discharge pressure (these two parameters are actually measured) to determine the pump flow rate, using these parameters on a digital pump chart. This procedure was applied to all other months by using GCS flow rates. Table 20 shows the power consumption for the Grundfos CRE15-3 that was obtained by the GCS, the pump curve and Eq. (4.33).

Table 20. Power consumption of the Grundfos VSP (determined by three approaches) from February to August with calculation of percent difference [$\dot{W}_2$ and $\dot{W}_3$ were based on the Siemens flow rate]

	February 15-22	March 7-14	April 11-18	May 9-14	July 4-11	August 1-8
$\dot{W}_1$ (kW)	7.74	6.40	6.81	6.81	5.90	6.47
$\dot{W}_2$ (kW)	6.01	5.53	5.49	5.46	4.96	5.13
$\dot{W}_3$ (kW)	5.90	5.47	5.43	5.41	4.91	4.89
e_1 (%)	22.4	13.5	19.4	19.8	15.9	20.7
e_2 (%)	23.1	14.5	20.2	20.5	16.7	24.4
e_3 (%)	1.0	1.1	1.1	0.9	1.0	4.7

The recorded GCS power ($\dot{W}_1$) is the highest among the three approaches because it depends on the flow rates that were recorded by GCS, which were, on average, 20-45 gpm higher than the Siemens flow rates (see Table 19). The computed differences between the power values that were obtained using the three different approaches were determined using Eqs. (4.28), (4.29), and (4.30).

e_1 and e_2 have the highest differences because both difference depend upon $\dot{W}_1$ which was the largest among the three approaches. Meanwhile, e_3 was very low because it depended upon $\dot{W}_2$ and $\dot{W}_3$; and both power values were determined based on the Siemens flow rate.

Table 21 shows the same calculations of the power consumption and the differences as for Table 20. However, the pump curve power and the computed power were found using the GCS flow rate.

Table 21. Power consumption of the Grundfos VSP (determined by three approaches) from February to August with calculation of percent difference [$\dot{W}_2$ and $\dot{W}_3$ were based on the GCS flow rate]

	February 15-22	March 7-14	April 11-18	May 9-14	July 4-11	August 1-8
$\dot{W}_1$ (kW)	7.74	6.40	6.81	6.81	5.90	6.47
$\dot{W}_2$ (kW)	7.64	6.40	6.59	6.48	5.64	6.35
$\dot{W}_3$ (kW)	7.59	6.35	6.55	6.43	5.55	6.10
e_1 (%)	1.3	0.0	3.2	4.8	4.5	1.9
e_2 (%)	1.9	0.8	3.8	5.6	5.9	5.7
e_3 (%)	0.7	0.8	0.6	0.8	1.5	3.9

Since all of the power consumption values in Table 21 were based on the GCS flow rate, $\dot{W}_1$, $\dot{W}_2$, and $\dot{W}_3$ were very close to each other; and the differences were very small in comparison to those of Table 20.

Tables 20 and 21 show that the recorded GCS ($\dot{W}_1$) power was always higher than power determined from the other methods, while the computed power by Eq. (4.33) ($\dot{W}_3$) was the lowest. In general, the power results in Table 21 are not trustworthy because the GCS flow rate was used.

The difference was computed between each pair of methods in order evaluate which one was more trustworthy. $\dot{W}_2$ and $\dot{W}_3$ power values in Table 20 were determined based on the Siemens flow meter flow rate. On average, e_3, which was based on these power values, was very low in comparison to the other two differences. Therefore, $\dot{W}_2$ and $\dot{W}_3$ were considered to be the most trustworthy for the Grundfos CRE15-3 power evaluation.

More specifically, $\dot{W}_2$ was best because it was determined as outputs from digital pump curve based on the current operating conditions (flow rate and net pressure head). Furthermore, these parameters were recorded from calibrated and tested instruments, while $\dot{W}_3$ could be subject to additional error due to the efficiency factors (η_m, η_P, and η_{VFD}) being affected by pump aging.

In conclusion, Figs. 70 and 71 show the power consumption evaluation for the Worthington 824 CSP and Grundfos CRE15-3 VSP, respectively, between February and August of 2016. These graphs show the three approaches of evaluating the power consumption. The method that was considered the most trustworthy in this study is given in the next paragraph.

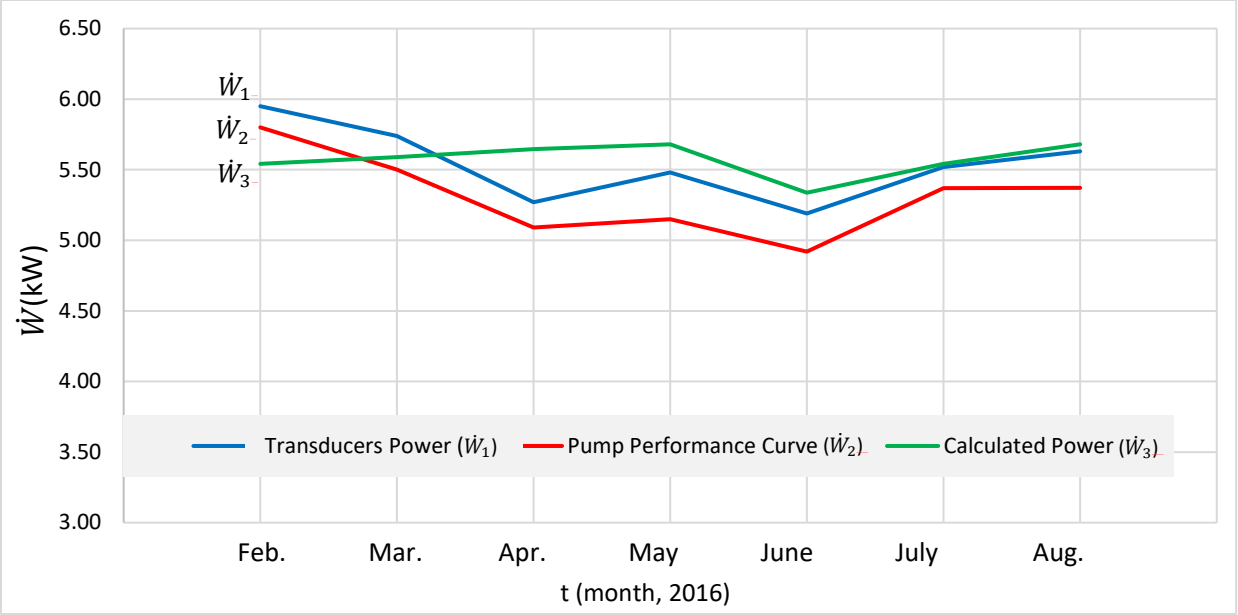

Fig. 70. Power consumption evaluation for the Worthington CSP for February - August, 2016

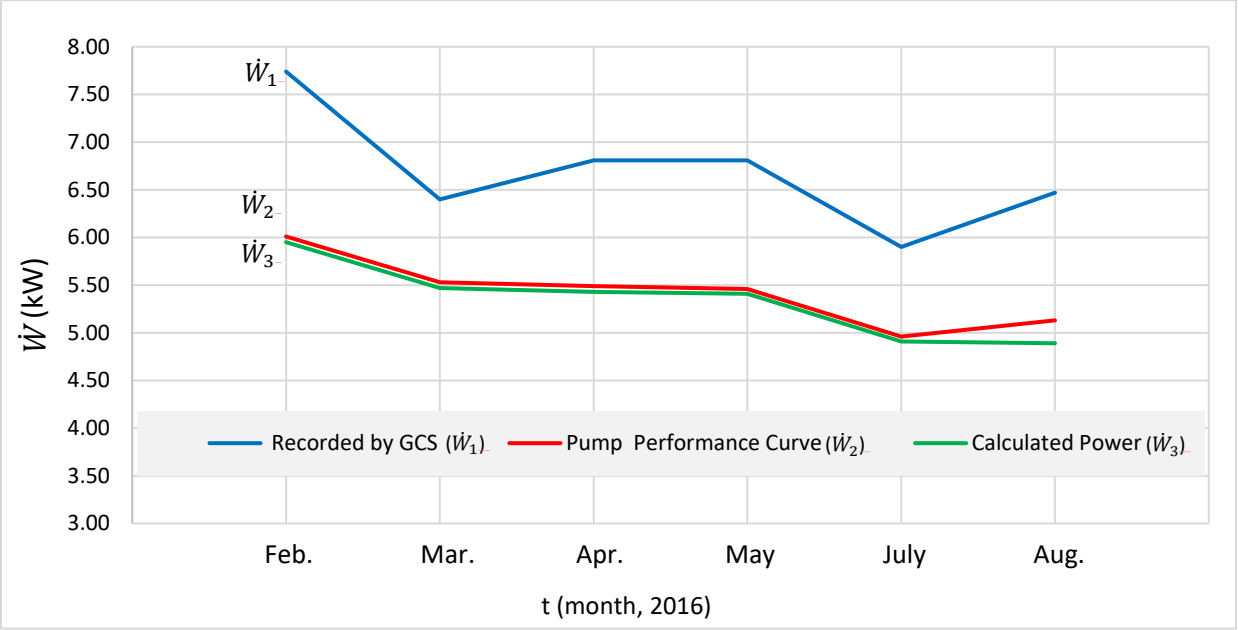

Fig. 71. Power consumption evaluation for the Grundfos VSP for February - August, 2016

For the Worthington CSP, Fig. 70 shows that $\dot{W}_1$ and $\dot{W}_2$ agreed better, but $\dot{W}_1$ was considered as the most trustworthy method since it was based on measuring the power directly in the power supply conductors with high accuracy transducers. For the Grundfos VSP pumps, Fig. 71 shows that $\dot{W}_2$ and $\dot{W}_3$ agreed better, but $\dot{W}_2$ was considered as the most trustworthy method since the power was determined digitally based on current operating conditions.

Chapter Five: Energy Content of the Vent Condenser's Condensed Steam Line and Evaluation of Natural Convection Heat Losses

After the flow rate of the condensed steam was determined with the newly installed flow meter (i.e., Siemens Mag 5100 DN 25, see Section 2.1.2, Fig. 38 for the installed flow meter), mass and energy investigation around the vent condenser was performed. The energy content of the condensed steam that was sent back to the storage tank as liquid water was determined.

By knowing the condensed steam flow rate and applying mass and energy balances around the storage tanks, the volume flow rate and temperature of the condensate water that returned from the campus were determined.

The energy lost due to natural convection with surroundings around the vent condenser was computed in order to estimate the mass flow rate of the DA's vented steam, and flow rate of the steam and non-condensable gases that were vented to the atmosphere. Energy loss due to natural convection was determined for the DA's vented steam pipe line that goes to the vent condenser. By knowing the energy lost from that line, the specific enthalpy of saturated steam that leaves the DA was determined which helped to estimate the temperature of the steam at that point.

Temperatures around the KU SPP were measured in this study by using thermocouple temperature sensors; and a T-S diagram for the overall plant was developed in order to visualize the heat transfer and temperatures changes during the SPP thermodynamic cycle.

5.1 Energy Content of the Vent Condenser's Condensed Steam Line

A Siemens flow meter was installed in the condensed steam line in September of 2016 by the SPP's staff. So data was collected only after September 10, 2016. Energy content of the water in the condensed steam line was computed using mass flow rate and the temperature difference between the condensed steam and the condensate water in the storage tanks (see Eq. (5.34)). That temperature difference was employed because the energy of the condensed steam was added to the water in the storage tank. So the energy difference between the two streams was considered to be energy gained from the condensed steam line. The flow rate of the condensed steam varied as explained in Section 2.1.2.a, with respect of the temperatures of the inlet steam and the condensate water that flowed through the vent condenser.

It was noticed that the flow rate of the condensed steam changed drastically from a range of 0 to 5 gpm after September 20, 2016 as shown in Figs. 72 and 73. The condensed steam flow rate was steady around 2 gpm before that date (see Figs. 39-42 in Section 2.1.2.a).

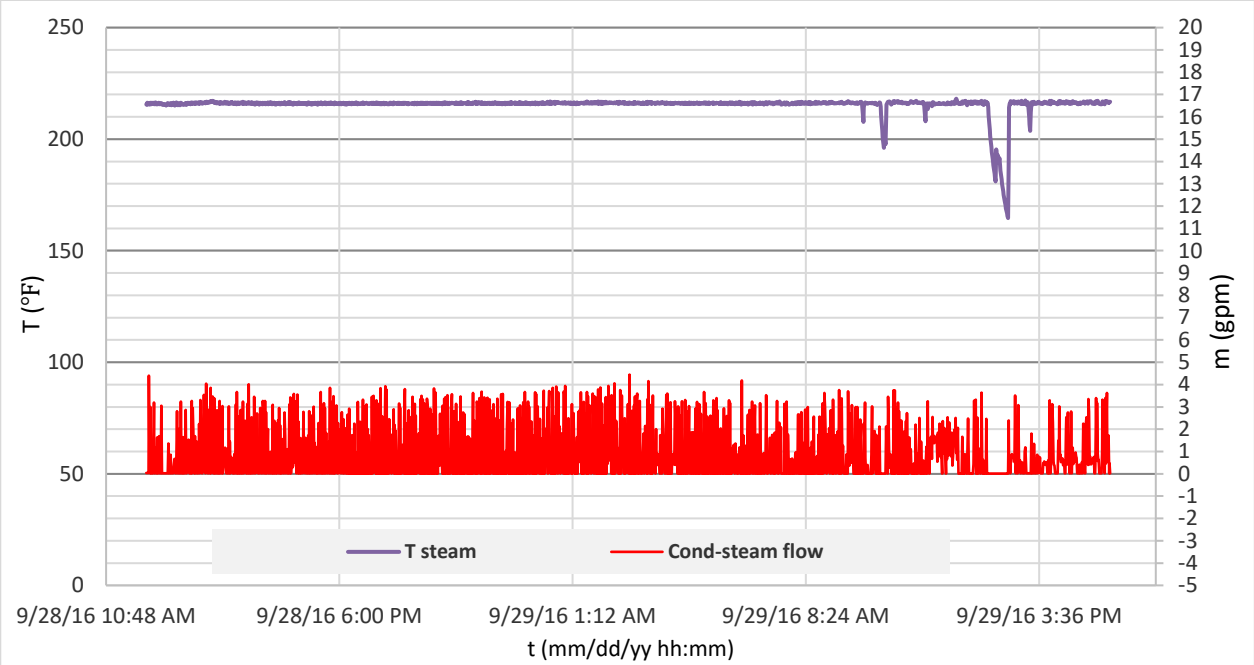

Fig. 72. Condensed steam flow rate for September 28-29, 2016

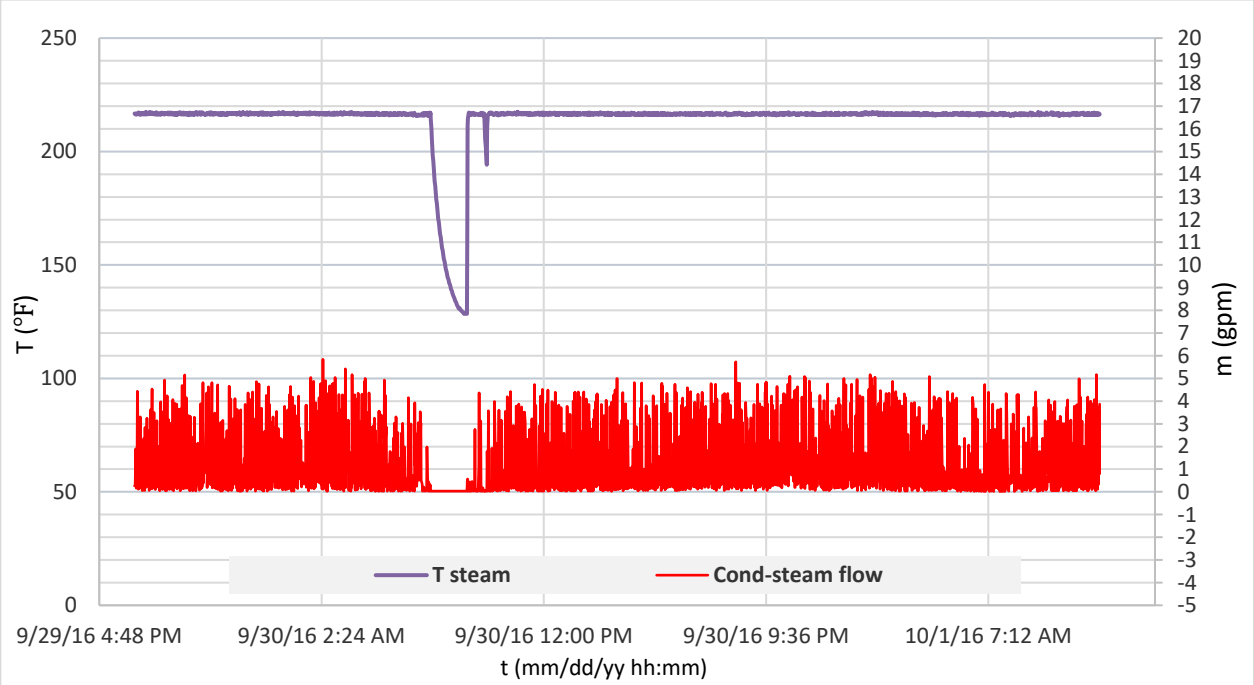

Fig. 73. Condensed steam flow rate for September 29-October 1, 2016

First, it was thought that change was due to a lower outside temperature which might cause that varying behavior. Then it was noticed that the valve, which vents the steam and non-condensable gases to the atmosphere, was closed. Closing that valve forced the gases to return to the storage tanks through the condensed steam line, which was the reason for turbulent flow. After the SPP staff was informed about this issue, the valve was opened.

Once the valve was opened, the flow rate measurement returned to normal as shown in Fig. 74, which is the same flow as that before September 20, 2016. This means that valve was closed from September 20 to November 13, 2016.

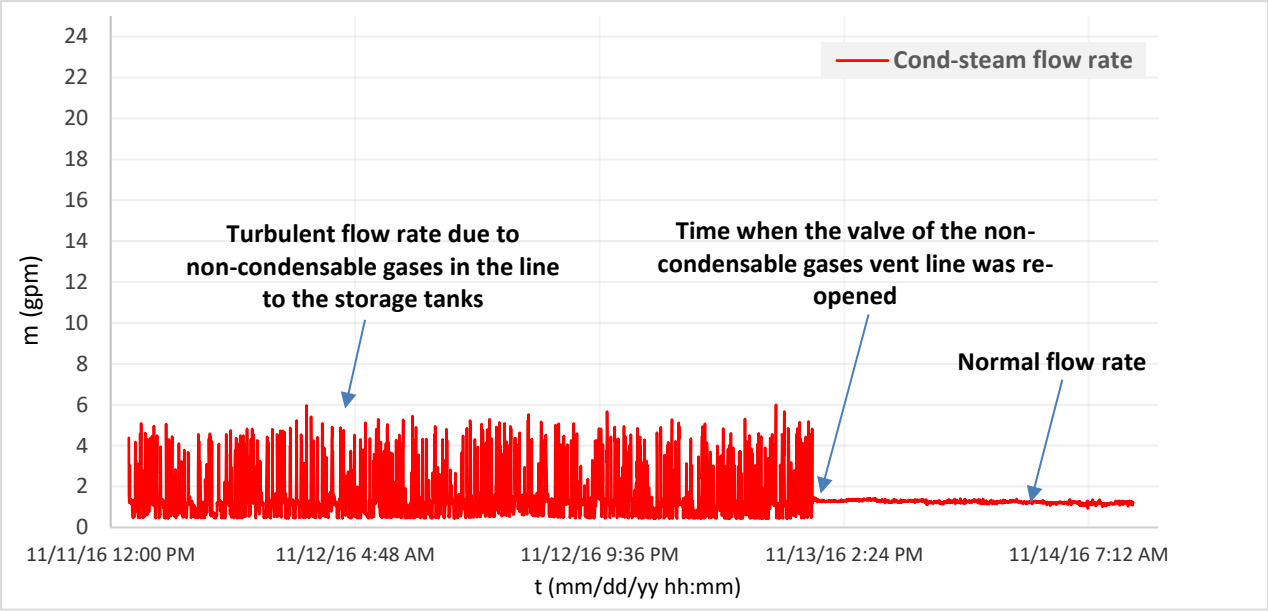

Fig. 74. Flow rate in the condensed steam line before and after re-opening the valve in the steam and non-condensable gases vent line on November 13, 2016

With the "closed valve" issue resolved, the condensed steam line energy could be computed. The energy added by the condensed steam line to the storage tanks was calculated from

$$Q_{add} = \dot{m}_{c\_st}\, C_p\, (T_{c\_st} - T_{tank}) \tag{5.34}$$

All terms are defined in the Nomenclature. Table 22 shows the computed energy added to the storage tanks for different periods between September and October of 2016. These energy values were computed minute-by-minute during these periods, then summed to obtain the total for each period.

Table 22. Energy added to the storage tanks by condensed steam line between September and October of 2016

Period	Q (Btu)	Period	Q (Btu)
Sept. 10-12, 2016	2,095,200	Oct. 12-14, 2016	1,817,397
Sept. 13-15, 2016	2,093,760	Oct. 15-17, 2016	1,961,627
Sept. 16-17, 2016	1,379,200	Oct. 18-20, 2016	1,638,400
Sept. 28-30, 2016	1,497,575	Oct. 21-23, 2016	1,837,296
Oct. 3-5, 2016	1,823,380	Oct. 24-26, 2016	1,589,718
Oct. 6-8, 2016	1,536,480	Oct. 27-29, 2016	1,932,131
Oct. 9-11, 2016	1,739,160	Oct. 30-31, 2016	1,188,422

Since the flow meter in the condensed steam line was installed late in 2016, it was not possible to compute the whole year's energy-added from data. Thus, a relationship was needed to predict approximately the energy added for other months based on the SPP's monthly generated steam.

An equation was produced, based on the relationship among the daily energy amounts in Table 22 and the generated steam in those periods. Figure 75 shows a linear fit of the data; and that curve was used to estimate the daily/monthly energy that might added to the storage tank by the condensed steam exiting the vent condenser.

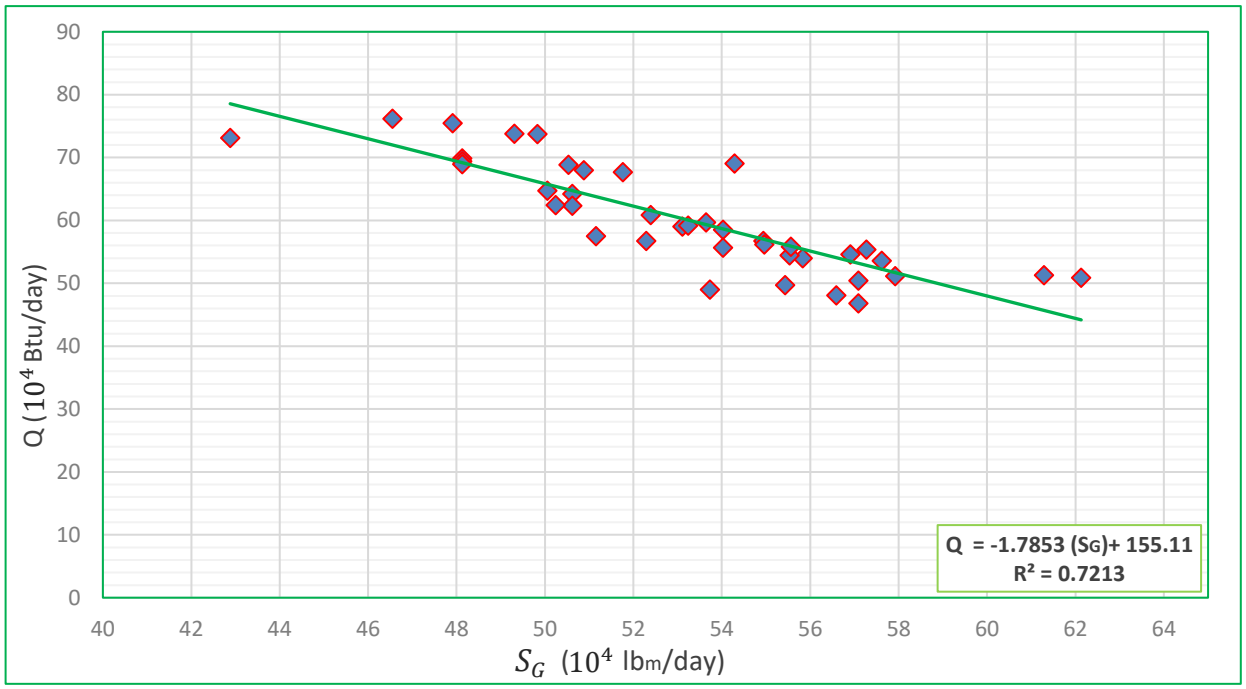

Fig. 75. Curve fit of the relationship between the condensed steam's energy content and boiler's generated steam

The resulting equation of the curve fit was

$$Q_i = -1.7853\ (S_G)_i + 155.11\ x\ 10^4 \tag{5.35}$$

However, this equation had a poor correlation coefficient (R^2=0.72), which yields estimated values having an accuracy between 84-120% [the accuracy is calculated as the ratio of the estimated energy to real energy].

This equation was used to estimate other months' energy values in 2016. Table 23 shows the estimated energy from January to December of 2016, based on the daily generated steam in those months (see App. B2 for monthly generated steam log sheets for January through October). The energy values for October and November in Table 23 were computed, based on the data gathered in those months.

Table 23. Energy added by the condensed steam line from the vent condenser to the storage tank for January to December, 2016

Month, 2016	Q (Btu)	Month, 2016	Q (Btu)
January	50,900,000 (estimated)	**July**	24,040,000 (estimated)
February	32,740,000 (estimated)	**August**	24,130,000 (estimated)
March	30,190,000 (estimated)	**September**	20,060,000 (estimated)
April	22,400,000 (estimated)	**October**	18,390,000 (computed)
May	17,660,000 (estimated)	**November**	29,060,000 (computed)
June	23,050,000 (estimated)	**December**	36,800,000 (estimated)

So, the total 2016 energy that was added by the condensed steam line to the storage tanks was about 2.92x10^8 Btu for the period of January-November of 2016. In this study, the steam generated value for December of 2016 was estimated based on 2014 and 2015 data (see App. C1, Table C1.4). So December's energy was computed based on an estimated steam generation of about $3x10^7$ lb_m. Thus, the 2016 energy added by the condensed steam line from the vent condenser was about $3.3x10^8$ Btu. This energy represents fuel savings of about 352,000 ft^3, assuming an average plant efficiency of 92%. The energy added by the condensed steam to the storage tanks saved about $880 for the SPP in 2016.

5.2 Evaluation of the DA's Vented Steam Flow Rate

The steam that entered the vent condenser was assumed to be saturated steam since the steam in the DA has saturated steam properties (i.e., 235 °F and 8 psig). In order to determine the mass flow rate of the DA's vented steam, computing the energy loss through the vent condenser casing was essential. This was done using a first law energy balance. The energy loss was due to free convection heat transfer from the vent condenser' walls to the surrounding air. Figure 76 shows flow and temperature conditions around the vent condenser that were used to determine the vented steam and non-condensable gases' mass flow rate.

A thermocouple (type J) was used to measure temperatures on the surfaces of the steam lines [33]. Another thermocouple (type K) was used to measure the air temperature, in order to find the properties of the air around equipment in the KU SPP [34]. An Omega data logger (type M-74) [35] was used to record the measured temperatures by both thermocouples.

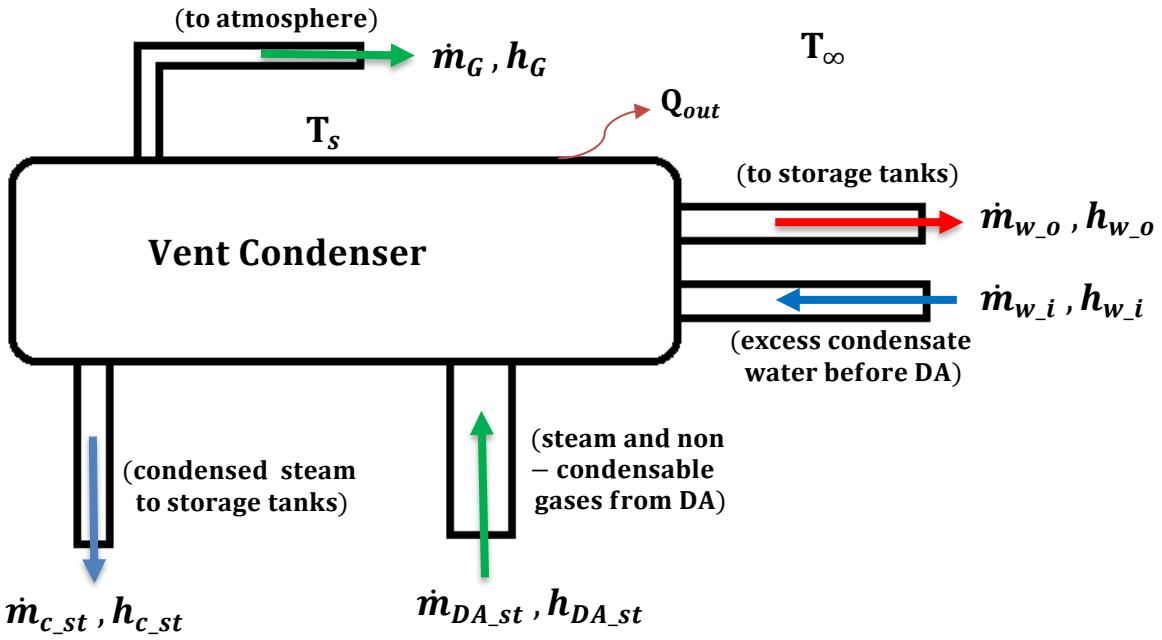

Fig. 76. Mass flow rates and specific enthalpies for the vent condenser's fluids

Assuming steady-state conditions, no kinetic and potential energy in the vent condenser and no work done, mass and energy balances were employed to determine the mass flow rate of the entering steam ($\dot{m}_{DA\_st}$) and of the steam and non-condensable gases ($\dot{m}_G$) that were vented to the atmosphere.

$$\sum \dot{m}_{in} = \sum \dot{m}_{out}$$

or, $$\dot{m}_{w\_i} + \dot{m}_{DA\_st} = \dot{m}_{w\_o} + \dot{m}_{c\_st} + \dot{m}_G \quad (5.36)$$

$$Q_{out} = (\dot{m}\, h)_{w\_i} + (\dot{m}\, h)_{DA\_st} - (\dot{m}\, h)_{w\_o} - (\dot{m}\, h)_{c\_st} - (\dot{m}\, h)_G \quad (5.37)$$

The heat loss by the vent condenser wall (Q_{out}) needed to be determined in order to solve Eq. (5.37) for $\dot{m}_G$ and $\dot{m}_{DA\_st}$. For the loss due to convection, the natural convection heat transfer coefficient (H_n) had to be calculated by [36]

$$H_n = Nu\,(\frac{K}{l_{cr}}) \quad (5.38)$$

Nusselt number (Nu) is a function of Grashoff number (Gr) and Prandtl number (Pr) [33]

$$Nu = \left[0.6 + \frac{0.387\ [(Gr)\ \ (Pr)]^{0.167}}{\left[1+\left(\frac{0.599}{Pr}\right)^{0.5625}\right]^{0.296}}\right]^2 \tag{5.39}$$

where Grashoff and Prandtl numbers are determined by [36]

$$Gr = \frac{(\rho_a)^2\ \beta\ g\ \Delta T\ (l_{cr})^3}{\mu^2} \tag{5.40}$$

$$Pr = \frac{\mu\ C_p}{K} \tag{5.41}$$

All terms are defined in the Nomenclature. Air properties are determined at the film temperature around the vent condenser's wall ($T_f = \frac{T_s+T_\infty}{2}$), and β is the coefficient of the thermal expansion $= \frac{1}{T_f}$ [36].

All needed data around the vent condenser, including the vent condenser's fluid flow rate, that was employed in all of the Eqs. (5.36)-(5.41) was recorded/determined at the same moment in order to have an accurate evaluation for the data gathered. The data gathered is given in Table 24.

Table 24. Data obtained on 10/01/16 at 12:12 PM around the vent condenser

$\dot{m}_{w\_i}\ (\frac{lb_m}{min})$	724.8	$C_p\ (\frac{Btu}{lb_m\ (°R)})$	0.2405
$\dot{m}_{w\_o}\ (\frac{lb_m}{min})$	724.8	$K\ (\frac{Btu}{hr\ (ft)°R})$	0.0154
$\dot{m}_{DA\_st}\ (\frac{lb_m}{min})$	--------	$\mu\ (\frac{lb_m}{ft\ (\sec)})$	$1.29x10^{-5}$
$\dot{m}_{c\_st}\ (\frac{lb_m}{min})$	8.1	$L_{V.C.}\ (ft)$	5.5
$\dot{m}_G\ (\frac{lb_m}{min})$	-------	$D_{V.C.}\ (ft)$	1.17
$h_{w\_i}\ (\frac{Btu}{lb_m})$	118.2	$T_s\ (°R)$	590
$h_{w\_o}\ (\frac{Btu}{lb_m})$	130	$T_\infty\ (°R)$	547
$h_{DA\_st}\ (\frac{Btu}{lb_m})$	1151.8	$\Delta T(°R) = (T_s - T_\infty)$	43
$h_{c\_st}\ (\frac{Btu}{lb_m})$	154.3	$T_f\ (°R)$	568
$h_G\ (\frac{Btu}{lb_m})$	134	$\beta\ (\frac{1}{°R})$	$1.76x10^{-3}$
$\rho_a\ (\frac{lb_m}{ft^3})$	0.075	$l_{cr}(ft)(\equiv\ D_{V.C.})$	1.17

All air properties were found using the film temperature (T_f) in the air tables [37]. All enthalpies were found from the saturated steam table [17]; and since most of the vented non-condensable gases were O_2, CO_2, and N_2, h_G was found using the air properties tables.

Using the data in Table 24, Grashoff and Prandtl numbers were determined by Eqs. (5.40) and (5.41), respectively, as $\mathrm{Gr} = 1.12x10^{8}$ and $\mathrm{Pr} = 0.727$. By applying Eq. (5.39), these give $\mathrm{Nu} = 53.267$.

Hence, by using Eq. (5.38), the natural convection heat transfer coefficient ($\mathrm{H_n}$) was found to be $0.7012\ \frac{Btu}{hr\,(ft^2)\,°R}$, where the diameter of the vent condenser was used as the characteristic length (l_{cr}) in Eqs. (5.38) and (5.40), according to the horizontal cylinder applications given in Ref. 33.

The heat loss due to natural convection was computed as [36]

$$Q_{out} = (H_n)(\pi\, D_{V.C.}\, L_{V.C.})(T_s - T_\infty) \tag{5.42}$$

So $Q_{out} = \left(0.7012\ \frac{Btu}{hr\,(ft^2)\,°\mathrm{R}}\right)(\pi)\ (1.17\ ft)\ (\ 5.5\ ft)(590\ R - 547\ R) = 595\ \frac{Btu}{hr}$

Using Eq. (5.37)

$$\left(595\frac{Btu}{60\ min}\right) = \left(724.8\ \frac{lb_m}{min}\right)\left(130\ \frac{Btu}{lb_m}\right) + \left(\ 8.1\ \frac{lb_m}{min}\right)\left(\ 154.3\ \frac{Btu}{lb_m}\right) + (\dot{m}_G)\left(\ 134\ \frac{Btu}{lb_m}\right) -$$

$$\left(\ 724.8\ \frac{lb_m}{min}\right)(118.2\ \frac{Btu}{lb_m}) - \left(\ \dot{m}_{DA\_st}\ \right)(1151.8\ \frac{Btu}{lb_m}) \tag{5.43}$$

Since the energy equation (Eq. (5.43)) has two unknowns (i.e., $\dot{m}_G$ and $\dot{m}_{DA\_st}$), the mass balance equation (Eq. (5.36)) was needed in order to solve for $\dot{m}_G$ and $\dot{m}_{DA\_st}$. Substituting flow rates of Table 24 into Eq. (5.36) gives

$\dot{m}_{DA\_st} = 8.1 + \dot{m}_G$

Using this mass flow rate relationship in Eq. (5.43), the mass flow rates were found as

$\dot{m}_G = 0.46\ \frac{lb_m}{min}$ and $\dot{m}_{DA\_st} = 8.55\ \frac{lb_m}{min}$

The determined amounts of $\dot{m}_G$ and $\dot{m}_{st}$ look reasonable when comparing with the measured $\dot{m}_{c\_st}$, because, when visually observing the outlet of the vented steam and non-condensable gases pipe line, there did not appear to be exiting products from the outlet.

These results give an idea about the flow rate of the steam entering the vent condenser and the flow rate of steam and non-condensable gases that vent to the atmosphere. Also, by knowing the flow rate of the DA's vented steam, it was possible to determine the heat loss around the line between the DA and vent condenser. The value of the heat loss was essential to determine the temperature of the steam that leaves the DA. See App. E1 for the heat loss and temperature calculations for the DA's vented steam pipe line.

5.3 KU SPP Storage Tanks' Mass and Energy Balances and BFW Loss

The temperature and flow rate of the condensate water that returns from the campus to the storage tanks are not known, since there is no temperature gauge or flow meter in that line. However, after installing the Siemens flow meter in the condensed steam line that went from the vent condenser to the storage tanks, it was possible to apply mass and energy balances around the storage tanks to determine both the temperature and flow rate of the returned condensate water. Figure 77 shows schematic of the storage tank with all of the input and output lines in the KU SPP.

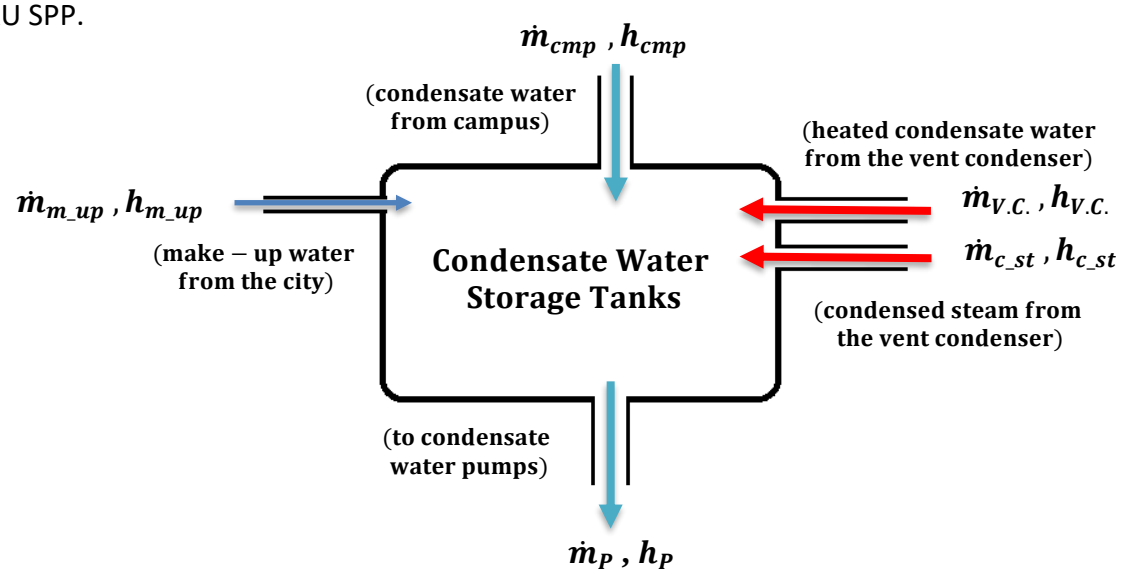

Fig. 77. Inlet and outlet fluid streams of the storage tanks in the KU SPP

By applying Eqs. (5.36) and (5.37) from Section 5.2, the mass flow rate and temperature of the campus returned condensate water were determined. Table 25 shows the recorded mass flow rates and determined specific enthalpies around the tanks. The flow rates in Table 25 were recorded for 10 minutes between 1:23 PM-1:32 PM on 9/19/2016. The enthalpy values were determined from the saturated steam table at the average recorded temperature of each line.

Table 25. Flow rates and enthalpies obtained between 1:23 PM and 1:32 PM on 9/19/2016

	$\dot{m}$ $(\frac{lb_m}{10\ \text{min}})$		h $(\frac{Btu}{lb_m})$
$\dot{m}_P$	13,267.7	h_P	136 (h_f @ 168 °F)
$\dot{m}_{V.C.}$	7,301.2	$h_{V.C.}$	144 (h_f @176 °F)
$\dot{m}_{c\_st}$	153.4	h_{c_st}	161 (h_f @193 °F)
$\dot{m}_{m\_up}$	582.9	h_{m_up}	63 (h_f @ 95 °F)
$\dot{m}_{cmp}$	-------	h_{cmp}	-------

According to Eq. (5.36), the mass balance in Fig. 77 is

$\dot{m}_P = \dot{m}_{cmp} + \dot{m}_{V.C.} + \dot{m}_{c\_st} + \dot{m}_{m\_up}$

$13{,}267.7 \frac{lb_m}{10\ min} = 7{,}301.2 \frac{lb_m}{10\ min} + 582.9 \frac{lb_m}{10\ min} + 153.4 \frac{lb_m}{10\ min} + \dot{m}_{cmp}$

which gives $\dot{m}_{cmp} = 5230.2\ lb_m$ for 10 minutes during that period. In order to determine the loss of the returned condensate water, use

$$\text{Loss of BFW } (\%) = \left[1 - \frac{\dot{m}_{cmp}}{(\dot{m}_P - \dot{m}_{V.C.} - \dot{m}_{c\_st})}\right](100) \quad (5.44)$$

$$= \left[1 - \frac{5230.2\ lb_m}{(13{,}267.7\ lb_m - 7{,}301.2\ lb_m - 153.4\ lb_m)}\right](100) = 10.03\%$$

The result from Eq. (5.44) show that 10.03% of the BFW was lost during that period due to the continuous blowdown from the boiler as well as the vented steam from the DA. In addition, there might be some other campus losses, such as steam pressure relief valves. After determining the mass flow rate of the returned condensate water, it was possible to determine the temperature by applying energy balance around the tank. So, rewriting Eq. (5.37) for the storage tanks gives

$$Q_{out} = (\dot{m}\ h)_{cmp} + (\dot{m}\ h)_{V.C.} + (\dot{m}\ h)_{C\_st} + (\dot{m}\ h)_{m\_up} - (\dot{m}\ h)_P \quad (5.45)$$

Assuming that the storage tanks are totally insulated, $Q_{out} = 0$; so writing Eq. (5.45) for h_{cmp} gives:

$$(13{,}267.7 \frac{lb_m}{10\ min})(136\ \frac{Btu}{lb_m}) = (7{,}301.2 \frac{lb_m}{10\ min})(144\ \frac{Btu}{lb_m}) + (153.4 \frac{lb_m}{10\ min})(161 \frac{Btu}{lb_m}) + (582.9 \frac{lb_m}{10\ min})(63\ \frac{Btu}{lb_m}) + (5230.2 \frac{lb_m}{10\ min})\ (\ h_{cmp})$$

Thus, h_{cmp}= 131.5 $\frac{Btu}{lb_m}$; which gives T = 163.5 °F (from the saturated liquid table; $T = T_{sat}@\ h_f = 131.5\ \frac{Btu}{lb_m}$), which is the computed temperature of the condensate water that returned from the campus. This temperature was helpful in Section 5.4 for drawing a more accurate T-S diagram. It can be noticed that the campus-returned condensate water gained about 5 °F (as compared with the 168 °F of the condensate water inside the tanks) because of using the heat exchangers in the KU SPP.

5.4 KU SPP's T-S Diagram

In a previous study [3], the KU SPP's cycle was represented on a T-S diagram. In this study, the T-S diagram was developed with respect to newly gathered data. Thermocouples (types K and J) [33, 34] were used in order to measure the steam temperatures more accurately. This diagram also indicates at which points in the plant there is energy lost or recovered, as well as the new changes in the SPP's equipment. Figure 78 schematically shows the KU SPP's equipment and fluid flow paths; and Fig. 79 shows the resulting T-S diagram.

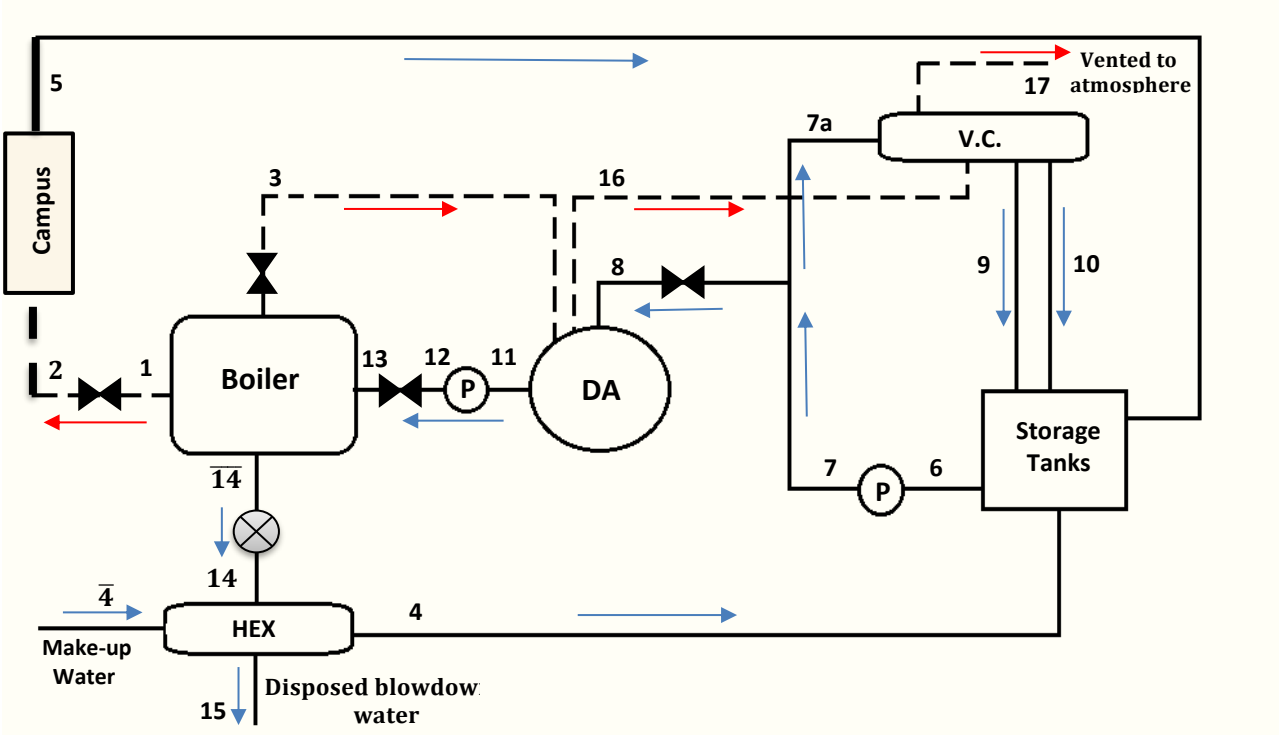

Fig. 78. Condensate water and steam flow processes in the KU SPP

(is a pressure reducer valve, and is the blowdown water flash tank)

Table 26 shows temperatures for each point in Fig. 78. Liquid water from different streams that have different temperatures and pressures is collected and mixed in the storage tanks at about 168 °F and 1.6 psig. The steam temperatures at points 1 and 2 were locally measured by using thermocouples on the pipes' surfaces; and the readings are subject to about ±0.75% error or 4 °F, according to the manufacturer's specifications (see App. E2).

The temperature of the returned condensate water from the campus is not known on site, but it was computed to be about 163 °F from Section 5.3. All other temperature in Table 26 were either recorded by temperature sensors or read from local gauges.

Table 26. Temperatures in the KU SPP cycle of Fig. 78

Location	T (°F)	Location	T (°F)
1	375	9	185
2	360	10	195
3	235	11	225
$\overline{4}$	65	$\overline{14}$	375
4	90	14	220
5	163	15	95
6	168	16	225
7	175	17	175

Figure 79 is the temperature-entropy diagram of the KU SPP. The main fluid cycle starts at the exit of the storage tanks, point 6 where all of the fluids are collected and mixed in the storage tanks. These fluids are: the returning campus condensate water (state 5), the heated condensate water (state 9), the condensed steam from the vent condenser (state 10), and the heated make-up water (state 4). All of these fluids have different temperatures and pressures, but they are mixed in the storage tank to yield a temperature and pressure of about 168 °F and 1.6 psig (state 6). From that point, the fluid is pumped by the condensate water pumps to about 44 psig (state 7) and then goes to the DA and the vent condenser.

The pressure drops to about 35 psig before it reaches the DA, and is then reduced to about 8 psig by the DA's control valve (state 8), while the pressure drops to about 30 psig at the vent condenser (state 7a) due to pipe fittings and frictional losses. Because of the deaeration process in the DA, the temperature increases to about 225 °F (state 11). Booster pumps increase the pressure to about 350 psig (state 12). Then it is reduced to about 170 psig (state 13) by a control valve before the boiler.

The produced steam exiting the boiler is at about 170 psig and 375 °F (saturated steam, state 1 in Fig. 79). That steam branches into two pipe lines: the main steam line goes to the campus at about 90 psig and 360 °F (superheated steam, state 2 in Fig. 79), and the auxiliary steam line goes to the DA with about 8 psig and 235 °F (superheated steam, state 3 in Fig. 79). The main steam flow condenses throughout the campus to return as liquid water (between the states 2 and 5, see the double line - which is double because the exact state change process is unknown)

In Fig. 79, the fluid properties (i.e., temperature, pressure, and phase status) are considered in the T-S diagram for each point. Since it is not possible to draw all of the pressure lines clearly because of the small space and distances between the points and lines, a scaled-up diagram that shows more clearly the pressure line for each point is shown in Fig. 80.

In Fig. 79, the dotted-lines in the saturated liquid and superheated steam regions represent process going through pressure reducer valves. The green dotted-line from state $\overline{14}$ to state 14 is the flash tank where the boiler's blowdown water is collected at about 7 psig and 220 °F, and then it is directed to the basement heat exchanger (the green dotted-line from state 14 to state 15) to be drained to the sewer system at about 95 °F after heating the make-up water.

The steam and non-condensable gases that are vented from the DA to the vent condenser are represented at state 16. From that point, most of the steam is condensed to liquid water, which is sent back to the storage tank (see the light brown dotted-line to state 10), and the rest of the steam and non-condensable gases is vented to the atmosphere (state 17). The light brown dotted-line from state 7 to state 9 is the excess condensate water from the DA that goes to the vent condenser to be heated to about 185 °F and is then sent back to the storage tank.

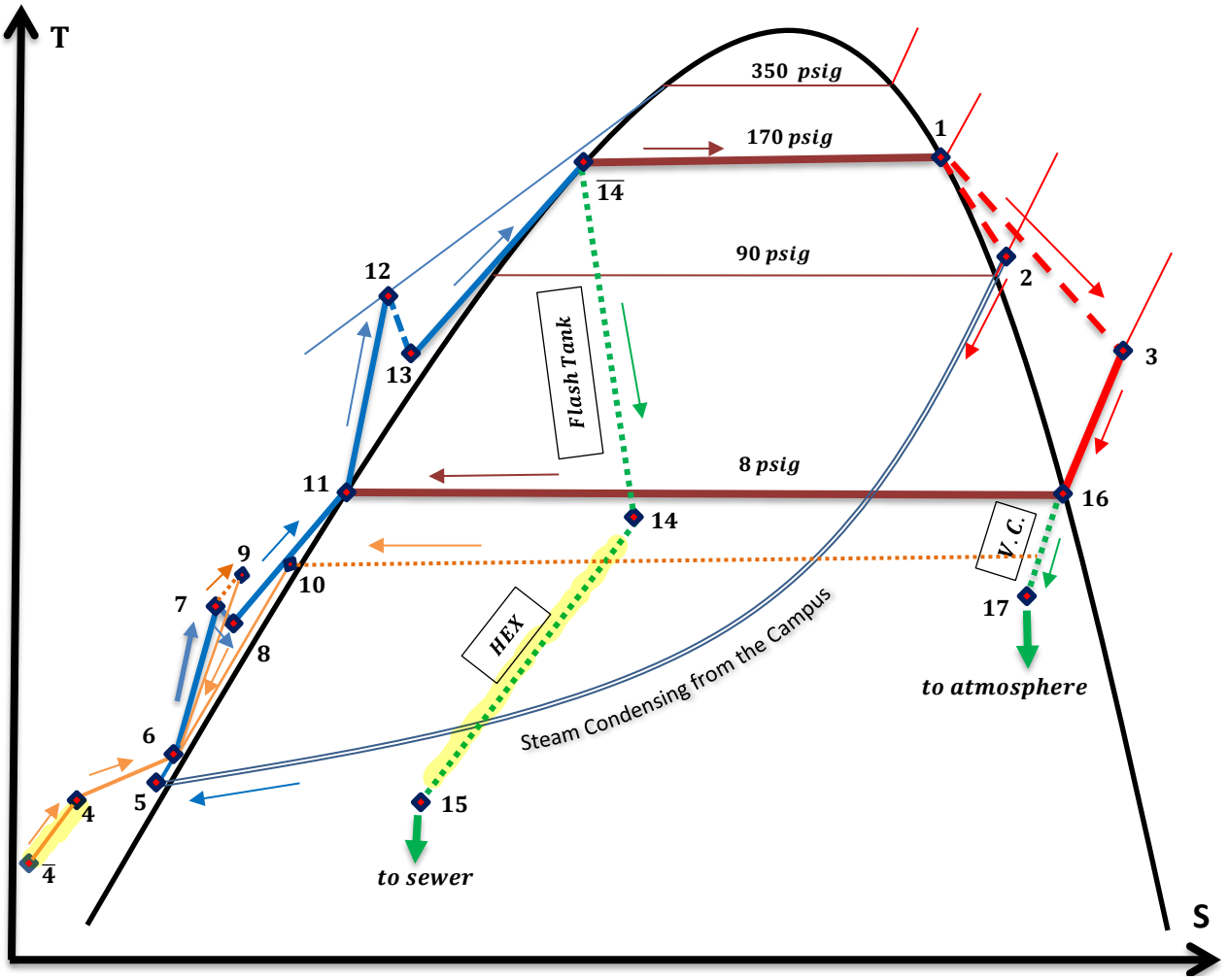

Fig. 79. T-S diagram (not to scale) [Solid blue is the main cycle's fluid in the subcooled region; solid light brown is for sub-cycle's fluids in subcooled region; solid maroon is for main cycle's fluid in the saturated region; red and dotted red is for the main steam in the superheated region]

Late in October of 2016, some systems and process changed in the KU SPP, which affected the T-S diagram. The main change was disconnecting the basement heat exchanger due to using an RO system to purify the make-up water. By using the RO system, the make-up pipe line was connected directly to the storage tanks without passing through the basement heat exchanger. This was changed because the blowdown water was reduced to very small flow since the RO system reduced TDS concentration tremendously, from 3000-4000 ppm to less than 100 ppm [38]. So the blowdown water is now drained directly to the sewer system without passing through the basement heat exchanger. The T-S diagram is upgraded in Fig. 81 to reflect this change. The state change 14-15 (HEX) is not there anymore, and the drain is dumped into the sewer from state 14, instead of state 15. Also, state 4 no longer exists since the make-up water is no longer heated. [Comparing the green highlighted dotted lines of Figs. 79 and 81 reveals these changes.]

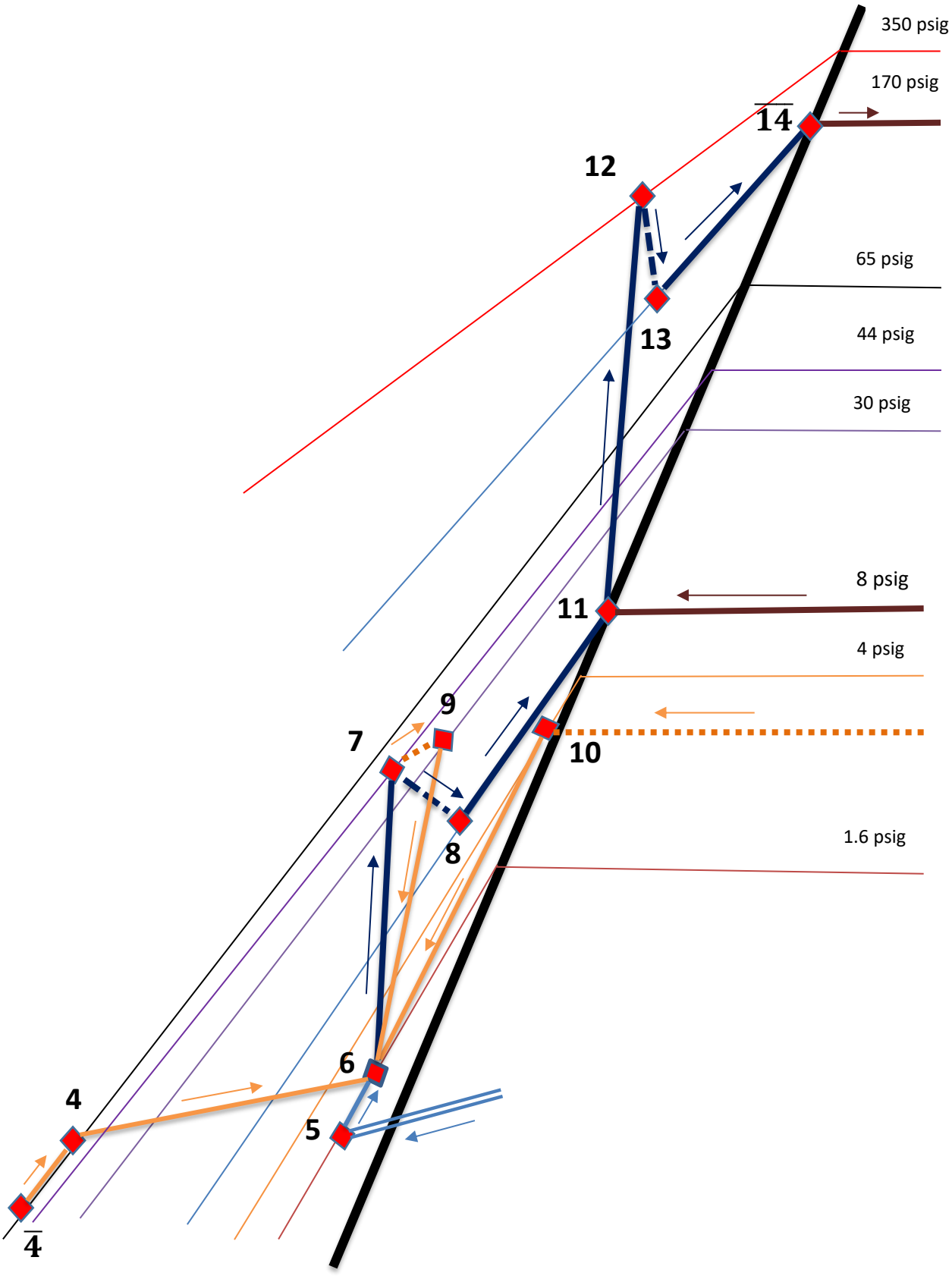

Fig. 80. Magnified saturated liquid line of the KU SPP's T-S diagram of Fig. 79

Disconnecting the basement heat exchanger affects the condensate water temperature inside the storage tanks because, previously, the make-up water was heated from about 65 °F to about 90 °F before it went to the storage tanks. However, after disconnecting the basement heat exchanger, it was found that the temperature of the condensate water inside the storage tanks dropped about 0.28 °F (this calculation was made using data from Section 5.3). So, state 6 in Fig. 81 was considered to be the same as it is in Fig. 79.

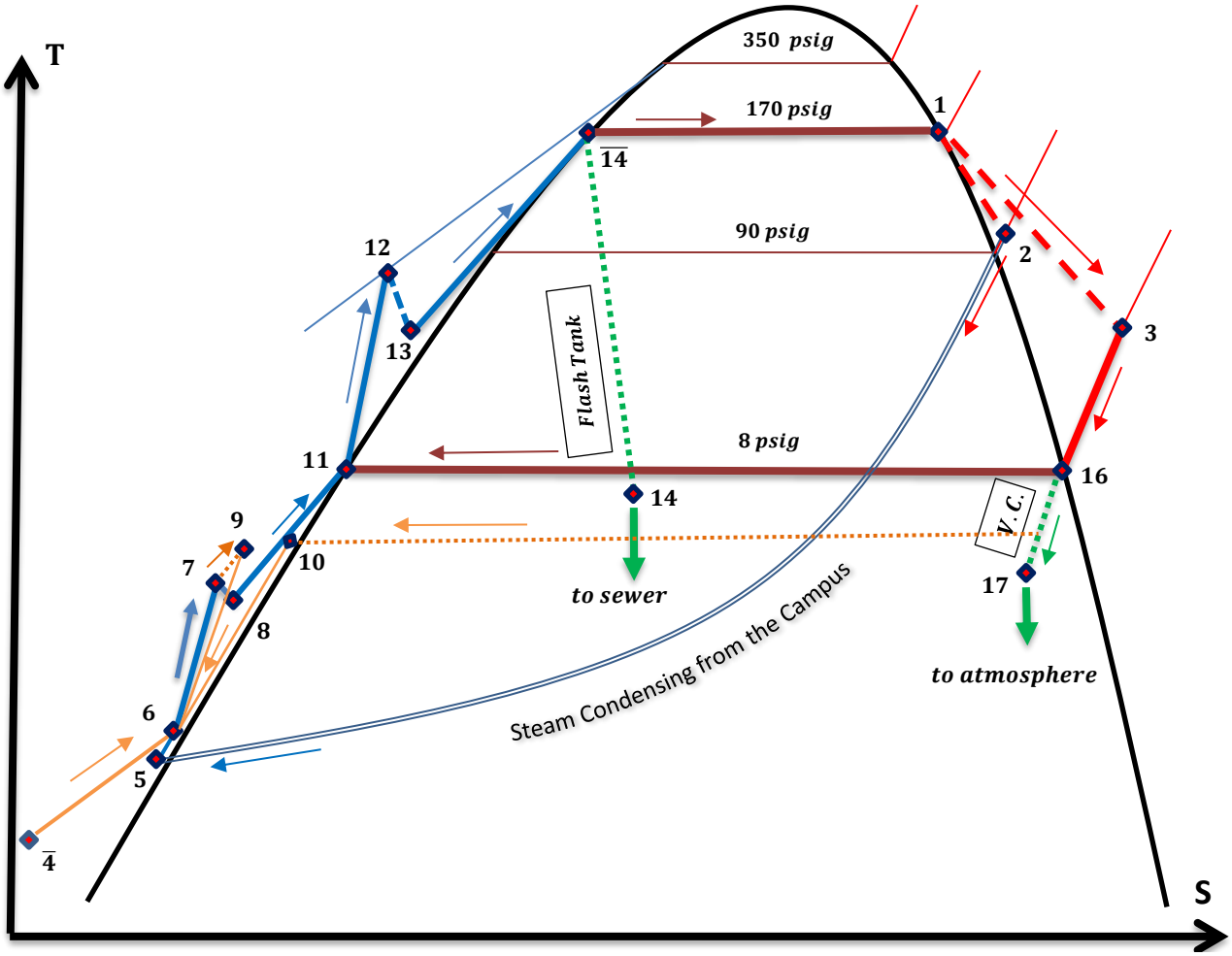

Fig. 81. T-S diagram after KU SPP personnel disconnected the basement heat exchanger (not to scale)

In conclusion, the 2016 energy added by the condensed steam line was about $3.3x10^8\ Btu$. This represented a fuel savings of about 352,000 ft^3, which was about $880 for the SPP. About 595 $\frac{Btu}{hr}$ was determined as a heat loss around the vent condenser due to natural convection. The determined heat loss was used to compute the flow rate of the DA's vented steam and of the steam and non-condensable gases that vented to the atmosphere (8.55 lb_m/min and 0.46 lb_m/min, respectively). KU SPP thermodynamic cycles were accurately depicted in T-S diagrams (Figs. 79, 80, and 81) based on the recorded operating conditions and recent changes in the plant.

Chapter Six: Conclusion and Recommendations for Future Work

6.1 Conclusion

The energy transferred by the heat recovery components in the KU SPP has been computed. Heat transfer rates were determined for the vent condenser and basement heat exchanger by employing the overall heat transfer coefficient in two assumed flow cases. The heat transfer rate when assuming the counter-flow direction was 40-60% higher than that when assuming the parallel-flow direction. The efficiency of the heat exchanger in the KU SPP (model SU-85-2) was determined to be 88%, based on the current operating conditions.

About $4.38\ x\ 10^9\ Btu$ was recovered by the vent condenser from the DA's vented steam in 2016. This energy was reclaimed as heated condensate water and condensed steam, which are added eventually to the BFW in the storage tanks. $8.92\ x\ 10^8\ Btu$ was reclaimed by using the basement heat exchanger from the boilers' blowdown water from January to September of 2016. The monthly energy savings were computed based on recorded minute-by-minute data from January to August of 2016. For the rest of the year, the energy savings was estimated based on the monthly steam generated by using energy curves that were produced based on the relationship between the steam generated and the energy savings for the first eight months.

The boiler efficiency was increased on average by 2% due to using the vent condenser and the basement heat exchanger as calculated from January to August of 2016. The total natural gas savings by using both heat exchangers in the KU SPP was about $5.64\ x\ 10^6\ ft^3$, which represents about \$ 14,110 based on the current natural gas price of \$2.5/1000 ft^3.

The power consumption by the condensate water CSP and VSP was evaluated using three different approaches. After analyzing the differences among between the three methods, it was concluded that the most trustworthy method was that of the power recording transducers for the Worthington pump; while for the Grundfos pump, the power that was determined by the pump curve was considered the most trustworthy among the three methods. Flow rate calibration curves were produced in order to correct the recorded flow rate of the Siemens flow meter downstream of the CSP and VSP. By using the produced calibration curves, the Siemens flow rate was increased by about a 7 gpm correction, according to the calibration results of Section 1.5.

All of the energy and power calculations were conducted based on calibrated flow rates, tested pressure sensors, and using more accurate instrumentation, such as internal temperature sensors instead of surface sensors. So, it was found that: the Siemens flow meters read about 7 gpm less than the actual value; the Omega pressure sensor was reading about 2 psig higher than the actual value; and the surface temperature sensors read about 2 °F less than the internal sensors.

About 595 $\frac{Btu}{hr}$ was determined as a heat loss around the vent condenser due to natural convection. This heat loss was employed with the energy and mass balances around the vent condenser to find the flow rate of the steam entering the vent condenser (8.55 $\frac{lb_m}{min}$), and the flow rate of the steam and non-condensable gases that vented to the atmosphere (0.46 $\frac{lb_m}{min}$). Also, by applying energy and mass balances around the storage tanks, it was found that 10% of the BFW was lost within the SPP and campus. A detailed T-S diagram (Fig. 79) was drawn for the KU SPP based on more accurate data; and it was modified (Fig. 81) due to the added RO system and the disconnected basement heat exchanger in the SPP.

6.2 Recommendations for Future Work

In the previous studies [2, 3], less power was consumed by VSP when the level control mode was used. However, more energy was wasted since the vent condenser was not used for with this mode, because the pressure head was not sufficient to reach the vent condenser. By using the DA on the first floor next to the vent condenser, it should be possible to pump in the level control mode while the vent condenser is also in service. So, it is recommended to gather new data for the first floor DA because added energy savings by the vent condenser and less power consumption by the VSP will result from using the DA and the vent condenser together when operating in the level control mode.

New Grundfos variable speed pumps for the BFW are installed. So it is recommended to conduct a comparative power consumption analysis to assess how much power would be saved by using the new pumps since they will run at lower pressure (270 psig, instead of the 350 psig that is provided by the current constant speed pumps).

Also, it was recommended to install a control system that can vary the flow rate of the make-up water to the storage tanks, instead of the on/off solenoid valve that is used now. By using this system, it should be possible to control the make-up water flow automatically based on the water level inside the storage tanks; and to protect the basement heat exchanger from thermal shock due to the sudden temperature changes caused by fully opening/closing the solenoid valve that used in the current system. However, the basement heat exchanger is no longer used, but the suggested system could be used for future work if the basement heat exchanger were employed again. This control system's design is given in detail in App. A4. Also, even if the basement heat exchanger is not used anymore, this system can still be used with the new make-up water pipe line that comes from the RO system to control the flow rate automatically based on the water level inside the storage tanks.

Moreover, it is recommended that the SPP measure and record digitally the flow rate of the steam generated as well as the make-up water since both of these flow rates are currently manually recorded by the staff on a log sheet.

Chapter Seven: References

1. U.S. Department of Energy, *Use a Vent Condenser to Recover Flash Steam Energy*. Available at: https://files.acrobat.com/a/preview/78e3a5bd-5a80-467e-a646-226d196df401 Date accessed: 9/30/2016.
2. Alabdullah, R.J., *Evaluation of Grundfos CRE 15-3 Variable Speed Centrifugal Pump and Worthington Constant Speed Centrifugal Pump Applications in KU Steam Power Plant*, Department of Mechanical Engineering. May 2015, (Mech. Eng. M.S. Thesis) University of Kansas; Lawrence, KS.
3. Nanda, A., *Comparative Analysis of Heat Exchangers and Continued Investigation of Variable Speed versus Constant Speed Pump Systems in KU's Steam Power Plant.* Department of Mechanical Engineering. May 2016, (Mech. Eng. M.S. Thesis) University of Kansas; Lawrence, KS.
4. Schmidt, F.P., *Comparative Analysis between Grundfos CRE 15-3 Variable Speed Centrifugal Pumps and a Worthington D-824 Constant Speed Centrifugal Pump in a KU Steam Power Plant Application*, Department of Mechanical Engineering. April 2014, (Mech. Eng. M.S. Thesis) University of Kansas; Lawrence, KS.
5. ARI Armaturen Steamline, LLP., *Deaerator & Feedtank Systems*. Available at: http://in.ari-armaturen.com/fileadmin/user_upload/ari-in/files/Deaerator-brochure_01.pdf Date accessed: 4/6/2016.
6. U.S. Department of Energy, *Energy Efficiency and Renewable Energy*. Available at: http://energy.gov/sites/prod/files/2014/05/f16/steam18_steam_systems.pdf Date accessed: 4/6/2016.
7. Industrial System, *Tray ST5 .005 cc/Liter Pressurized Deaerator*. Available at: http://www.industrialsteam.com/pdf/Industrial_Steam_Tray_ST5.pdf Date accessed: 4/2/2016.
8. Stork, *Spray-Type Deaerators*. Available at: http://www.pentol.com.pl/eng/dokumenty/STORK_spray-type-deaerator.pdf Date accessed: 4/2/2016.
9. Lee, H., *Thermal Design: Heat Sinks, Thermoelectrics, Heat Pipes, Compact Heat Exchangers, and Solar Cells*. Hoboken, NJ (2010): Wiley.
10. Bell & Gossett, *Type "SU" Heat Exchanger, "U" Tube Design*. Available at: http://documentlibrary.xylemappliedwater.com/wp-content/blogs.dir/22/files/2012/07/c-121.2b.pdf Date accessed: 4/7/2016.
11. Mowe, Kent, "*Re: Kent Mowe B&G SU85-2 Heat Exchanger*." Message to Akeel A. Abdulla. April 13, 2016 at 4:38 PM. E-mail.
12. Mercer, Mike, "Re: Heat Exchanger SU85-2." Message to Akeel A. Abdulla. May 17, 2016 at 5:01 PM. E-mail.
13. Ronald L. Dougherty, *ME637 course notes, Steam Power Plant, Power Plant Components Analysis*, *Condensers and Feed Water Heaters*. Department of Mechanical Engineering. Fall, 2015, University of Kansas; Lawrence, KS.

14 Bell & Gossett Shell-and-Tube Heat Exchanger, *SU-85-2*. Data available at: http://www.genemco.com/catalog/pdf/CJRP5186v2tubeheatexchanger.pdf Date accessed: 4/22/2016.

15 Omega Engineering, Inc., *TX92A-3 Transmitter*. Available at: https://files.acrobat.com/a/preview/41cc15c6-d048-4e4b-8920-2a35fbe9ea11 Date accessed: 6/13/2016.

16 Siemens, *SITRANS F M Mag 5100 W Flow Sensor*. Available at : http://w3.siemens.com/mcms/sensor-systems/en/process-instrumentation/flow-measurement/electromagnetic/pulsed-dc-meters/sensors/Pages/sitrans-f-m-mag-5100-w-for-water-applications.aspx Date accessed: 4/28/2016.

17 El-Wakil, M. M., *Power Plant Technology*. New York City, NY (1984): McGraw-Hill.

18 The Engineering Toolbox, *Water Specification and Properties*. Data available from: http://www.engineeringtoolbox.com/water-specific-volume-weight-d_661.html Date accessed: 4/6/2016.

19 The Engineering Toolbox, *Overall Heat Transfer Coefficients*. Data available from: http://www.engineeringtoolbox.com/overall-heat-transfer-coefficients-d_284.html Date accessed: 4/26/2016.

20 Fakheri, A., "*Heat Exchanger Efficiency*". *ASME Journal of Heat Transfer.* 2006; 129(9):1268-1276. doi:10.1115/1.2739620. Available at: https://files.acrobat.com/a/preview/38a8eacd-0675-4353-a522-0b04d5002a0d. Date accessed: 9/16/2016

21 Werth, G., Campus Energy Engineer, Personal Communication during the previous study with Anurag Nanda, October, 2015; KU Facilities Service; Lawrence, KS.

22 Mills, R., KU Power Plant Operator. Personal Communication, May, 2016; KU Steam Power Plant; Lawrence, KS.

23 U.S. Energy Information Administration, *Natural Gas*, *Natural Gas Prices*. Available from: http://www.eia.gov/dnav/ng/ng_pri_sum_dcu_nus_m.htm Date accessed: 8/5/2016.

24 Beckwith & Kuffel, Inc., *Centrifugal Pumps Fundamentals; Pump Characteristics Curve*. Data available at: http://www.b-k.com/technical-information/centrifugal-pump-fundamentals/system-curves Date accessed: 8/8/2016.

25 Applied Industrial Technologies, *Pump Formulas, Pump Input Power*. Available at: https://files.acrobat.com/a/preview/76f9d305-3def-42f6-9a4e-7826edf4a843 Date accessed: 8/6/2016.

26 Veris Power Monitoring Sensor, *Current Transducer H8044-0100-2*. Available at: https://files.acrobat.com/a/preview/6466c5dd-412c-42ca-a69c-e72f250e5d1d Date accessed: 9/19/2016.

27 Grundfos System, *Specification of HYDRO MPC E 2CRE15-03 3X460V BASIS*. Available at: https://files.acrobat.com/a/preview/62768241-7d73-4e0e-8e6e-1f7c8529a172 Date accessed: 8/15/2016.

28 Gems Sensors & Controls, "Suresite® Mini Alloy Visual Level Gauges", Gems Sensors & Controls, Plainville, CT (2012). Available at: http://www.gemssensors.com/en/Products/Level/Visual-Indicators/SureSite Date accessed: 9/16/2016.

29 Grundfos, *CRE15-3 Variable Speed Pump Performance Curve, Hydro MPCE 2CRE15-03 3X460 V Basis*. Available at: http://product-selection.grundfos.com/product-detail.product-detail.html?from_suid=14710679973620505389090901042&pumpsystemid=120312966&qcid=101284231 Date accessed: 9/22/2016.

30 Vemco, Inc., *Pump Head for Open and Closed Systems*. Available at: https://files.acrobat.com/a/preview/ecf928cd-48ea-4f44-a382-d36251b1752e Date accessed: 8/16/2016.

31 Igor J. Karassik; Joseph P. Messina; Paul Cooper; Charles C. Heald: *Pump Handbook,* fourth edition*. Power Pump Theory*. New York City, NY (2001): McGraw-Hill.

32 Engineering Tool Box, *Water Specific Gravity*. Available at: http://www.engineeringtoolbox.com/water-temperature-specific-gravity-d_1179.html Date accessed: 9/22/2016.

33 Omega Engineering, Inc., *J Thermocouple Sensor, XCIB-4, OSTW Termination*. Available at: https://files.acrobat.com/a/preview/5b1ee6d1-0769-48b8-bdfa-f183c86dc69f Date accessed: 10/23/2016.

34 Omega Engineering, Inc., *K Thermocouple Sensor, 5SRTC Model*. Available at: https://files.acrobat.com/a/preview/3d8fcf79-8180-48d3-a33a-645140e2a737 Date accessed: 10/23/2016.

35 Omega Engineering, Inc., *OM-74 Thermocouple Data Logger*. Available at: https://files.acrobat.com/a/preview/c0ad529a-0e6a-42ae-b351-374609c3a1b3 Date accessed: 10/23/2016.

36 Rajput, R. K., *Heat and Mass Transfer in SI Units*. Ram Nagar, New Delhi (2006): S. Chand & company.

37 Van Wylen, J., and Sonntag, R. E., *Fundamentals of Classical Thermodynamics*, Air Property Tables and Charts (English Units). New York City, NY (1973): Wiley.

38 Ullery, R., KU Power Plant Operator. Personal Communication, November, 2016; KU Steam Power Plant; Lawrence, KS.

39 Onset Computer Corporation, *Hobo Data Logger UX120-006M. Available at:* https://files.acrobat.com/a/preview/c8c5b388-0a91-4912-bc13-2a39921f8ea0 Date accessed: 1/5/2016.

40 Onset Computer Corporation, *TMC6-HE Temperature Sensor*. Available at: https://files.acrobat.com/a/preview/314ceefd-5949-4c45-87b7-892e1d7bf12e Date accessed: 5/9/2016.

41 Badger Recordall Flow Meters, *Turbo 450*. Available at: https://files.acrobat.com/a/preview/d761efd4-e5c2-4e3a-a8e0-5d687de2a23b Date accessed: 8/15/2016.

42 Indelac Actuator, *SR and SX Nema7*. Available at: https://files.acrobat.com/a/preview/db66782f-4cda-4716-bad7-1f5a2bf4962d Date accessed: 2/12/2016.

43 Flowline Level Transmitter, *EchoPod DL24*. Available at:
https://files.acrobat.com/a/preview/4a56b9a5-1b00-4e47-bbe3-dd53bd3c0329
Date accessed: 8/9/2016.

44 Cadillac Meter, *CMAG Magnetic Flow Meter*. Available at:
https://files.acrobat.com/a/preview/5f165611-6395-47ee-83b1-23b5adba9b77
Date accessed: 3/15/2016.

45 Omega Engineering, Inc., *Resistance Temperature detector PR-12-2-100-SL*. Available at:
https://files.acrobat.com/a/preview/9ca727ea-83cb-47fa-ae59-c6ed7bc1dc72
Date accessed: 9/5/2016.

46 Omega Engineering, Inc., *Magnetic Meter FMG-3000 Series Blind Version*. Available at:
https://files.acrobat.com/a/preview/2e8b791a-ba7d-408f-b324-9d275459937f
Date accessed: 15/1/2016.

47 Onset Computer Corporation, *Hobo Cable 4-20 mA*. Available at:
https://files.acrobat.com/a/preview/a3e344cb-aa68-4ff1-b499-c844b3b902a9
Date accessed: 6/7/2016.

48 Flowserve, *Worthington D824 Centrifugal Pump*, Available at:
https://files.acrobat.com/a/preview/79c909bf-b19c-422e-be63-172b884de2d6
Date accessed: 5/1/2016.

49 Omega Engineering, Inc., *Pressure Transducer 0-200 psig PX43 Series*. Available at:
https://files.acrobat.com/a/preview/99741a2c-5805-44b6-9321-e24b697f2c86
Date accessed: 3/5/2016.

50 Danfoss, *Pressure Transducer MBS3000*. Available at:
https://files.acrobat.com/a/preview/0ff2d129-8761-4017-8dfc-588302d8c6a5
Date accessed: 4/19/2016.

51 Omega Engineering, Inc., *K/J Thermocouple Temperature Tolerance*. Available at:
https://files.acrobat.com/a/preview/1cf152de-481e-429a-a645-bfb40ff3127e
Date accessed: 9/15/2016.

Appendices

Appendix A1: Onset HOBO Data Logger (UX120-006M) (reproduced from Ref. 39)

HOBO® 4-Channel Analog Data Logger (UX120-006M) Manual

The HOBO 4-Channel Analog data logger has 16-bit resolution and can record up to 1.9 million measurements or events. The four external channels accept a variety of sensors, including temperature and split-core AC current sensors as well as 4-20 mA and voltage input cables (sold separately). Using HOBOware®, you can easily configure an alarm to trip when the sensor reading rises above or falls below a measurement that you specify. Or, you can set up burst logging in which the logger records data at a different interval during certain conditions. The logger can also calculate minimum, maximum, average, and standard deviation statistics. This easy-to-use data logger has a built-in LCD screen to check current readings and to monitor logging status, battery use, and memory consumption in between readouts.

HOBO 4-Channel Analog Data Logger

UX120-006M

Included Items:

- Command™ strip
- Double-sided tape
- Hook & loop strap
- Two AAA 1.5 V alkaline batteries

Required Items:

- HOBOware 3.6 or later
- USB cable (included with software)

Sensors and cables available at www.onsetcomp.com.

Specifications

Logger with Cable Type	CABLE-4-20mA	CABLE-2.5-STEREO	CABLE-ADAP5	CABLE-ADAP10	CABLE-ADAP24
Measurement Range	0 to 20.1 mA	0 to 2.5 V	0 to 5.0 V	0 to 10 V	0 to 24 V
Accuracy	±0.001 mA ±0.2% of reading	±0.1 mV ±0.1% of reading	±0.2 mV ±0.3% of reading	±0.4 mV ±0.3% of reading	±1.0 mV ±0.3% of reading
Resolution	0.3 µA	40 µV	80 µV	160 µV	384 µV

Logger	
Operating Range	Logging: -20° to 70°C (-4° to 158°F); 0 to 95% RH (non-condensing); Launch/Readout: 0° to 50°C (32° to 122°F) per USB specification
Logging Rate	1 second to 18 hours, 12 minutes, 15 seconds
Logging Modes	Fixed interval (normal), burst, or statistics
Memory Modes	Wrap when full or stop when full
Start Modes	Immediate, push button, date & time, or next interval
Stop Modes	When memory full, push button, or date & time
Restart Mode	Push button
Time Accuracy	±1 minute per month at 25°C (77°F), see Plot A
Power Source	Two AAA 1.5 V alkaline batteries, user replaceable, and USB cable
Battery Life	1 year, typical with logging rate of 1 minute and sampling interval of 15 seconds or greater
Memory	4 MB (1.9 million measurements, maximum)
Download Type	USB 2.0 interface
Full Memory Download Time	Approximately 1.5 minutes
LCD	LCD is visible from 0° to 50°C (32° to 122°F); the LCD may react slowly or go blank in temperatures outside this range
Size	10.8 x 5.41 x 2.54 cm (4.25 x 2.13 x 1 in.)
Weight	107.5 g (3.79 oz)
Environmental Rating	IP50
CE	The CE Marking identifies this product as complying with all relevant directives in the European Union (EU).

Note: The HOBO U-Shuttle (U-DT-1) is not compatible with this logger.

17384-D

Specifications (continued)

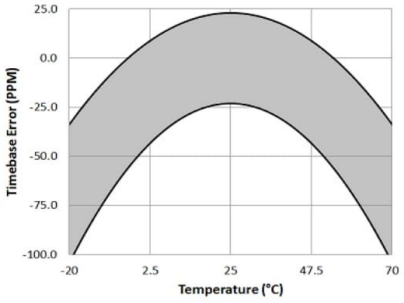

Plot A: Time Accuracy

Logger Components and Operation

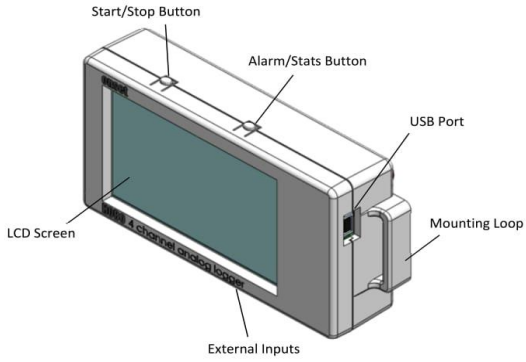

Start/Stop Button: Press this button for 3 seconds to start or stop logging data, or to resume logging on the next even logging interval. This requires configuring the logger in HOBOware with a push button start or stop, and with "Resume logging on next button push" selected (see *Setting up the Logger*). You can also press this button for 1 second to record an internal event (see *Recording Internal Logger Events*) or to turn the LCD screen on if the option to turn off the LCD has been enabled (see *Setting up the Logger*).

Alarm/Stats Button: Use this button to clear a tripped alarm (see *Setting up Alarms*) or to switch between statistics, alarm readings, and the current sensor reading.

Mounting Loops: Use the two mounting loops (only one visible in the diagram) to mount the logger with the hook-and-loop strap (see *Mounting the Logger*).

External Inputs: Use these 2.5 mm jacks (not visible in the diagram) to connect up to 4 sensors (see *Connecting External Sensors*).

USB Port: Use this port to connect the logger to the computer via USB cable (see *Setting up the Logger* and *Reading Out the Logger*).

LCD Screen: This logger is equipped with an LCD screen that displays details about the current status. This example shows all symbols illuminated on the LCD screen followed by definitions of each symbol in the table.

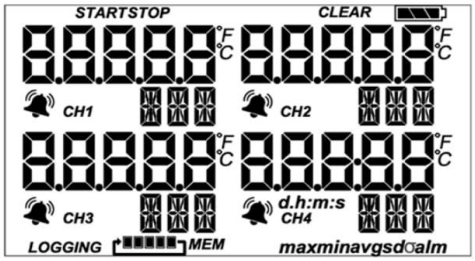

LCD Symbol	Description
START	The logger is waiting to be launched. Press and hold the Start/Stop button for 3 seconds to launch the logger.
STOP	The logger has been launched with push button stop enabled; press and hold the Start/Stop button for 3 seconds to stop the logger. **Note**: If you also launched the logger with a push button start, this symbol will not appear on the display for 30 seconds.
CLEAR	An alarm is ready to be cleared. This will only appear if "Cleared with button press" was selected in the HOBOware alarm settings. Press the Alarm/Stats button for 3 seconds to clear the alarm.
	The battery indicator shows the approximate battery power remaining.
86.2°F	This is an example of a temperature reading from a temperature sensor. Temperature units are determined by the settings in HOBOware. To switch between Celsius and Fahrenheit, change the Display Preferences in HOBOware before launching the logger.
	A sensor reading is above or below the high or low alarm that you configured. Press and release the Alarm/Stats button until the "alm" symbol (described later in this chart) is displayed on the screen. This symbol at left will clear depending on how alarms were configured in HOBOware. If the alarm was configured to clear when the logger is relaunched, this symbol will remain on the LCD. Otherwise, it will clear when the sensor reading is back within the alarm limits or by pressing the Alarm/Stats button for 3 seconds.
CH1	This is the channel number associated with the sensor reading (channel 1 for this example). Up to four channels are visible at one time.
AMP	This is an example of the units entered for the sensor, which appears to the right of the channel number. The unit type is determined by what was entered in the LCD Units field for that sensor in HOBOware. See *Setting up the Logger* for more details. Note that units for temperature sensors are displayed as °F or °C only.
05:38 m:s	The logger has been configured to start logging on a particular date/time. The display will count down in days, hours, minutes, and seconds until logging begins. In this example, 5 minutes and 38 seconds remain until logging will begin.

Appendix A2: Surface Temperature Sensor (TMC6-HE) (reproduced from Ref. 40)

TMCx-HE Temperature Sensor

For use with HOBO® U12 and UX120-006M data loggers and ZW data nodes

Specifications

Measurement Range	-40° to 100°C (-40° to 212°F)
Accuracy with U12	±0.25°C from 0° to 50°C (±0.45°F from 32° to 122°F), insert probe 2.3 cm (0.9 inches) minimum; see Plot A
Accuracy with ZW	±0.21°C from 0° to 50°C (±0.38°F from 32° to 122°F), insert probe 2.3 cm (0.9 inches) minimum; see Plot B
Accuracy with UX120-006M	±0.15°C from 0° to 50°C (±0.27°F from 32° to 122°F), insert probe 2.3 cm (0.9 inches) minimum; see Plot C
Resolution with U12	0.03° at 20°C (0.05° at 68°F)
Resolution with ZW	0.02°C at 25°C (0.04°F at 77°F)
Resolution with UX120-006M	0.002° at 25°C (0.003° at 77°F)
Drift	<0.1°C (<0.2°F) per year
Response time in air	2 min. typical to 90% in air moving 1 m/sec (2.2 mph)
Response time on a pipe	Typically 2 times faster than the TMCX-HD. Typically less than 1 minute to 90%.
Housing	Copper-plated sensor tip
Dimensions	0.9 x 5.8 cm (0.38 x 2.30 inches)
Weight	34 g (1.1 oz)

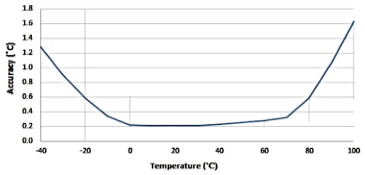

Plot A: U12 Accuracy*

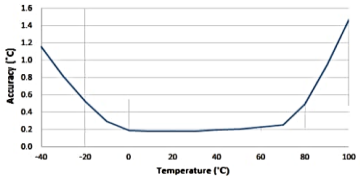

Plot B: ZW Accuracy*

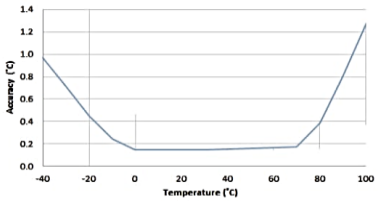

Plot C: UX120-006M Accuracy*

*Accuracy shown in plots outside the 0 to 50°C range is typical.

Items Included:

- 2 tie wraps
- 1 #6 screw
- Thermal compound

Mounting the Sensor

Use a small amount of the enclosed thermal compound between the flat part of the sensor tip and the surface where the sensor is being deployed to enhance the contact between the two.

Sensor mounted on pipe using two tie wraps:

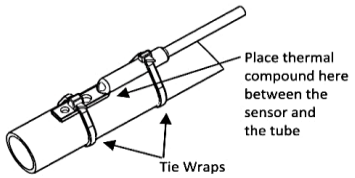

Sensor mounted on wall using #6 screw:

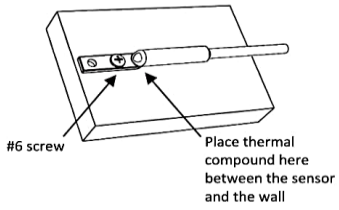

Appendix A3: **Recordall Turbo 450 Flow Meter** (reproduced from Ref. 41)

Cold Water Recordall® Turbo 450 Meter	Size 3" (DN 80 mm)	Technical Brief

DESCRIPTION

Badger Meter offers the 3" Turbo Series meter in Cast Bronze and a Low Lead Alloy. The Low Lead Alloy (Trade Designation: Turbo Series LL-NS) version complies with ANSI/NSF Standard 61, Annex G and carries the NSF-61 Mark on the product.

APPLICATIONS: For use in measurement of potable cold water in commercial and industrial services where flow is in one direction only.

OPERATION: Water flows into the meter's measuring element contacting the multi-vaned rotor. Flow readings are obtained by rotor revolutions transmitted by magnetic drive coupling through the meter's cover plate to the sealed register. Magnetic drive is achieved by a right angle worm drive, coupling the rotor to a vertical transmission spindle, driving a gear set rotating the magnet carrier. A ceramic magnet in a carrier rotates around a vertical axis. Through the magnetic coupling, rotor rotation is transmitted to a follower magnet which transmits rotation to the register gearing.

The turbo measuring element is designed to greatly reduce wear by reducing friction potential between the moving parts of the rotor and bearing system. Less wear, in this critical area of the design, provides the utility manager with a lower life cycle cost for meter application. Throughout the normal operating range of the meter, the rotor floats between the thrust bearing system.

OPERATING PERFORMANCE: The Badger® Recordall Turbo 450 meter meets and exceeds registration accuracy for the low flow rate, normal operating flow rate, and maximum continuous operation flow rate as specifically stated in AWWA Standard C701.

CONSTRUCTION: The Badger Recordall Turbo 450 meter construction which complies with ANSI and AWWA C701 standards, consists of three basic components: meter housing, measuring element and permanently sealed register. The housing is bronze, with round flanges. The measuring element consists of the transmission coupling, measuring element insert, rotor, inlet and outlet straightening vanes with nose cones, and calibration ring assembly. The unique inlet and outlet straightening vanes minimize swirl from piping arrangements upstream as well as downstream.

To simplify maintenance, the register and measuring element can be removed without removing the meter housing from the installation. No change gears are required for accuracy calibration. Interchangeability of certain parts between 1 1/2" - 4" like-sized meters also minimizes spare parts inventory investment.

MAGNETIC DRIVE: Direct magnetic drive, through the use of high-strength magnets, provides positive, reliable and dependable register coupling for straight-reading, remote or automatic meter reading options.

SEALED REGISTER: The standard register consists of a straight-reading odometer-type totalization display, 360° test circle with center sweep hand and flow finder to detect leaks. Register gearing consists of self-lubricating thermoplastic gears to minimize friction and provide long life. Permanently sealed; dirt, moisture, tampering and lens fogging problems are eliminated. Multi-position register simplifies meter installation and reading. Automatic meter reading and close proximity systems are available for all Recordall Turbo meters. (See back of sheet for additional information.) All reading options are removable from the meter without disrupting water service.

TAMPER-RESISTANT FEATURES: Customer removal of the register to obtain free water can be prevented if the tamper detection seal wire screw or TORX® tamper resistant seal screw is added to the meter. Both can be installed at the meter site or at the factory. A tamper resistant calibration plug seal provides protection from unauthorized personnel.

STRAINER: A separate strainer is recommended to protect the measuring element. See Technical Brief PS-T-1 for strainer dimensions.

MAINTENANCE: Badger Recordall Turbo meters are designed and manufactured to provide long-term service with minimal maintenance. When maintenance is required, it can be performed easily either at the meter installation or at any other convenient location. As an alternative to repair by the utility, Badger offers various maintenance and meter component exchange programs to fit the needs of the utility.

CONNECTIONS: Companion flanges for installation of meters on various pipe types and sizes are available in cast iron or bronze as an option.

TEST PLUG: An optional 2" NPT test plug puts an end to removing and reinstalling meters during field accuracy and pressure testing.

Turbo 450 with Optional 2" Test Plug

SPECIFICATIONS

Typical Operating Range (100% ± 1.5%)	5 - 550 GPM (1.1 to 124.9 m³/h)
Maximum Continuous Operation	450 GPM (102.2 m³/h)
Maximum Intermittent Flow	550 GPM (124.9 m³/h)
Typical Low Flow (Min. 95%)	4 GPM (0.9 m³/h)
Pressure Loss at Maximum Continuous Operation	1.8 PSI (.12 bar at 102.2 m³/h)
Maximum Operating Temperature	120°F (49°C)
Maximum Operating Pressure	150 PSI (10 bar)
Meter Flanges	3" Round AWWA 125 pound class
Register	Straight reading, permanently sealed magnetic drive standard. Automatic Meter Reading and Close Proximity units optional.
Registration	100,000,000 Gallons 100 gallons/sweep hand revolution. 10,000,000 Cubic Feet 10 cubic ft./sweep hand revolution. 1,000,000 m³ 1 m³/sweep hand revolution. 100,000,000 Imperial Gallons 100 Imperial Gallons/sweep hand revolution.

MATERIALS

Housing	Cast Bronze (B81), Low Lead Alloy
Turbo Head	Cast Bronze (B81), Low Lead Alloy
Nose Cone and Straightening Vanes	Thermoplastic
Rotor	Thermoplastic
Rotor Radial Bearings	Lubricated Thermoplastic
Rotor Thrust Bearings	Sapphire Jewels
Rotor Bearing Pivots	Passivated 316 Stainless Steel
Calibration Mechanism	Stainless Steel and Thermoplastic
Magnet	Ceramic
Register Lid and Shroud	Thermoplastic, Bronze
Trim	Stainless Steel

BadgerMeter, Inc.

RTS-T-3

9-10

PRESSURE LOSS CHART

Rate of Flow, in Gallons per Minute

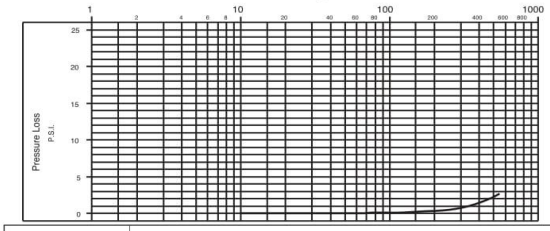

ACCURACY CHART

Rate of Flow, in Gallons per Minute

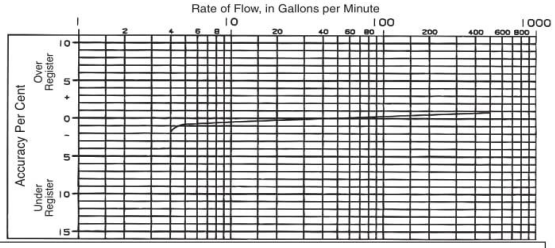

Meter & Pipe Size	DIMENSIONS								
	Length A	Width B	Height C	Flange D	Bolt Circle E	Centerline F	No. Bolts	Net Weight	Shipping Weight
3" RD (DN 80)	12" (305mm)	7 1/2" (191mm)	8 11/16" (220mm)	3/4" (19mm)	6" (152mm)	3 11/32" (85mm)	4	31 lb. (14.1kg)	34 lb. (15.4 kg)

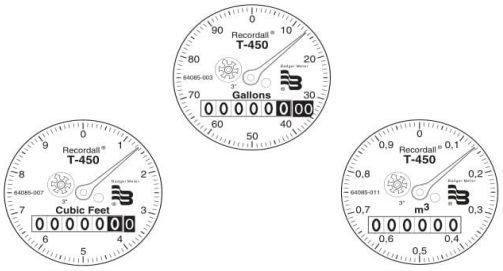

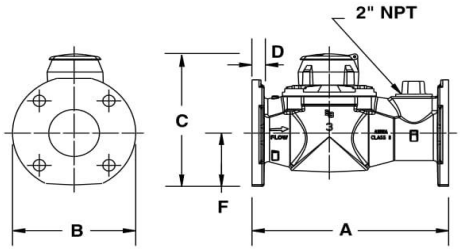

PROPER INSTALLATION: The following installation guidelines will insure optimum field performance and reliability when installing a Badger Turbo meter.

1. A strainer is recommended to insure optimum flow conditioning and protection for the turbo meter measuring element.
2. When using a strainer, five (5) diameters of straight pipe separating the strainer upstream of the meter is recommended.
3. ONLY full-open gate valves should be used immediately upstream of the meter. Butterfly valves MUST be five (5) pipe diameters or more upstream of the meter. Full-open gate or butterfly valves can be used downstream.
4. DO NOT install pressure reducing devices or check valves upstream of the meter.
5. Unweighted check valves MUST be located at least three (3) pipe diameters downstream of the meter.
6. Pressure reducing devices and externally weighted check valves MUST be located at least five (5) pipe diameters downstream of the meter.

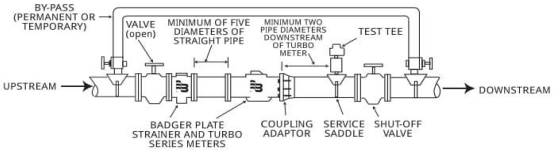

Please see our website at
www.badgermeter.com
for specific contacts.

Due to continuous research, product improvements and enhancements, Badger Meter reserves the right to change product or system specifications without notice, except to the extent an outstanding contractual obligation exists.

BadgerMeter, Inc.
P.O. Box 245036, Milwaukee, WI 53224-9536
(800) 876-3837 / Fax: (888) 371-5982
www.badgermeter.com

Appendix A4: Electrically Actuated Flow Control System

As explained briefly in Section 1.3.1, an idea was suggested to use an electric flow control valve in the make-up water pipe line instead of the solenoid valve (S.V.) in that pipe line. By using an actuated valve to control the flow of the make-up water to the storage tank, the solenoid valve upstream the tank would not be needed anymore. That is because the control valve would maintain and control the flow rate, according to the desired condensate water level inside the tank by using an ultrasonic level transmitter on the tank. The ultrasonic transmitter would reflect the condensate water level as an analog signal 4-20 mA, which then would be sent to the actuator valve that would control the flow in the make-up line based on the provided signal. Figure A4.a shows a schematic of the suggested system in the make-up pipe line and the storage tank.

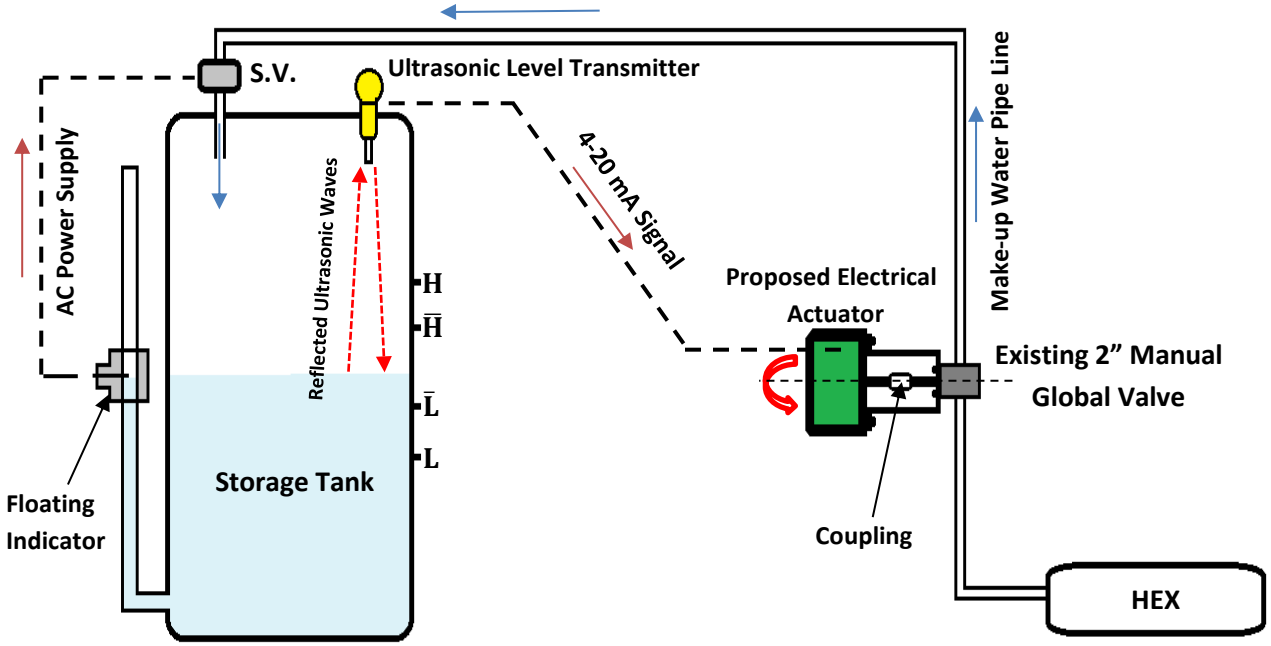

Fig. A4.a. Current and suggested make-up flow control systems

For the current control system, the solenoid valve shown in Fig. A4.a is normally closed, and it is controlled (open or closed) by controlling its AC power supply through a mechanical floating system. That system has a lever that moves, up or down according to the water level inside the pipe next to the tank (see Fig. A4.a). The indicator cuts off the AC power when the water level at position H, so the solenoid will be closed since it is normally closed. When the level reaches position L inside the tank, the floating indicator turns on the AC power to open the solenoid valve. However, this operating procedure caused a problem for the KU SPP staff because the temperature of the basement heat exchanger drastically changed between about 70 °F to about 200 °F due to the solenoid valve suddenly opening/closing.

That caused thermal stress shock to the heat exchanger tubes' walls, which led to failure of the metal and leakage for two previous heat exchangers in the SPP.

The suggested idea was based on keeping the water continuously flowing, so that the temperature changed gradually through the heat exchanger in order to avoid thermal shock. Since it was not possible for the staff to cut and weld the make-up water pipe line, because the whole SPP would have to shut down in order to install a control valve, it was possible to use a 2 in manual globe valve that is already in the pipe line by installing an electrical actuator that would be coupled to the manual valve's stem, as shown in Fig. A4.a. However, the actuator would need a 4-20 mA signal to operate; so an ultrasonic level transmitter was proposed for installation in the tank, which would provide that type of signal.

The ultrasonic level transmitter could be adjusted to provide a signal of 4 to 20 mA to reflect the desired limits of the minimum and maximum water level inside the storage tanks. If the water level was at position $\overline{\mathrm{L}}$ as shown in Fig. A4.a, the ultrasonic transmitter would provide a 4 mA signal which would be sent to the actuator to open the globe valve in the make-up line. When the water level reached position $\overline{\mathrm{H}}$, a 20 mA signal would be provided by the ultrasonic level transmitter which would be sent to the actuator to close the globe valve. The globe valve would always be partially open when the water level was between the positions $\overline{\mathrm{L}}$ and $\overline{\mathrm{H}}$. So this system would cause the temperature to change gradually through the heat exchanger, since the manual valve would open and close gradually, in place of the solenoid valve's suddenly action.

In addition, another idea was proposed in order to make the system more efficient by avoiding the fully closed/open positions completely. This concept would maintain the water flow at all times through the heat exchanger. This would be achieved by adjusting the actuator to be about 95% closed (or whatever the proper percentage should be after some trial runs), instead of 100% closed, when the provided signal was 20 mA (the level at the position $\overline{\mathrm{H}}$). In this case, the make-up water would flow through the heat exchanger all of the time.

Furthermore, the actuator design has a fail-safe mode as protection for the system. The fail-safe mode forces the actuator to be fully closed or fully open (to be selected by KU SPP) in case the power supply or the input signal from the ultrasonic transmitter fails. Moreover, the old system (i.e., the solenoid valve with float indicator) could be used as further protection in the make-up line when the suggested control system failed. When the water level went higher than $\overline{\mathrm{H}}$, reaching position H, the solenoid valve would close. This extra protection could prevent the storage tanks from overflow when both the proposed system and its fail-safe mode did not work. For that reason, the high and the low levels for the proposed control system were chosen to be within the limits of the current system. The proposed equipment for the new system is shown in Apps. A4-1 and A4-2.

Appendix A4-1: 200 in-lb SR Electrical Actuator (reproduced from Ref. 42)

INDELAC MODEL
SR & SX

MADE IN U.S.A PRODUCT

(200 & 300 IN-LB) NEMA 7

The S series NEMA 7 rotary electric actuator was designed solely for applications within the SR & SX torque range used in hazardous locations. These heavy-duty reversing actuators are used in place of model SD, SR, SDX, and SX when the area used in requires enclosure rating of Class I Groups C & D and Class II Groups E, F, & G div. I and II. These compact actuators are equipped with spur gear drive and, as in all ICI actuators, can withstand all conditions without suffering gear failure.

SPECIFICATIONS

TORQUE	SR SX	200 In-Lb 300 In-Lb	(22.6 Nm) (33.9 Nm)
CYCLE TIME	5 sec. / 90° 115 Vac & 230 Vac 10 sec. / 90° with 75% duty cycle		
DUTY CYCLE	25% (standard) 115 Vac & 230 Vac 75% (optional) 12 Vdc, 24 Vdc / Vac & 115Vac Ext.		
ENCLOSURE	NEMA 7, C, US certified by CSA		

CSA Std. C22.2 No. 139-1982 - Electrically Operated Valves
CSA Std. C22.2 No. 25-1966 - Enclosures for Use in Class II, Group E, F and G Hazardous Locations
CSA Std. C22.2 No. 30-M1986 - Explosion-Proof Enclosures for Use in Class I Hazardous Locations
UL Std. No. 429:1999 - Electrically Operated Valves
UL Std. No. 1203:2000 - Explosion-Proof and Dust-Ignition-Proof Electrical Equipment for use in Hazardous Location

COATING	Thermally bonded polyester powder
POSITION IND.	Visual indicator (optional) Wired for light indication
SWITCHES	SPDT snap action, 15 Amps @ 250 Vac
LUBRICATION	Permanent
WEIGHT	14 Lbs
INSTALLATION	Universal
TEMP. RANGE	-40°F to 150°F Heater & Thermostat required 0°F & below
MODULATING	Available also with poisition indicator and manual override
OVERRIDE	Manual, not declutching (optional) Declutching manual override (optional)

Access Online Product Page

Scan the QR Code

INDELAC CONTROLS, INC. FLORENCE, KY 41042 TOLL FREE: 1-800-662-9424 www.INDELAC.com

TECHNICAL DRAWINGS & WIRING DIAGRAM

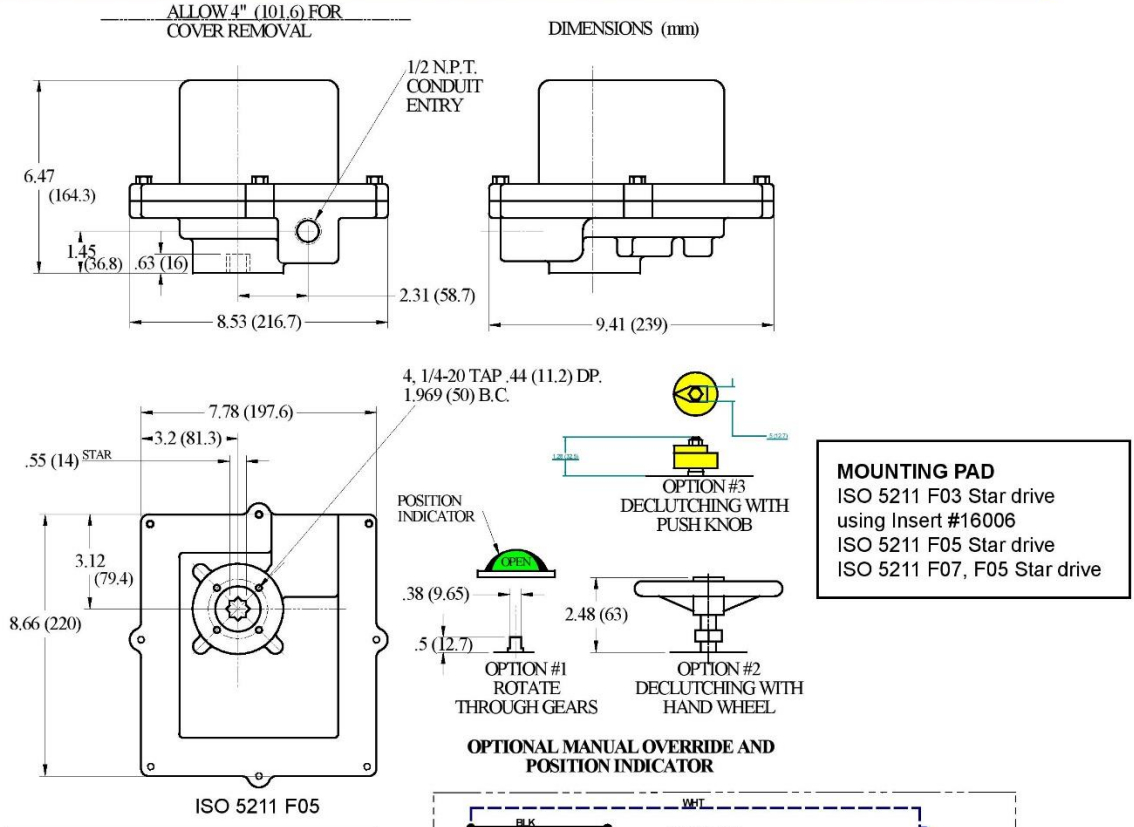

MOUNTING PAD
ISO 5211 F03 Star drive
using Insert #16006
ISO 5211 F05 Star drive
ISO 5211 F07, F05 Star drive

ISO 5211 F05

MOTOR SPECIFICATIONS
Permanent split capacitor
115 Vac / 1Ph / 50-60 Hz (standard)
with thermal over load protection

115 Vac (Std.)	FL	0.38
	LR	0.75
115 Vac Ext'ed Duty	FL	0.38
	LR	0.75
24 Vac	FL	0.7
	LR	3.2
24 Vdc	FL	0.7
	LR	3.2
12 Vdc	FL	1.3
	LR	4.2
208 Vac/1Ph/60Hz	FL	0.21
	LR	0.42
230 Vac/1Ph/60Hz	FL	0.18
	LR	0.38

FL = Full Load, LR = Lock Rotor

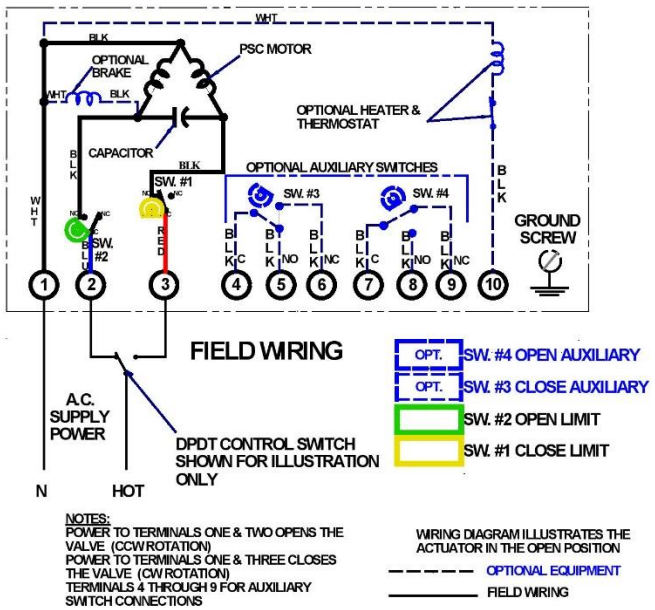

NOTES:
POWER TO TERMINALS ONE & TWO OPENS THE VALVE (CCW ROTATION)
POWER TO TERMINALS ONE & THREE CLOSES THE VALVE (CW ROTATION)
TERMINALS 4 THROUGH 9 FOR AUXILIARY SWITCH CONNECTIONS

WIRING DIAGRAM ILLUSTRATES THE ACTUATOR IN THE OPEN POSITION
OPTIONAL EQUIPMENT
FIELD WIRING

<u>Appendix A4-2:</u> EchoPod DL24 Ultrasonic Level Transmitter (reproduced from Ref. 43)

EchoPod® DL24 Ultrasonic Level Transmitter, Switch & Controller

FLOWLINE®

Application

The general purpose ultrasonic level transmitter provides continuous level measurement up to 9.8' (3m) with a 4-20 mA signal output, and is configured via our free Webcal software. The level sensor has 4 programmable relays with selectable hysteresis and fail-safe logic. The embedded level controller can lower cost by replacing external control hardware. This non-contact liquid level sensor is ideally suited for corrosive, sticky or dirty liquids, and is widely selected for day tank, skid, IBC, sump and process tank level applications.

RoHS Compliant CE FM APPROVED

Features

- Level detection, switch and control functions up to 9.8' (3m)
- Configuration is fast and easy via WebCal software and USB adapter
- Narrow 2" beam width and short 4" dead band optimized for small tanks
- Four programmable relays for switch, pump or valve control and fail-safety
  - 1 pump or valve with 3 alarms
  - 2 pumps (lead-lag) with 2 alarms
  - 2 pumps (duplexing) with 2 alarms
  - 4 independent switch point alarms
- PVDF transducer and 6P polycarbonate enclosure for corrosive liquids
- Automatic temperature compensation for accurate measurement

Success

About 1.3M polyethylene tanks are sold in North America each year ranging in size from 1 to 15,000 gallons. Most of these are less than 6' in height with capacities under 500 gallons. The largest markets are industrial manufacturing, municipal, agriculture and residential in chemical, water & wastewater applications. Over the past 10 years, customers have moved toward the use of smaller storage tanks with increased automation to lower cost. Today, mini-bulk tanks are a major product category. Flowline has developed a new multi-function sensor to meets the needs of this growing market. The DL24 EchoPod puts non-contact level measurement, relay switch and advanced control functions in the palm of your hand.

Compatible Products

DataLoop™ Level Indicator

LI25

DataView™ Level Controller

LI55

Commander™ Multi-Tank Level Controller

LI90

DataPoint™ Level Controller

LC52

EchoPod® DL24 Ultrasonic Level Transmitter, Switch & Controller

FLOWLINE®

Specifications

Range:	9.8' (3m)
Accuracy:	± 0.2% of range
Resolution:	0.039" (1mm)
Dead band:	4" (10cm)
Beam width:	2" (5.08cm)
Configuration:	WebCal® PC Windows® USB 2.0
Memory:	Non-volatile
Supply voltage:	24 VDC (loop)
Consumption:	0.5W
Loop resist.:	400Ω max
Signal output:	4-20 mA, two-wire
Signal invert:	4-20 mA or 20-4 mA
Signal fail-safe:	4 mA, 20 mA, 21 mA, 22 mA or hold last
Contact type:	(4) SPST relays
Contact rating:	60 VA, 1A maximum
Contact fail-safe:	Power loss: Hold last Echo loss: Open, close or hold last
Hysteresis:	Selectable
Process temp.:	F: 20° to 140° C: -7° to 60°
Temp. comp.:	Automatic
Ambient temp.:	F: -31° to 140° C: -35° to 60°
Pressure:	MWP = 30 PSI (2 bar)
Enclosure rating:	Type 6P, encapsulated, corrosion resistant & submersible
Encl. material:	Polycarbonate
Trans. material:	PVDF
Cable jacket mat:	Polyurethane
Cable type:	9-conductor, shielded
Cable length:	48" (1.2m)
Process mount:	1" NPT (1" G)
Mount gasket:	Viton®
Classification:	General purpose
Compliance:	CE, RoHS
Approvals:	cFMus

Dimensions

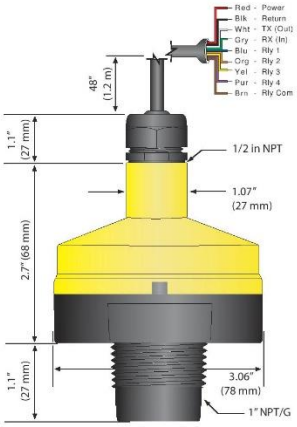

Configuration

LI99-1001

The level sensor is configurable via our free WebCal PC software and Fob USB adapter. The sensors are offered with and without Fobs. Fobs are universal and can be used to configure any WebCal compatible product.

Download your free copy of WebCal in English or Chinese at www.flowline.com/webcal.php.

Fittings

For optimum performance, install the level sensor using the below recommended or direct equivalent fittings.

	P/N	Description
	LM52-1400	2" NPT x 1" NPT (Sch. 40)
	LM52-1800	2" NPT x 1" NPT (Sch. 80)
	LM52-1410	2" Socket x 1" NPT (Sch. 40)
	LM52-1810	2" Socket x 1" NPT (Sch. 80)
	LM52-1850	1" NPT Flange - 150# (Sch. 80)
	LM50-1001-1	1" NPT Bracket, Polypropylene

Ordering

DL24-□□

Process mount (1)
- ***0*** *NPT (US)*
- ***1*** *G (Metric)*

Fob USB adapter (2)
- ***0*** *Without Fob*
- ***1*** *With Fob*

Notes

1) Install the level sensor using Flowline installation fittings or equivalents.
2) The level sensor is configured via our WebCal software and one LI99-1001 Fob USB adapter. The level sensor is offered with and without a Fob. Fobs are universal and can be used to configure any WebCal compatible product. WebCal is a free download from our website at www.flowline.com/webcal.php.

 • 10500 Humbolt Street Los Alamitos, CA 90720 • 562.598.3015 • www.flowline.com • DS204200 REV A

Appendix A5: Cadillac Magnetic Flow Meter (reproduced from Ref. 44)

Cadillac Meter

ACCURATE & RELIABLE ENERGY METERS

GENERAL INFORMATION

Cadillac® Magnetic Flow Meter CMAG Series

CENTRAL STATION STEAM CO.® 15615 SW 74TH AVE., STE #150 TIGARD, OR 97224 PHONE: 888-556-3913 FAX: 503-624-6131 @ WWW.CADILLACMETER.COM

Rev 0613

METER INSTALLATION

Cadillac CMAG Piping Requirements

Installation requirements have been redefined with the Cadillac magnetic flow meter.

Employing coil and plate shaping techniques the Cadillac® meter provides a uniform magnetic flux shaping within the flow tube. This allows the meter to measure and sample uniformly the entire flow tube area.

In addition, the electronics provide high frequency DC square wave signal generation and flow signal sampling. When combined these two techniques eliminate all straight run flow profiling requirements, significantly decrease signal to noise ratio, and increase low flow accuracy.

In practice, this means the Cadillac magnetic flow meters may be installed next to elbows, tees, valves, etc. without any effect in meter accuracy or stability. (See Illustrations). This also allows the CMAG to be installed in gravity flow applications with a turndown of 300:1 @ +/- 0.25% accuracy.

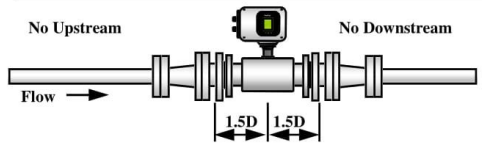

D = nominal flow meter diameter

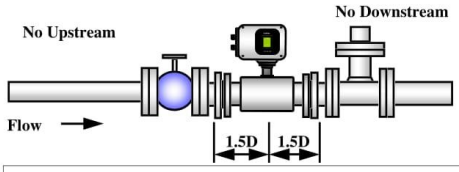

Traditional Magmeter Piping Requirements

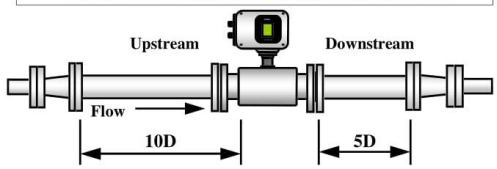

D = nominal flow meter diameter

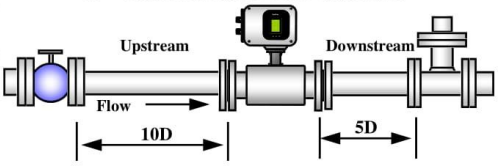

In comparison, the straight pipe run requirements for all other magnetic flow meters are as follows:

Downstream of the meter:
- ◊ Expander (2-5) diameters
- ◊ Tee - (2-5) diameters
- ◊ Elbow - (2-5) diameters
- ◊ Valves - (2-10) diameters

- **Upstream of the meter:**
  - ◊ Expander - (10) diameters
  - ◊ Tee - (5) diameters
  - ◊ Elbow - (5) diameters
  - ◊ Valves - (10) diameters

Unlike other technologies such as the Cadillac® Vortex flow meter, magnetic flow meters do not have a low flow cutoff, essentially allowing the meter to read to zero. With such a wide flow range capability for the technology, most applications can be addressed with meters at full line size.

The Cadillac® magnetic flow meter has a 304 stainless steel body and is always sold with integral grounding rings installed. The primary reason for providing grounding rings is to contain the magnetic field within the meter body and to assure the liquid potential is grounded properly. As a consequence, the induced voltage is remarkably free of noise allowing the meter to reliably measure extremely low fluid velocities. The table below lists minimum and maximum 4-20 madc output spans for each meter size, in GPM for liquids and lbs/hr for condensate.

CMAG	Liquid Flow Range Table		Condensate Flow Range Table	
Meter Body (inches) Size	Minimum Volumetric (gal/min) Range	Maximum Volumetric (gal/min) Range	Minimum Condensate (lbs/hr) Range	Maximum Condensate (lbs/hr) Range
0.50"	0.00 - 0.250	0.00 - 25.00	0.00 - 125.0	0.00 - 12,500
1.0"	0.00 - 0.750	0.00 - 75.00	0.00 - 375.0	0.00 - 37,500
1.5"	0.00 - 1.750	0.00 - 175.0	0.00 - 875.0	0.00 - 875,000
2.0"	0.00 - 3.000	0.00 - 300.0	0.00 - 1,500	0.00 - 150,000
3.0"	0.00 - 8.000	0.00 - 800.0	0.00 - 4,000	0.00 - 400,000
4.0"	0.00 - 12.50	0.00 - 1,250	0.00 - 6,250	0.00 - 625,000
6.0"	0.00 - 25.00	0.00 - 2,500	0.00 - 12,500	0.00 - 1,250,000
8.0"	0.00 - 50.00	0.00 - 5,000	0.00 - 25,000	0.00 - 2,500,000
10.0"	0.00 - 75.00	0.00 - 7,500	0.00 - 37,500	0.00 - 3,750,000

Low velocity "Turndown Accuracy" of the CMAG has allowed it to address applications, which were not possible for volumetric flow meters in the past. Below is the turndown accuracy for the CMAG:

- ♦ (**+/- 0.25%**) of rate at **300:1** turndown with 1.5 diameters of straight piping from meter centerline up/downstream.
- ♦ (**+/- 0.50%**) of rate from **300:1 to 400:1** turndown with 1.5 diameters of straight piping from meter centerline up/downstream.
- ♦ (**+/- 1.00%**) of rate from **400:1 to 500:1** turndown with 1.5 diameters of straight piping from meter centerline up/downstream.

CENTRAL STATION STEAM CO.® 15615 SW 74TH AVE., STE #150 TIGARD, OR 97224 PHONE: 888-556-3913 FAX: 503-624-6131 @ WWW.CADILLACMETER.COM

Rev 0613

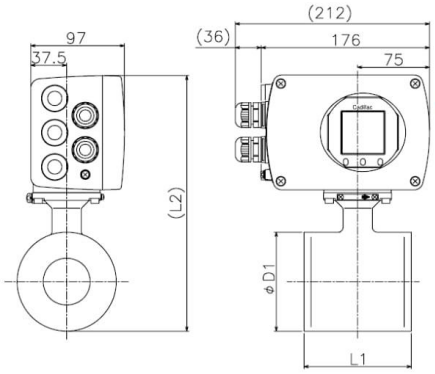

Cadillac Meter

ACCURATE & RELIABLE ENERGY METERS

Unit: inch (mm)

CMAG Flanged ANSI class 150 dimensions					
Meter Size (inch)	L1 (inch)	L2 (inch)	L3 (inch)	No. of Bolts	Weight (lbs)
1/2	5.51	7.99	9.88	4	21
1	6.30	8.23	10.71	4	25
1 1/2	6.69	8.58	11.34	4	28
2	7.09	9.13	12.20	4	32
3	9.06	10.04	13.66	4	62
4	9.45	10.31	14.45	8	72
6	10.24	11.22	16.73	8	115
8	11.81	12.20	18.70	8	145
10	13.78	13.18	21.06	12	210
12	15.75	14.37	23.15	12	355
14	17.72	14.72	24.37	12	460

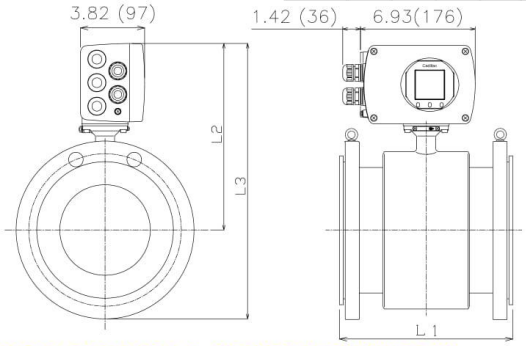

CMAG Wafer ANSI class 150/300 dimensions				
Meter Size (inch)	L1 (inch)	L2 (inch)	D1 (inch)	Weight (lbs)
1/2	2.76	9.33	1.93	17
1	3.15	8.90	2.60	21
1 1/2	3.94	9.80	3.35	25
2	4.33	10.43	4.02	29
3	4.33	11.46	5.00	35
4	4.72	12.72	6.26	40

CADILLAC® MAGNETIC FLOW METER GENERAL SPECIFICATIONS

- Meter will consist of a full-bore body with encapsulated and rigidly retained set of coils.
- Meter available with remote or integral electronics with indication and totalization.
- Meter operates at ± 0.25% accuracy without flow profiling or piping straight run exceeding 1.5 diameters.
- Meter operates with minimum 300 to 1 turndown at stated operating accuracy.
- Meter available with pulse and analog (4-20 mA) outputs.
- Meter will provide instantaneous and totalized flow available at local indicator or remotely through outputs.
- Meter measures flow using Faraday's law (Induce voltage is directly proportional to the velocity of the conductive liquid)
- Meter K-factor is stable and not influenced by external piping or mounting orientation.
- Meter will have uniform magnetic field flux distribution eliminating piping straight run and flow profiling.
- Meter will measure fluids with conductivity greater than or equal to 3.0 uS/cm.
- Meter will be calibrated to/and provided with NIST calibration certificate.

CADILLAC® MAGMETER MODEL NUMBER STRUCTURE

CMAG		Cadillac Magnetic Flow Meter
	A	Size 0.5"
	B	Size 1"
	C	Size 1.5"
	D	Size 2"
	E	Size 3"
	F	Size 4"
	G	Size 6"
	H	Size 8"
	I	Size 10"
	J	Size 12"
	K	Size 14" (Consult factory for larger sizes)
	II	Integral Converter with Indicator/Totalizer
	RC	Remote Converter
	W	Wafer Body (Ceramic Liner only) - available thru 4"
	F	Flanged Body
	150	ANSI Class 150
	300	ANSI Class 300
	S	Electrode Material - 316L SS (Std w/ Poly & EPDM)
	H	Electrode Material - Hastelloy C (std w/PFA)
	X	Electrode Material - Other
	C	Liner Material - PFA (Teflon) - (Temp rated 250˚F)
	U	Liner Material - Polyurethane (NSF approved)
	D	Liner Material - EPDM (Rubber)
	A	Liner Material - Ceramic (Temp rated 350˚F w/RC)
	S	Ground Ring Material - 316 Stainless Steel
	H	Ground Ring Material - Hastelloy C
	X	Ground Ring Material - Other
	FM	FM Approvals

CMC		CMAG Remote Converter
	R	Remote Mounting
	I	Indicator/Totalizer
	U	Universal Mounting Bracket
	XXFT	Interconnecting Cable (length in feet)
	FM	FM Approvals

APPLICATION NOTE:

The Cadillac® magnetic flow meter is an excellent choice for gravity flow applications. However for proper flow meter operation the piping and flow tube must be full at all times. This requires the meter to be mounted in such a way to provide a "Wet Leg" as illustrated below.

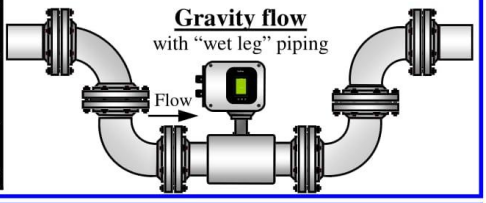

CENTRAL STATION STEAM CO.® 15615 SW 74TH AVE., STE #150 TIGARD, OR 97224 PHONE: 888-556-3913 FAX: 503-624-6131 @ WWW.CADILLACMETER.COM

Rev 0613

<u>Appendix A6:</u> RTD Temperature Probe (PR-12-2-100-SL) (reproduced from Ref. 45)

Replacement Probes
For Connection Head Assemblies Spring Loaded for Use in Thermowells

PR-12-2-100-SL Series

MADE IN USA — ACCURACY IEC CLASS A (±0.15°C @ 0°C)

- Replacement Probes Used with Connection Heads or Enclosures
- Pt100 Class A Wire Wound Sensing Element
- Includes Two ½ NPT Mounting Threads
- Probe is Spring Loaded to Mounting Fitting so Sensor Will Have Positive Contact with Thermowell Bore
- Temperature Range -200 to 500°C (-328 to 932°F) [260°C (500°F) Max at Wire Connection End]
- Available in ⅛, 3⁄16 and ¼" Diameters

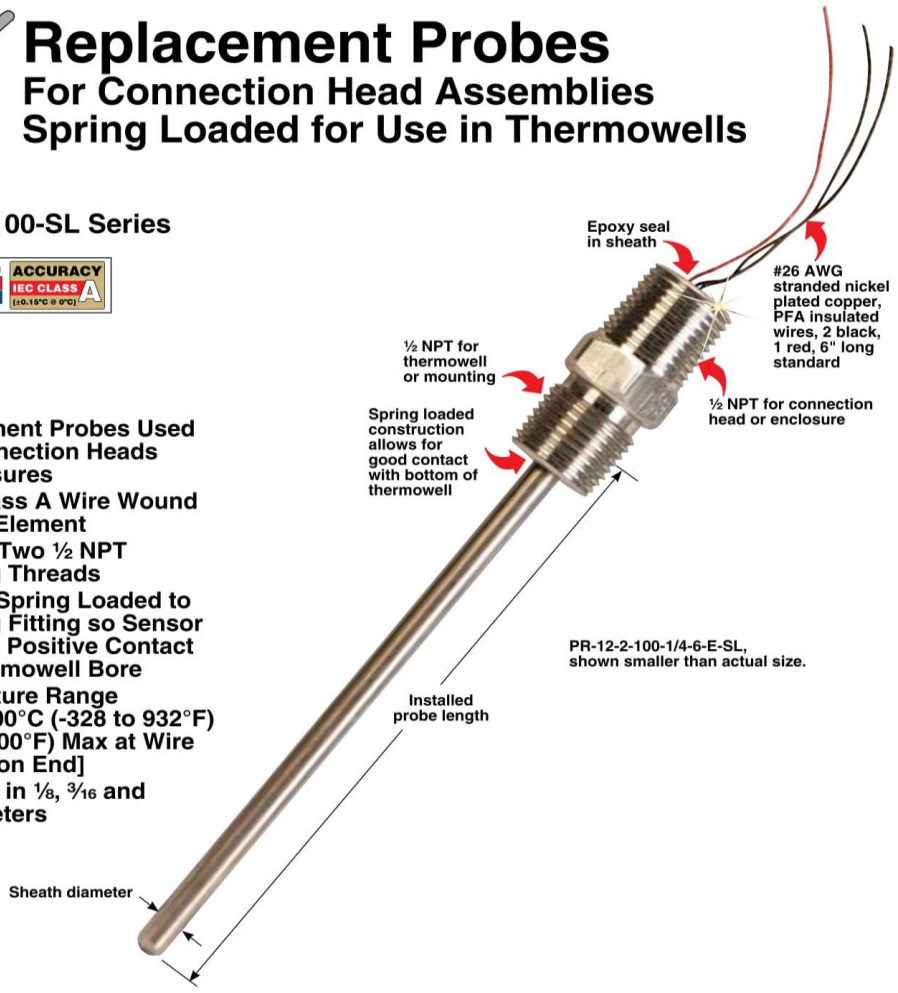

To Order *Visit omega.com/pr-12-rp for Pricing and Details*

Model No.	Number of Lead Wires	Resistance at 0°C	Sensor Accuracy	Sheath Length
PR-12-2-100-(*)-6-E-RP-SL	3	100Ω	Class A	6"
PR-12-2-100-(*)-9-E-RP-SL	3	100Ω	Class A	9"
PR-12-2-100-(*)-12-E-RP-SL	3	100Ω	Class A	12"
PR-12-2-100-(*)-18-E-RP-SL	3	100Ω	Class A	18"
PR-12-2-100-(*)-24-E-RP-SL	3	100Ω	Class A	24"

Notes: (*) *Specify ⅛, 3⁄16 or ¼" probe diameter. Lead wires are individual wires 6" long standard.*
*For 2-wire construction, change **"-2"** in model number to **"-1"**, for 4-wire construction, change to **"-3"** (color code is red/black, red/red/black or red/red/black/black), additional cost.*
For special probe lengths, change sheath length in model number to required sheath length in inches, additional cost per inch above 24".
*For lead wires other than 6" long, add lead wire length in inches after the **"-SL"** in the model number additional cost per foot.*
*For fiberglass insulated lead wires, add **"-GG"** to the model number for additional price.*
***Ordering Examples: PR-12-2-100-1/4-6-E-RP-SL,** spring loaded ¼" OD by 6" long probe with ½ x ½ NPT mounting threads, 100 Ω Pt100 Class A element and three 6 long PFA insulated extension wires.*
***PR-12-3-100-3/16-18-E-RP-SL-12-GG,** spring loaded 3⁄16" OD by 18" long probe with ½ x ½ NPT mounting threads, 100 Ω Pt100 Class A element and four 12" long fiberglass extension wires.*

C-97

<u>Appendix A6-1:</u> Omega Signal Transmitter (TX92A-3) (reproduced from Ref. 15)

1.4 Available Ranges

As specified in Table 1-1, the transmitter has 10 ranges. Depending upon the range, the transmitter can measure temperature span as narrow as 180°F or as wide as 1000°F. A multi-turn, top-accessible potentiometer provides fine span tuning. A second top-accessible, multi-turn potentiometer provides a zero adjustment which allows placement of the 4-mA output temperature within +/- 25% for Fahrenheit and +/- 10% for Celsius of nominal span (refer to Section 3.0, Calibrating the Transmitter, for more details). Models TX92A-*-L are transmitters with the 4-20mA output linearized to temperature.

Table 1-1. Range/Models

Range	Model	
-40 to 140°F	TX92A-1	TX92A-1-L
0 to 200°F	TX92A-2	TX92A-2-L
0 to 300°F	TX92A-3	TX92A-3-L
0 to 500°F	TX92A-4	TX92A-4-L
0 to 750°F	TX92A-5	TX92A-5-L
0 to 1000°F	TX92A-6	TX92A-6-L
-0 to 100°C	TX92A-7	TX92A-7-L
-0 to 150°C	TX92A-8	TX92A-8-L
-0 to 250°C	TX92A-9	TX92A-9-L
-0 to 400°C	TX92A-10	TX92A-10-L

2.0 CONNECTING POWER AND SIGNAL INPUTS

1. Verify that the transmitter is connected for the correct power voltage rating.
2. Connect the power supply to pin 4 and the resistance load to pin 5.
3. Connect the sensor to pins 1, 2 and 3.

The transmitter has no power on switch, so it will be in operation as soon as you apply power.

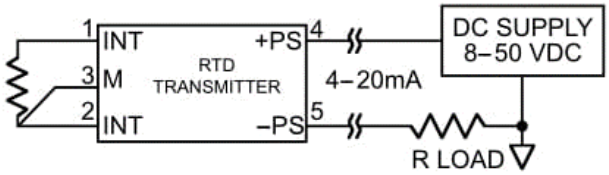

Figure 2-1 Power Input Setup

+PS and -PS screws accept 2mm (13 gauge) or lighter wire. Input range is 8-50 Vdc.

Table 2-1. Screw-Terminal Pin Assignment

1	RTD
2	RTD
3	M (Sense)
4	+Power/Signal Output
5	-Power/Signal Output

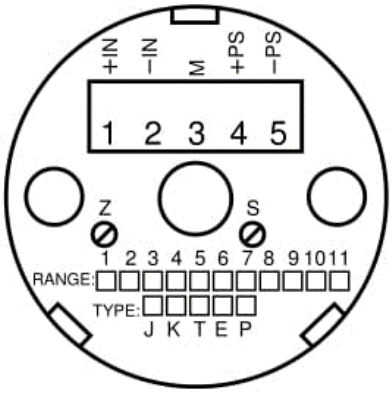

Figure 2-2 Pin Assignment

3.0 CALIBRATING THE TRANSMITTER

Calibration Setup:

1. Insert the reference RTD.
2. Connect RTD simulator.
3. Connect DMM monitor and power supply.

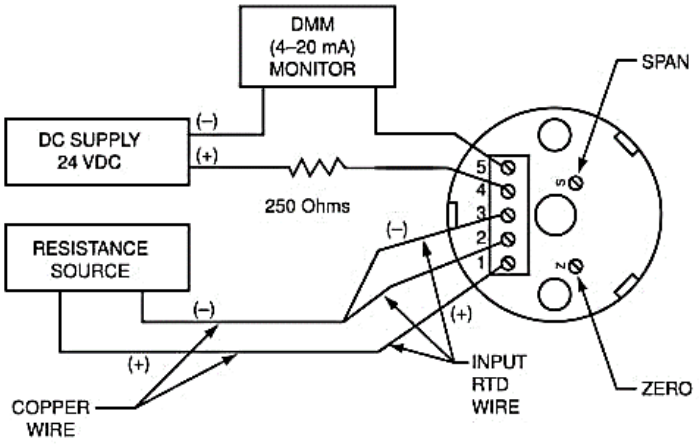

Figure 3-1. Calibration Setup (Resistance Source)

To calibrate the transmitter, follow these steps (refer to Figure 3-1):

1. Locate the model number in Table 3-1 or 3-2 and set the resistance source to the LO-IN value.
2. Adjust the Zero potentiometer until the milliammeter reads 4.00 mA.
3. Set the resistance source to the HI-IN value (in your appropriate table) and read the output current on the milliammeter.
4. Adjust the Span potentiometer to obtain the 20 mA on the milliammeter.
5. Set the resistance source to LO-IN resistance. If the output current is not 4.00 mA, repeat steps 2 through 7.
6. When calibration is complete, remove the transmitter from the setup.

Appendix A7: Materials for Modifying the Calibration Setup

Table A7.1. List of needed materials for modifying the calibration setup

Material	Quantity	Unit Price $	Total Price $
Pipe, 1 in x 10 ft, PVC	2	10.72	21.44
Elbow, 90 Deg, 1 in, Slip, PVC	4	2.97	11.88
Reducer Bush, 1-1/2 x ¾, PVC	1	6.31	6.31
Elbow, 90 Deg, 1-1/2 in, FN, PVC	1	6.34	6.34
Tee, 1-1/2 in, FNPT, PVC	1	13.26	13.26
Flange, 1 in, FNPT, PVC	2	11.79	23.58
Flange Gasket, 1 in Diameter	10	4.3	43.00
Cement, PVC, 16 oz, Blue	1	12.96	12.96
Submersible Water Pump, 500 gph	1	46	46
Water Hose, 5/8 in	50 ft.	15	15
Flat Vessel, 22 in x 16 in x 6 in	1	6.5	6.5
Cable Tie, 12 in	1 set	5	5
Bushing, 1 in, PVC	2	6.5	13
Bushing, 2 in, PVC	1	9.25	9.25
Hose Metal Clamp	2	0.9	1.8
Bolt, M16-2 Zinc-Plated Hex	8	1.25	10
Nut and Flat Washer, M16-2 Zinc-plated	8	0.5	4
Teflon Tape	3	0.75	2.25
Sand Paper	1 set	3	3
Brush	1	1.5	1.5
Total			256.07

Appendix A7-1: Re-designing the Calibration Setup

Since the calibration setup was re-located to the Lab B171, the structure of the setup frame was re-designed to fit the lab ceiling height. The height of the ceiling there is about 104 in, while the height of the setup was about 110 in, so it was necessary to re-design the frame. The first idea was to remove the wheels from the setup in order to reduce the frame height; but then it was found that would reduce just 5 in, as shown in Fig. A7.a. Then it was suggested to move the upper frame panel, which supports the tank, to a lower level because it could move down about 10 in. This was more than enough to reduce the total height of the setup to about 100 in in order to fit inside the lab, as shown in Fig. A7.b.

Figure A7.c shows a picture of the final setup with the new piping and flow meters. The power supply for the Grundfos pump was also modified in order to have adequate power capacity in Lab B171. For the power supply changes, see Fig. A7.d.

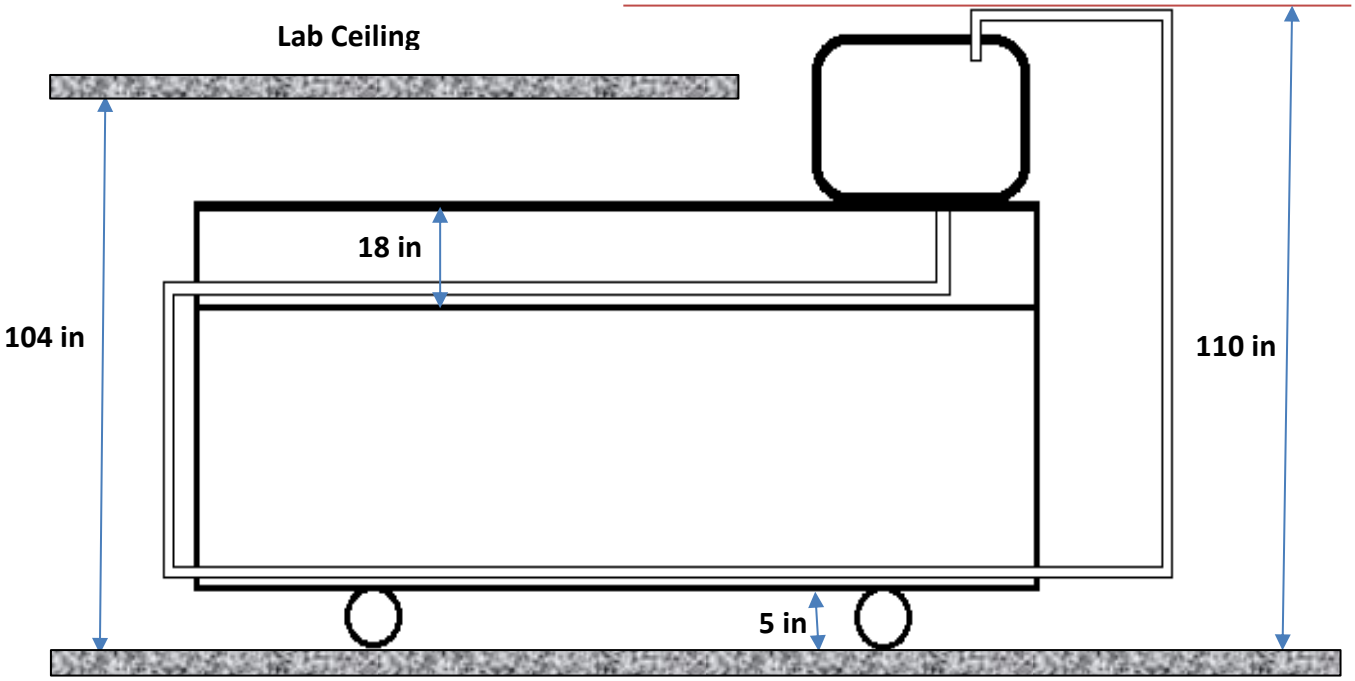

Fig. A7.a. The original design of the setup from a previous study [2]

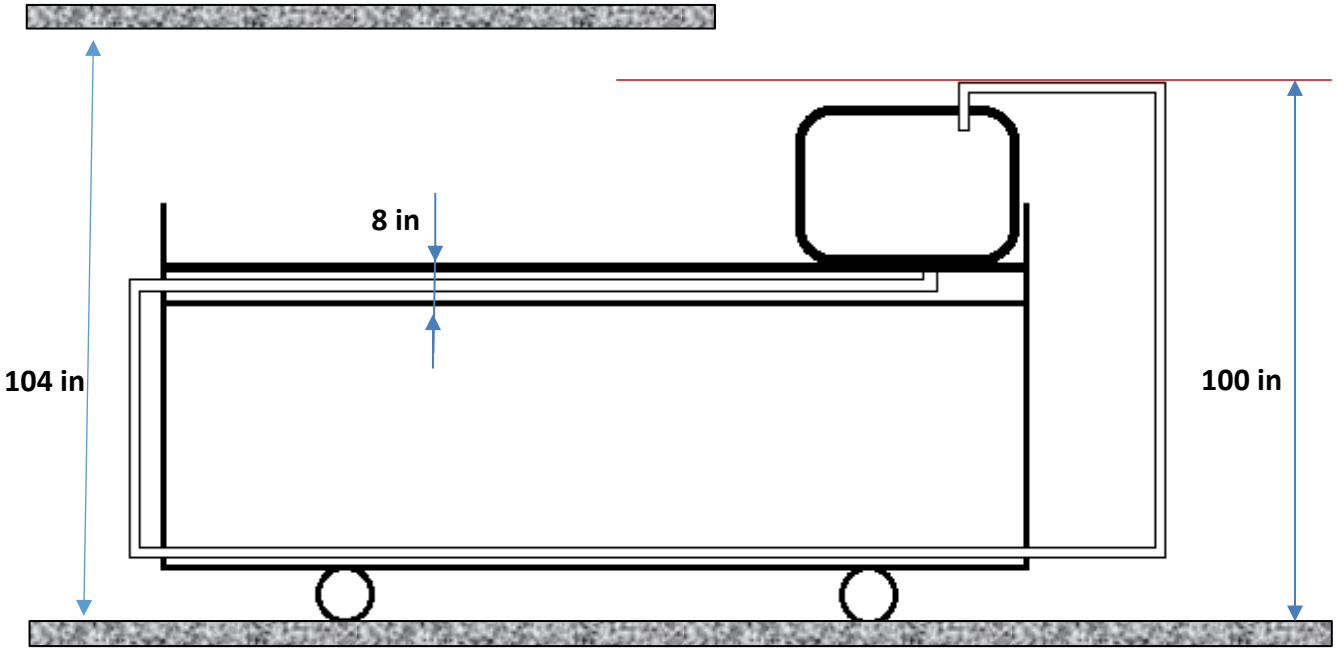

Fig. A7.b. The modified design of the setup to fit the Lab B171 height

Appendix A7-2: Modified Setup with Wiring Changes

Fig. A7.c. The modified calibration setup in Lab B171

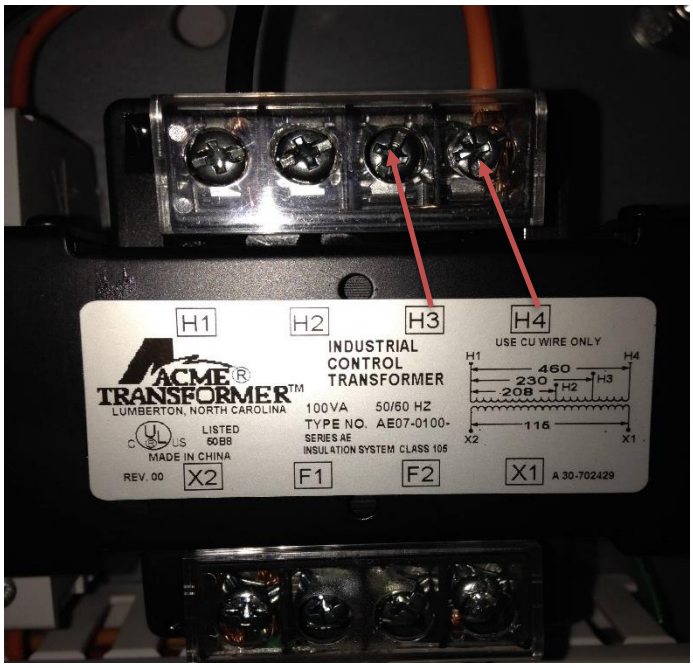

Fig A7.d. Changed wiring of the pump to 460 VAC

When the calibration setup was used by Alabdullah [2], the supplied voltage was 230 VAC where it was located in the ME lab. However, the only available power supply in Lab B171 was 460 VAC; so it was necessary to change the wiring on the Grundfos control panel to fit the 480 VAC of the Lab's power supply outlet. As shown in the picture of the wiring diagram in Fig. A7d, with 230 VAC, the black conductor was connected to pin H1, while the red conductor was connected to pin H3. In order to use 460 VAC, the black conductor was connected to pin H1, but the red conductor was connected to pin H4.

Appendix A7-3: Calibration Test Data and Error Calculations

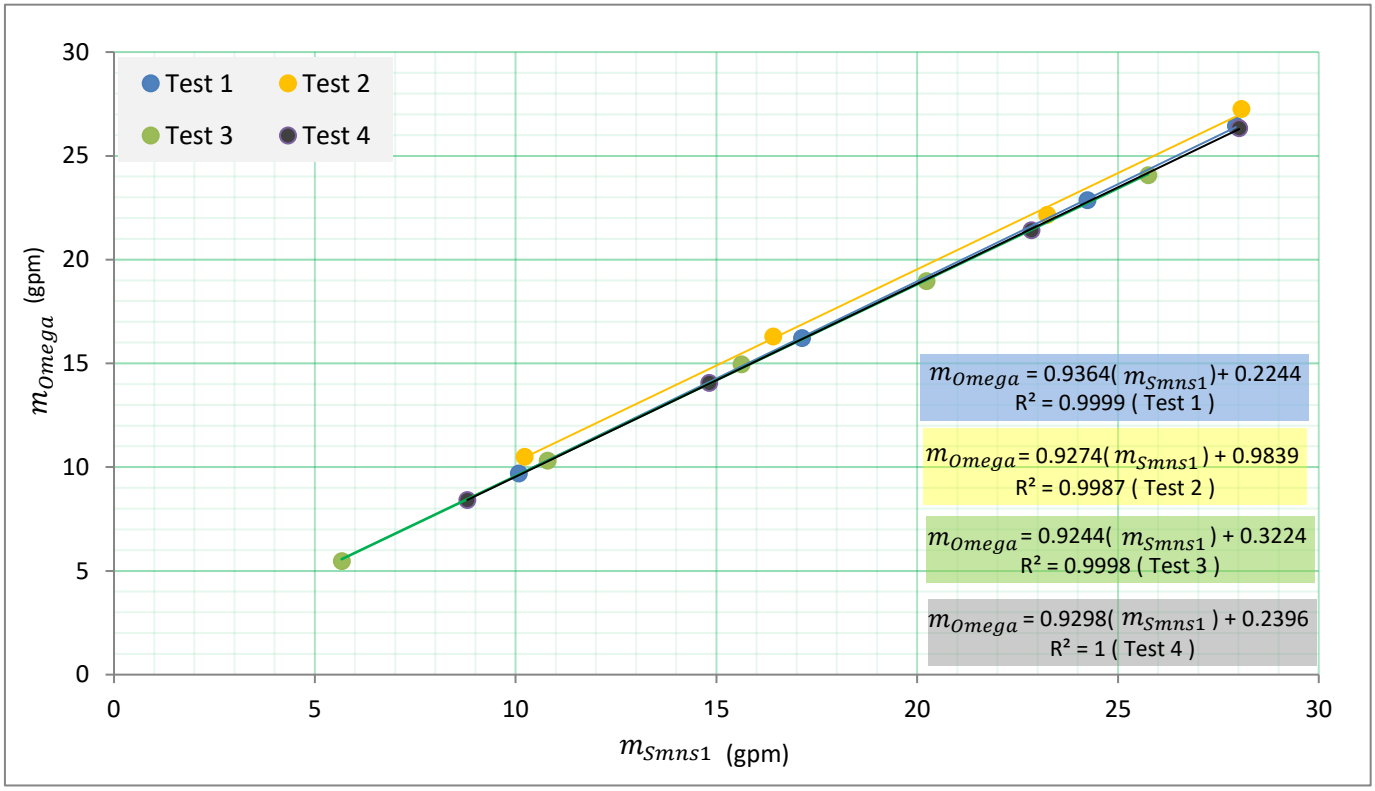

Fig. A7.e. Tests 1-4 recorded data at different time intervals; and the maximum and minimum tested flow rates

Calibration Error Calculations

The following equations were used to evaluate the error, average error, RMS error, and the standard deviation of errors in Table 1.

$$e_j\ (\%) = \frac{m_{Omega} - m_{Smns1}}{m_{Omega}}(100) \qquad \text{(A7-3a)}$$

$$e_{avg} = \frac{1}{n}\sum_{j=1}^{j=n}[e_j] \qquad \text{(A7-3b)}$$

$$\sigma_e = \{[\frac{1}{n}\sum_{j=1}^{j=n}(e_j - e_{avg})^2]\}^{0.5} \qquad \text{(A7-3c)}$$

$$e_{RMS} = \{[\frac{1}{n}\sum_{j=1}^{j=n}(e_j)^2]\}^{0.5} \qquad \text{(A7-3d)}$$

Appendix A7-4: **CSP and VSP Siemens Flow Meter Calibration Data**

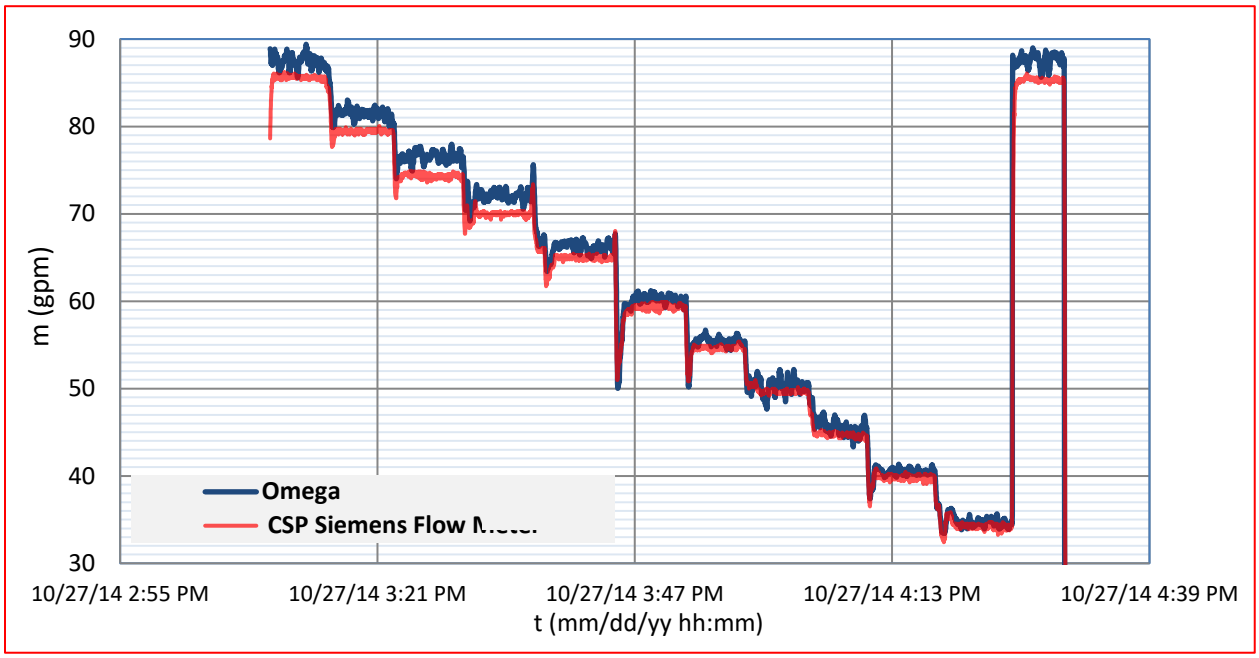

Fig. A7.f. Calibration curve for the Siemens flow meter located downstream of the Worthington pump

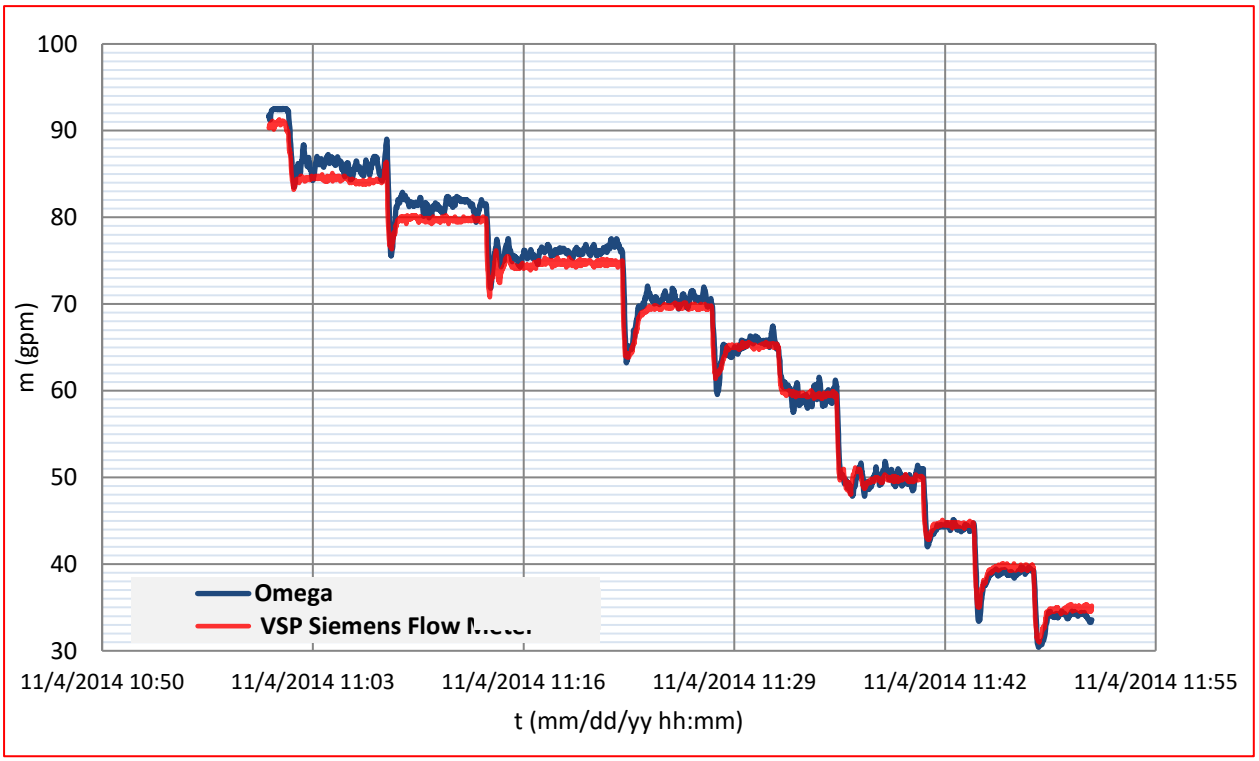

Fig. A7.g. Calibration curve of the Siemens flow meter located downstream of the Grundfos pump

<u>Appendix A8:</u> Siemens Mag5000 Flow Meter (reproduced from Ref. 16)

SITRANS F M MAG 5100 W Sensor

The SITRANS F M MAG 5100 W with its patented liners of hard rubber NBR or ebonite and EPDM is a sensor for all water applications such as ground water, drinking water, cooling water, waste water, sewage or sludge applications. Application examples: Water abstraction, Water distribution network, Waste water and as custody transfer water meter or cooling meter.

Details

Measuring range	0 to 10 m/s
Nominal Sizes	From DN 15 to DN 2000 (1" to 78")
Accuracy	0.2 % ±2.5 mm/s
Operating Pressure	Max. 16 bar (Max. 150 psi)
Ambient temperature	From -40 to 70 °C (-40 to 158 °F)
Medium Temperature	From -10 to 70 °C (14 to 158 °F)
Liners	EPDM NBR hard rubber Ebonite hard rubber
Electrodes	Hastelloy C-276 Built-in grounding electrodes
Material	Carbon steel, with corrosion resistant two-component epoxy coating
Drinking Water Approvals	EPDM: WRAS, NSF/ANSI Standard 61, DVGW 270, ACS and BelgAqua NBR: NSF/ANSI Standard 61, WRAS Ebonite: WRAS
Custody Transfer Approvals	OILM R 49 MI-001 PTB K7.2 (Germany) BEV OE12/C040 (Austria)
General approval	MCERTS Sira Certificate No. MC080136/00

Dimensional drawings

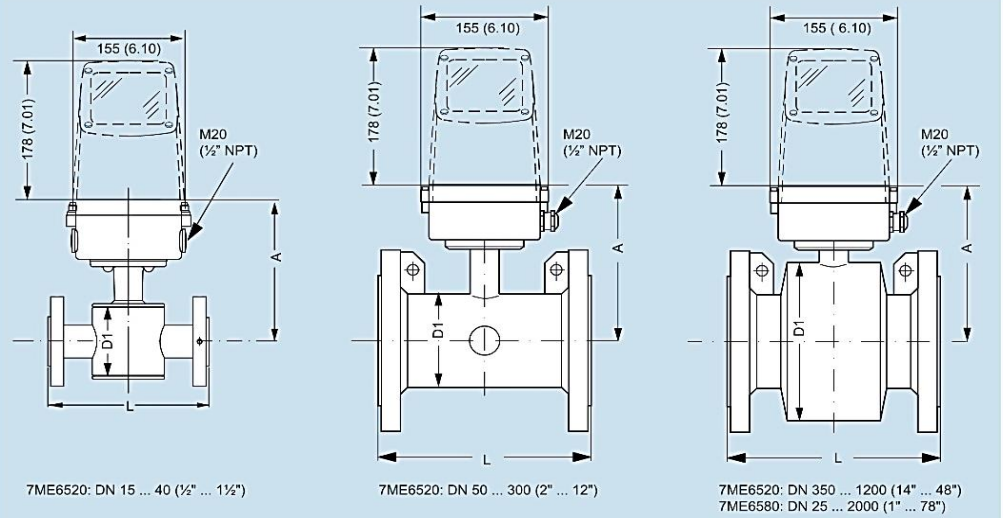

7ME6520: DN 15 ... 40 (½" ... 1½")

7ME6520: DN 50 ... 300 (2" ... 12")

7ME6520: DN 350 ... 1200 (14" ... 48")
7ME6580: DN 25 ... 2000 (1" ... 78")

7ME6520 NBR or EPDM liner						7ME6580 Ebonite liner					
Nominal size		A		D1		A		D1		L	
[mm]	[inch]	[mm]	[inch]	[mm]	[inch]	[mm]	[inch]	[mm]	[inch]	[mm]	[inch]
15	½	177	7.0	77	3.0	-	-	-	-	200	7.9
25	1	187	7.4	96	3.8	187	7.4	104	4.09	200	7.9
40	1½	202	8.0	127	5.0	197	7.8	124	4.88	200	7.9
50	2	188	7.4	76	3.0	205	8.1	139	5.47	200	7.9
65	2½	194	7.6	89	3.5	212	8.3	154	6.06	200	7.9
80	3	200	7.9	102	4.0	222	8.7	174	6.85	200	7.9
100	4	207	8.1	114	4.5	242	9.5	214	8.43	250	9.8
125	5	217	8.5	140	5.5	255	10.0	239	9.41	250	9.8
150	6	232	9.1	168	6.6	276	10.9	282	11.1	300	11.8
200	8	257	10.1	219	8.6	304	12.0	338	13.31	350	13.8
250	10	284	11.2	273	10.8	332	13.1	393	15.47	450	17.7
300	12	310	12.2	324	12.8	357	14.1	444	17.48	500	19.7
350	14	382	15.0	451	17.8	362	14.3	451	17.76	550	21.7
400	16	407	16.0	502	19.8	387	15.2	502	19.76	600	23.6
450	18	438	17.2	563	22.2	418	16.5	563	22.16	600	23.6
500	20	463	18.2	614	24.2	443	17.4	614	24.17	600	23.6
600	24	514	20.2	715	28.2	494	19.4	715	28.15	600	23.6
700	28	564	22.2	816	32.1	544	21.4	816	32.13	700	27.6
750	30	591	23.3	869	34.2	571	22.5	869	34.21	750	29.5
800	32	616	24.3	927	36.5	606	23.9	927	36.5	800	31.5
900	36	663	26.1	1032	40.6	653	25.7	1032	40.63	900	35.4
1000	40	714	28.1	1136	44.7	704	27.7	1136	44.72	1000	39.4
	42	714	28.1	1136	44.7	704	27.7	1136	44.72	1000	39.4
	44	765	30.1	1238	48.7	755	29.7	1238	48.74	1100	43.3
1200	48	820	32.3	1348	53.1	810	31.9	1348	53.07	1200	47.2
1400	54	-	-	-	-	925	36.4	1574	65.94	1400	55.1
1500	60	-	-	-	-	972	38.2	1672	65.83	1500	59.1
1600	66	-	-	-	-	1025	40.4	1774	75.39	1600	63
1800	72	-	-	-	-	1123	44.2	1974	77.72	1800	70.9
2000	78	-	-	-	-	1223	48.1	2174	85.59	2000	78.7

- not available

The SITRANS F M MAG 5000 is a microprocessor-based transmitter engineered for high performance, easy installation, commissioning and maintenance. The transmitter is truly robust, cost-effective and suitable for all-round applications and has a measuring accuracy of ± 0.4% of the flow rate (incl. sensor).

Application Examples: Water and waste water, General process industry, Food & beverage industry

Details

Accuracy	0.4 % ±1 mm/s
Input / output	1 current output 1 digital output 1 relay output
Communication	HART
Display	Background illumination with alphanumeric text, 3 x 20 characters
Enclosure	IP67 (NEMA 4x/6) IP20 (NEMA 2)
Power supply	12-24 V a.c./d.c. 115-230 V a.c.
Ambient temperature	From -20 to 50 °C (-4 to 122 °F)
Approvals	MI-001 Danak PTB OIML R49
Ex-approvals	FM/CSA Class 1, Div 2

Appendix A9: Omega FMG3002-PP Magnetic Flow Meter (reproduced from Ref. 46)

SAFETY INSTRUCTIONS
1. Depressurize and vent system prior to installation or removal.
2. Confirm chemical compatibility before use.
3. Do not exceed maximum temperature/pressure specifications.
4. Wear safety goggles or face shield during installation/service.
5. Do not alter product construction.
6. Disconnect power before attempting any service or wiring.

2. Specifications

Wetted Materials:
- Sensor body, electrodes and grounding ring:
  - -PP: Polypropylene and 316L Stainless Steel
  - -PVDF and 316L Stainless Steel
- O-rings: FPM standard; EPDM, (Perfluoroelastomer optional)

Other Materials:
- Case: PBT
- Ground terminal: 316 Stainless Steel

Power Requirements
- 4 to 20 mA: 21.6 to 26.4 VDC, 22.1 mA maximum; 400 mV p-p maximum ripple voltage
- Frequency: 5 to 26.4 VDC, 15 mA maximum
- Reverse polarity and short circuit protected

Performance
- Pipe Size Range: FMG-3000: ½ in. to 4 in.; FMG-3100: 5 in. to 8 in.; FMG-3200: 10 in. to 12 in.
- Flow Range: Minimum: 0.05 m/s (0.15 ft/s); Maximum: 10 m/s (33 ft/s)
- Linearity: ±(1% reading + 0.01 m/s); ±(1% reading + 0.033 ft/s)
- Repeatability: ±0.5% of reading @ 25 °C
- Minimum Conductivity: 20 µS/cm

Output Specifications
Current output (4 to 20 mA)
- Programmable and eversible
- Loop Accuracy: 32 µA max. error (@ 25 °C @ 24 VDC)
- Temp. drift: ±1 µA per °C max.
- Power Supply Rejection: ±1 µA per V
- Isolation: Low voltage: <48 VAC/DC from electrodes and auxiliary power
- Maximum Cable: 300 m (1000 ft)
- Maximum Loop Resistance: 300 Ω
- Error Condition: 22.1 mA

Frequency output:
- Max. Pull-up Voltage: 30 VDC
- Short Circuit Protected: ≤ 30 V @ 0 Ω pull-up for one hour
- Reverse Polarity Protected - 40 V
- Overvoltage Protected to 40 V with pull-up resistor
- Max. Current Sink: 50 mA, current limited
- Maximum cable: 300 m (1000 ft)

Environmental Requirements
- Storage Temperature: -20 to 70 °C (-4 to 158 °F)
- Relative Humidity: 0 to 95% (non-condensing)
- Operating Temperature
  - Ambient: -10 to 70 °C (14 to 158 °F)
  - Media: 0 to 85 °C (32 to 185 °F)

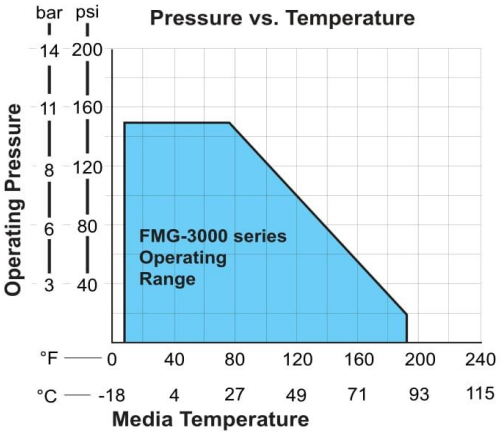

Max. Operating Pressure: 10.3 bar @ 25 °C (150 psi @ 77 °F)
1.4 bar @ 85 °C (20 psi @ 185 °F)

Tests, Approvals & Standards
- NEMA 4X
- CE

Dimensions

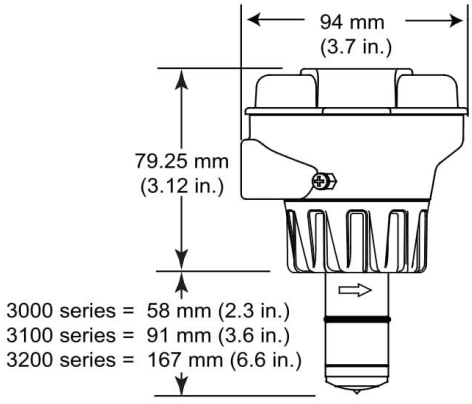

4

3. Installation: Pipe fittings

Omega offers a wide selection of installation fittings that control the position of the Magmeter electrodes in relation to the dimensions of the pipe. You will find a complete list of order numbers for installation fittings in the Calibration tables on pages 8-12.

Type	Description
Plastic tees	• 0.5 to 2 inch versions • MPVC or CPVC
PVC Glue-on Saddles	• Available in 10 and 12 inch sizes only • Cut 2-1/2 inch hole in pipe • Weld in place using solvent cement
PVC Saddles	• 2 to 4 inch, cut 1-7/16 inch hole in pipe • 6 to 8 inch, cut 2-1/8 inch hole in pipe
Iron Strap-on saddles	• 2 to 4 inch, cut 1-7/16 inch hole in pipe • Over 4 inch, cut 2-1/8 inch hole in pipe • Special order 14 in. to 36 in.

Type	Description
Iron, Carbon Steel, 316 SS Threaded tees	• 0.5 to 2 in. versions • Mounts on threaded pipe ends
Carbon steel & stainless steel Weld-on Weldolets	• 2 to 4 inch, cut 1-7/16 inch hole in pipe • Over 4 inch, cut 2-1/8 inch hole in pipe
Fiberglass tees FPT	• 1.5 in. to 2 in. PVDF insert
Metric Union Fitting	• For pipes from DN 15 to 50 mm • PP or PVDF

4. Selecting a Location

- The FMG-3000 requires a full pipe and a fully developed turbulent flow profile for accurate measurement.
- If the piping system harbors air pockets or bubbles, take steps to locate the sensor so the air pockets will not contact the electrodes.
- In vertical installations, assemble the unit so the conduit ports are facing downward. This prevents condensation inside the conduit from being directed into the electronics housing.
- Chemical injection systems can temporarily alter the fluid conductivity and cause anomalies in the magmeter measurement. To avoid this problem, install the Magmeter UPSTREAM of the injection point.

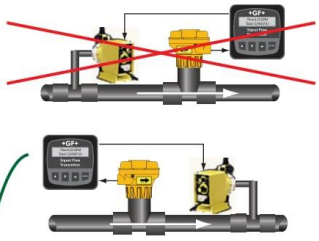

Select a location with sufficient distance of straight pipe immediately upstream of the sensor.

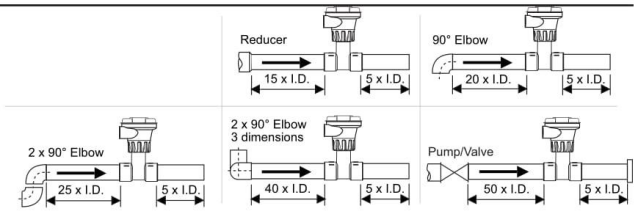

Locating the sensor in a trap or where the flow is upward helps to protect the sensor from exposure to air bubbles when the system is in operation.

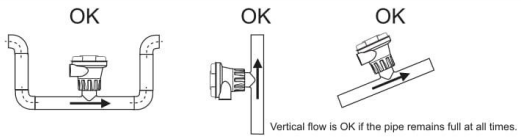

These configurations are not recommended because it is difficult to keep the pipe full.

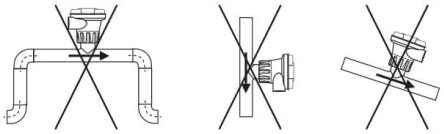

In a gravity-flow system, the tank must be designed so the level does not drop below the outlet.

This causes the pipe to draw air in from the tank. If air bubbles pass across the Magmeter electrodes, the output will become erratic.

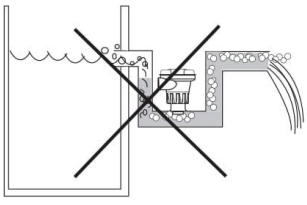

6. General Installation and Grounding Tips

Sensor conditioning
The Magmeter output signal may be unstable immediately after installation. Allowing the sensor to soak in a full pipe (or in any container of water) for 24 hours will stabilize the performance.

- Very low conductivity fluids may require a longer conditioning period. The Magmeter may not operate properly in fluids where the conductivity is less than 20 µS/cm.

Grounding
The FMG-3000 Magmeter is unaffected by moderate levels of electrical noise. However, in some applications it may be necessary to ground portions of the system to eliminate electrical interference. The grounding requirements will vary with each installation.

One or more of the following steps may be applied if the FMG-3000 Magmeter is affected by electrical noise:

① The ground terminal on the outside of the yellow housing is connected internally to the grounding ring at the tip of the sensor. Connect a wire (14 AWG/1.5 mm^2 recommended) from this terminal directly to a local Earth ground.

② Install fluid grounding devices immediately upstream and downstream of the Magmeter.
Connect the fluid grounds to the Earth ground terminal on the FMG-3000.
Use flanged grounding rings or metal electrodes on plastic pipes, or metal clamps on metal pipes.
Fluid grounds must be in direct contact with the fluid, and as near to the Magmeter as possible.

③ The shield from the output cable must be terminated at the remote instrument ONLY.
This shield must not be connected at both ends!

④ Connect an additional wire (minimum AWG 14/1.5 mm^2) from the remote instrument ground to the Magmeter ground terminal.

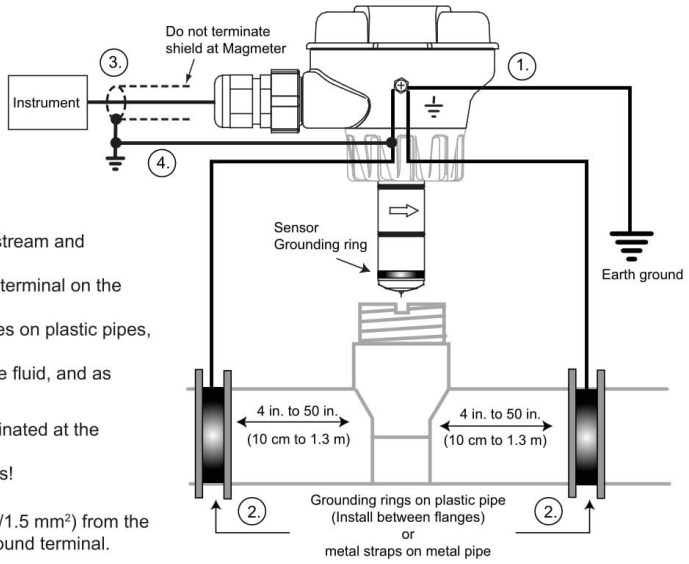

---

7. Wiring the FMG-3002, 3102 and 3202 Magmeter with 4 to 20 mA Loop Output

The FMG-3002, 3102 and 3202 Magmeters are traditional 2-wire passive 4 to 20 mA loop transmitters.

- External loop power (24 VDC ±10%) is required.
- **The maximum loop resistance the Magmeter can accomodate is 300 Ω.**
- All FMG-3002, 3102 and 3202 Magmeters are shipped from the factory with the 4 to 20 mA output scaled for 0 to 5 m/s (0 to 16.4 ft/s). The Calibration charts on pages 8-12 list the 20 mA setpoint for each installation fitting. Use this information to program the 4 to 20 mA range of the loop device (PLC, Datalogger, recorder, etc.)

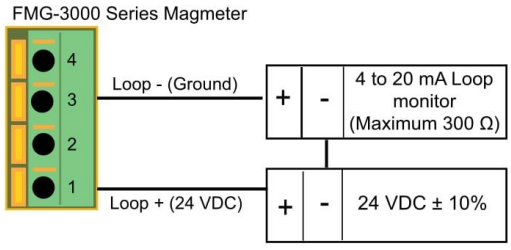

<u>Appendix B1:</u> HOBO Output Signal Cable 4-20 mA (reproduced from Ref. 47)

4-20mA Input Cable (CABLE-4-20mA)

For use with HOBO® U12 and UX120-006M data loggers and ZW data nodes

Specifications

Measurement range	0 to 20.1 mA
Accuracy with U12	±0.02 mA ±2.5% of absolute current
Accuracy with ZW	±0.015 mA ±2.0% of absolute current
Accuracy with UX120-006M	±0.001 mA ±0.2.% of absolute current
Resolution with U12 and ZW	0.03% of full scale
Resolution with UX120-006M	0.002% of full scale
Cable length	47 cm (18.5 inches)

This cable measures currents from 0 to 20.1 mA and must be connected so that the current flows through, and with the proper polarity, as shown below. Do not expose to current above 20 mA or negative current. Do not cut off the end of the gray cable where it connects to the blue and yellow wires as that contains the precision resistor required for current measurements.

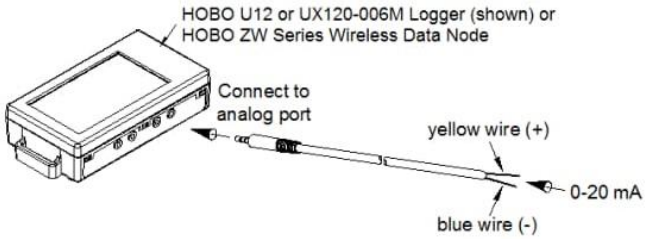

onset
HOBO Data Loggers

2943-D MAN-4-20mA

Appendix B2: KU SPP Daily Log Sheets (January-October, 2016)

Makeup Water	%	JAN 2016	#1	#2	#7	#8	HRS. on OIL	OIL Gals.	GAS FEET M. No. 1	No. 2	No. 7	No. 8	Steam Lbs. No. 1	No. 2	No. 7	No. 8	By GAS STEAM LBS.	By OIL STEAM LBS.	TOTAL STEAM GENERATED	BOILER EFF.
21,380	15.1	1			x	x					525,000	722,500			537,700	636,000	1,174,300		1,174,300	83
23,580	17.2	2			x	x					522,500	688,800			530,700	605,100	1,135,800		1,135,800	83
24,880	17.3	3			x	x					591,900	673,800			601,100	590,200	1,191,300		1,191,300	83
25,320	13.7	4			x	x					770,000	871,900			770,400	760,800	1,531,200		1,531,200	83
29,020	16.5	5			x	x					724,400	847,500			724,900	738,500	1,463,400		1,463,400	83
26,500	17.0	6			x	x					621,300	770,000			625,600	671,100	1,296,700		1,296,700	83
25,060	18.2	7			x	x					529,400	693,800			534,600	605,900	1,140,500		1,140,500	83
22,500	16.0	8			x	x					545,600	706,900			549,100	618,200	1,167,300		1,167,300	83
37,200	20.5	9			x	x					748,800	878,100			744,600	763,000	1,507,600		1,507,600	83
38,120	18.0	10			x	x					895,600	1,016,300			881,600	877,600	1,759,200		1,759,200	83
38,180	21.9	11			x	x					703,800	856,300			702,200	742,900	1,445,100		1,445,100	83
38,980	22.9	12			x	x					683,100	839,400			685,600	729,800	1,415,400		1,415,400	83
33,090	22.5	13			x	x					566,900	648,400			571,800	648,400	1,220,200		1,220,200	83
23,970	19.6	14			x	x					520,000	571,300			522,800	494,800	1,017,600		1,017,600	83
20,340	13.6	15			x	x					648,100	668,800			653,600	584,100	1,237,700		1,237,700	83
23,720	13.9	16			x	x					730,000	787,500			732,800	687,300	1,420,100		1,420,100	83
24,660	11.4	17			x	x					943,800	990,600			930,600	861,400	1,792,000		1,792,000	83
22,510	10.8	18			x	x					868,100	1,005,000			860,600	872,400	1,733,000		1,733,000	83
20,520	10.3	19			x	x					810,000	956,900			811,100	834,800	1,645,900		1,645,900	83
19,910	10.6	20			x	x					756,900	913,100			760,800	798,900	1,559,700		1,559,700	83
20,810	11.4	21			x	x					729,400	889,400			735,000	778,800	1,513,800		1,513,800	83
21,850	11.7	22			x	x					753,100	910,600			758,600	796,700	1,555,300		1,555,300	83
23,020	12.7	23			x	x					723,800	886,300			731,500	776,600	1,508,100		1,508,100	83
21,610	14.5	24			x	x					571,900	754,400			577,900	660,600	1,238,500		1,238,500	83
22,290	13.8	25			x	x					643,100	783,800			649,300	686,900	1,336,200		1,336,200	83
21,620	13.7	26			x	x					624,400	768,100			633,900	674,600	1,308,500		1,308,500	83
23,140	16.0	27			x	x					586,900	688,100			594,100	602,900	1,197,000		1,197,000	83
21,260	16.4	28			x	x					572,500	574,400			576,200	498,800	1,075,000		1,075,000	83
17,950	15.4	29			x	x					681,900	337,900			679,000	287,000	966,000		966,000	82
31,280	23.8	30	x		x	x			238,100		427,500	356,900	254,200		467,300	367,900	1,089,400		1,089,400	81
20,910	18.6	31	x			x			491,900			571,300	437,900			493,900	931,800		931,800	82
785,180	15.7								730,000	0	20,019,700	23,628,100	692,100	0	20,135,000	20,746,500	41,573,600	0	41,573,600	

Makeup Water	%	FEB 2016	#1	#2	#7	#8	HRS. on OIL	OIL Gals.	GAS FEET M. No. 1	No. 2	No. 7	No. 8	Steam Lbs. No. 1	No. 2	No. 7	No. 8	By GAS STEAM LBS.	By OIL STEAM LBS.	TOTAL STEAM GENERATED	BOILER EFF.
20,960	16.6	1	x			x			565,000			630,000	501,800			547,800	1,049,600		1,049,600	82
21,140	16.3	2	x			x			586,300			644,400	517,600			558,700	1,076,300		1,076,300	82
24,550	15.2	3	x			x			748,800			787,500	656,700			687,300	1,344,000		1,344,000	82
27,830	17.0	4	x			x			732,500			820,600	644,000			717,900	1,361,900		1,361,900	82
24,760	15.7	5	x			x			684,400			800,600	604,600			701,800	1,306,400		1,306,400	82
19,140	14.2	6	x			x			550,600			711,900	492,600			625,600	1,118,200		1,118,200	82
20,590	15.7	7	x			x			540,000			692,500	483,000			608,100	1,091,100		1,091,100	82
29,110	18.2	8	x			x			716,300			804,400	628,700			701,300	1,330,000		1,330,000	82
22,910	13.7	9	x			x			718,800			870,000	630,900			759,500	1,390,400		1,390,400	82
22,080	14.0	10	x			x			706,300			791,300	621,300			690,400	1,311,700		1,311,700	82
20,530	13.2	11	x			x			685,000			781,300	606,400			685,100	1,291,500		1,291,500	82
23,910	14.9	12	x			x			711,900			798,100	628,700			700,000	1,328,700		1,328,700	82
24,460	12.7	13	x			x			918,800			920,000	800,600			802,800	1,603,400		1,603,400	82
20,980	14.4	14	x			x			641,300			734,400	566,600			640,100	1,206,700		1,206,700	82
18,860	14.6	15	x			x			541,900			676,900	483,900			590,600	1,074,500		1,074,500	82
19,810	15.3	16	x			x			536,900			682,500	479,900			596,800	1,076,700		1,076,700	82
19,240	16.5	17	x			x			465,000			633,800	416,500			551,700	968,200		968,200	82
16,500	19.0	18				x			176,300			647,500	158,400			560,900	719,300		719,300	82
13,920	18.2	19				x						725,000				635,300	635,300		635,300	83
15,760	19.2	20				x						774,400				679,900	679,900		679,900	83
25,900	24.6	21				x						1,000,500				873,300	873,300		873,300	83
20,230	16.4	22	x			x			342,500			820,000	311,100			711,800	1,022,900		1,022,900	82
17,510	14.0	23	x			x			463,100			711,300	413,900			622,100	1,036,000		1,036,000	82
21,130	15.5	24	x			x			535,600			746,900	476,900			652,300	1,129,200		1,129,200	82
19,010	13.4	25	x		x	x			543,800		413,100	318,100	485,200		415,200	277,800	1,178,200		1,178,200	82
17,930	13.9	26	x		x				486,300		635,600		434,000		639,600		1,073,600		1,073,600	82
18,960	19.8	27	x		x				261,900		555,600		238,000		555,600		793,600		793,600	82
19,360	23.5	28			x						686,900				682,500		682,500		682,500	83
23,020	24.1	29	x		x				53,800		745,600		61,300		731,900		793,200		793,200	82
	#####	30															0		0	
	#####	31															0		0	
610,090	16.1								13,913,100	0	3,036,800	18,523,900	12,342,600	0	3,024,800	16,178,900	31,546,300	0	31,546,300	

Makeup Water	%	MAR 2016	#1	#2	#7	#8	HRS. on OIL	OIL Gals.	GAS FEET M. No. 1	No. 2	No. 7	No. 8	Steam Lbs. No. 1	No. 2	No. 7	No. 8	By GAS STEAM LBS.	By OIL STEAM LBS.	TOTAL STEAM GENERATED	BOILER EFF.
34,720	24.7	1	x		x				473,800		763,800		413,400		754,300		1,167,700		1,167,700	82
18,380	15.4	2	x		x				433,100		608,100		385,000		607,300		992,300		992,300	82
26,230	23.0	3	x		x				417,500		575,600		370,600		574,400		945,000		945,000	82
20,570	20.2	4	x		x				233,100		636,300		207,400		636,100		843,500		843,500	82
23,600	26.9	5			x						733,800				728,000		728,000		728,000	83
18,700	24.1	6			x						648,800				643,100		643,100		643,100	83
13,290	18.9	7			x						590,600				583,600		583,600		583,600	83
18,700	23.3	8			x						674,400				666,300		666,300		666,300	83
16,920	19.3	9			x						737,500				728,000		728,000		728,000	83
16,330	19.8	10			x						688,100				684,700		684,700		684,700	83
20,310	25.7	11			x						658,800				655,800		655,800		655,800	83
16,690	21.7	12			x						641,900				637,000		637,000		637,000	83
12,170	18.0	13			x						570,000				561,800		561,800		561,800	83
14,920	21.1	14			x						598,800				587,100		587,100		587,100	83
14,990	21.0	15			x						603,100				592,400		592,400		592,400	83
20,880	23.1	16			x						765,600				751,200		751,200		751,200	83
24,550	26.9	17			x						768,800				756,400		756,400		756,400	83
27,830	25.0	18	x		x				161,300		806,300		132,100		791,400		923,500		923,500	82
20,880	17.1	19	x		x				401,300		652,500		357,000		654,500		1,011,500		1,011,500	82
18,060	14.6	20	x		x				453,100		617,500		402,900		621,700		1,024,600		1,024,600	82
18,920	16.6	21	x		x				296,900		688,100		261,600		682,500		944,100		944,100	82
16,330	20.1	22			x						690,000				674,200		674,200		674,200	83
13,130	18.6	23			x						602,500				587,100		587,100		587,100	83
31,350	25.8	24	x		x				286,900		789,400		241,900		765,600		1,007,500		1,007,500	82
20,300	18.3	25	x		x				353,100		613,800		308,900		611,600		920,500		920,500	82
16,410	17.5	26	x		x				181,300		628,800		156,200		624,300		780,500		780,500	82
20,940	18.4	27	x		x				203,800		791,900		165,800		776,600		942,400		942,400	82
19,730	19.7	28	x		x				191,200		670,600		167,600		665,400		833,000		833,000	82
18,530	21.1	29			x						738,800				728,900		728,900		728,900	83
12,490	16.3	30			x						642,500				634,800		634,800		634,800	83
25,450	27.7	31			x						779,400				761,300		761,300		761,300	83
612,300	20.9								4,086,400	0	20,976,100	0	3,570,400	0	20,727,400	0	24,297,800	0	24,297,800	

Makeup Water	%	APR 2016	#1	#2	#7	#8	HRS. on OIL	OIL Gals.	GAS FEET M. No. 1	No. 2	No. 7	No. 8	Steam Lbs. No. 1	No. 2	No. 7	No. 8	By GAS STEAM LBS.	By OIL STEAM LBS.	TOTAL STEAM GENERATED	BOILER EFF.
24,360	21.7	1			x						960,600				930,100		930,100		930,100	83
19,040	19.3	2			x						840,000				817,300		817,300		817,300	83
13,510	16.8	3			x						682,500				666,300		666,300		666,300	83
13,570	16.8	4			x	x					391,300	333,800			384,100	284,400	668,500		668,500	81
17,615	21.4	5				x						783,800				682,500	682,500		682,500	83
18,205	22.6	6				x						768,100				669,400	669,400		669,400	83
20,500	23.4	7				x						836,900				726,300	726,300		726,300	83
24,800	25.8	8				x						921,900				797,600	797,600		797,600	83
17,290	18.3	9				x						903,100				782,300	782,300		782,300	83
10,460	14.9	10				x						656,300				581,400	581,400		581,400	83
23,080	25.0	11				x						878,800				766,500	766,500		766,500	83
19,560	20.5	12	x			x			148,800			779,400	111,600			679,000	790,600		790,600	79
13,590	16.4	13				x						786,300				687,300	687,300		687,300	83
16,100	21.3	14				x						717,500				627,400	627,400		627,400	83
13,450	19.2	15				x						666,300				582,300	582,300		582,300	83
10,740	16.1	16				x						629,400				552,600	552,600		552,600	83
10,440	15.5	17				x						630,600				558,700	558,700		558,700	83
12,060	15.9	18				x						720,000				629,600	629,600		629,600	83
12,270	16.1	19				x						721,300				631,800	631,800		631,800	83
14,160	18.1	20				x						745,600				650,100	650,100		650,100	83
16,920	21.6	21				x						750,600				651,400	651,400		651,400	83
13,540	17.4	22				x						738,800				645,300	645,300		645,300	83
14,060	20.5	23				x						650,000				569,600	569,600		569,600	83
10,850	17.0	24				x						604,400				529,800	529,800		529,800	83
13,750	19.6	25				x						666,300				581,000	581,000		581,000	83
13,030	18.9	26				x						655,000				572,300	572,300		572,300	83
12,340	17.0	27	x			x			328,100			352,500	297,100			307,100	604,200		604,200	79
15,850	21.1	28	x						715,000				623,400				623,400		623,400	81
17,810	22.9	29	x						741,900				644,400				644,400		644,400	81
11,460	17.2	30	x						632,500				554,300				554,300		554,300	81
	#####	31															0		0	
464,410	19.5								2,566,300	0	2,874,400	16,896,700	2,230,800	0	2,797,800	14,745,700	19,774,300	0	19,774,300	

Makeup Water	%	May 2016	#1	#2	#7	#8	HRS. on OIL	OIL Gals.	GAS FEET M. No. 1	GAS FEET M. No. 2	GAS FEET M. No. 7	GAS FEET M. No. 8	Steam Lbs. No. 1	Steam Lbs. No. 2	Steam Lbs. No. 7	Steam Lbs. No. 8	By GAS STEAM LBS.	By OIL STEAM LBS.	TOTAL STEAM GENERATED	BOILER EFF.
14,290	20.4	1	x						666,900				582,800				582,800		582,800	82
15,420	19.9	2	x						743,100				644,400				644,400		644,400	82
14,170	19.2	3	x						705,000				612,100				612,100		612,100	82
16,570	23.8	4	x						665,000				578,400				578,400		578,400	82
19,500	28.9	5	x						646,900				560,400				560,400		560,400	82
13,740	21.8	6	x						600,600				523,700				523,700		523,700	82
11,270	19.4	7	x						550,600				482,600				482,600		482,600	82
11,500	18.3	8	x						596,900				520,600				520,600		520,600	82
12,500	18.3	9	x						655,000				567,400				567,400		567,400	82
16,220	24.8	10	x						624,400				542,500				542,500		542,500	82
13,500	20.7	11	x		x				345,600		255,000		298,800		242,800		541,600		541,600	80
13,660	20.6	12			x						561,900				550,800		550,800		550,800	83
16,020	22.7	13			x						604,400				584,900		584,900		584,900	83
23,320	26.1	14			x						766,300				742,400		742,400		742,400	83
16,590	26.5	15			x						531,300				519,300		519,300		519,300	83
	#####	16															0		0	
	#####	17															0		0	
7,490	#####	18															0		0	
	#####	19															0		0	
19,050	28.2	20			x	x					335,600	205,600			328,100	232,800	560,900		560,900	79
10,625	15.9	21			x						569,400				556,100		556,100		556,100	83
9,965	16.8	22			x	x					287,500	228,800			290,400	201,300	491,700		491,700	82
9,720	15.3	23				x						601,300				527,200	527,200		527,200	83
10,110	15.1	24				x						631,300				554,300	554,300		554,300	83
8,620	13.5	25				x						598,800				530,700	530,700		530,700	83
10,420	15.3	26				x						643,800				565,700	565,700		565,700	83
11,010	15.2	27				x						688,100				599,400	599,400		599,400	83
9,280	14.6	28				x						594,400				527,600	527,600		527,600	83
9,210	15.2	29				x						562,500				501,400	501,400		501,400	83
8,620	14.9	30				x						538,800				481,700	481,700		481,700	83
9,220	14.7	31				x						585,600				521,500	521,500		521,500	
361,610	20.0								6,800,000	0	3,911,400	5,879,000	5,913,700	0	3,814,800	5,243,600	14,972,100	0	14,972,100	

Makeup Water	%	JUN 2016	#1	#2	#7	#8	HRS. on OIL	OIL Gals.	GAS FEET M. No. 1	GAS FEET M. No. 2	GAS FEET M. No. 7	GAS FEET M. No. 8	Steam Lbs. No. 1	Steam Lbs. No. 2	Steam Lbs. No. 7	Steam Lbs. No. 8	By GAS STEAM LBS.	By OIL STEAM LBS.	TOTAL STEAM GENERATED	BOILER EFF.
10,610	17.8	1				x						552,500				493,500	493,500		493,500	83
11,540	19.5	2				x						550,600				491,800	491,800		491,800	83
11,910	20.1	3				x						553,800				490,900	490,900		490,900	83
10,220	18.6	4				x						508,800				456,300	456,300		456,300	83
10,100	18.3	5				x						514,400				458,500	458,500		458,500	83
10,920	19.0	6				x						530,600				476,400	476,400		476,400	83
11,450	19.6	7				x						545,000				486,100	486,100		486,100	83
10,300	18.5	8			x	x					201,900	307,500			189,400	273,900	463,300		463,300	82
10,400	19.7	9			x						461,300				437,100		437,100		437,100	82
10,510	20.5	10			x						450,000				426,100		426,100		426,100	82
9,360	19.8	11			x						417,500				392,900		392,900		392,900	82
9,440	19.8	12			x						421,900				396,400		396,400		396,400	82
10,150	19.0	13			x						466,900				443,200		443,200		443,200	82
10,640	20.5	14			x						457,500				431,400		431,400		431,400	82
10,650	21.2	15			x						440,000				416,500		416,500		416,500	82
10,060	19.6	16			x						449,400				425,300		425,300		425,300	82
10,640	21.4	17			x						438,100				412,600		412,600		412,600	82
9,770	20.3	18			x						421,300				398,600		398,600		398,600	82
9,780	20.6	19			x						417,500				393,300		393,300		393,300	82
10,490	20.3	20			x						450,600				428,800		428,800		428,800	82
11,250	21.9	21			x						452,500				426,600		426,600		426,600	82
10,520	20.9	22			x						447,500				418,300		418,300		418,300	82
10,950	21.0	23			x						460,000				432,300		432,300		432,300	82
11,220	20.8	24			x						476,900				447,100		447,100		447,100	82
10,090	20.6	25			x						435,000				406,400		406,400		406,400	82
9,677	19.9	26			x						431,900				402,900		402,900		402,900	82
10,680	19.9	27			x						471,900				444,500		444,500		444,500	82
11,300	20.9	28			x						471,300				448,000		448,000		448,000	82
10,530	19.4	29			x						474,400				451,500		451,500		451,500	82
9,590	17.4	30			x						481,900				458,100		458,100		458,100	82
	#####	31															0		0	
314,747	19.9								0	0	10,097,200	4,063,200	0	0	9,527,300	3,627,400	13,154,700	0	13,154,700	

Makeup Water	%	JUL 2016	#1	#2	#7	#8	HRS. on OIL	OIL Gals.	GAS FEET M. No. 1	No. 2	No. 7	No. 8	Steam Lbs. No. 1	No. 2	No. 7	No. 8	By GAS STEAM LBS.	By OIL STEAM LBS.	TOTAL STEAM GENERATED	BOILER EFF.
9,230	16.7	1			x						481,900				459,400		459,400		459,400	82
9,290	16.9	2			x						480,000				455,900		455,900		455,900	82
9,830	17.2	3			x						500,600				473,800		473,800		473,800	82
8,850	16.8	4			x						463,800				436,600		436,600		436,600	82
8,970	17.0	5			x						471,900				438,800		438,800		438,800	82
16,420	30.5	6			x						479,400				446,300		446,300		446,300	82
15,130	28.1	7			x						480,600				447,600		447,600		447,600	82
11,890	21.8	8			x						480,600				451,900		451,900		451,900	82
10,070	20.1	9			x						441,300				415,200		415,200		415,200	82
10,390	21.1	10			x						434,400				407,800		407,800		407,800	82
10,190	19.7	11			x						460,600				430,100		430,100		430,100	82
10,250	18.9	12			x						479,400				449,800		449,800		449,800	82
8,990	16.7	13			x						475,600				447,100		447,100		447,100	82
11,120	20.1	14			x	x					194,400	331,900			182,000	276,100	458,100		458,100	81
8,930	15.7	15				x						550,600				471,200	471,200		471,200	82
7,130	14.1	16				x						496,900				420,900	420,900		420,900	82
7,650	15.9	17				x						471,900				398,100	398,100		398,100	82
8,500	16.2	18				x						510,600				435,800	435,800		435,800	82
8,720	16.5	19				x						516,300				439,700	439,700		439,700	82
8,950	16.8	20				x						520,600				442,300	442,300		442,300	82
9,180	18.1	21				x						495,000				420,900	420,900		420,900	82
7,900	15.9	22				x						485,600				413,000	413,000		413,000	82
7,730	15.9	23				x						474,400				402,500	402,500		402,500	82
8,150	16.7	24				x						479,400				406,000	406,000		406,000	82
8,820	15.9	25				x						541,300				461,100	461,100		461,100	82
9,470	17.7	26				x						522,500				443,200	443,200		443,200	82
9,760	18.6	27				x						514,400				436,600	436,600		436,600	82
11,120	20.6	28				x						526,300				447,100	447,100		447,100	82
9,540	17.4	29				x						534,400				455,400	455,400		455,400	82
8,800	17.5	30				x						493,100				417,400	417,400		417,400	82
8,320	16.8	31			x	x					227,500	234,400			213,500	197,800	411,300		411,300	81
299,290	18.3								0	0	6,552,000	8,699,600	0	0	6,155,800	7,385,100	13,540,900	0	13,540,900	

Makeup Water	%	AUG 2016	#1	#2	#7	#8	HRS. on OIL	OIL Gals.	GAS FEET M. No. 1	No. 2	No. 7	No. 8	Steam Lbs. No. 1	No. 2	No. 7	No. 8	By GAS STEAM LBS.	By OIL STEAM LBS.	TOTAL STEAM GENERATED	BOILER EFF.
9,180	17.8	1			x						451,300	3,800			429,200		429,200		429,200	82
9,340	18.4	2			x						445,600				421,300		421,300		421,300	82
8,630	18.4	3			x						414,400				388,900		388,900		388,900	82
8,720	20.4	4			x						380,000				355,300		355,300		355,300	82
8,540	18.2	5			x						410,000				388,500		388,500		388,500	82
8,300	19.0	6			x						385,600				362,300		362,300		362,300	82
8,470	19.2	7			x						388,100				366,600		366,600		366,600	82
10,230	28.8	8			x						307,100				294,600		294,600		294,600	81
15,030	31.8	9			x						413,100	4,700			392,900		392,900		392,900	80
13,380	27.1	10			x						444,400				409,500		409,500		409,500	82
17,710	36.6	11			x						433,100				401,200		401,200		401,200	82
14,000	26.6	12			x						469,400				437,500		437,500		437,500	82
13,030	26.7	13			x						433,100				404,300		404,300		404,300	82
6,180	12.8	14			x						430,600				400,300		400,300		400,300	82
15,020	26.9	15			x						494,400				462,900		462,900		462,900	82
16,260	28.2	16			x						508,800				477,800		477,800		477,800	82
14,920	27.0	17			x						490,600				458,100		458,100		458,100	82
18,290	33.1	18			x						491,300				458,900		458,900		458,900	82
26,260	48.1	19			x						484,400				453,300		453,300		453,300	82
20,560	36.2	20			x						497,500				470,800		470,800		470,800	82
20,040	35.4	21			x						496,300				469,900		469,900		469,900	82
21,690	36.9	22			x						518,100				487,800		487,800		487,800	82
26,060	45.4	23			x						511,900				476,900		476,900		476,900	82
19,500	34.0	24			x						509,400				476,400		476,400		476,400	82
18,750	33.1	25			x						502,500				470,300		470,300		470,300	82
18,650	31.7	26			x						520,600				488,700		488,700		488,700	82
15,520	29.3	27			x						471,900				440,100		440,100		440,100	82
15,810	30.2	28			x						467,500				434,900		434,900		434,900	82
17,230	30.7	29			x						500,600				466,400		466,400		466,400	82
17,140	29.9	30			x						509,400				476,400		476,400		476,400	82
18,250	30.3	31			x					60,231	530,000				500,100		500,100		500,100	82
470,690	29.1								0	60,231	14,311,000	8,500	0	0	13,422,100	0	13,422,100	0	13,422,100	

Makeup Water	%	SEP 2016	#1	#2	#7	#8	HRS. on OIL	OIL Gals.	GAS FEET M. No. 1	No. 2	No. 7	No. 8	Steam Lbs. No. 1	No. 2	No. 7	No. 8	By GAS STEAM LBS.	By OIL STEAM LBS.	TOTAL STEAM GENERATED	BOILER EFF.
16,410	26.6	1			x						539,400				512,800		512,800		512,800	82
17,710	29.1	2			x						531,900				505,800		505,800		505,800	82
16,550	30.5	3			x						475,000				450,200		450,200		450,200	82
16,470	30.7	4			x						472,500				444,900		444,900		444,900	82
15,580	28.9	5			x						475,000				447,600		447,600		447,600	82
18,510	32.9	6			x						503,800				466,400		466,400		466,400	82
16,210	29.0	7			x						500,000				464,600		464,600		464,600	82
16,010	28.6	8		x	x					48,048	500,000				464,200		464,200		464,200	82
14,570	25.0	9			x						517,500				483,000		483,000		483,000	82
15,950	27.6	10			x						504,400				479,100		479,100		479,100	82
16,040	27.7	11			x						508,100				481,300		481,300		481,300	82
15,830	26.0	12			x						537,500				506,200		506,200		506,200	82
15,740	25.7	13			x						535,000				508,800		508,800		508,800	82
24,590	41.0	14		x	x					118,220	527,500				498,300		498,300		498,300	82
17,510	28.1	15		x	x					32,597	523,100			23,200	494,400		517,600		517,600	82
17,090	26.1	16			x						570,000				542,900		542,900		542,900	82
15,400	25.3	17			x						530,000				505,300		505,300		505,300	82
15,100	25.6	18			x						508,800				489,100		489,100		489,100	82
15,790	27.1	19			x						510,600				484,300		484,300		484,300	82
16,090	28.3	20			x						498,800				472,100		472,100		472,100	82
18,550	31.9	21			x						510,000				483,000		483,000		483,000	82
21,130	36.6	22		x	x					6,313	508,100				478,600		478,600		478,600	82
17,550	31.3	23			x						491,300				465,500		465,500		465,500	82
16,120	30.3	24			x						470,000				441,900		441,900		441,900	82
17,560	29.6	25			x						516,300				491,800		491,800		491,800	82
23,480	35.3	26	x		x				28,988		576,300				552,100		552,100		552,100	82
24,910	39.4	27	x		x				15,775		556,900				525,400		525,400		525,400	82
26,140	38.0	28	x		x				2,760		600,000				570,900		570,900		570,900	82
32,150	49.7	29	x		x				131,402		566,300				537,300		537,300		537,300	82
25,280	37.6	30			x						586,300				558,300		558,300		558,300	82
	#####	31															0		0	82
556,020	31.1								178,925	205,178	15,650,400	0	0	23,200	14,806,100	0	14,829,300	0	14,829,300	

Makeup Water	%	OCT 2016	#1	#2	#7	#8	HRS. on OIL	OIL Gals.	GAS FEET M. No. 1	No. 2	No. 7	No. 8	Steam Lbs. No. 1	No. 2	No. 7	No. 8	By GAS STEAM LBS.	By OIL STEAM LBS.	TOTAL STEAM GENERATED	BOILER EFF.
24,900	38.1	1			x						570,600				542,500		542,500		542,500	82
24,710	38.1	2			x						563,100				538,600		538,600		538,600	82
25,530	38.3	3			x				22,060		574,400		13,600		539,000		552,600		552,600	82
34,220	51.2	4			x						595,600				555,200		555,200		555,200	82
31,310	46.2	5			x						593,100				562,200		562,200		562,200	82
31,630	48.4	6			x						571,900				542,900		542,900		542,900	82
39,130	53.3	7			x						641,300				609,400		609,400		609,400	82
29,530	48.8	8			x						520,600				502,700		502,700		502,700	82
30,230	51.2	9			x						504,400				489,600		489,600		489,600	82
26,740	43.1	10			x				10,489	16,204	530,000		2,600		512,800		515,400		515,400	82
26,910	42.5	11	x		x				327,256	39,077	286,300		252,000		273,400		525,400		525,400	82
28,020	39.9	12	x	x					438,900	456,711			312,400	269,900			582,300		582,300	80
28,370	34.6	13	x	x					31,253	890,100			21,000	659,300			680,300		680,300	82
20,900	29.4	14		x						803,022				590,600			590,600		590,600	80
18,110	29.8	15		x						696,486				504,400			504,400		504,400	80
14,030	25.0	16		x						642,114				465,500			465,500		465,500	80
20,360	33.0	17	x	x					66,750	500,250			63,900	447,600			511,500		511,500	80
16,790	26.7	18	x	x					508,800	275,000			332,100	190,800			522,900		522,900	80
18,850	28.2	19	x						842,500				555,600				555,600		555,600	80
26,930	36.5	20	x						924,400				612,900				612,900		612,900	80
22,120	29.6	21	x						945,600				621,300				621,300		621,300	80
20,730	32.4	22	x						801,300				531,100				531,100		531,100	80
18,110	30.5	23	x						740,000				493,100				493,100		493,100	80
22,650	32.6	24	x						871,900				576,200				576,200		576,200	80
21,700	33.3	25	x						817,500				540,300				540,300		540,300	80
20,320	30.4	26	x						836,900				554,300				554,300		554,300	80
23,100	33.5	27	x			x			515,600			299,400	337,800			234,900	572,700		572,700	77
19,310	32.0	28				x						621,300				500,500	500,500		500,500	82
17,360	33.6	29				x						550,600				428,800	428,800		428,800	82
21,520	33.5	30				x						652,500				532,400	532,400		532,400	83
20,340	31.5	31				x						663,100				536,400	536,400		536,400	83
744,460	36.7								8,701,208	4,318,964	5,951,300	2,786,900	5,820,200	3,128,100	5,668,300	2,233,000	16,849,600	0	16,849,600	

<u>Appendix B3:</u> Bell & Gossett SU-85-2 Heat Exchanger (reproduced from Ref. 14)

Bell & Gossett Shell and Tube Heat Exchanger	
Mfg: Bell & Gossett	**Model: SU-85-2**
Stock No. CJRP5186.2	**Serial No. 0-44554**

Bell & Gossett Shell and Tube Heat Exchanger. Model: SU-85-2. S/N: 0-44554. Nat'l Bd: 560585. MAWP @ 350 °F: 150 psi. Number of tubes: 22. Tube dimensions: 11/16 in. x 60 in. L. Inlets: (1) 2 in. dia. tube (media), (1) 3 in. dia. S-line fitting (product). Outlets: 1-1/4 in. dia. pipe outlet (media), (1) 3 in. dia. S-line fitting (product). Overall dimensions: 66 in. L x 33 in. W x 12 in. H.

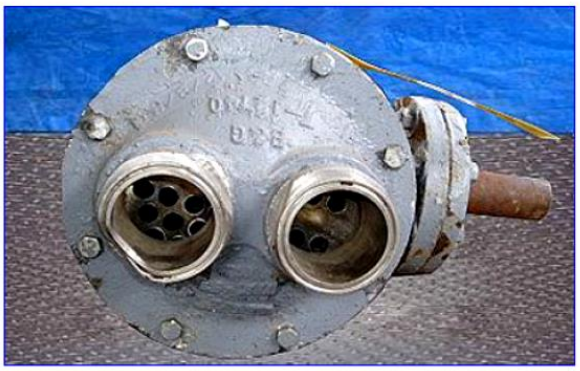

Appendix C1: Steam Generated and Accuracy of Estimated Energy Savings

Table C1.1. Energy savings that were estimated by using Eq. (3.18)

Month	S_G $(\frac{lb_m}{30\ days})$	Computed Q $(\frac{Btu}{30\ days})$	Estimated Q by Eq. (3.18) $(\frac{Btu}{30\ days})$	Accuracy (-) $(\frac{Estimated\ Q}{Computed\ Q})$
January	40,230,000	265,870,000	267,750,000	**1.01**
February	32,630,000	292,110,000	283,900,000	**0.97**
March	23,510,000	305,250,000	311,900,000	**1.02**
April	19,770,000	325,100,000	329,260,000	**1.01**
May	16,640,000	343,100,000	349,560,000	**1.02**
June	13,150,000	396,280,000	384,760,000	**0.97**
July	13,100,000	400,890,000	385,440,000	**0.96**
August	13,080,000	377,880,000	385,690,000	**1.02**

The values of "Computed Q" shown in Table C1.1 were given in Section 3.1. Equation (3.18) (see Section 3.1.2) was developed based on the relationship between the computed energy savings and steam generated between January to August of 2016. This equation was employed to estimate the energy savings for September to December of 2016, based on the steam generated during these months. So in order to evaluate the validity of Eq. (3.18), a relationship was similarly developed from January-July data to predict the August's energy savings as a test. So, Eq. (C1.a) was found as a polynomial relationship between these months (January-July). The accuracy of predicting August's energy savings was 103% (Table C1.2) with respect to the actual value that was computed based on the data gathered.

$$Q_i(\frac{Btu}{30\ days}) = \frac{(S_G(\frac{lb_m}{30\ days}))_i}{0.1712((S_G(\frac{lb_m}{30\ days}))_i\ x\ 10^{-8})^2 + 0.3382\left((S_G(\frac{lb_m}{30\ days}))_i\ x\ 10^{-8}\right) - 0.0136} \qquad \text{(C1.a)}$$

Table C1.2. The accuracy of using Eq. (C1.a) to predict August's energy savings

Month	S_G $(\frac{lb_m}{30\ days})$	Computed Q $(\frac{Btu}{30\ days})$	Estimated Q by Eq. (C1.a) $(\frac{Btu}{30\ days})$	Accuracy (-) $(\frac{Estimated\ Q}{Computed\ Q})$
January	40,230,000	265,870,000	267,900,000	**1.01**
February	32,630,000	292,110,000	283,770,000	**0.97**
March	23,510,000	305,250,000	311,900,000	**1.02**
April	19,770,000	325,100,000	329,730,000	**1.01**
May	16,640,000	343,100,000	350,970,000	**1.02**
June	13,150,000	396,280,000	388,600,000	**0.98**
July	13,100,000	400,890,000	389,330,000	**0.97**
August	13,080,000	377,880,000	**389,600,000**	**1.03**

Table C1.3. Basement heat exchanger's energy savings estimated by using Eq. (3.20)

Month	$\dot{m}_{m-up}$ $(\frac{lb_m}{30\ days})$	Computed Q $(\frac{Btu}{30\ days})$	Estimated Q by Eq. (3.20) $(\frac{Btu}{30\ days})$	Accuracy (-) $(\frac{Estimated\ Q}{Computed\ Q})$
January	760,000	193,210,000	175,210,000	**0.91**
February	631,000	138,960,000	128,660,000	**0.93**
March	593,000	134,710,000	116,640,000	**0.87**
April	464,000	83,560,000	83,140,000	**0.99**
May	393,000	84,260,000	76,680,000	**0.91**
June	315,000	62,680,000	56,490,000	**0.90**
July	290,000	54,100,000	53,330,000	**0.99**

Table C1.4. KU SPP's generated steam for the years 2014 [2], 2015 [3], and 2016 [App. B2]

Month	2014	2015	2016
January	------	37,821,700 lb_m	41,573,600 lb_m
February	------	38,179,100 lb_m	31,546,300 lb_m
March	------	27,418,400 lb_m	24,297,800 lb_m
April	20,085,100 lb_m	19,858,400 lb_m	19,774,300 lb_m
May	13,838,600 lb_m	15,015,900 lb_m	14,972,100 lb_m
June	13,903,500 lb_m	14,563,600 lb_m	13,154,700 lb_m
July	13,015,900 lb_m	14,423,800 lb_m	13,540,900 lb_m
August	13,637,200 lb_m	14,359,000 lb_m	13,422,100 lb_m
September	14,175,800 lb_m	14,286,400 lb_m	14,829,300 lb_m
October	17,721,800 lb_m	18,118,300 lb_m	16,849,600 lb_m
November	31,515,000 lb_m	26,090,300 lb_m	-------
December	35,417,400 lb_m	33,367,700 lb_m	-------

Appendix C2: Basement Heat Exchanger Temperature Analysis

Figures C2.a shows the recorded inlet, outlet, and rise temperatures of the basement heat exchanger in March, 2, 2016. A temperature analysis was conducted on these temperatures in order to determine when the solenoid valve was open or closed. This analysis was conducted based on the behavior of the inlet temperature of the make-up water for the reasons explained in Section 3.2. All temperature readings, when the solenoid valve was closed, were ignored since they were not the actual temperatures because there was no make-up water flowing. For example, it can be seen in Fig. C2.a that the actual temperature of the inlet make-up water was about 54 °F, while the many 60-90 °F inlet and outlet temperature pulses represent when the solenoid valve was closed. These temperature pulses happened because the heat exchanger's metal components and all of its connected pipe lines were overheated by the boiler's hot blowdown water.

In this case, any temperature higher than around 54 °F was not considered in the energy calculation. So, it can be seen that all of the readings when the valve was closed (the temperature pulses) were removed from Fig. C2.a to yield Fig. C2.b, while the remaining readings in Fig. C2.b were only when the solenoid valve was open.

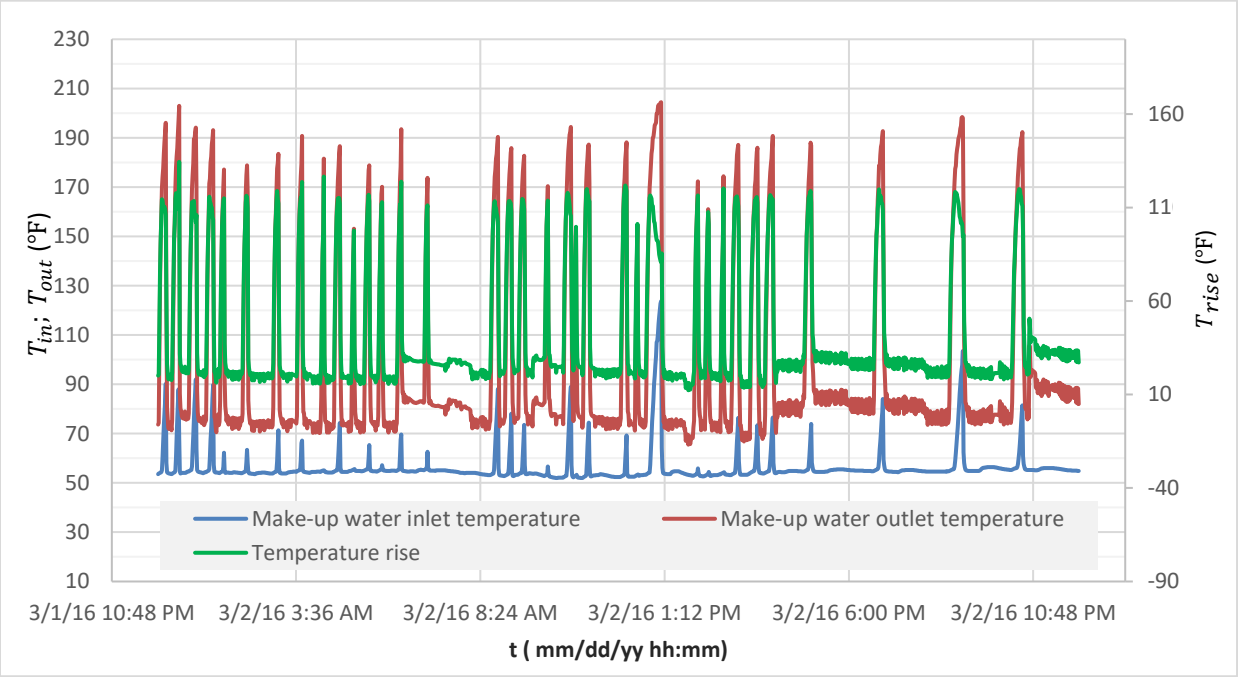

Fig. C2.a. Basement heat exchanger's inlet, outlet, and rise temperatures of the make-up water on March 2, 2016

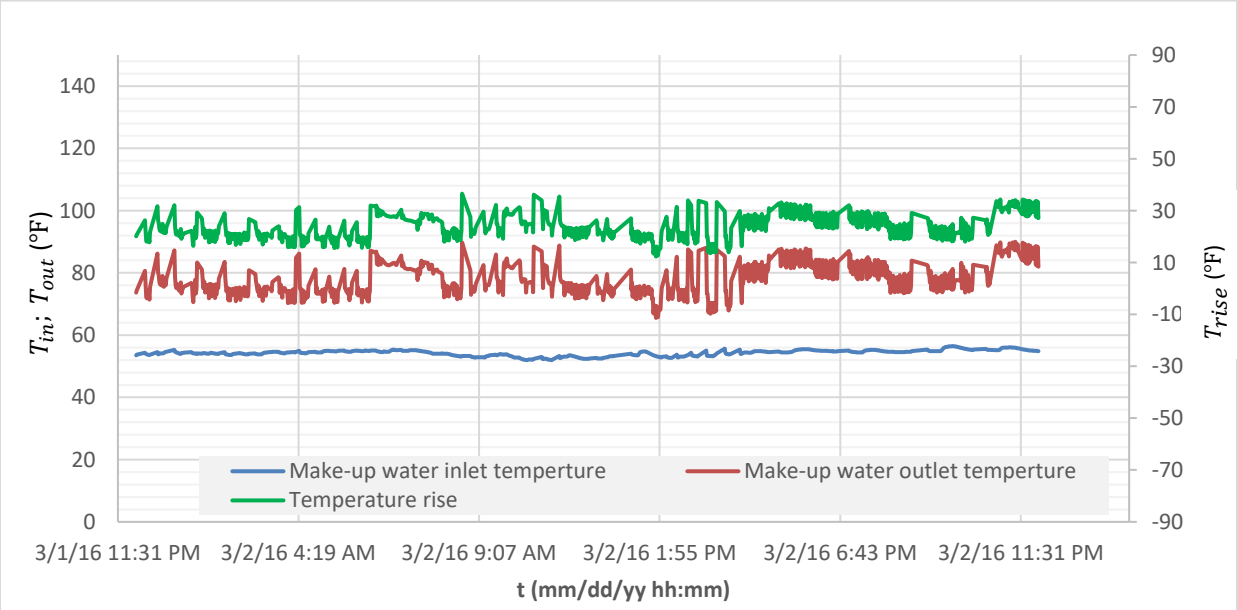

Fig. C2.b. Basement heat exchanger's analyzed inlet, outlet, and rise temperatures of the make-up water on March 2, 2016

Appendix D1: Worthington D-824 CSP Specifications and Performance Curves

(reproduced from Ref. 48)

FLOWSERVE

Construction Datasheet

Customer	:	Pump / Stages	: D824-3X2X5F / 1
Customer reference	: Douglas Pump	Based on curve no.	: A-19446
Item number	: -	Flowserve reference	: 363650489
Service	:	Date	: April 8, 2015

Construction

Nozzles	Size	Rating	Face	Pos'n
Suction	3.00	125#	FF	End
Discharge	2.00	125#	FF	Top

Casing mounting	: Foot
Casing split	: Radial
Impeller type	: Closed Impeller
Bearing type (radial)	: N/A
Bearing number (radial)	: N/A
Bearing type (thrust)	: N/A
Bearing number (thrust)	: N/A
Bearing lubrication	: Other
Rotation (view from cplg)	: CW per Hyd. Institute

Materials

Casing	: Cast Iron 25
Impeller	: Bronze
Case wear ring	: N/A
Impeller wear ring	: N/A
Inducer	: N/A
Shaft	: Steel
Sleeve	: Bronze

Baseplate, Coupling and Guard

Baseplate type	: N/A
Baseplate material	: N/A
Coupling manufacturer	: N/A
Coupling size	:
Coupling / Shaft guard	: N/A

Weights (Approx.)

Bareshaft pump(nett)	: 58.0 lb
Baseplate(nett)	: -
Driver(nett)	: 127.0 lb
Shipping gross weight/vol.	: 212.7 lb / 6199 cu.in

Testing

Hydrostatic test	: None
Performance test	: None
NPSH test	: None

Paint and Package

Pump paint	: FPD Standard
Base grout surface prep	: FPD Std.
Shipment type	: Domestic

Driver Information

Manufacturer	: Flowserve Choice
Power	: 10.00 hp / 7.46 kW
Service factor (req'st / act)	: 1.0 / -
Speed	: 3600
Orientation / Mounting	: Horizontal / Foot and flange
Driver Type	: NEMA
Frame-size / material	: 215JM / Aluminum
Enclosure	: TEFC
Hazardous area class	: -
Explosion 'T' rating	: -
Volts / Phase / Hz	: 230/460 / 3 / 60 Hz
Amps-full load/locked rotor	: 12.00 A / 72.10 A
Motor starting	: Direct on line (DOL)
Insulation	: F
Temperature rise	: 80 C
Bearings	: Ball
Lubrication	: Grease
Motor mounted by	: Flowserve

Sound Pressure (dBA @ 1.0 m)

Driver, expected	: -
Pump & driver, estimated	: -

Seal Information

Arrangement	: Sgl. Int. O-Ring
Size	: 1.375
Manufacturer / Type	: Flowserve / PAC 51
Material code (Man'f/API)	: BCFXF / -
Internal neck bushing	: N/A

Gland

Gland material	: N/A
Flush	: N/A
Vent	: N/A
Drain	: N/A
Auxiliary seal device	: N/A

Piping

Seal flush plan	: None
Seal flush construction	: -
Seal flush material	: -
Aux seal flush plan	: None
Aux seal flush construction	: -
Aux seal flush material	: -

Notes

-

-

-

-

Bronze Adapter Wear Ring

-

Affinity v1.3.5

3 of 3

FLOWSERVE

Hydraulic Datasheet

Customer	:	Pump / Stages	: D824-3X2X5F / 1
Customer reference	: Douglas Pump	Based on curve no.	: A-19446
Item number	: -	Flowserve reference	: 363650489
Service	:	Date	: April 8, 2015

Operating Conditions

Capacity	: 282.9 USgpm
Water capacity (CQ=1.00)	: -
Normal capacity	: -
Total developed head	: 86.44 ft
Water head (CH=1.00)	: -
NPSH available (NPSHa)	: Ample
NPSHa less NPSH margin	: -
Maximum suction pressure	: 0.0 psig

Liquid

Liquid type	: Other
Temperature / Spec. Gravity	: 60 F / 1.000
Solid Size - Actual / Limit	: - / 0.50 in
Viscosity / Vapor pressure	: 1.00 cSt / -

Materials / Specification

Material column code	: STD
Pump specification	: General Industrial

Other Requirements

Hydraulic selection : No specification
Construction : No specification
Test tolerance : Hydraulic Institute Level B
Driver Sizing : Max Power(MCSF to EOC)with SF

Performance

Hydraulic power	: 6.18 hp	Impeller diameter	
Pump speed	: 3550 rpm	Rated	: 5.05 in
Pump overall efficiency (CE=1.00)	: 77.5 %	Maximum	: 5.25 in
		Minimum	: 4.40 in
NPSH required (NPSH3)	: 11.1 ft	Suction specific speed	: 9190 US units
Rated power	: 7.97 hp	Minimum continuous flow	: 38.5 USgpm
Maximum power	: 9.04 hp	Maximum head @ rated dia	: 101.36 ft
Driver power	: 10.00 hp / 7.46 kW	Flow at BEP	: 282.9 USgpm
Casing working pressure	: 43.9 psig	Flow as % of BEP	: 100.0 %
(based on shut off @ cut dia/rated SG)		Efficiency at normal flow	: -
Maximum allowable	: 175.0 psig	Impeller dia ratio (rated/max)	: 96.2 %
Hydrostatic test pressure	: 265.0 psig	Head rise to shut off	: 17.3 %
Est. rated seal chamb. press.	: -	Total head ratio (rated/max)	: 82.6 %

CURVES ARE APPROXIMATE, PUMP IS GUARANTEED FOR ONE SET OF CONDITIONS; CAPACITY, HEAD, AND EFFICIENCY.

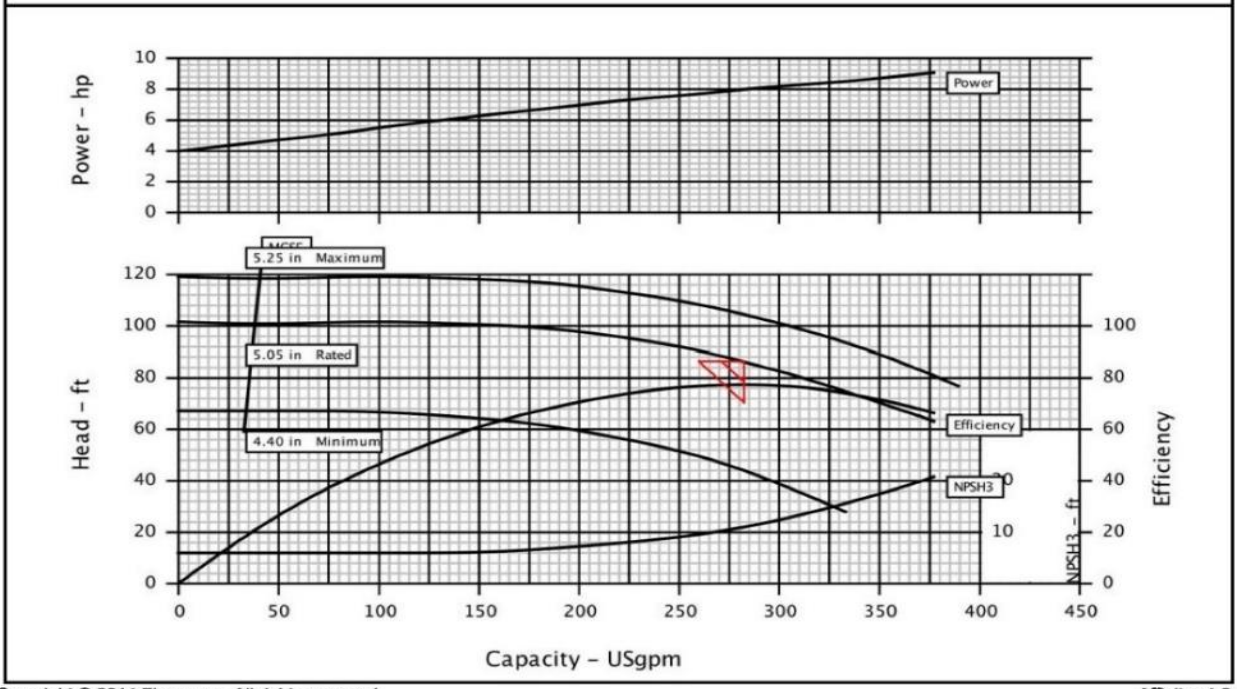

Affinity v1.3.

FLOWSERVE

Pump size & type	: D824-3X2X5F
Based on curve no.	: A-19446
Number of stages	: 1

Customer	:	Capacity	: 282.9 USgpm
Item number	: -	Head	: 86.44 ft
Service	:	Specific gravity	: 1.000
Flowserve reference	: 363650489	Pump speed	: 3550 rpm
Date	: April 8, 2015	Test tolerance	: Hydraulic Institute Level B

CURVES ARE APPROXIMATE, PUMP IS GUARANTEED FOR ONE SET OF CONDITIONS; CAPACITY, HEAD, AND EFFICIENCY.

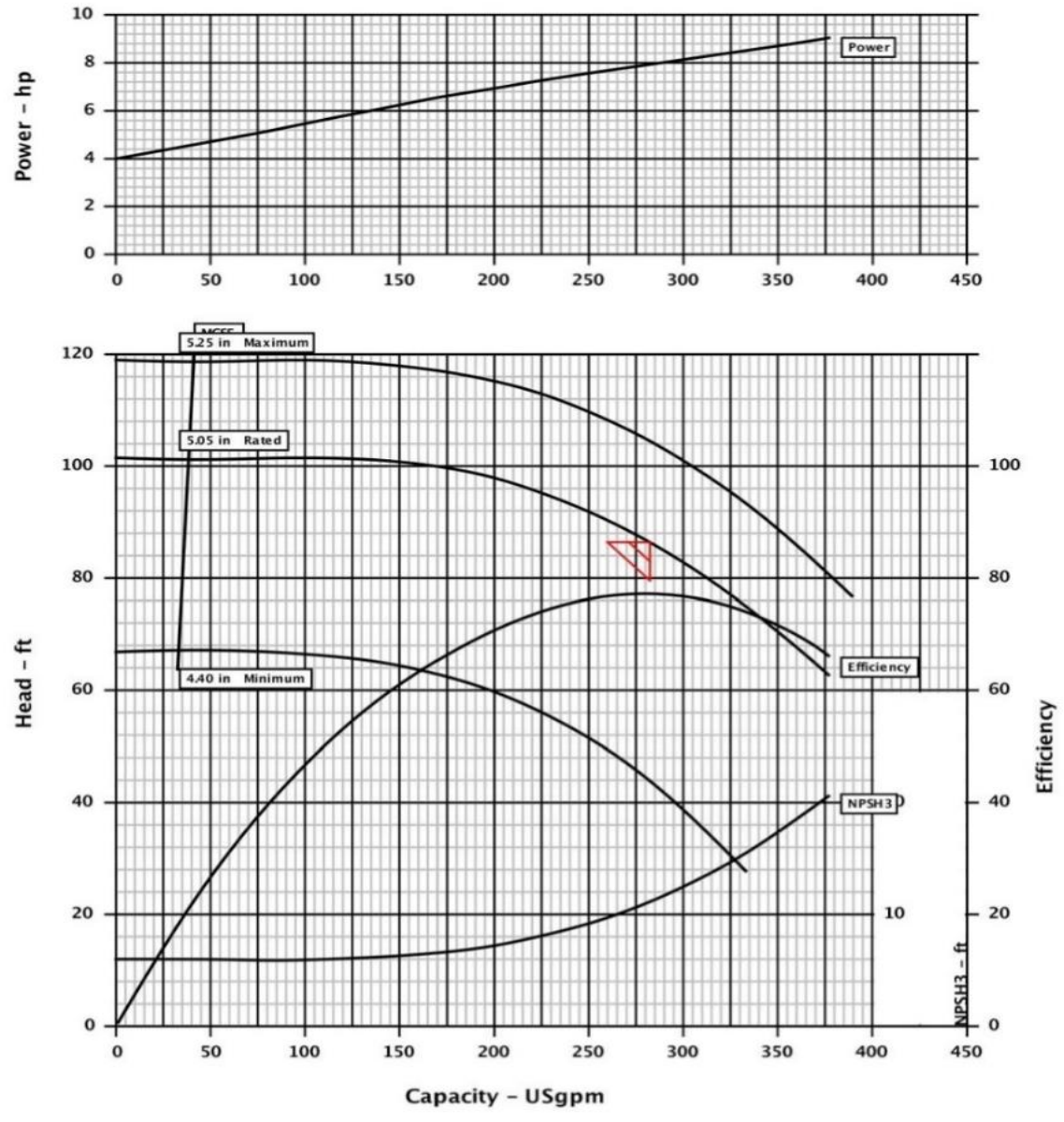

Affinity v1.3.

Appendix D1-1: Worthington D-824 Motor Tag

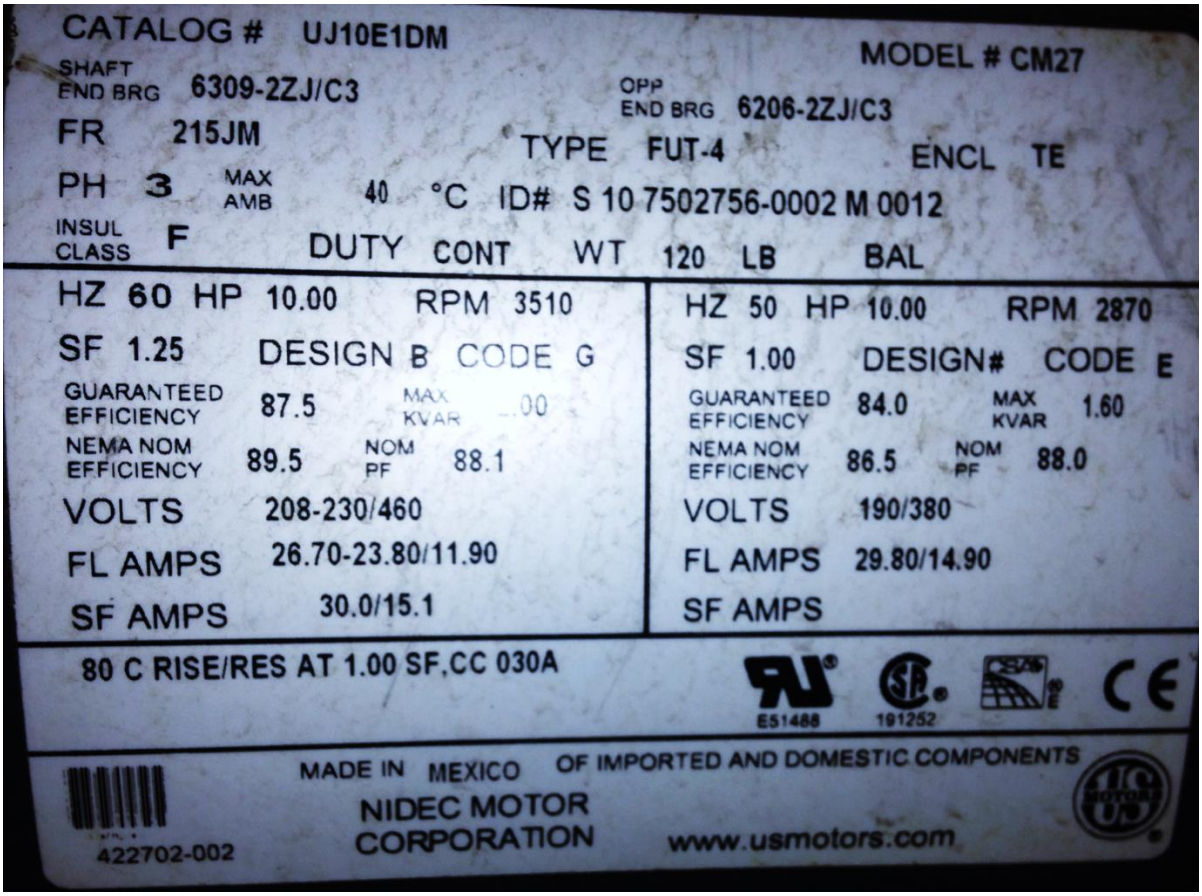

Fig. D1. Worthington motor tag in the KU SPP shows the motor efficiency (0.875 at 60Hz).

Appendix D2: Grundfos CRE15-3 Specifications and Performance Curves

(reproduced from Ref. 27)

GRUNDFOS

Company name: University of Kansas - Steam Power Plant
Created by:
Phone: -
Fax: -
Date: -

Description	Value
General information:	
Product name:	HYDRO MPC E 2CRE15-03 3X460V BASIS
Position	
Product No.:	95055132
EAN:	5700836977051
Price:	On request
Technical:	
Max flow:	244 US gpm
Max flow system:	244 US gpm
Head max:	200 ft
Impellers main:	3
Main pump name:	CRE15-03
Main pump Number:	96541270
Number of pumps:	2
Non-ret. valve:	at discharge side
Installation:	
Maximum operating pressure:	232 psi
Maximum inlet pressure:	145 psi
Flange standard:	ANSI
Pump inlet:	102
Pump outlet:	102
Pressure stage:	CL 150
Liquid:	
Liquid temperature range:	32 .. 140 °F
Electrical data:	
Power (P2) main pump:	7.51 HP
Main frequency:	60 Hz
Rated voltage:	3 x 3X460-480V, 60 Hz
Starting main:	electronically
Rated current of system:	20.8 A
Enclosure class (IEC 34-5):	UL Type 3R/12
Controls:	
Control type:	E
Operation unit:	CU 352
Tank:	
Diaphragm tank:	No
Others:	
Net weight:	650 lb
Language:	EN
Product range:	NAMREG
Configuration file Hydro MPC:	95043547

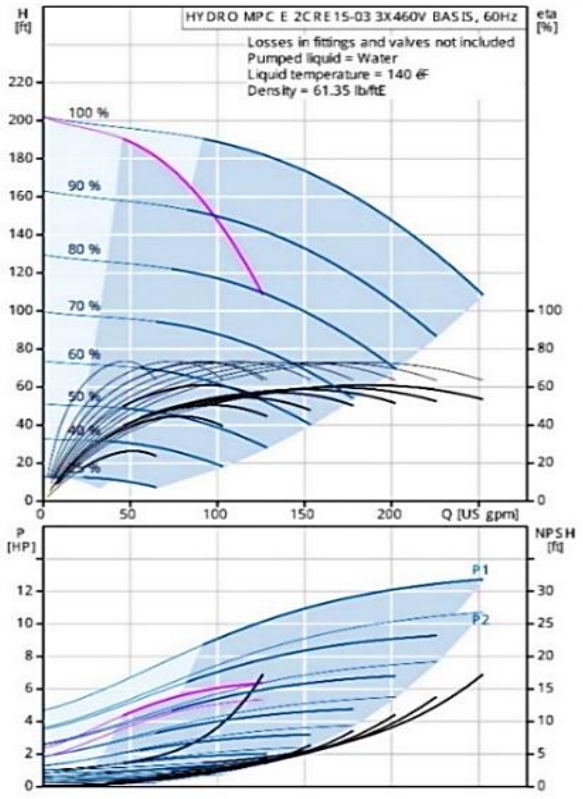

Printed from Grundfos Product Center [2015.02.029]

GRUNDFOS 1/2

Company name:	University of Kansas - Steam Power Plant
Created by:	
Phone:	-
Fax:	-
Date:	-

95055132 HYDRO MPC E 2CRE15-03 3X460V BASIS 60 Hz

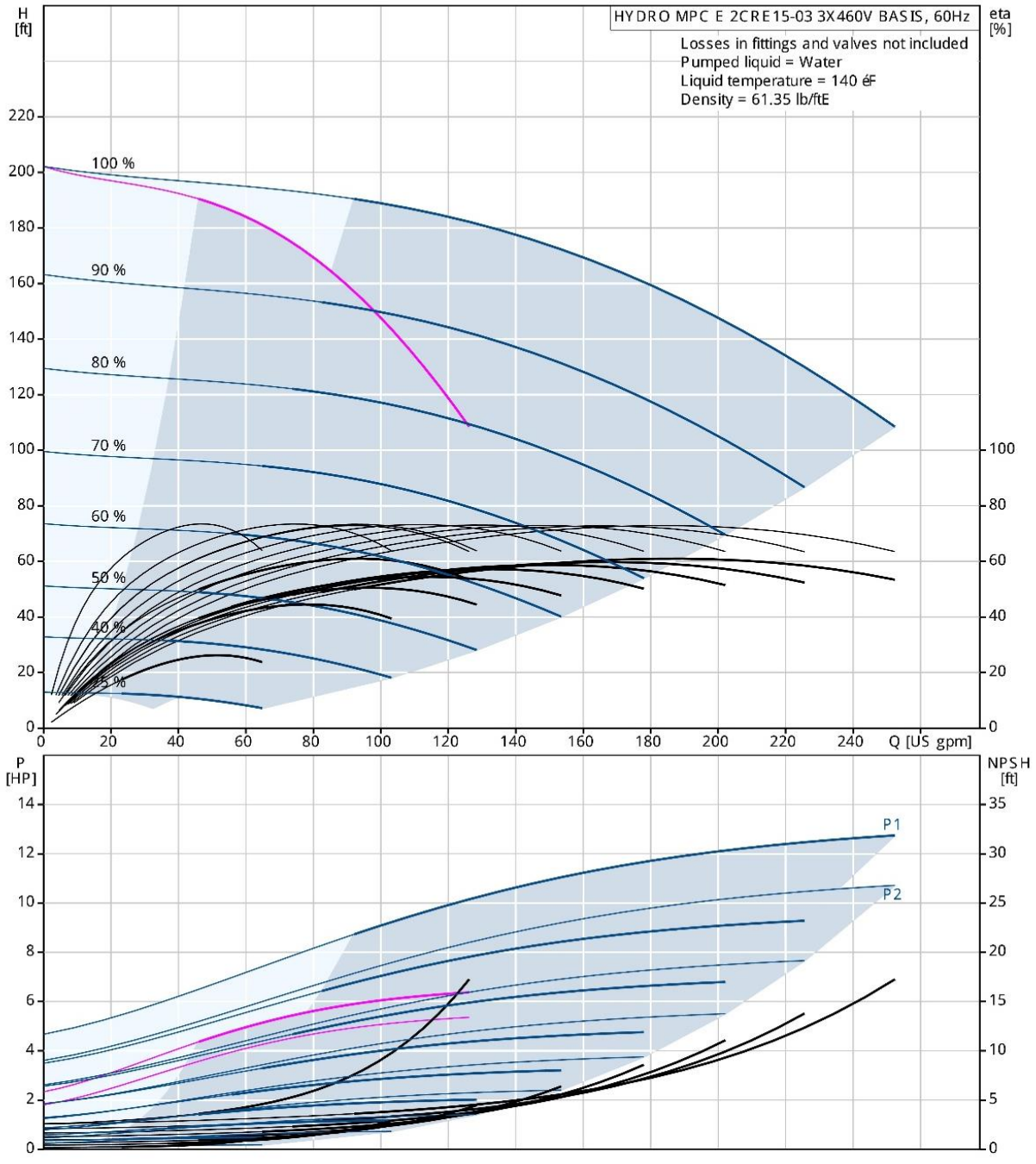

Appendix D2-1: Grundfos E Product PC Tools

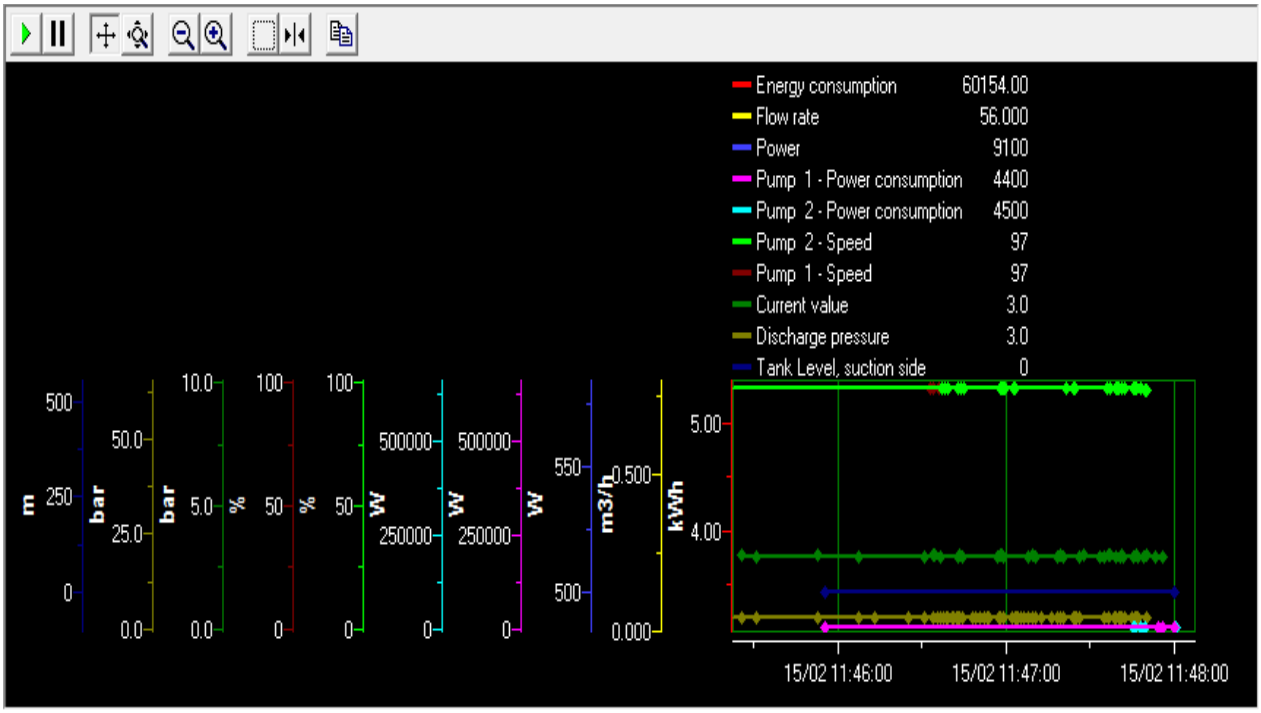

Fig. D2. Grundfos PC Tools software used to monitor and record pump operating conditions from the Grundfos control panel

Appendix D3: **Omega Pressure Sensor (PX43E0-200GI) Data Sheet**
(reproduced from Ref. 49)

HEAVY-DUTY FLUSH DIAPHRAGM TRANSMITTER
½ NPT THREAD

4 to 20 mA Output
0-50 to 0-750 psi
0-3 to 0-50 bar

1 bar = 14.5 psi
1 kg/cm² = 14.22 psi
1 atmosphere = 14.7 psi = 29.93 inHg = 760.2 mmHg = 1.014 bar

PX43 Series

MADE IN USA NIST CE OMEGADYNE RoHS
Standard

- **Stainless Steel Construction**
- **Processing or Industrial Applications**
- **Rugged Flush Diaphragm for Measurement of Difficult Fluids**
- **3 m (10') Cable with Conduit Connection for Installation in Harsh Environments**
- **Heavy-Duty ½ NPT Fitting**
- **4 to 20 mA Output for Noise-Free Transmission**

OMEGA's PX43 is a high-accuracy, current output, industrial pressure transmitter with a heavy-duty flush diaphragm. It is designed for use with food and industrial fluids and slurries that are difficult to measure because of sticking or plugging of orifices. Its hermetically sealed, all stainless steel construction make it suitable for the harshest industrial environments. Ten feet of 2-conductor shielded cable is standard with a second ½ NPT fitting on the body for conduit installation. Pressure ranges from 0 to 50 up to 0 to 750 psi are available to cover most processing and industrial applications.

SPECIFICATIONS

Excitation: 10 to 40 Vdc
Output: 4 to 20 mA 10% adj
Zero Balance: 4 mA +10% -2% adj
Accuracy: 0.5% linearity, hysteresis and repeatability combined
Operating Temp Range: -46 to 121°C (-50 to 250°F)
Compensated Temp Range: 16 to 71°C (60 to 160°F)
Thermal Effects:
Span: 0.003% of rdg/°F
Zero: 0.0045% of FSO/°F
Proof Pressure: 150% of range
Burst Pressure: 300% of range

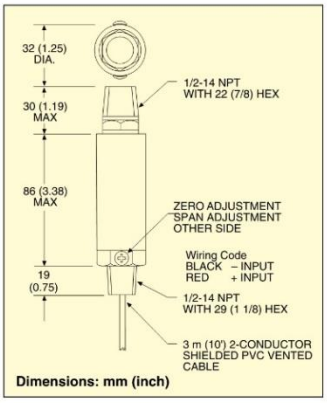

Dimensions: mm (inch)

Wetted Parts: 17-4 PH stainless steel with 316 stainless steel diaphragm
Pressure Port: ½-14 NPT male
Electrical Connection: 3 m (10') 2-conductor shielded vented cable with ½-14 NPT fitting

To Order Visit omega.com/px43-i for Pricing and Details

RANGE		MODEL NO.	COMPATIBLE METERS*
0 to 50 psig	0 to 3.4 bar	**PX43E0-050GI**	DP41-E, DP25B-E, DP24-E
0 to 60 psig	0 to 4.1 bar	**PX43E0-060GI**	DP41-E, DP25B-E, DP24-E
0 to 100 psig	0 to 6.9 bar	**PX43E0-100GI**	DP41-E, DP25B-E, DP24-E
0 to 200 psig	0 to 13.8 bar	**PX43E0-200GI**	DP41-E, DP25B-E, DP24-E
0 to 300 psig	0 to 20.7 bar	**PX43E0-300GI**	DP41-E, DP25B-E, DP24-E
0 to 500 psig	0 to 34.5 bar	**PX43E0-500GI**	DP41-E, DP25B-E, DP24-E
0 to 750 psig	0 to 51.7 bar	**PX43E0-750GI**	DP41-E, DP25B-E, DP24-E

Comes complete with 5-point NIST traceable calibration.
Metric ranges available – consult Engineering.

** See **omega.com** for compatible meters.*

***Ordering Examples:* PX43E0-100GI,** 100 psi gage model with stainless steel wetted parts, 3 m (10') cable, 4 to 20 mA output. **PX43E0-050GI,** 50 psi gage model with stainless steel wetted parts, 3 m (10') cable, 4 to 20 mA output.

Appendix D4: Veris Power Monitoring H8044-0100-2 Current Transducer
(reproduced from Ref. 26)

VERIS INDUSTRIES H804X SERIES INSTALLATION GUIDE

WIRING

Typical 208/480 VAC 3Ø, 3- or 4-Wire Installation

Model 8043/44

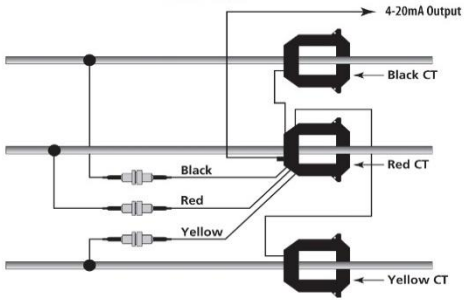

Model 8041/42 (Use on balanced loads only)

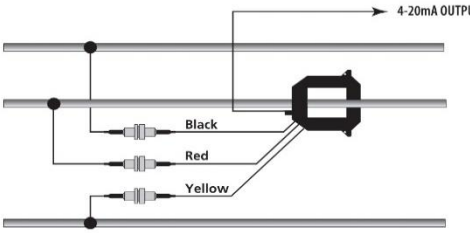

NOTE: Multiply output by 3 for proper kW indication

Typical 240/120 VAC 1Ø, 3-Wire Installation

Model 8043

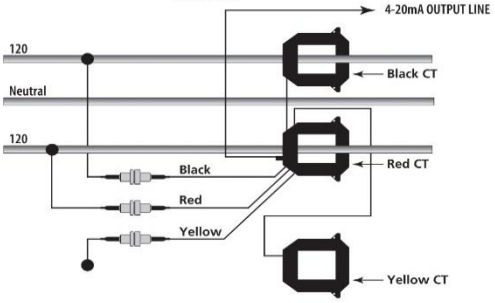

Model 8041

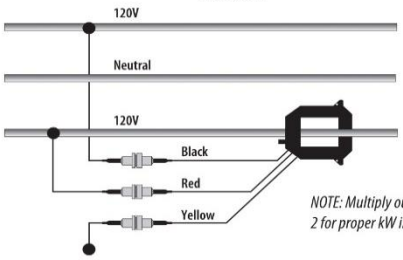

NOTE: Multiply output by 2 for proper kW indication

Typical 277 VAC 1Ø, 2-Wire Installation

Model 8044

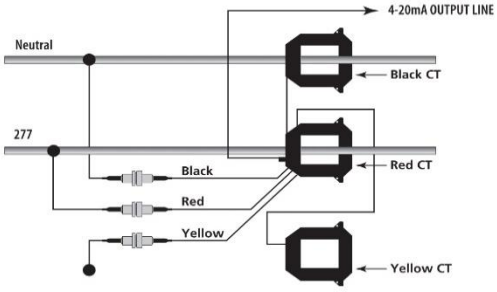

Model 8042

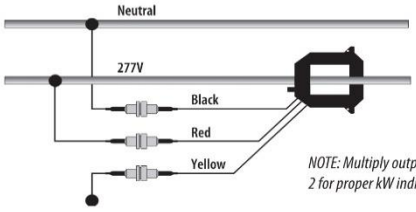

NOTE: Multiply output by 2 for proper kW indication

Alternative 277 VAC 1Ø, 2-Wire Installation

Model 8042

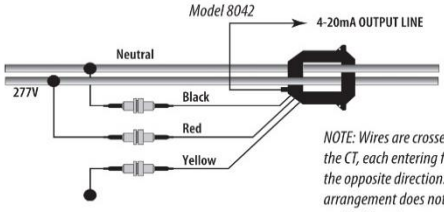

NOTE: Wires are crossed through the CT, each entering from the opposite direction. This arrangement does not require multiplying the output data.

TROUBLESHOOTING

Problem	Solution
Status LED does not blink	Check fuses and voltage connections. Status LED should blink regardless of CTs or output connections.
Readings seem highly inaccurate.	• Check that each CT is installed on the conductor with the corresponding color voltage input lead attached. In most cases, incorrect wiring will cause the STATUS LED to blink RED (slowly). However, a power factor lower than 0.5 could cause the LED to blink this way, even if the unit is installed properly. • It does not matter which side of the CT faces towards the load. • If current is below 7% of full scale maximum for the CT, use a smaller CT or wrap each wire through the CT multiple times • If using the single-phase H8042, use an amp-clamp to ensure that all three phases are passing the same approximate current. If phases are unbalanced, try the H8043/H8044 models.
Meter goes offline when load is switched off.	Voltage leads must be connected on the Line side of the conductor. The power meter cannot communicate without voltage.
Status LED blinks red.	• If the LED blinks quickly (i.e., about 5 blinks in two seconds), then use a higher rated CT. • If the LED blinks slowly (i.e., about 1 blink in two seconds) the CTs are not installed on the correct conductors, or the power factor is less than 0.5. The meter can accurately measure these low PFs, but few loads operate normally at such a low power factor.

NOTES

1. DO NOT GROUND THE SHIELD INSIDE THE ELECTRICAL PANEL. All wires, including the shield should be insulated to prevent accidental contact to high voltage conductors.
2. The cable should be mechanically secured where it enters the electrical panel.
3. The cable should be shielded twisted pair wire BELDEN 1120A or similar.

WARNING: After wiring the cable, remove all scraps of wire or foil shield from the electrical panel. This could be DANGEROUS if wire scraps come into contact with high voltage wires!

MAXIMUM READINGS

Model	3Ø Power (kW)	1Ø Power (kW)
H8041-0100-2	36.03	24.00
H8041-0300-2	108.1	72.00
H8041-0400-3	144.1	96.00
H8041-0800-3	288.2	192.0
H8041-0800-4	288.2	192.0
H8041-1600-4	576.4	384.0
H8041-2400-4	864.6	576.0
H8042-0100-2	83.14	55.43
H8042-0300-2	249.4	166.3
H8042-0400-3	332.6	221.7
H8042-0800-3	665.1	443.4
H8042-0800-4	665.1	443.4
H8042-1600-4	1330	886.7
H8042-2400-4	1995	1330
H8043-0100-2	36.03	36.03
H8043-0300-2	108.1	108.1
H8043-0400-3	144.1	144.1
H8043-0800-3	288.2	288.2
H8043-0800-4	288.2	288.2
H8043-1600-4	576.4	576.4
H8043-2400-4	864.6	864.6
H8044-0100-2	83.14	83.14
H8044-0300-2	249.4	249.4
H8044-0400-3	332.6	332.6
H8044-0800-3	665.1	665.1
H8044-0800-4	665.1	665.1
H8044-1600-4	1330	1330
H8044-2400-4	1995	1995

Appendix D5: CSP Recorded Data for May-July

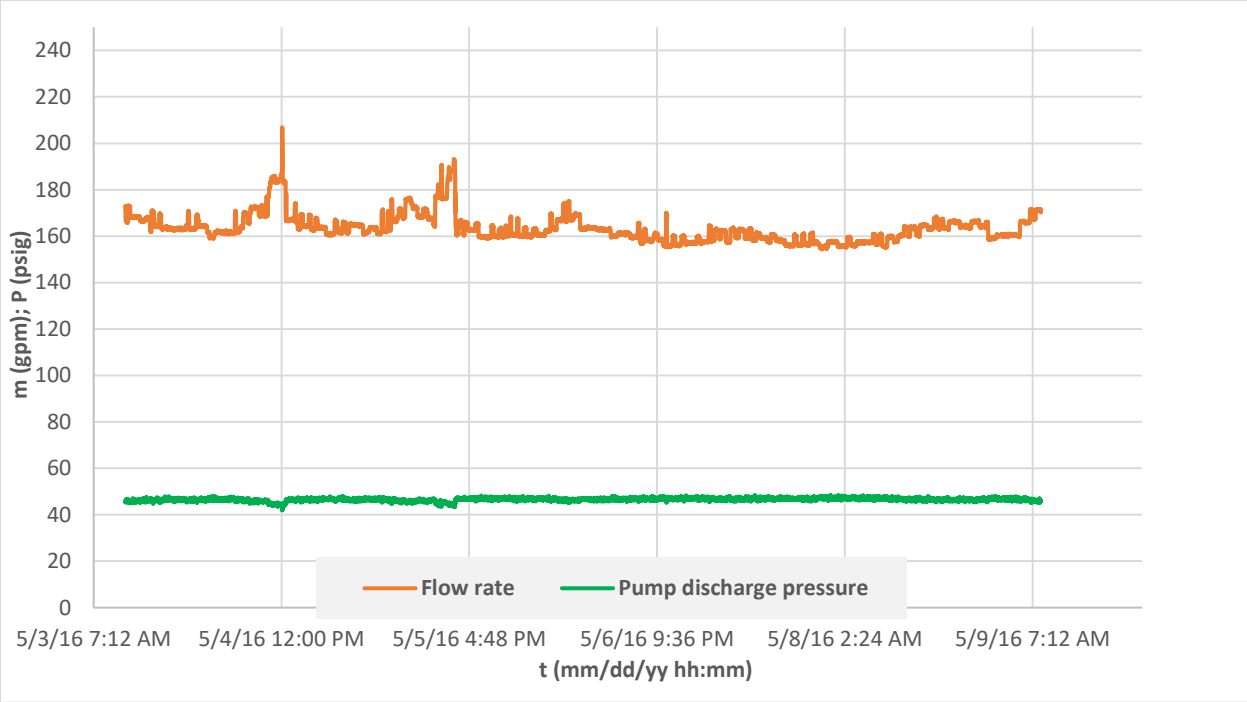

Fig. D5.a. Flow rate and discharge pressure of the Worthington pump in May

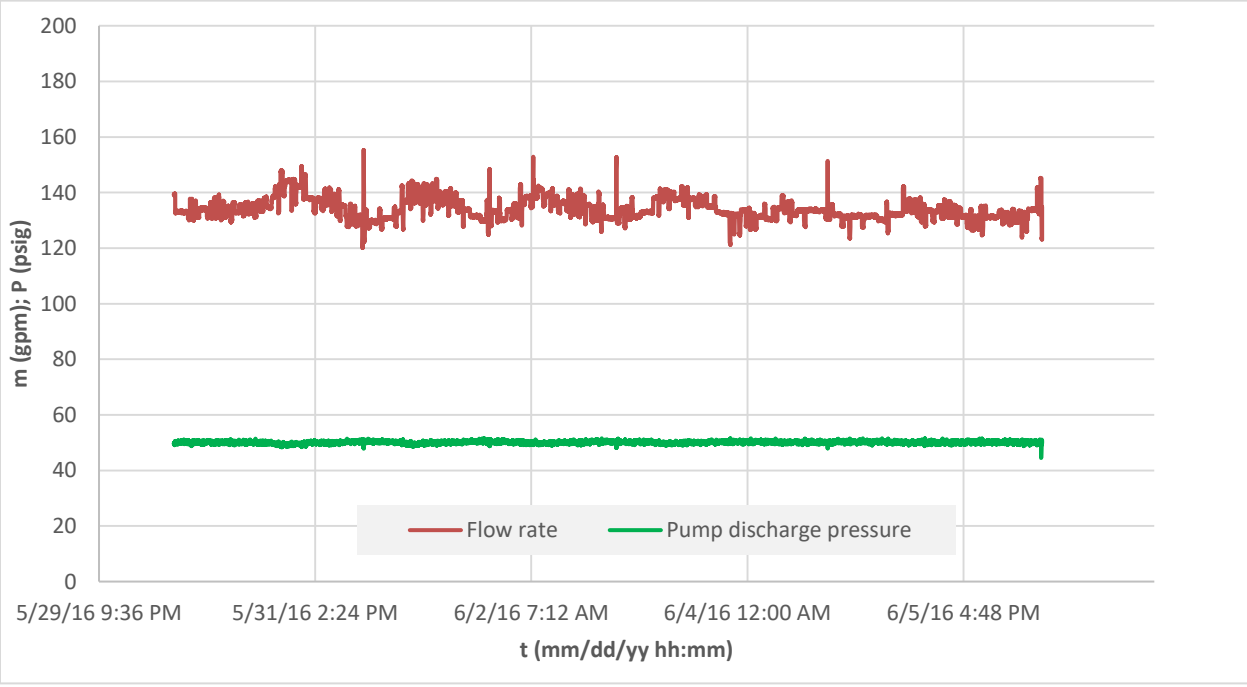

Fig. D5.b. Flow rate and discharge pressure of the Worthington pump in June

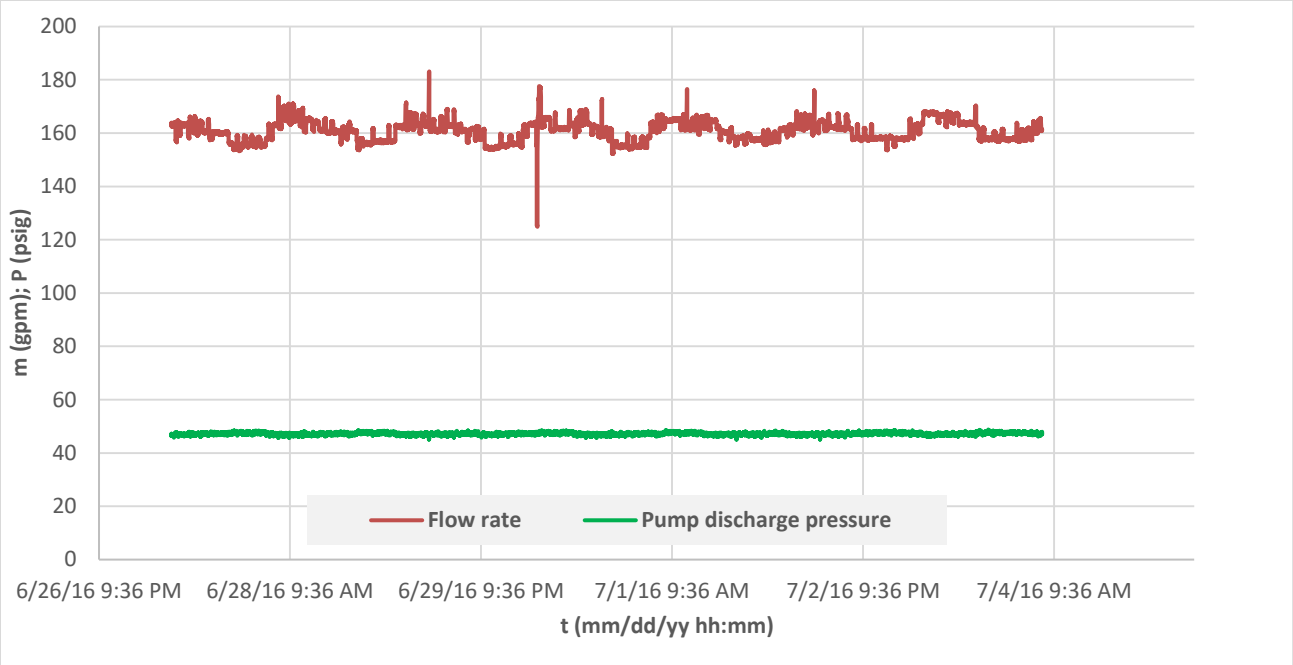

Fig. D5.c. Flow rate and discharge pressure of the Worthington pump in July

Appendix D6: Danfoss MBS3000 Pressure Transducer Data Sheet

(reproduced from Ref. 50)

ENGINEERING TOMORROW

Data sheet

Pressure transmitter for general industrial purposes

MBS 3000 and MBS 3050

The compact pressure transmitter, type MBS 3000, is designed for use in almost all industrial applications, and offers a reliable pressure measurement, even under harsh environmental conditions.

The compact heavy duty pressure transmitter MBS 3050 with integrated pulse-snubber is designed for use in hydraulic applications with severe medium influences like cavitation, liquid hammer or pressure peaks and offers a reliable pressure measurement, even under harsh environmental conditions.

The flexible pressure transmitter programme covers different output signals, absolute or gauge (relative) versions, measuring ranges from 0 – 1 to 0 – 600 bar. A wide range of pressure and electrical connections are available.

Excellent vibration stability, robust construction, and a high degree of EMC/EMI protection equip the pressure transmitter to meet the most stringent industrial requirements.

Features

- Designed for use in severe industrial and hydraulic environments
- Resistant to cavitation, liquid hammer and pressure peaks (MBS 3050)
- Enslosure and wetted parts of acid-resistant stainless steel (AISI 316L)
- Pressure ranges in relative (gauge) or absolute from 0 up to 600 bar
- All standard output signals: 4 – 20 mA, 0 – 5 V, 1 – 5 V, 1 – 6 V, 0 – 10 V, 1 – 10 V
- A wide range of pressure and electrical connections
- Temperature compensated and laser calibrated
- For use in zone 2 explosive atmospheres

Application and media conditions for MBS 3050

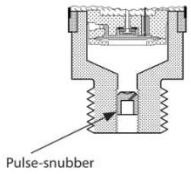

Application

Cavitation, liquid hammer and pressure peaks may occur in hydraulic systems with changes in flow velocity, e.g. fast closing of a valve or pump starts and stops.

The problem may occur on the inlet and outlet side, even at rather low operating pressures.

Media condition

Clogging of the nozzle may occur in liquids containing particles. Mounting the transmitter in an upright position minimizes the risk of clogging, because the flow in the nozzle is limited to the start-up period until the dead volume behind the nozzle orifice is filled. The media viscosity has only little effect on the response time. Even at a viscosities up to 100 cSt, the response time will not exceed 4 ms.

Technical data

Performance (EN 60770)

Accuracy (incl. non-linearity, hysteresis and repeatability)		≤ ± 0.5% FS (typ.)
		≤ ± 1% FS (max.)
Non-linearity BFSL (conformity)		≤ ± 0.2% FS
Hysteresis and repeatability		≤ ± 0.1% FS
Thermal zero point shift		≤ ± 0.1% FS / 10K (typ.)
		≤ ± 0.2% FS / 10K (max.)
Thermal sensitivity (span) shift		≤ ± 0.1% FS / 10K (typ.)
		≤ ± 0.2% FS / 10K (max.)
Response time	Liquids with viscosity < 100 cSt	< 4 ms
	Air and gases (MBS 3050)	< 35 ms
Overload pressure (static)		6 × FS (max. 1500 bar)
Burst pressure		6 × FS (max. 2000 bar)
Durability, P: 10 – 90% FS		>10 × 10^6 cycles

Electrical specifications

Nom. output signal (short-circuit protected)	4 – 20 mA	0 – 5, 1 – 5, 1 – 6 V	0 – 10 V, 1 – 10 V
Supply voltage [U_B], polarity protected	9 – 32 V	9 – 30 V	15 – 30 V
Supply – current consumption	–	≤ 5 mA	≤ 8 mA
Supply voltage dependency	≤ ± 0.1% FS / 10 V		
Current limitation	28 mA (typ.)	–	
Output impedance	–	≥ 25 kΩ	
Load [R_L] (load connected to 0 V)	$R_L \leq (U_B - 9V) / 0.02$ A	$R_L \geq 10$ kΩ	$R_L \geq 15$ kΩ

Technical data
(continued)

Environmental conditions

Sensor temperature range		Normal	-40 – 85 °C
		ATEX Zone 2	-10 – 85 °C
Media temperature range			115 - (0.35 × Ambient temp.)
Ambient temperature range (depending on electrical connection)			See page 6
Compensated temperature range			0 – 80 °C
Transport/storage temperature range			-50 – 85 °C
EMC – Emission			EN 61000-6-3
EMC – Immunity			EN 61000-6-2
Insulation resistance			> 100 MΩ at 100 V
Mains frequency test			Based on SEN 361503
Vibration stability	Sinusoidal	15.9 mm-pp, 5 Hz – 25 Hz	IEC 60068-2-6
		20 g, 25 Hz – 2 kHz	
	Random	7.5 g_{rms}, 5 Hz – 1 kHz	IEC 60068-2-64
Shock resistance	Shock	500 g / 1 ms	IEC 60068-2-27
	Free fall	1 m	IEC 60068-2-32
Enclosure (depending on electrical connection)			See page 6

Explosive atmospheres

Zone 2 applications	CE Ex II 3G Ex nA IIA T3 Gc -20C<Ta<+85C	EN60079-0; EN60079-15

When used in ATEX Zone 2 areas at temperatures <-10 °C the cable and plug must be protected against impact.

Mechanical characteristics

Materials	Wetted parts	EN 10088-1; 1.4404 (AISI 316 L)
	Enclosure	EN 10088-1; 1.4404 (AISI 316 L)
	Electrical connections	See page 6
Net weight (depending on pressure connection and electrical connection)		0.2 – 0.3 kg

Appendix E1: Evaluation of the Heat Loss in the DA-Vent Condenser Steam Pipe Line

Evaluating the heat loss due to natural convection from the steam pipe line between the DA and the vent condenser was important to determine the lost energy through that pipe line's wall. Evaluating the heat loss in this pipe line was helpful to estimate the temperature of the vented steam that left the DA after the deaeration process. That steam inside the deaerator has a measured temperature and pressure of about 235 °F and 8 psig, which is saturated steam, according to the steam tables. Figure E1.a shows a schematic of the steam pipe line between the DA and the vent condenser in the KU SPP. The specific enthalpy of the steam that enters the vent condenser was assumed to be the saturated enthalpy (h_{sat2}) at 216 °F. The steam temperature inside the DA was known (235 °F), but the temperature of the steam that left the DA after the deaeration process was not known. So the specific enthalpy of the steam leaving the DA (h_{sat1}) was needed in order to determine the temperature there. In order to determine h_{sat1}, the heat loss from the pipe line shown in Fig. E1.a was required which can be written as

$$Q_{out} = \dot{m}_{DA\_st}(h_{sat1} - h_{sat2}) \quad \text{(E1.1)}$$

Heat loss was computed in Section 5.2; but, here, it must be calculated for two cases: for the vertical and horizontal pipe lines shown in Fig. E1.a. This is because the natural convection heat transfer coefficient (H_n) is computed differently for vertical and horizontal pipe applications [36].

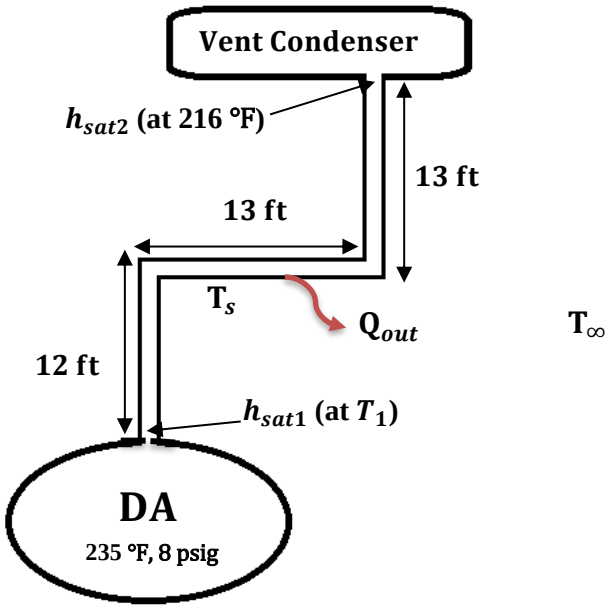

Fig. E1.a. Schematic of the vented steam pipe line between the DA and vent condenser

The property data shown in Table E1.1 are for air around the steam pipe line. In addition, dimensions of the vertical and horizontal pipe lines are included.

Table E1.1. Data gathered on 10/01/16 at 12:12 PM around the DA's vented steam pipe line

ρ_a $(\frac{lb_m}{ft^3})$	0.0712
C_p $(\frac{Btu}{lb_m\,^\circ\mathrm{R}})$	0.2404
K $(\frac{Btu}{hr\,ft\,^\circ R})$	0.0152
μ $(\frac{lb_m}{ft\,sec})$	$1.27x10^{-5}$
L_V (ft)	25
L_H (ft)	13
D (ft)	0.34
T_s $(^\circ R)$	561
T_∞ $(^\circ R)$	550
$\Delta T(^\circ R) = (T_s - T_\infty)$	11
T_f $(^\circ R)$	555.5
β $(\frac{1}{^\circ R})$	$1.88x10^{-3}$

<u>For the vertical pipe lines</u>

For vertical pipe application, the Nusselt number is [36]

$$\mathrm{Nu} = \left[0.825 + \frac{0.387\,(Gr\,Pr)^{0.167}}{\left[1+\left(\frac{0.492}{Pr}\right)^{0.5625}\right]^{0.296}}\right]^2 \qquad \text{(E1.2)}$$

Equations (5.40) and (5.41) in Section 5.2 were used to calculate Gr and Pr numbers. From those equations, Gr number was found to be $3.31x10^{11}$, and Pr number was found to be 0.723, which, using Eq. (E1.2), gave $\mathrm{Nu} = 685.9$. Substituting Nu and Table E1.1 properties into Eq. (5.38), gave $\mathrm{H_n} = 0.42\ \frac{Btu}{hr\,(ft^2)\,^\circ R}$, where the characteristic length was 25 ft (for vertical cylinder application [36])

Thus, by using Eq. (5.42), $Q_V = 122.5\ \frac{Btu}{hr}$.

For the horizontal pipe line

Equations (5.38)-(5.41) in Section 5.2 were used to determine $\mathrm{Gr}, \mathrm{Pr}, \mathrm{Nu}$, and $\mathrm{H_n}$ since this part of pipe line is a horizontal cylinder. Gr number was found to be $7.88x10^5$, and Pr number was found to be 0.723, which gave $\mathrm{Nu} = 12.45$ and $\mathrm{H_n} = 0.56\ \frac{Btu}{hr\ (ft^2)\ ^\circ R}$. Hence, from Eq. (5.42)

$Q_H = 85\ \frac{Btu}{hr}$.

Then summing Q_V and Q_H, total heat loss in both pipe lines was

$Q_{out} = 207.5\ \frac{Btu}{hr}$

Since the mass flow rate of the steam leaving the DA was the same as that entering the vent condenser, the steam mass flow rate determined in Section 5.2 [by applying mass and energy balances around the vent condenser (see Eq. (5.43))] was used in Eq. (E1.1). However, the determined mass flow rate of the steam in the vented steam pipe line ($\dot{m}_{DA\_st}$) was slightly different that that found in Section 5.2 (8.56 $\frac{lb_m}{min}$, instead of 8.55 $\frac{lb_m}{min}$) because of different air properties around the DA's steam pipe lines as shown in Table E1.1.

By using Eq. (E1.1)

$207.5\ \frac{Btu}{60\ min} = 8.56\ \frac{lb_m}{min}\ (h_{sat1} - 1151.8)\ \frac{Btu}{lb_m}$

Here, h_{sat2} was found 1151.8 $\frac{Btu}{lb_m}$ from the saturated steam table at 216 °F.

So after solving Eq. (E1.1), the specific enthalpy of the steam leaving the DA was found to be 1152.2 $\frac{Btu}{lb_m}$, which is almost the same as that entering the vent condenser. That was because the heat loss (Q_{out}) through the pipe wall was very small, which did not significantly affect the specific enthalpy along the pipe line. So the temperature of the steam leaving the DA was found to be about 218 °F.

Appendix E2: Thermocouple K/J Temperature Tolerance Table (reproduced from Ref. 51)

Thermocouple Tolerances
(Reference Junction at 0°C)

American Limits of Error ASTM E230-ANSI MC 96.1

ANSI Code		Standard Limits†		Special Limits†	
J	Temp Range	>0 to 750°C	>32 to 1382°F	0 to 750°C	32 to 1382°F
	Tolerance Value	2.2°C or 0.75%	4.0°F or 0.75%	1.1°C or 0.4%	2.0°F or 0.4%
K	Temp Range	>0 to 1250°C	>32 to 2282°F	0 to 1250°C	32 to 2282°F
	Tolerance Value	2.2°C or 0.75%	4.0°F or 0.75%	1.1°C or 0.4%	2.0°F or 0.4%
	Temp. Range*	-200 to 0°C	-328 to 32°F		
	Tolerance Value	2.2°C or 2.0%	4.0°F or 2.0%		
T	Temp Range	>0 to 350°C	>32 to 662°F	0 to 350°C	32 to 662°F
	Tolerance Value	1.0°C or 0.75%	1.8°F or 0.75%	0.5°C or 0.4%	1°F or 0.4%
	Temp. Range*	-200 to 0°C	-328 to 32°F		
	Tolerance Value	1.0°C or 1.5%	1.8°F or 1.5%		
E	Temp Range	>0 to 900°C	>32 to 1652	0 to 900°C	32 to 1652°F
	Tolerance Value	1.7°C or 0.5%	3°F or 0.5%	1.0°C or 0.4%	1.8°F or 0.4%
	Temp. Range*	-200 to 0°C	-328 to 32°F		
	Tolerance Value	1.7°C or 1.0%	3°F or 1.0%		
N	Temp Range	>0 to 1300°C	>32 to 2372°F	0 to 1300°C	32 to 2372°F
	Tolerance Value	2.2°C or 0.75%	4.0°F or 0.75%	1.1°C or 0.4%	2.0°F or 0.4%
	Temp. Range*	-270 to 0°C	-454 to 32°F		
	Tolerance Value	2.2°C or 2.0%	4.0°F or 2.0%		
R S	Temp Range	0 to 1450°C	32 to 2642°F	0 to 1450°C	32 to 2642°F
	Tolerance Value	1.5°C or 0.25%	2.7°F or 0.25%	0.6°C or 0.1%	1°F or 0.1%
B	Temp Range	800 to 1700°C	1472 to 3092°F	Not	
	Tolerance Value	0.5%	0.5%	Established	
G*C*D*	Temp Range	0 to 2320°C	32 to 4208°F	Not	
	Tolerance Value	4.5°C or 1.0%	9°F or 1.0%	Established	

** Not official symbol or standard designation* *† Whichever value is greater.*

Note: *Material is normally selected to meet tolerances above 0°C. If thermocouples are needed to meet tolerances below 0°C, the purchaser shall state this as selection of material is usually required.*

IEC Tolerance Class EN 60584-2; JIS C 1602

IEC Code		Class 1	Class 2	Class 3††
J	Temp Range	-40 to 375°C	-40 to 333°C	
	Tolerance Value	±1.5°C	±2.5°C	Not
	Temp. Range	375 to 750°C	333 to 750°C	Established
	Tolerance Value	±0.4% Reading	±0.75% Reading	
K N	Temp Range	-40 to 375°C	-40 to 333°C	-167 to 40°C
	Tolerance Value	±1.5°C	±2.5°C	±2.5°C
	Temp. Range	375 to 1000°C	333 to 1200°C	-200 to -167°C
	Tolerance Value	±0.4%	±0.75% Reading	±1.5% Reading
T	Temp Range	-40 to 125°C	-40 to 133°C	-67 to 40°C
	Tolerance Value	±0.5°C	±1°C	±1°C
	Temp. Range	125 to 350°C	133 to 350°C	-200 to -67°C
	Tolerance Value	±0.4% Reading	±0.75% Reading	±1.5% Reading
E	Temp Range	-40 to 375°C	-40 to 333°C	-167 to 40°C
	Tolerance Value	±1.5°C	±2.5°C	±2.5°C
	Temp. Range	375 to 800°C	333 to 900°C	-200 to -167°C
	Tolerance Value	±0.4% Reading	±0.75% Reading	±1.5% Reading
R S	Temp Range	0 to 1100°C	0 to 600°C	
	Tolerance Value	±1°C	±1.5°C	Not
	Temp. Range	1100 to 1600°C	600 to 1600°C	Established
	Tolerance Value	±[1 + 0.3% x (Rdg-1100)]°C	±0.25% Reading	
B	Temp Range			600 to 800°C
	Tolerance Value	Not		+4°C
	Temp. Range	Established	600 to 1700°C	800 to 1700°C
	Tolerance Value		±0.25% Reading	±0.5% Reading

†† Material is normally selected to meet tolerances above -40°C. If thermocouples are needed to meet limits of Class 3, as well as those of Class 1 or 2, the purchaser shall state this, as selection of material is usually required.